Smoothened regulation in the Hedgehog signaling pathway

Smoothened regulation in the Hedgehog signaling pathway

A dissertation presented

by

Daniel Nedelcu

to

The Division of Medical Sciences

in partial fulfillment of the requirements

for the degree of

Doctor of Philosophy

in the subject of

Cell Biology

Harvard University

Cambridge, Massachusetts

August 2013

Thesis Advisor: Adrian Salic Daniel Nedelcu

Abstract

Hedgehog signaling is a pathway essential in embryonic development, adult stem cell maintenance, and is implicated in the formation and progression of cancer. Signaling in this pathway is triggered when the secreted protein Hedgehog binds to its membrane receptor, Patched. Patched normally inhibits the seven-spanner transmembrane protein Smoothened (Smo). Binding of Hedgehog inhibits Patched resulting in Smo derepression. Active Smo then triggers the activation of the cytoplasmic steps of the signaling pathway. The regulation of Smo is poorly understood mechanistically.

Oxysterols bind Smo and potently activate vertebrate Hedgehog signaling. However, it is unknown if oxysterols are important for normal Hedgehog signaling, and whether antagonizing oxysterols can inhibit the Hedgehog pathway. I developed azasterols that block Hedgehog signaling by inhibiting the oxysterol-binding site of Smo. I show that the binding site for oxysterols maps to the extracellular, cysteine-rich domain of Smoothened, which is distinct from the site bound by other small molecule Smo modulators. Smo mutants that abolish oxysterol binding no longer respond to oxysterols and cannot be maximally activated by the Hedgehog ligand. My results show that oxysterol binding to vertebrate Smoothened is required for high level Hedgehog signaling. Importantly, I found that targeting the oxysterol binding site is an effective strategy to block Smoothened activity.

Signal transduction in the vertebrate Hedgehog pathway is spatially restricted to the primary cilium. I explored the mechanism of ciliary localization of Smo, and identified two degenerate ciliary localization sequences within its cytosolic tail. I further identified a cytosolic

domain of Smo, which is essential but not sufficient for activation of downstream components. Finally, I show that while the ciliary localization aspect is unique to vertebrates, signaling to downstream components is conserved across phyla.

My findings indicate that Smo is a modular protein, wherein each module serves a specific role and reflects a distinct mechanism of regulation. This suggests a model wherein Smo is at the confluence of several distinct regulatory inputs: an oxysterol regulated module, a second small-molecule regulated module, and a ciliary localization module, as well as a module for downstream signalling – which all converge for maximal activation.

Acknowledgements

First I would like to thank my wife for standing by my side over these years, as well as for putting up with my occasionally crazy passions. To say that my life would have ben much emptier had she not tolerated all four of my cats in our midst would be an understatement.

I would like to thank my parents and brother who never objected too much as I experimented with chemistry in the kitchen of my childhood. This little hobby back then has instilled an everlasting passion in me without which the current work would not exist.

I want to thank my advisor, Adrian Salic, for his relentless mentoring and guidance over the years. I would then like to thank the other members of the Salic lab who have contributed creatively to my development as a scientist. First, I would like to thank Jing Liu and Cindy Jao for making all the chemical compounds without which my project would not have been possible. I would like to thank Hanna Tukachinsky for introducing me to the rockstar blue energy drink, without which my years in the Salic lab would have been a lot less productive; for sharing the same delayed working schedule which ensured I would not be; and for always challenging my hypotheses until I had a sound answer. My grad school experience would have been much more lonely, were it not for the many late nights we spent together in lab each doing our own experiments while everyone else was soundly asleep in their homes. I would like to thank the rest of the – current or former – members of the Salic lab: Lyle Lopez for bringing music to everyone's ears in lab every single day, Kostadin Petrov for being such an energetic presence in my bay, and Ryan Kuzmickas for keeping my spirits up when experiments would fail.

I would like to thank the members of my dissertation advisory committee – Drs. John Blenis, Danesh Moazed and Malcolm Whitman – for their guidance and constructive advice over the years.

Last but not least, I would like to thank my first biology teacher, Dorin Dochinoiu, for arousing my interest in science at a time when I should have still been playing with toy cars; and my high school chemistry teacher, Bruno Bednar, who encouraged me to ask questions and then devise experiments to answer them.

Table of Contents

List of Figures and Illustrations

List of Symbols, Abbreviations and Nomenclature

Symbol	Definition
Shh	Sonic hedgehog
Ptc	Patched, the Shh receptor
Smo	Smoothened
SuFu	Suppressor of Fused
Gli	Glioma-associated
Ci	Cubitus interruptus
Cos2	Costal2
20-OHC	20(S)-hydroxycholesterol
22-NHC	22-azacholesterol

Chapter 1: General Introduction

1.1 Signaling in Embryonic development

The development of complex structures such as individual organs or limbs requires a crosstalk between adjacent cell populations in order to establish different cell fates and spatial organization. This section will review the principal signalling pathways involved in embryonic development.

Morphogenesis of the Drosophila embryo begins with specification of the anterior-posterior (A/P) and dorsal-ventral (D/V) axes before the egg is laid. These processes rely on maternal mRNAs deposited in the oocyte as it matures in the developing follicle; *bicoid* and *oskar* mRNAs localize at opposite ends of the oocyte and form opposite gradients along the A/P axis. Upon fertilization, translation of the *bicoid* and *oskar* maternal mRNAs forms opposite gradients of the morphogens across the dividing cells to maintain the A/P axis throughout the early stages of embryonic development (Jones et al., 2011). Subsequently, the embryo is divided along the A-P axis into a series of 14 segments (Gehring, 2012).

In a series of classic genetic experiments, Nusslein-Volhard and Wieschaus identified three classes of mutants which caused early lethality during embryonic development in Drosophila. These three classes of mutant phenotypes correspond to multiple genes involved in embryonic patterning, and highlight three levels of spatial and temporal organization. First, gap genes specify broad region of the embryo encompassing the multiple segments. Pair-rule genes then subdivide the embryo in similar regions in every other segment. Finally, segment polarity genes (such as *patched*, *wingless* and *hedgehog*) are turned on in all segments to control portions within each segment; mutations in segment polarity genes cause similar deletions across all

segments, with the remaining part of the segment duplicated in a mirror-like fashion. Taken together, these three classes of mutants suggest a hierarchical organization of segmentation genes to specify the final body plan. The segment polarity genes stand out because the mutants affect components of only two signaling pathways – *wingless* and *hedgehog*.

Wingless (*wg*) is a secreted protein homologous to the vertebrate *Wnt*, and is involved in maintenance of *engrailed*; *wg* binds to its receptor Frizzled (Fz), a seven transmembrane domain protein with homology to G-protein coupled receptors, and turns on downstream transcription via the nuclear effector Pan (Brunner et al., 1997). Hedgehog (Hh) codes for a secreted morphogen and is transcribed upon Engrailed activation. Early in embryonic development, *wg* and *hh* function to specify the parasegment boundary (Bokor and DiNardo, 1996) while later they are involved in patterning of the nervous system and the imaginal discs. In Drosophila, imaginal discs are precursors of the adult appendages; during embryogenesis, the discs are patterned to reflect their specific fate, and upon metamorphosis to the adult fly, they build the adult exoskeleton. During the third larval instar, *wg* is responsible for patterning the region around the margins of wing imaginal discs (Couso et al., 1994). *engrailed* activity leads to production of *hedgehog* in the posterior compartment of imaginal discs, which establishes a gradient along the A-P axis. *Hedgehog* signaling from the posterior compartment turns on *Decapentaplegic* (Dpp) in the anterior compartment, which in turn maintains Wg production.

The Hedgehog (Hh) signaling pathway in vertebrates is also responsible for correct patterning and differentiation during embryonic development of most tissues and organs; the Hh pathway has also been implicated in postembryonic tissue homeostasis by regulating

proliferation and differentiation of adult stem cells (Beachy et al., 2004; Trowbridge et al., 2006). In the vertebrate embryo, the hedgehog ligand is initially expressed in the notochord and guides specification of all ventral cell types such as motor neurons in the developing neural tube, which will later on become the spinal cord (Jessell, 2000). Later in development, hedgehog signaling is required for limb formation and specification of digit identity in the developing limb bud (reviewed by (Johnson et al., 1994)).

While vertebrates lack segments as seen in arthropods like Drosophila, the formation of somites is an analogous process of division along the anterior-posterior axis that specifies a segmented body plan. The somites are structures along the anterior-posterior axis of the embryo that will eventually become vertebrae, skeletal muscle and skin. In somites, Shh secreted from the adjacent neural tube regulates the differentiation of the ventral sclerotome (Fan and Tessier-Lavigne, 1994; Marigo and Tabin, 1996). Mutations of Shh manifest themselves at this stage as defects of the spine and ribs (Chiang et al., 1996).

Mysregulation of Hh signaling leads to birth defects and a number of sporadic cancers in humans (Beachy et al., 2004; Hooper and Scott, 2005; Ingham and McMahon, 2001; Rubin and de Sauvage, 2006). The Hedgehog pathway regulates both differentiation and proliferation in the cardiovascular system; in early embryonic development, it plays a crucial role during morphogenesis of the heart by determining left/right asymmetry, and directing the correct looping of the heart tube (Cooper et al., 2005). Hedgehog signaling is implicated in maintenance and repair of adult cardiovascular tissues and regulates angiogenesis. Hh signaling induces angiopoietins and VEGF, leading to coronary neovascularization in the adult heart**;** treatment

with recombinant Shh induces neovascularization and confers protection against ischemic injury in a surgically induced mouse hind-limb ischemia model (Pola et al., 2001). Furthermore, transient intra-myocardial gene transfer of Shh induces recovery from myocardial ischemia in adult mice and pigs (Kusano et al., 2005). Aberrant activation of Hedgehog signaling leads to neovascularization of tumors and is a central step in tumor growth in a variety of cancers. In the absence of a steady blood supply, tumors are severely restricted in growth; many tumors secrete Shh to signal the surrounding stroma and attract blood vessel formation, allowing progressive growth in both tumor size and metastatic potential (Folkman, 2002; Yamazaki et al., 2008).

1.2 Hedgehog pathway overview

The Hh pathway structure remains mainly conserved from *Drosophila* to humans, although some differences exist (Varjosalo et al., 2006). This section will examine the individual components of the Hh pathway and their regulation in arthropods and in vertebrates.

The secreted protein Hedgehog (Hh in *Drosophila*, or one of three vertebrate orthologs, primarily Sonic hedgehog, Shh) is synthesized as a precursor protein which undergoes a cholesterol-catalyzed self-cleavage and palmitoylation. The processed N-terminal fragment is then secreted in a process that depends on the 12-spanner Dispatched and is further assisted by Scube (Tukachinsky et al., 2012). On the receiving end (Figure 1.1), signaling is triggered when the secreted Hh ligand binds to its membrane receptor, the 12-spanner protein Patched (Ptc)(Stone et al., 1996). Ptc normally inhibits the 7-pass transmembrane protein Smoothened

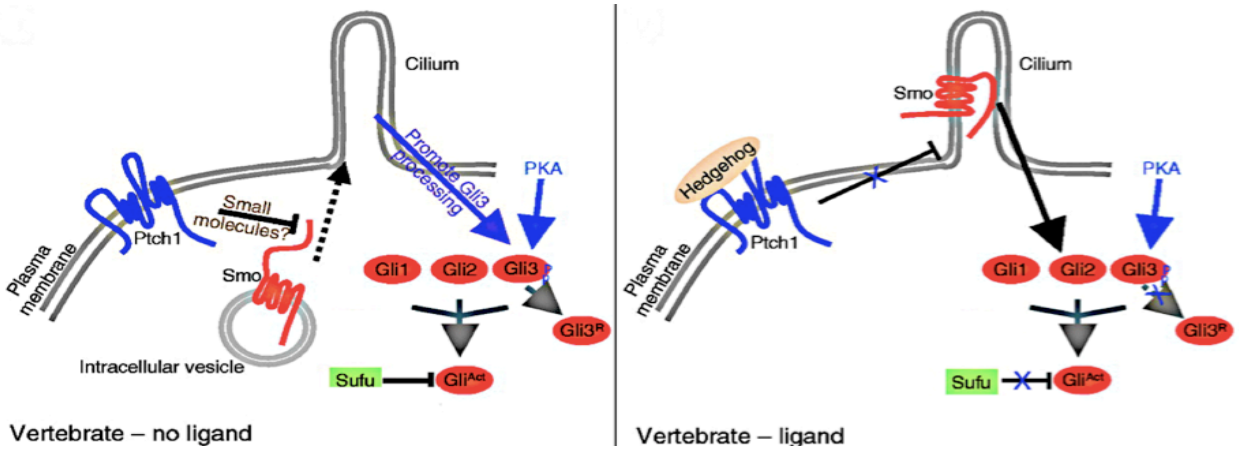

Figure 1.1 Overview of the Hedgehog pathway components in the receiving cell
In the absence of stimulation Ptc prevents Smo from entering the primary cilium; upon stimulation by Sonic hedgehog ligand, the inhibition is relieved and Smo can enter the cilium where it signals downstream effectors (adapted from (Huangfu and Anderson, 2005))

(Smo). When bound by Hh, Patched is inhibited resulting in Smo activation. Active Smo then triggers the activators of the cytoplasmic steps of the signaling pathway, and ultimately induces transcription of the Hh target genes which include Gli1 and Ptc (Rohatgi and Scott, 2007).

Regulation of Smo is critical for Hh signaling; however, the way Smo is activated and inhibited is poorly understood mechanistically. Ptc does not directly bind Smo (Denef et al., 2000), and acts catalytically to inhibit it (Taipale et al., 2002). The non-stoichiometric inhibition of oncogenic Smo suggests that Ptc regulates Smo indirectly, by affecting the concentration of an intermediate modulator (Chen et al., 2002a), and several lines of evidence point to a small-molecule mediator (Chen et al., 2002b; Taipale et al., 2002) whose identity remains unknown. Furthermore, in a cellular context, Smo is constitutively active in the absence of Ptc (Rohatgi et al., 2007); however, it is not known whether Smo is intrinsically in the active conformation, or is kept active by a ubiquitous activator molecule – and Ptc may act indirectly on Smo by interfering

with this activator. Ptc may regulate the abundance of a Smo modulator; nevertheless, in the absence of direct biochemical evidence, the mechanism of Smo inhibition remains an open question.

While Hedgehog, Patched and Smoothened as well as the Ci/Gli transcription factors are conserved from Drosophila to vertebrates, the pathway components downstream of Smo have diverged significantly. Moreover, despite sequence conservation of Smo throughout species, the presence of additional regulatory sequences in the cytoplasmic tail of *Drosophila* Smo suggests a divergent, specialized mechanism of downstream signaling (Varjosalo et al., 2006). In Drosophila and in the absence of signaling, the zinc-finger transcription factor Cubitus interruptus (Ci) forms two separate complexes, one containing the kinesin-like protein Costal2 (Cos2) and the serine/threonine kinase Fused (Fu), and a small fraction exists in a separate complex containing the Suppresor of Fused, Su(Fu); the complexed Ci is then proteolytically cleaved to a repressor form. Cos2 is anchored to microtubules in the cytosol and thus sequesters Ci in the cytosol. Cos2 inhibits the vast majority of available Ci while Sufu only plays a minor role (Varjosalo 2006). Pathway activation leads to accumulation of Smo, which binds Cos2 directly; this in turn destabilizes the Ci-Cos2 complex , releases Ci and inhibits the proteolytic cleavage of Ci. The full-length Ci-activator form translocates to the nucleus where it transcribes the hedgehog target genes. Smo binds Cos2 through its C-terminal domain, while the vertebrate Smo does not interact with Cos2; interestingly, the Drosophila C-terminal domain renders vertebrate Smo sensitive to Cos2 in a chimeric protein (Varjosalo et al., 2006).

In vertebrates, the Glioma-associated family of transcription factors (Gli1, 2 and 3) are the homologs of Ci. Gli forms a complex with Suppresor of Fused (SuFu) in the cytosol, and is proteolyzed to a short repressor form. Pathway activation leads to destabilization of the Gli-SuFu complex, which inhibits the proteolytic cleavage of Gli and frees the active Gli-A form to translocate to the nucleus and transcribe the Hedgehog target genes (Tukachinsky et al., 2010). Of the three Gli proteins present in vertebrates, Gli3 is processed robustly to the repressor form in the absence of signaling (Wang et al., 2000), while pathway activation stabilizes the full-length Gli3 activator form which translocates to the cilium along with SuFu (Tukachinsky et al., 2010). Gli1 only exists in the activator form and is not processed to a repressor (Dai et al., 1999; Kaesler et al., 2000; Park et al., 2000), while Gli2 is primarily in the active form but is kept repressed by binding to SuFu in the cytosol (Pan et al., 2006; Tukachinsky et al., 2010). The primary mediator of transcriptional activation is Gli2, while the primary mediator of transcriptional repression is Gli3 (Bai et al., 2002; Persson et al., 2002; Wang et al., 2000); as a direct target of Hh signaling, Gli1 is not essential for Hedgehog signaling but forms a positive feedback loop to amplify the transcriptional output of the pathway (Park et al., 2000). Early on in embryonic development, mouse knockouts of the positive regulators Shh, Smo or Gli2 show severe defects in specifying left-right asymmetry, in establishing midline structures such as the notochord or floor plate; later in embryonic development, gross morphological defects include holoprosencephaly, cyclopia, absence of motor neurons in the ventral neural tube, and defects in limb development (Chiang et al., 1996; Ding et al., 1998; Kim et al., 2001; Tsukui et al., 1999; Zhang et al., 2001).

Strikingly, mouse knockouts of the Fu kinase homolog (Stk36) are viable and have normal Hh signaling (Wilson et al., 2009). The closest vertebrate homologs of Cos2 are Kif27 and Kif7. The mouse Fu homolog interacts directly with Kif27, and together are essential for assembly of the central pair of microtubule dublets in motile cilia, but have no role in Hedgehog signaling (Wilson et al., 2009). Separately, Kif7 is a ciliary protein which acts downstream of Smo and does not bind Smo directly (Varjosalo et al., 2006). In the absence of signaling, Kif7 localizes at the base of the primary cilium; activation of the hedgehog pathway triggers a redistribution of Kif7 along the entire length of the cilium, and it accumulates at the distal tip of the cilium. Furthermore, mutations in the motor domain of Kif7 disable this movement, impair the formation of the Gli3 repressor form, and result in ectopic Hh pathway activation; this is similar to the effect of a complete loss of Kif7, which also recapitulates the Gli3-null phenotype (Endoh-Yamagami et al., 2009; Liem et al., 2009).

1.3 Ptc and the Sterol Sensing Domain

Several proteins involved in cholesterol biosynthesis or homeostasis contain a conserved sterol sensing domain (SSD), a region of five transmembrane domains which appears conserved across a variety of proteins involved in cholesterol biosynthesis, homeostasis or trafficking – but despite the conservation, the SSD has no known function. This section will review cholesterol biosynthesis and the role of the SSDs in cholesterol homeostasis in cells, before returning to Patched and examining what role the SSD might play in its function.

Cholesterol in cells is synthesized starting from acetate. The rate-limiting step of the cholesterol biosynthetic pathway involves the production of mevalonate in the ER through the catalytic action of the 3-hydroxy-3-methylglutaryl-coenzyme A reductase (HMG-CoA reductase); statins potently inhibit this step and are highly successful in the clinic to control cholesterol levels in circulation and thus prevent cardiovascular disease. Mevalonate is subsequently transformed through a number of steps into squalene which undergoes cyclization to lanosterol, the first compound to bear the four ring structure of sterols. Lanosterol is then transformed into cholesterol in 19 steps catalyzed by 9 different enzymes (Fakheri and Javitt, 2011).

Two enzymes in the cholesterol biosynthetic pathway contain SSDs. HMG-CoA reductase contains an SSD that is not required for its catalytic function but appears essential for the accelerated proteasomal degradation of HMG-CoA induced by sterols (Gil et al., 1985; Sever et al., 2003). The ER protein Insig-1 binds to the SSD of HMG-CoA reductase, and binding of sterols to Insig-1 greatly enhances this interaction and accelerates the degradation of HMG-CoA. This provides feedback inhibition in the sterol biosynthetic pathway. Separately, 7-dehydrocholesterol reductase (DHCR7) is an SSD-containing enzyme which catalyzes the transformation of 7-dehydrocholesterol into cholesterol, the last step in the biosynthesis of cholesterol; DHCR7 also catalyzes the transformation of cholesta-5,7,34-trienol into desmosterol.

Cholesterol levels in cells of vertebrates are tightly regulated. The majority of cholesterol in vertebrates comes from the diet and is derived from lipoprotein particles that transport

cholesterol and cholesterol esters from the gut throughout the organism. Thus, in the presence of cholesterol, cells must keep the endogenous production of cholesterol off; this occurs by turning off the transcription of HMG-CoA reductase and of cholesterol uptake receptors. Sterols facilitate the binding of Insig to the HMG-CoA reductase SSD and induce its accelerated proteolysis to further shunt the cholesterol biosynthesis (Sever et al., 2003). The promoter region of the HMG-CoA gene contains a sterol regulatory element, a region of DNA to which the sterol regulatory element binding protein (SREBP) binds. The N-terminal end of SREBP is a transcription factor, while its C-terminal end interacts with the SREBP cleavage-activating protein (SCAP) in the ER. SCAP contains an SSD, and in the presence of sterols SCAP binds Insig, which causes the SCAP-SREBP complex to be retained in the ER. In the absence of sterols, the interaction of SCAP with Insig is abolished, and the SCAP-SREBP complex translocates to the Golgi where the Golgi-resident zinc metalloproteases S1P and S2P cleave SREBP into its transcriptionally active form. The cytosolic N-terminal fragment of SREBP then enters the nucleus where it activates transcription of sterol regulatory element-containing genes (Rawson, 2003).

Interestingly, sterol binding correlates with the presence of an SSD in a protein but is not restricted to SSD-containing proteins: while cholesterol binds to SCAP and causes it to bind Insigs, the more soluble oxysterols bind directly to Insigs and cause them to bind SCAP in return (Radhakrishnan et al., 2007). A search for proteins that bind oxysterols, including 25-hydroxycholesterol, has identified the Niemann-Pick type C1 (NPC1) protein as an unexpected mediator of intracellular sterol transport. Cholesterol is transported through circulation in

complexes with lipoproteins and enters cells via receptor-mediated endocytosis in vesicles that fuse with the lysosomes. NPC1 is a transmembrane protein that functions in lysosomes where it binds cholesterol and dissociates it from lipoproteins; NPC1 also binds certain oxysterols bearing an –OH group at the 24, 25 or 26 positions, but not oxysterols with –OH groups at the 7, 19 or 20 position. It then transports the sterols from lysosomes to the endoplasmic reticulum. Patients deficient in NPC1 accumulate large amounts of cholesterol in the endosomal-lysosomal system (Infante et al., 2008a). NPC1 has a low specificity for substrates as long as they are lipophilic or at least amphiphilic; in a remarkable assay, NPC1 expressed in outer membrane of E. coli bacteria transports acriflavine and oleic acid from the periplasmic space across the plasma membrane into the cytosol (Davies et al., 2000). NPC1 has 13 transmembrane helices and contains a sterol-sensing domain embedded within helices 3-7 that resembles the SSD of SCAP. However, both SCAP and NPC1 bind sterols through a soluble, luminal loop near the N-terminal end, and thus the role of the SSD remains unclear (Infante et al., 2008b; Motamed et al., 2011). Separately, NPC2 is a soluble glycoprotein which lacks an SSD altogether. NPC2 fails to bind oxysterols but binds cholesterol and facilitates its transport between membrane compartments (Cheruku et al., 2006; Infante et al., 2008b); defects in NPC2 account for 5% of Niemann-Pick Type C disease cases (Wilson et al., 2009). NPC1 and NPC2 act together in a sequential mechanism wherein NPC2 captures cholesterol released from LDL particles and transfers it to NPC1; NPC1 then transports cholesterol out of lysosomes and to the various cellular membrane compartments by incorporating it in the membrane of outbound vesicles (Infante et al., 2008c).

Two homologs of Patched exist in vertebrates, Patched 1 and Patched 2; however, only Ptc1 is the primary receptor for hedgehog ligands in vertebrates (and from here on will be referred to as Ptc), while Ptc2 plays only a minor role as Ptc2-null mice are born alive without the gross abnormalities or cancer susceptibility associated with Ptc1 defects (Lee et al., 2006). Mutations in Patched that result in constitutive activation of Shh signaling are linked to Gorlin Syndrome. Nevoid Basal Cell Carcinoma Syndrome (NBCCS), also known as Gorlin Syndrome or Gorlin-Goltz Syndrome, is a familial cancer syndrome characterized by an abundance of basal nevoid cell carcinomas. These Ptc mutations show autosomal dominant inheritance, and trigger tumor formation through loss of heterozygosity in individual cells – this results in extremely variable expressivity of symptoms throughout the entire lifespan of individuals affected. Age of onset varies greatly between 2 and 65 years of age, and symptoms include skeletal as well as numerous basal cell carcinomas occurring at a young age, jaw cysts, palmar and plantar pits, and occasionally cognitive impairment (Jones et al., 2011).

Ptc associates with accessory membrane proteins such as the transmembrane proteins Cdo or Boc, or the GPI-anchored Gas1 to bind the Hedgehog ligand. These proteins have overlapping roles in soaking up the Hedgehog ligand, and thus limiting its range, but also form co-receptors with Ptc and together appear essential for proper Hedgehog signal transduction (Allen et al., 2011; Izzi et al., 2011; Zheng et al., 2010). Ptc is highly conserved from *Drosophila* to humans and shares homology with NPC1. Both Ptc and NPC1 contain an SSD, and are distantly related to the bacterial proton-driven small molecule transporters of the Resistance-Nucleation-cell Division (RND) superfamily (Davies et al., 2000; Rohatgi and Scott, 2007;

Tseng et al., 1999). Several members of this family actively translocate lipophilic small molecules across the cell membrane with broad specificity. In bacteria, several RND permeases are efflux pumps that account for multidrug resistance, as is the case with MexD in *P. aeruginosa*;. Furthermore, RND permeases function as homotrimers, and biochemical evidence suggests that Ptc forms trimers under physiological conditions through its C-terminal domain (Lu et al., 2006).

The SSD of Ptc is critical for its function, and this function is independent of binding of the Hedgehog ligand. Several mutations, including some mutations observed in patients with Gorlin Syndrome, map to conserved residues within the SSD that are essential for the activity of functional RND transporters (Taipale et al., 2002), of SCAP, or of NPC1 (Martin et al., 2001; Strutt et al., 2001). These mutations abolish the ability of Ptc to repress Smo and result in constitutive hedgehog pathway activity, but do not affect the binding of the Hedgehog ligand to Ptc. Taken together, the data suggest that Ptc may function as a small molecule transporter; nevertheless, no such activity of Ptc has yet been demonstrated and no known binding substrates exist (Rohatgi and Scott, 2007; Taipale et al., 2002).

1.4 Smo and G-Protein Coupled Receptors

One class of receptors involved in mediating cellular signalling and transducing the extracellular signal to the inside of the cell are seven-pass transmembrane-domain G-protein Coupled Receptors (GPCRs). This section will first review GPCRs, and then will examine the similarities and differences between GPCRs and Smo.

Canonical GPCRs exist in a conformational equilibrium between two distinct states – a ground, "inactive" form and an "activated" one. Binding the ligand triggers the switch between the two states. Despite significant diversity in their sequences, GPCRs share structural homology: the seven transmembrane helices form a bundle, a barrel-like cavity where ligands bind; the three extracellular loops as well as the N-terminal region are stabilized by a series of disulfide bridges and function to modulate ligand access to the transmembrane core, while the intracellular loops and the C-terminal tail relay the signal to the associated G protein. The extracellular disulfide bridges are structurally essential, as reducing agents or mutagenesis impairs the receptor (Gill et al., 2008).

The most numerous family of GPCRs is by far the Class A rhodopsin/β-adrenergic receptor family; in these receptors the extracellular loop 2 is often the longest extracellular loop (although exceptions exist) and ligands bind inside the transmembrane domain barrel. Class B GPCRs share a common N-terminal fold which interacts with ligands directly but it is not clear whether transmembrane domains contribute to the creation ligand binding pocket (Javitt, 2002b). Class C GPCRs contain a "venus flytrap module" in the N-terminal domain which binds ligands directly; the signal is relayed from the ligand-bound extracellular N-terminus to the transmembrane core through allosteric coupling. Finally, the Frizzled (Fz) class GPCRs are characterized by the presence of a Cysteine-Rich Domain in the N-terminal, which in the case of Frizzled binds the canonical ligand Wnt (Janda et al., 2012).

Smo resembles GPCRs and shares significant homology with Fz. The Fz family of receptors contains a conserved large extracellular Cysteine-Rich Domain (CRD) at the N-

terminal end. Fzs bind their cognate ligand through the CRD and signal to downstream components through their cytoplasmic tails (Bhanot et al., 1996; Janda et al., 2012); however, the CRD of Smo serves no known function (Chen et al., 2002b; Hooper, 2003; Rohatgi and Scott, 2007). Furthermore, Fzs form coreceptors with a Low-Density Lipoprotein Receptor-related protein in order to signal, while no such complex is known to exist for Smo.

GPCRs bind ligands on the extracellular side of the transmembrane barrel; this leads initially to a small conformational change within the transmembrane region, which in turn results in more significant structural rearrangements on the cytosolic side. A common mechanism for GPCR activation conserved across many class A receptors involves the relocation of transmembrane domains 3 and 7 upon agonist binding, which leads to a reconfiguration of the TM3-TM5 and TM5-TM6 interfaces; together, these coordinated movements bring together the extracellular ends of the TM helices while moving the cytosolic ends further apart (Javitt, 2002b). This creates a cleft-like pocket where the Gα subunit of the heterotrimeric G protein can bind and downstream signaling is activated ((Venkatakrishnan et al., 2013) provide a comprehensive review of the structural changes accompanying agonist binding).

Signaling downstream of canonical GPCRs occurs primarily through associated heterotrimeric GTP-binding regulatory proteins (G proteins). Heterotrimeric G proteins are activated by the conformational switch of the GPCR induced by ligand binding. This in turn triggers the dissociation of the inhibitory Gβγ subunits dimer from Gα; in mammals there are four families of Gα proteins (i.e. Gs, Gq/11, Gi/o, and G12/13), as well as 5 Gβ and 12Gγ isoforms, leading to over 1000 heterotrimeric combinations of subunit isoforms possible, and the

exact combination of the heterotrimer determines the specificity of its interactions with GPCRs (Dingus et al., 2002; Javitt, 2002a). Interestingly, more than one active state conformation may exist for a given receptor, as different ligands can modulate different conformational changes in GPCRs, biasing the receptor to preferentially bind one or more G proteins, or in turn to couple the receptor to other cytosolic effectors such as scaffold proteins like the β-arrestins – thus altering their signaling output or altogether shifting the response of the receptor to a parallel downstream cascade (Bjorkhem, 2007; Gill et al., 2008). More recently, the subunits Gβγ themselves have been implicated as direct messengers that relay the signal downstream of GPCRs directly, rather than the signal proceeding through the Gα subunit (reviewed by (Smrcka, 2008)). In the end, a two-step desensitization process limits the duration of activated GPCR signaling: extensive phosphorylation by G-protein coupled receptor kinases (GRKs) stops the interaction with G proteins, and β-arrestins trigger internalization and recycling of phosphorylated receptors from the cell surface (Chen et al., 2004).

Smo is reminiscent of functional GPCRs and is likely triggered by an unknown endogenous ligand. Smo is highly druggable, and a number of small molecule modulators of Smo activity exist: both agonists such as the synthetic small molecules SAG (Chen et al., 2002b) or purmorphamine (Wu et al., 2004), as well as antagonists such as the plant alkaloid cyclopamine (Taipale et al., 2000) or the synthetic compounds SANT-1 (Chen et al., 2002b) and Vismodegib (Robarge et al., 2009). While the canonical Wnt signal transduction occurs through a protein cascade that involves β-catenin and is independent of G protein coupling, several Frizzled receptors couple to heterotrimeric G protein subunits $G\alpha_o$ (Katanaev et al., 2005) and

$G\alpha_S$ (Nichols et al., 2013) to trigger non-canonical effects such as the regulation of the actin cytoskeleton through activation of Rho and Rac small GTPases (Angers and Moon, 2009). Evidence for G protein activation by Smo is scarce, but co-expression of G protein subunits along with Smoothened in baculovirus-infected insect cells indicates that Smo specifically activates several members of the G_i family, which inhibit the production of cAMP (Riobo et al., 2006; Varjosalo et al., 2006); human Smo also appears to activate $G\alpha_i$-mediated pigment aggregation in *Xenopus* melanophores, although whether this interaction is direct remains unknown (DeCamp et al., 2000). Further evidence for a potential involvement of G proteins comes from the functional similarities Smo shares with other GPCRs: activated Smo can be phosphorylated in a G-protein-coupled receptor kinase 2 (GRK2) dependent manner, and leads to accumulation and binding of β-Arrestin (Chen et al., 2004). Interestingly, a Smo mutant lacking the cytosolic tail which is unable to signal through Gli can nevertheless interact with $G\alpha_i$; this suggests that the interaction of Smo and $G\alpha_i$ is mediated through the cytosolic loops of Smo, and further suggests that this activity is independent of the canonical hedgehog signaling pathway (Polizio et al., 2011). Finally, Smo promotes fibroblast migration through activation of $G\alpha_I$ in a Gli-independent mechanism, suggesting the possibility that the GPCR-like function of Smo is involved in a function outside of canonical Hh signaling.

A conformational change of Smo upon stimulation of the Hh pathway has been suggested (Zhao et al., 2007). The fact that Smo is susceptible to small molecule modulation points to a possible mechanism of regulation through an endogenous small molecule. Cyclopamine binds directly to the seven transmembrane domain region and stabilizes the inactive

conformation(Chen et al., 2002a). Furthermore, oncogenic mutations (such as the SmoM2 mutant which corresponds to a tryptophane to a leucine point mutation towards the cytosolic end of the seventh transmembrane domain (Xie et al., 1998)) that render Smo insensitive to both Patched and cyclopamine, and which result in constitutive downstream signaling, could act simply by sterically impairing the ground state conformation and instead favouring a less ordered, intermediate conformation as evidenced by an increased retention in the endoplasmic reticulum (Chen et al., 2002a). SAG binding stabilizes oncogenic Smo and rescue it from ER retention, while overexpression of Ptc or addition of a more potent cyclopamine derivative revert such activated Smo mutants to the stable, inactive conformation (Chen et al., 2002a; Taipale et al., 2000; Zhao et al., 2007). The data point to a common mechanism of Smo inhibition by regulation of its conformational equilibrium. Furthermore, cyclopamine affinity for oncogenic Smo increases with Ptc overexpression, suggesting that Ptc shifts Smo to an inactive-state conformation similar to that recognized and stabilized by cyclopamine; the non-stoichiometric inhibition of oncogenic Smo suggests that Ptc regulates Smo indirectly, by affecting the concentration of an intermediate modulator (Chen et al., 2002a).

1.5 Sterols and the Hedgehog pathway

Hh signal transduction in vertebrates depends on proper sterol metabolism, as defects in sterol biosynthesis phenocopy Hh signal transduction defects. This section will review the evidence implicating sterols as regulators of the Hedgehog pathway.

Smith-Lemli-Opitz (SLOS), lathosterolosis and desmosterolosis are three human disorders that result in defects in the last stages of cholesterol biosynthesis. In mouse models of SLOS and lathosterolosis, which lack the enzymes 7-dehydrocholesterol reductase or lathosterol 5-desaturase respectively, the formation of Shh cholesterol-modified ligand is unaffected, but the response of cells to the secreted Shh ligand is impaired. Furthermore, non-specific depletion of sterols from cell membranes blocks Shh transduction at the level of Smo (Cooper et al., 2003). The SmoM2 mutation disrupts the ligand binding pocket of Smo and significantly decreases the affinity of Smo for ligands, as the inhibitors Cyclopamine, SANT-1 and Vismodegib show markedly higher IC_{50} values towards the M2 mutant than towards wildtype Smo (Chen et al., 2002b; Taipale et al., 2000; Yauch et al., 2009). However, the constitutive, ligand-independent SmoM2 (also called SmoA1 in the human protein) is not affected by sterol depletion (Cooper et al., 2003). Inhibition of the sterol biosynthetic pathway at various steps suggests that a cholesterol derivative, but not a steroid, is critical for Hh signaling (Corcoran and Scott, 2006). Two endogenous oxysterols, 20α-hydroxycholesterol (20-OHC, Figure 1.2) and 25-hydroxycholesterol (25-OHC, Figure 1.2), strongly activate the Hh pathway at the level of Smo and rescue the sterol-depletion defects (Corcoran and Scott, 2006; Dwyer et al., 2007; Nachtergaele et al., 2012; Rohatgi et al., 2007). 20-OHC and 25-OHC are so far the only endogenous molecules known to modulate Smo activity; 20-OHC acts directly on Smo as an allosteric agonist (Nachtergaele et al., 2012), yet whether it is the endogenous modulator of Smo is unclear. Together, this evidence suggests that endogenous regulation of Smo may involve a

hydrophobic small molecule such as a cholesterol derivative – however, the identity of such modulator remains unknown.

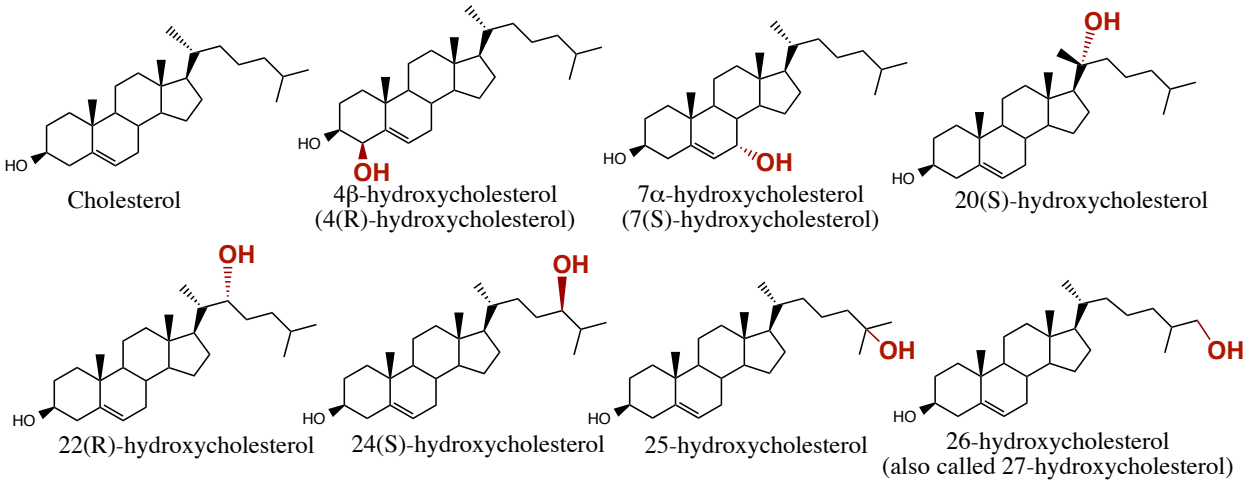

Figure 1.2 Structures of cholesterol and oxysterols

Several enzymes are known that catalyze the transformation of cholesterol into particular oxysterols (the structures of which are shown in Figure 1.2); these are generally cytochrome P450 hydroxylases. For instance, CYP3A4 forms 4β-hydroxycholesterol (Gill et al., 2008); CYP7A1 is responsible for the synthesis of 7α-hydroxycholesterol, the precursor to all bile acids (however, a separate, non-enzymatic path also exists to generate this particular oxysterol as an autoxidation product of cholesterol); CYP46 synthesizes 24(S)-hydroxycholesterol in neurons and is 100-fold enriched in the brain over other tissues, while CYP27A1 in mitochondria catalyzes the production of 26-hydroxycholesterol which is the major circulating oxysterol in humans and also an intermediate of the bile acid biosynthesis (Bjorkhem, 2007; Gill et al., 2008; Javitt, 2002a). The only known exception is the cholesterol 25 hydroxylase which forms 25-OHC from cholesterol; it belongs to a larger family of transmembrane enzymes that catalyze

oxidations using a di-iron cofactor in the catalytic site instead of a heme iron center (Lund et al., 1998).

Importantly, 20(S) and 22(R)-hydroxycholesterol form a special case as no single hydroxylase produces either of them as the stable end product. Instead, they are produced for a brief period as intermediates in the conversion of cholesterol to pregnenolone through the action of the cytochrome $P450_{SCC}$ sidechain cleavage enzyme (also known as CYP11A1 in humans) in the adrenal glands (reviewed in (Gill et al., 2008) and (Javitt, 2002b). Naturally occurring 20(S)-hydroxycholesterol was found in the brain and placenta, but its origin remains unclear (Lin et al., 2003). Several specific inhibitors of the $P450_{SCC}$ have been identified: the synthetic derivative 22-azacholesterol (Counsell et al., 1971) and 22-thiacholesterol (Miao et al., 1995) are both potent competitive inhibitors of P450Scc and block the formation of pregnenolone.

Since the majority of mutations associated with Hedgehog pathway defects in humans map to Ptc and result in constitutive derepression of Smo, and because Smo is easily druggable, there is significant interest in developing Smo-specific pharmacological inhibitors for therapeutic use ((Mas and Ruiz i Altaba, 2010) provide a comprehensive review of the inhibitors currently in clinical trials). One such compound, Vismodegib (formerly known as GDC-0449) has received approval from the U.S. Food and Drug Administration in 2012 as a treatment for basal cell carcinoma (Dubey et al., 2013). Vismodegib is the first Hh pathway inhibitor to receive authorization, and is in further clinical trials for a number of other cancers and metastatic solid tumors including medulloblastoma, recurrent glioblastoma multiforme, advanced stomach cancer, gastroesophageal junction cancer, pancreatic cancer, metastatic colorectal cancer, small

cell lung cancer, basal-cell nevus syndrome, multiple myeloma, chondrosarcoma, ovarian and prostate cancers (Mas and Ruiz i Altaba, 2010; Sandhiya et al., 2013). Vismodegib binds the same site as cyclopamine on Smo and displaces cyclopamine in competitive experiments (Rominger et al., 2009). A crystal structure of Smo with an inhibitor bound at the cyclopamine site shows the ligand binding pocket buried deep within the transmembrane domain, with a cap formed by the extracellular loops 2 and 3. Interestingly, a mutation in the extracellular loop of Smo renders it insensitive to inhibition by Vismodegib while keeping its signaling function intact. The D473H mutation was isolated from a medulloblastoma patient treated with Vismodegib (Yauch et al., 2009); residue D473 maps to the interface between the transmembrane helix 6 and the extracellular loop 3, and the mutation likely disturbs a hydrogen-bonding network within the ligand binding pocket (Wang et al., 2013).

Separately, two classes of glucocorticoid compounds were identified in a recent screen for small molecules that affect the ciliary localization of Smo (Wang et al., 2012). One class of compounds which contains fluocinolone acetonide (a common over-the-counter glucocorticoid medication used routinely as an anti-inflammatory topical treatment in dermatology (Scholtz, 1961)) behaves similar to cyclopamine in that they push Smo to the cilium in the inactive conformation and the compounds compete with a fluorescent cyclopamine derivative for binding Smo (Wang et al., 2012). A second class of compounds inhibited Smo translocation to the cilium, synergized with Vismodegib to block Hedgehog signaling at the level of Smo, and inhibited both wildtype as well as Smo mutants refractory to inhibition by Vismodegib (Wang et al., 2012). This second class of compounds do not directly compete with cyclopamine, indicating

that they may act elsewhere on Smo, or act indirectly on Smo. In this regard, the compounds behave closer to the protein kinase A (PKA) activator forskolin, and most likely act on Smo like forskolin through an indirect mechanism (see Section 1.8 for more effects of forskolin on the Hh pathway). An example of this class of compounds is budesonide (Wang et al., 2012). It is worth mentioning that glucocorticoids elicit their anti-inflammatory action by binding to and activating the glucocorticoid receptor, a member of the nuclear receptor family of transcription factors (Vandevyver et al., 2013). Whether budesonide acts directly on Smo, or indirectly through a separate mechanism is not known.

1.6 The primary cilium

The primary cilium is a unique organelle comprising a hair-like membrane projection surrounding a bundle of microtubules, which forms the axoneme. The primary cilium is a highly conserved structure, which exists in most eukaryotic cells and serves as an anchoring point to a variety of receptors including some GPCRs to increase their local concentration; the cilium thus serves as a cellular antenna for sensing the presence of nutrients or growth factors. Structurally, the cilium consists of three distinct regions - the axoneme forms the majority of the cilium and is attached to the basal body through the transition zone. The basal body is a complex of proteins formed around one of the two centrioles in the cell and functions to assemble and elongate the cilium. In addition to the primary cilium, some organisms also contain a separate flagellum which is a specialized, beating cilium; primary cilia contain 9 pairs of microtubules in a barrel-like arrangement across the axoneme, while motile cilia contain two additional central pairs of

microtubules attached to a flagellar motor complex. The primary cilium lacks the central pairs of microtubules and is therefore a rigid structure. No protein synthesis takes place at the primary cilium, thus any protein found at the cilium must be transported there; this includes the tubulin building blocks required for elongation of the cilium.

Microtubules are a major component of the cellular cytoskeleton and are involved in a variety of cellular processes, such as vesicular transport, cytokinesis and in particular cell division. The precursor of microtubules, tubulin is a globular protein, and its two most common isoforms (α and β) form heterodimers that are used as assembly blocks in the formation of microtubules. The microtubules are polarized, with the α-Tubulin subunit of the heterodimers exposed at the – end, and the β-Tubulin subunit exposed at the + end. Polymerization of tubulin dimers occurs at the + end of microtubules, when a new heterodimer attaches in its GTP-bound form to pre-existing tubulin polymers and subsequently hydrolyzes GTP to GDP. Microtubules are highly dynamic structures, and their length and stability is controlled by the balance between assembly and disassembly at both the + and the – ends; the net result of these processes at the – end is a shortening of the microtubule, while a net lengthening can be observed at the + end. Furthermore, microtubules suffer a variety of modifications, with acetylation being a hallmark of stable microtubules such as those in the primary cilium. Two families of ATP-dependent molecular motors provide bi-directional transport of cargo along microtubules: kinesins walk on microtubules towards the + end in a stepwise manner, while dyneins transport cargo along microtubules in the opposite direction. Ciliary microtubules are anchored with the – end to the

basal body, and the + end extends into the tip of the cilium; this translates to microtubule assembly occurring primarily at the tip of the cilium.

Genetic screens have identified two protein assemblies involved in ciliary transport – the intraflagellar transport IFT-A and IFT-B complexes (Ou et al., 2005). Defects in IFT-A components lead to accumulation of proteins along the cilium and at the ciliary tip, causing a bulging at the tip. In contrast, defects in IFT-B components lead to short or nonexistent cilia. One possible explanation is that IFT-B is involved in anterograde transport which would be required for extension of the cilium, while IFT-A along with cytoplasmic dynein mediates retrograde transport; a core component of IFT-B is the plus-directed motor kinesin II which brings cargo. Older evidence however suggests that IFT-A and IFT-B complexes function together in both anterograde and retrograde transport, as they associate with each other prior to movement along the cilium. The key player in ciliary transport and ciliary assembly is the BBSome, a complex of proteins essential for ciliary formation which catalyzes the assembly of IFT complexes at the base of the cilium. The IFT-A/IFT-B complexes transport both cargo and the BBSome to the distal end of the cilium where the complex dissociates and the cargo is unloaded. The BBSome at the ciliary tip then facilitates the reassociation of the IFT-A and IFT-B, which in turn recycles both components as well as cargo (which includes the BBSome) back to the base of the cilium. While IFT-A appears critical for retrograde transport, a defect in BBS-1 which renders the BBSome unable to associate with IFT-A/IFT-B and thus unable to reach the ciliary tip, leads to the accumulation of IFT-B complexes at the ciliary tip. This suggests that the BBSome functions to associate IFT-A to IFT-B in both the basal body and at the ciliary tip, and

that the association between IFT-A and IFT-B is maintained throughout both anterograde and retrograde transport (Wei et al., 2012).

1.7 Mechanisms of ciliary translocation

No protein synthesis takes place at the primary cilium, thus any protein found at the cilium must be transported there. This section will review the mechanism of ciliary translocation and the structural requirements for ciliary localization

The ciliary membrane has a unique lipid composition that is different from that of the plasma membrane (Tyler et al., 2009). Notably, sterols are enriched at (and distributed uniformly throughout) the ciliary shaft membrane, but are absent from the base of the cilium (Montesano, 1979). The highly curved membrane at the base of the cilium consists of a condensed lipid zone and may itself act as a diffusion barrier for integral membrane proteins or lipid-anchored proteins and lipids to restrict their movement into the ciliary membrane through lateral diffusion (Rohatgi and Snell, 2010). Furthermore, a ring in the transition zone consisting of Septin2 along with the B9 complex and the products several other ciliopathy genes forms a diffusion barrier at the base of the cilium that restricts access of membrane proteins into the ciliary membrane; this resembles the diffusion barrier found in the nuclear pore that restricts entry of soluble cytosolic proteins into the nucleus (Chih et al., 2012; Hu et al., 2010). The B9 complex is essential for both the ciliary translocation as well as for the sequestration of transmembrane proteins in the ciliary membrane (Chih et al., 2012). The septin diffusion barrier blocks the diffusion of a GPI-linked membrane-anchored fluorescent protein but does not restrict access of ciliary transport proteins

such as IFT88 into the ciliary membrane; these are instead inserted by IFT proteins and by the BBSome into the ciliary membrane directly above the septin diffusion barrier (Nachury et al., 2010).

At present, trafficking of proteins to the primary cilium is poorly understood mechanistically. One possibility is that ciliary entry is limited through a diffusion barrier at the base of the cilium, similar to how a size-selective diffusion barrier at the nuclear pore restricts entry into the nucleus. The size exclusion limit is around 30-40 kDa for both nuclear and ciliary entry by diffusion; proteins below the limit float in freely, while proteins above the limit are restricted from entering the cilium by diffusion alone, and instead require active transport (Kee et al., 2012). Members of the importin and Ran-GTPase families are required for ciliary entry and transport, as they are for nuclear import (Dishinger et al., 2010). In nuclear entry, importins recognize and bind the basic residues of the NLS, and move the cargo proteins through the nuclear pore complex; the importins then release the cargo upon binding to Ran-GTP, which is highly enriched in the nucleus, and are shuttled back to the cytosol where hydrolysis of the Ran-GTP to Ran-GDP restarts the process (Macara, 2001; Stewart, 2007). At the base of the primary cilium, importins and Ran along with the BBSome load cargo onto IFT-A/IFT-B complexes for transport to the distal end of the cilium (Fan and Margolis, 2011). Furthermore, nucleoporins localize to the base of the cilium as they do in the nuclear pore, and nucleoporin-blocking agents such as a truncated importin-β1 block entry of the kinesin-2 Kif17 motors into the ciliary compartment (Kee et al., 2012). However, it must be noted that the exact nature of the ciliary pore (and whether it actually exists) remains unknown.

While the simple diffusion barrier model above explains the ciliary import of soluble proteins, a different mechanism must account for the entry of membrane or lipid-anchored proteins into the primary cilium. Trafficking of membrane proteins between cellular compartments occurs through vesicles coated with the cage proteins COPI, COPII or clathrin (Faini et al., 2013). It is unlikely that whole vesicles would enter the ciliary lumen directly since the size of the smallest vesicles is larger than the 60nm spacing available between the transition fibers that anchor the transition zone of the primary cilium to the ciliary membrane (Anderson, 1972; Nachury et al., 2010). Instead, vesicles containing membrane proteins originating from the trans-Golgi fuse either to the membrane compartment at the base of the cilium and deliver their cargo there; or to the plasma membrane, and the cilium-directed cargo then moves into the ciliary membrane through lateral diffusion (Nachury et al., 2010). It must be noted that the directed vesicular trafficking mechanism from the Golgi to the base of the cilium is currently the preferred model for selective sorting of protein and lipids to the primary cilium (Rohatgi and Snell, 2010). A single component of the IFT-B complex, IFT20, also has a function independent of the IFT B complex and couples vesicular traffic from the Golgi to the canonical IFT components at the primary cilium. IFT20 is the only IFT protein in the Golgi; it localizes primarily to the trans-Golgi network as well as to post-Golgi vesicles that fuse with the base of the cilium (Follit et al., 2006), and moves dynamically between the Golgi and the primary cilium along with ciliary-targeted cargo (Keady et al., 2011). The light-detecting outer segments of vertebrate photoreceptors are highly specialized structures derived from the primary cilium and function as anchoring points for the light-sensitive GPCRs of the opsin family. In rod cells of the

retina, IFT20 binds the photopigment rhodopsin directly, both as part of the IFT particle as well as outside of it, and loss of IFT20 leads to accumulation of opsins in the Golgi network of the cell body (Keady et al., 2011). In the Hh pathway, however, Smo translocates to the primary cilium primarily through lateral movement from the plasma membrane, a mechanism that is distinct from the common vesicular trafficking to the ciliary base (Milenkovic et al., 2009).

One mechanism for regulation of proteins at the primary cilium is through regulation of their transport to and from the primary cilium. Ciliary access is tightly regulated as ciliary proteins must contain a ciliary localization sequence (CLS); interestingly, functional CLS resemble nuclear localization sequences and are stretches of basic residues (Dishinger et al., 2010) or a motif of adjacent hydrophobic and basic residues immediately C-terminal to the seventh transmembrane domain of olfactory GPCRs (Dwyer et al., 2001). Ciliary transport also resembles nuclear entry; members of the importin and Ran-GTPase families are required for ciliary entry, as they are for nuclear import (Dishinger et al., 2010). In nuclear import, importins recognize and bind the NLS of the cargo proteins, and move them through the nuclear pore complex in a Ran-GTPase dependent manner. At the cilium, importins and Ran along with the BBSome load cargo at the base of the cilium onto IFT-A/IFT-B complexes for transport to the distal end of the cilium (Fan and Margolis, 2011). Membrane proteins enter the base of the cilium through both vesicular trafficking as well as through lateral diffusion from the cell membrane. A septin ring in the transition zone forms a diffusion barrier at the base of the cilium that restricts access into the ciliary membrane; this is similar to the diffusion barrier found in the nuclear pore (Hu et al., 2010). However, it must be noted that other CLS exist, such as the

conserved AX[S/A]XQ motif found in the third intracellular loop of many ciliary-targeted GPCRs; this sequence is bound directly by the BBSome rather than by importins, and facilitates ciliary entry through a parallel mechanism (Berbari et al., 2008; Jin et al., 2010).

Lipid modifications of soluble proteins or protein domains result in attachment to the plasma membrane and affect sorting into the various cellular compartments. The addition of either a C15 (farnesyl) or a C20 (geranylgeranyl) fatty acid linker through S-prenylation of C-terminal cysteines in a conserved CAAX motif results in attachment to the inner leaflet of the plasma membrane (Fu and Casey, 1999); similarly, N-terminal myristoylation attaches a C14 fatty acid sidechain to N-terminal glycine residues and leads to incorporation in lipid rafts (Gordon et al., 1991). Separately, glycophosphatidylinositol (GPI) anchors can tether the C-terminus end of proteins to the plasma membrane (Low, 1989). Finally, S-palmitoylation of cysteine residues anchors soluble proteins to the plasma membrane via a C16 fatty acid sidechain (Munday and Lopez, 2007). Of these lipid modifications, palmitoylation and myristoylation are often encountered among ciliary proteins, and myristoylation motifs are enriched in ciliary proteins of Chlamydomonas (Pazour et al., 2005). Palmitoylation and myristoylation move proteins into lipid rafts, which are detergent-insoluble, cholesterol-rich microdomains of the plasma membrane; at the same time, prenylation prevents proteins from entering lipid rafts due to the branched bulky structure of the prenyl groups which disfavours the liquid-ordered phase domains of lipid rafts (Melkonian et al., 1999). Interestingly, the ciliary membrane is enriched in sterols, sphingolipids and glycolipids which are constituents of lipid rafts, and contains a high degree of liquid order indicative of lipid raft microdomains (Tyler et al., 2009).

Despite the fact that the CLSs identified to date do not share significant sequence homology to each other, a majority of them incorporate in lipid rafts via palmitoyl and/or myristoyl modifications (for instance fibrocystin, cystin, and calflagin) (Follit et al., 2010; Godsel and Engman, 1999; Tao et al., 2009). Myristoylation addresses proteins without transmembrane domains to the plasma membrane (as in the case of the flagellar calcium-binding protein calflagin in African trypanosomes, (Emmer et al., 2009)) or to the ciliary membrane as in the case of the ciliopathy protein nephrocystin-3 (NPHP3) (Godsel and Engman, 1999; Wright et al., 2011). Several proteins involved in myristoylated protein trafficking localize to the cilium: Unc119 binds myristoylated proteins, while the small GTPase Arf-like 3 (ARL3) along with the Retinitis pigmentosa 2 protein, which acts as the Arl3 GTPase-activating protein (GAP), release myristoylated cargo proteins from Unc119; all three proteins are enriched at the transition zone (Wright et al., 2011). Separately, cysteine residues next to blocks of basic amino acids are targets of palmitoylation (Bijlmakers and Marsh, 2003), and in the case of calflagin, palmitoylation provides a secondary signal that relocates the myristoylated calflagin from the plasma membrane to the ciliary membrane (Emmer et al., 2009). Furthermore, palmitoylation of an 18-aminoacid stretch which was recently identified as the CLS of fibrocystin is essential for correct ciliary targeting (Follit et al., 2010). Mutations that abolish the palmitoylation of certain CLSs also prevent targeting to the primary cilium (Emmer et al., 2009; Follit et al., 2010), and defects in the calflagin palmitoyltransferase TbPAT7 which acylates the CLS of calflagin recapitulate the behaviour of the lipidation-defective mutants (Emmer et al., 2009). This suggests that despite their similarity, the stretches of basic residues of the NLS and those of certain CLSs probably

serve completely different functions – in the case of the NLS they bind importins and facilitate movement through the nuclear pore, whereas in the case of the CLS they serve as palmitoylation signals to link the CLS to lipid membranes. It is conceivable that ciliary targeting depends on partitioning into membrane microdomains or lipid rafts with a unique lipid composition; a precedent along these lines exists – targeting of proteins to the apical membrane in epithelial cells requires the association of cargo targeted to the apical membrane with lipid rafts (Simons and Toomre, 2000).

While myristoylation is a static modification that is generally applied to proteins through a co-translational process, palmitoylation is a reversible modification and palmitoylation–depalmitoylation dynamics can coordinate protein sorting as evidenced by the cycling of the Ras oncogene between the Golgi and the plasma membrane: the cytosolic Ras is palmitoylated at the Golgi membrane and then shuttles on vesicles to the plasma membrane where it is depalmitoylated and recycled to the cytosol through a non-vesicular pathway for another round of palmitoylation; this process ensures a constant supply of Ras at the plasma membrane, while at the same time maintains a high turnover rate of Ras at the plasma membrane that prevents it from accidentally entering other membrane compartments in the cell (Goodwin et al., 2005). Regulated trafficking to the cilium may involve a similar dynamic mechanism.

1.8 Hedgehog signaling at the primary cilium

The spatial localization of the Hedgehog pathway components in vertebrates provides an additional layer of regulation, as primary cilia are essential for transduction of the Hedgehog

signal across the membrane (Huangfu and Anderson, 2005). This section will review the Hh signaling in vertebrates in the context of the primary cilium, and will highlight the key differences between the regulation of the Hh pathway in flies and in vertebrates.

In the absence of signal, Smo appears primarily in intracellular vesicles, while Ptc localizes to the base of the primary cilium. Upon activation by Shh, Ptc is internalized which allows Smo to accumulate at the primary cilium where the intracellular components of the Hh signaling pathway reside, to physically associate with the ciliary protein Evc2, and to activate downstream signaling; Smo also localizes to the cilium when overexpressed (Dorn et al., 2012; Rohatgi et al., 2007; Singla and Reiter, 2006). Smo translocates to the primary cilium primarily through lateral movement from the plasma membrane (Milenkovic et al., 2009). However, the ciliary localization sequences of Ptc or Smo are not known.

In vertebrates, the major negative hedgehog pathway regulator SuFu inhibits Gli proteins in the cytosol by forming a complex with them. Upon pathway activation at the level of Ptc or Smo, the SuFu-Gli complexes travel to the primary cilium, where the activated Smo triggers their rapid dissociation; the liberated full-length Gli (the unproteolysed activator form, Gli-A) then enters the nucleus and starts transcribing the Hh target genes. Pharmacologic activation of protein kinase A (PKA) by forskolin uncouples Smo activation from the SuFu-Gli complex dissociation, inhibits ciliary entry of the SuFu-Gli complex and prohibits the derepression of Gli. Furthermore, the loss of SuFu triggers maximal pathway response, and these cells do not require cilia for signaling, providing further evidence that the net result of the ciliary steps of the Hedgehog pathway is the liberation of full-length Gli (Svard et al., 2006; Tukachinsky et al.,

2010). In contrast, Drosophila cells lack a primary cilium, which explains the divergent signaling mechanism downstream of Smo through Costal2 in the cytosol, and the relatively minor role of Su(fu) as a negative regulator in flies (Svard et al., 2006).

Knockout of the negative regulators Ptc and Sufu leads to constitutive pathway activity, which results in ventralization of the neural tube, polydactyly and inverted cardiac looping in the embryo. Ectopic activation of the Hedgehog pathway directly causes a number of tumors in humans including sporadic medulloblastoma, a common but devastating childhood brain tumor; mouse knockout models recapitulate these tumors (Goodrich et al., 1997; Svard et al., 2006). Furthermore, reactivation of the Hh pathway is observed in a variety of cancers as they metastasize and enhances their metastatic potential (Yoo et al., 2011).

Several IFT proteins have been implicated in Hedgehog signaling. IFT172 and IFT88 are present in the same IFT-B complex and are essential for ciliogenesis; both proteins are required for normal activation of the Hh pathway and for establishing correct left-right asymmetry in the developing embryo. Mice lacking IFT172 or IFT88 have an open neural tube that lacks the groove normally observed on the ventral midline, as well as random looping of the heart tube, and die in utero at E10.5-13.5; this phenotype is characteristic for defects in Hh signaling, and loss of IFT172 prevents processing of Gli3 to the repressor form which results in a higher basal transcriptional level of Hh target genes (Huangfu and Anderson, 2005; Huangfu et al., 2003). The mouse Kif3a is an essential subunit of the kinesin-II anterograde IFT motor, while Dnchc2 is an essential subunit of the retrograde IFT motor complex. Defects in Kif3a result in a failure of ciliary assembly and blocks hedgehog signaling (Ko et al., 2009). Loss of either Kif3a or Dnchc2

results in lack of ventral neural types, which is similar to the loss of IFT172 and IFT88 (Huangfu and Anderson, 2005; Huangfu et al., 2003). Interestingly, the loss of IFT88 or Kif3a homologs in Drosophila does not impair Hh signaling; this is in line with the divergent signal transduction mechanism downstream of Smo in Drosophila, which does not involve the primary cilium (Han et al., 2003; Ray et al., 1999).

A different set of IFT-B proteins, IFT25 and IFT27 form a binary complex that is conserved throughout vertebrates but is missing in Drosophila. The IFT25-IFT27 complex is not required for ciliogenesis, but appears essential for transduction of the Hh signal in vertebrates; the loss of IFT25 leads to mislocalization of Ptc, Smo and Gli2 at the cilium and disrupts the Hh pathway response upon stimulation. In these animals, Gli2 does not accumulate at the cilium in response to signaling, while Patched and Smo are constitutively localized at the cilium regardless of the presence or absence of the Hh ligand. Interestingly, the cilia of these animals appear morphologically normal, and also show normal localization as well as normal amounts of other IFT proteins such as IFT88; the animals survive to birth but show severe abnormalities indicative of Hh signaling defects: cleft palate, incorrect alignment of the sternal vertebrae, and polydactyly (Keady et al., 2012). Thus, rather than facilitating transport to the primary cilium, the IFT25-IFT27 complex enables the dynamic redistribution of Hh pathway components in response to signaling. Furthermore, this dynamic is critical to establishing the correct enrichment of pathway components in the cilium versus the rest of the cell in both the OFF state (Ptc at cilium, Smo and Gli2 outside the cilium) and the ON state (Ptc outside the cilium, Smo at the cilium and Gli2 accumulated at the tip of the cilium and in the nucleus) of the Hh pathway.

Any ciliary-bound protein must cross through the ciliary transition zone in order to reach the axoneme. Multiple ciliopathy proteins reside at the transition zone and are involved in ciliary assembly and trafficking; this includes proteins whose defects result in human ciliopathies such as Meckel syndrome (MKS), Joubert syndrome and Nephronophthisis (NPHP) (Garcia-Gonzalo et al., 2011). Interestingly, while the disease phenotypes are different, the molecular aetiologies of the different ciliopathies overlap. For instance, the defining features of MKS are occipital encephalocele, kidney cysts and polydactyly, while JBTS patients show primarily brainstem and cerebellar malformations; however, mutations in a subset of six genes originally identified in MKS such as CEP290 can cause JBTS or a related ciliopathy, COACH (short for cerebellar vermis hypoplasia, oligophrenia, ataxia, coloboma and hepatic fibrosis) (Garcia-Gonzalo et al., 2011). Of particular relevance is the JBTS protein Tectonic (Tctn1), as it is a modulator of Hh signaling and acts at a level downstream of Smo (Reiter and Skarnes, 2006). Tctn1 is required for ciliogenesis in a tissue-specific manner and forms a transition zone complex with other MKS and JBTS proteins that includes membrane components as well as the two other vertebrate homologs of Tctn1 – Tctn2 and Tctn3 (Garcia-Gonzalo et al., 2011). $Tctn1^{-/-}$ mice die in-utero at E13.5-E16.5, and show morphological defects such as holoprosencephaly which are indicative of impaired Hedgehog signaling in the neural floorplate (Reiter and Skarnes, 2006). Loss of Tctn1 blocks the transition zone localization of the proteins Mks1 and Tmem67, but does not affect the localization of Septin2 or of the IFT-A, IFT-B or BBSome complexes. This suggests that the action of Tctn1 is required at the transition zone. Intriguingly, Tctn1 acts as both a positive as well as a negative regulator on the Hedgehog pathway. This can be explained by the role of cilia

in the partial proteolytic processing of Gli to the Gli-R repressor form, as well as by the role of cilia in the dissociation of the SuFu-Gli complex and the release of the full-length Gli-A activator form from the inhibitory effect of SuFu. In the absence of Tctn1, neither of these processes occurs; the net effect is a combination of the reduced function of both Gli-A and Gli-R. What the role of Tctn1 is in the context of the ciliary transition zone, and whether the Tctn1-containing complex interacts with the SuFu-Gli complex is not clear.

1.9 Aims of this dissertation

Over the last three decades, genetics studies in model organisms such as flies, fish, mice and chick have made great progress in identifying the Hedgehog pathway components. However, a mechanistic understanding of various key aspects remains lacking. In this dissertation I describe experiments both in-vitro and in the tissue culture system that were used to answer several mechanistic questions.

In Chapter 2 I show that oxysterols which potently activate Hedgehog signaling bind Smo at a site in the extracellular, cysteine-rich domain which is distinct from the site bound by cyclopamine and the other small molecule Smo modulators. I describe azasterols that block Hedgehog signaling by inhibiting the oxysterol-binding site of Smo. My results show that oxysterol binding to vertebrate Smoothened is required for high-level Hedgehog signaling, and that targeting the oxysterol binding site is an effective strategy to block Smoothened activity.

In Chapter 3 I explore the mechanism of ciliary localization of Smo. I map the ciliary localization domain to the cytosolic tail of Smo and identify two degenerate ciliary localization

sequences within its cytosolic tail. I further identify a cytosolic domain of Smo, which is essential but not sufficient for activation of downstream components. Finally, I show that while the ciliary localization aspect is unique to vertebrates, signaling to downstream components is conserved across phyla.

In Chapter 4 I discuss the significance of my findings and suggest future experiments to address the open questions raised by my work. My findings indicate that Smo is a modular protein, wherein each module serves a specific role and reflects a distinct mechanism of regulation. This suggests a model wherein Smo is at the confluence of several distinct regulatory inputs: an oxysterol regulated module, a second small-molecule regulated module, and a ciliary localization module, as well as a module for downstream signalling – which all converge for maximal activation.

1.10 References

Allen, B.L., J.Y. Song, L. Izzi, I.W. Althaus, J.S. Kang, F. Charron, R.S. Krauss, and A.P. McMahon. 2011. Overlapping roles and collective requirement for the coreceptors GAS1, CDO, and BOC in SHH pathway function. *Dev Cell*. 20:775-787.

Anderson, R.G. 1972. The three-dimensional structure of the basal body from the rhesus monkey oviduct. *J Cell Biol*. 54:246-265.

Angers, S., and R.T. Moon. 2009. Proximal events in Wnt signal transduction. *Nat Rev Mol Cell Biol*. 10:468-477.

Bai, C.B., W. Auerbach, J.S. Lee, D. Stephen, and A.L. Joyner. 2002. Gli2, but not Gli1, is required for initial Shh signaling and ectopic activation of the Shh pathway. *Development*. 129:4753-4761.

Beachy, P.A., S.S. Karhadkar, and D.M. Berman. 2004. Tissue repair and stem cell renewal in carcinogenesis. *Nature*. 432:324-331.

Berbari, N.F., A.D. Johnson, J.S. Lewis, C.C. Askwith, and K. Mykytyn. 2008. Identification of ciliary localization sequences within the third intracellular loop of G protein-coupled receptors. *Mol Biol Cell*. 19:1540-1547.

Bhanot, P., M. Brink, C.H. Samos, J.C. Hsieh, Y. Wang, J.P. Macke, D. Andrew, J. Nathans, and R. Nusse. 1996. A new member of the frizzled family from Drosophila functions as a Wingless receptor. *Nature*. 382:225-230.

Bijlmakers, M.J., and M. Marsh. 2003. The on-off story of protein palmitoylation. *Trends Cell Biol*. 13:32-42.

Bjorkhem, I. 2007. Rediscovery of cerebrosterol. *Lipids*. 42:5-14.

Bokor, P., and S. DiNardo. 1996. The roles of hedgehog, wingless and lines in patterning the dorsal epidermis in Drosophila. *Development*. 122:1083-1092.

Brunner, E., O. Peter, L. Schweizer, and K. Basler. 1997. pangolin encodes a Lef-1 homologue that acts downstream of Armadillo to transduce the Wingless signal in Drosophila. *Nature*. 385:829-833.

Chen, J.K., J. Taipale, M.K. Cooper, and P.A. Beachy. 2002a. Inhibition of Hedgehog signaling by direct binding of cyclopamine to Smoothened. *Genes Dev*. 16:2743-2748.

Chen, J.K., J. Taipale, K.E. Young, T. Maiti, and P.A. Beachy. 2002b. Small molecule modulation of Smoothened activity. *Proc Natl Acad Sci U S A*. 99:14071-14076.

Chen, W., X.R. Ren, C.D. Nelson, L.S. Barak, J.K. Chen, P.A. Beachy, F. de Sauvage, and R.J. Lefkowitz. 2004. Activity-dependent internalization of smoothened mediated by beta-arrestin 2 and GRK2. *Science*. 306:2257-2260.

Cheruku, S.R., Z. Xu, R. Dutia, P. Lobel, and J. Storch. 2006. Mechanism of cholesterol transfer from the Niemann-Pick type C2 protein to model membranes supports a role in lysosomal cholesterol transport. *J Biol Chem*. 281:31594-31604.

Chiang, C., Y. Litingtung, E. Lee, K.E. Young, J.L. Corden, H. Westphal, and P.A. Beachy. 1996. Cyclopia and defective axial patterning in mice lacking Sonic hedgehog gene function. *Nature*. 383:407-413.

Chih, B., P. Liu, Y. Chinn, C. Chalouni, L.G. Komuves, P.E. Hass, W. Sandoval, and A.S. Peterson. 2012. A ciliopathy complex at the transition zone protects the cilia as a privileged membrane domain. *Nat Cell Biol*. 14:61-72.

Cooper, A.F., K.P. Yu, M. Brueckner, L.L. Brailey, L. Johnson, J.M. McGrath, and A.E. Bale. 2005. Cardiac and CNS defects in a mouse with targeted disruption of suppressor of fused. *Development*. 132:4407-4417.

Cooper, M.K., C.A. Wassif, P.A. Krakowiak, J. Taipale, R. Gong, R.I. Kelley, F.D. Porter, and P.A. Beachy. 2003. A defective response to Hedgehog signaling in disorders of cholesterol biosynthesis. *Nature genetics*. 33:508-513.

Corcoran, R.B., and M.P. Scott. 2006. Oxysterols stimulate Sonic hedgehog signal transduction and proliferation of medulloblastoma cells. *Proc Natl Acad Sci USA*. 103:8408-8413.

Counsell, R.E., M.C. Lu, S. el-Masry, and P.A. Weinhold. 1971. Inhibition of cholesterol side-chain cleavage by azacholesterols. *Biochem Pharmacol*. 20:2912-2915.

Couso, J.P., S.A. Bishop, and A. Martinez Arias. 1994. The wingless signalling pathway and the patterning of the wing margin in Drosophila. *Development*. 120:621-636.

Dai, P., H. Akimaru, Y. Tanaka, T. Maekawa, M. Nakafuku, and S. Ishii. 1999. Sonic Hedgehog-induced activation of the Gli1 promoter is mediated by GLI3. *J Biol Chem*. 274:8143-8152.

Davies, J.P., F.W. Chen, and Y.A. Ioannou. 2000. Transmembrane molecular pump activity of Niemann-Pick C1 protein. *Science*. 290:2295-2298.

DeCamp, D.L., T.M. Thompson, F.J. de Sauvage, and M.R. Lerner. 2000. Smoothened activates Galphai-mediated signaling in frog melanophores. *J Biol Chem*. 275:26322-26327.

Denef, N., D. Neubuser, L. Perez, and S.M. Cohen. 2000. Hedgehog induces opposite changes in turnover and subcellular localization of patched and smoothened. *Cell*. 102:521-531.

Ding, Q., J. Motoyama, S. Gasca, R. Mo, H. Sasaki, J. Rossant, and C.C. Hui. 1998. Diminished Sonic hedgehog signaling and lack of floor plate differentiation in Gli2 mutant mice. *Development*. 125:2533-2543.

Dingus, J., B.S. Tatum, G. Vaidyanathan, and J.D. Hilderbrandt. 2002. Purification of G protein beta gamma from bovine brain. *Methods Enzymol*. 344:194-208.

Dishinger, J.F., H.L. Kee, P.M. Jenkins, S. Fan, T.W. Hurd, J.W. Hammond, Y.N. Truong, B. Margolis, J.R. Martens, and K.J. Verhey. 2010. Ciliary entry of the kinesin-2 motor KIF17 is regulated by importin-beta2 and RanGTP. *Nat Cell Biol*. 12:703-710.

Dorn, K.V., C.E. Hughes, and R. Rohatgi. 2012. A Smoothened-Evc2 complex transduces the Hedgehog signal at primary cilia. *Dev Cell*. 23:823-835.

Dubey, A.K., S. Dubey, S.S. Handu, and M.A. Qazi. 2013. Vismodegib: the first drug approved for advanced and metastatic basal cell carcinoma. *Journal of postgraduate medicine*. 59:48-50.

Dwyer, J.R., N. Sever, M. Carlson, S.F. Nelson, P.A. Beachy, and F. Parhami. 2007. Oxysterols are novel activators of the hedgehog signaling pathway in pluripotent mesenchymal cells. *J Biol Chem*. 282:8959-8968.

Dwyer, N.D., C.E. Adler, J.G. Crump, N.D. L'Etoile, and C.I. Bargmann. 2001. Polarized dendritic transport and the AP-1 mu1 clathrin adaptor UNC-101 localize odorant receptors to olfactory cilia. *Neuron*. 31:277-287.

Emmer, B.T., C. Souther, K.M. Toriello, C.L. Olson, C.L. Epting, and D.M. Engman. 2009. Identification of a palmitoyl acyltransferase required for protein sorting to the flagellar membrane. *J Cell Sci*. 122:867-874.

Endoh-Yamagami, S., M. Evangelista, D. Wilson, X. Wen, J.W. Theunissen, K. Phamluong, M. Davis, S.J. Scales, M.J. Solloway, F.J. de Sauvage, and A.S. Peterson. 2009. The mammalian Cos2 homolog Kif7 plays an essential role in modulating Hh signal transduction during development. *Current biology : CB*. 19:1320-1326.

Faini, M., R. Beck, F.T. Wieland, and J.A. Briggs. 2013. Vesicle coats: structure, function, and general principles of assembly. *Trends Cell Biol*. 23:279-288.

Fakheri, R.J., and N.B. Javitt. 2011. Autoregulation of cholesterol synthesis: physiologic and pathophysiologic consequences. *Steroids*. 76:211-215.

Fan, C.M., and M. Tessier-Lavigne. 1994. Patterning of mammalian somites by surface ectoderm and notochord: evidence for sclerotome induction by a hedgehog homolog. *Cell*. 79:1175-1186.

Fan, S., and B. Margolis. 2011. The Ran importin system in cilia trafficking. *Organogenesis*. 7:147-153.

Folkman, J. 2002. Role of angiogenesis in tumor growth and metastasis. *Semin Oncol*. 29:15-18.

Follit, J.A., L. Li, Y. Vucica, and G.J. Pazour. 2010. The cytoplasmic tail of fibrocystin contains a ciliary targeting sequence. *J Cell Biol*. 188:21-28.

Follit, J.A., R.A. Tuft, K.E. Fogarty, and G.J. Pazour. 2006. The intraflagellar transport protein IFT20 is associated with the Golgi complex and is required for cilia assembly. *Mol Biol Cell*. 17:3781-3792.

Fu, H.W., and P.J. Casey. 1999. Enzymology and biology of CaaX protein prenylation. *Recent Prog Horm Res*. 54:315-342; discussion 342-313.

Garcia-Gonzalo, F.R., K.C. Corbit, M.S. Sirerol-Piquer, G. Ramaswami, E.A. Otto, T.R. Noriega, A.D. Seol, J.F. Robinson, C.L. Bennett, D.J. Josifova, J.M. Garcia-Verdugo, N. Katsanis, F. Hildebrandt, and J.F. Reiter. 2011. A transition zone complex regulates mammalian ciliogenesis and ciliary membrane composition. *Nature genetics*. 43:776-784.

Gehring, W.J. 2012. The animal body plan, the prototypic body segment, and eye evolution. *Evol Dev*. 14:34-46.

Gil, G., J.R. Faust, D.J. Chin, J.L. Goldstein, and M.S. Brown. 1985. Membrane-bound domain of HMG CoA reductase is required for sterol-enhanced degradation of the enzyme. *Cell*. 41:249-258.

Gill, S., R. Chow, and A.J. Brown. 2008. Sterol regulators of cholesterol homeostasis and beyond: the oxysterol hypothesis revisited and revised. *Prog Lipid Res*. 47:391-404.

Godsel, L.M., and D.M. Engman. 1999. Flagellar protein localization mediated by a calcium-myristoyl/palmitoyl switch mechanism. *EMBO J*. 18:2057-2065.

Goodrich, L.V., L. Milenkovic, K.M. Higgins, and M.P. Scott. 1997. Altered neural cell fates and medulloblastoma in mouse patched mutants. *Science*. 277:1109-1113.
Goodwin, J.S., K.R. Drake, C. Rogers, L. Wright, J. Lippincott-Schwartz, M.R. Philips, and A.K. Kenworthy. 2005. Depalmitoylated Ras traffics to and from the Golgi complex via a nonvesicular pathway. *J Cell Biol*. 170:261-272.
Gordon, J.I., R.J. Duronio, D.A. Rudnick, S.P. Adams, and G.W. Gokel. 1991. Protein N-myristoylation. *J Biol Chem*. 266:8647-8650.
Han, Y.G., B.H. Kwok, and M.J. Kernan. 2003. Intraflagellar transport is required in Drosophila to differentiate sensory cilia but not sperm. *Current biology : CB*. 13:1679-1686.
Hooper, J.E. 2003. Smoothened translates Hedgehog levels into distinct responses. *Development*. 130:3951-3963.
Hooper, J.E., and M.P. Scott. 2005. Communicating with Hedgehogs. *Nat Rev Mol Cell Biol*. 6:306-317.
Hu, Q., L. Milenkovic, H. Jin, M.P. Scott, M.V. Nachury, E.T. Spiliotis, and W.J. Nelson. 2010. A septin diffusion barrier at the base of the primary cilium maintains ciliary membrane protein distribution. *Science*. 329:436-439.
Huangfu, D., and K.V. Anderson. 2005. Cilia and Hedgehog responsiveness in the mouse. *Proc Natl Acad Sci USA*. 102:11325-11330.
Huangfu, D., A. Liu, A.S. Rakeman, N.S. Murcia, L. Niswander, and K.V. Anderson. 2003. Hedgehog signalling in the mouse requires intraflagellar transport proteins. *Nature*. 426:83-87.
Infante, R.E., L. Abi-Mosleh, A. Radhakrishnan, J.D. Dale, M.S. Brown, and J.L. Goldstein. 2008a. Purified NPC1 protein. I. Binding of cholesterol and oxysterols to a 1278-amino acid membrane protein. *J Biol Chem*. 283:1052-1063.
Infante, R.E., A. Radhakrishnan, L. Abi-Mosleh, L.N. Kinch, M.L. Wang, N.V. Grishin, J.L. Goldstein, and M.S. Brown. 2008b. Purified NPC1 protein: II. Localization of sterol binding to a 240-amino acid soluble luminal loop. *J Biol Chem*. 283:1064-1075.
Infante, R.E., M.L. Wang, A. Radhakrishnan, H.J. Kwon, M.S. Brown, and J.L. Goldstein. 2008c. NPC2 facilitates bidirectional transfer of cholesterol between NPC1 and lipid bilayers, a step in cholesterol egress from lysosomes. *Proc Natl Acad Sci U S A*. 105:15287-15292.
Ingham, P.W., and A.P. McMahon. 2001. Hedgehog signaling in animal development: paradigms and principles. *Genes Dev*. 15:3059-3087.
Izzi, L., M. Levesque, S. Morin, D. Laniel, B.C. Wilkes, F. Mille, R.S. Krauss, A.P. McMahon, B.L. Allen, and F. Charron. 2011. Boc and Gas1 each form distinct Shh receptor complexes with Ptch1 and are required for Shh-mediated cell proliferation. *Dev Cell*. 20:788-801.
Janda, C.Y., D. Waghray, A.M. Levin, C. Thomas, and K.C. Garcia. 2012. Structural basis of Wnt recognition by Frizzled. *Science*. 337:59-64.
Javitt, N.B. 2002a. 25R,26-Hydroxycholesterol revisited: synthesis, metabolism, and biologic roles. *J Lipid Res*. 43:665-670.

Javitt, N.B. 2002b. Cholesterol, hydroxycholesterols, and bile acids. *Biochem Biophys Res Commun*. 292:1147-1153.
Jessell, T.M. 2000. Neuronal specification in the spinal cord: inductive signals and transcriptional codes. *Nat Rev Genet*. 1:20-29.
Jin, H., S.R. White, T. Shida, S. Schulz, M. Aguiar, S.P. Gygi, J.F. Bazan, and M.V. Nachury. 2010. The conserved Bardet-Biedl syndrome proteins assemble a coat that traffics membrane proteins to cilia. *Cell*. 141:1208-1219.
Johnson, R.L., R.D. Riddle, and C.J. Tabin. 1994. Mechanisms of limb patterning. *Curr Opin Genet Dev*. 4:535-542.
Jones, E.A., M.I. Sajid, A. Shenton, and D.G. Evans. 2011. Basal cell carcinomas in gorlin syndrome: a review of 202 patients. *J Skin Cancer*. 2011:217378.
Kaesler, S., B. Luscher, and U. Ruther. 2000. Transcriptional activity of GLI1 is negatively regulated by protein kinase A. *Biol Chem*. 381:545-551.
Katanaev, V.L., R. Ponzielli, M. Semeriva, and A. Tomlinson. 2005. Trimeric G protein-dependent frizzled signaling in Drosophila. *Cell*. 120:111-122.
Keady, B.T., Y.Z. Le, and G.J. Pazour. 2011. IFT20 is required for opsin trafficking and photoreceptor outer segment development. *Mol Biol Cell*. 22:921-930.
Keady, B.T., R. Samtani, K. Tobita, M. Tsuchya, J.T. San Agustin, J.A. Follit, J.A. Jonassen, R. Subramanian, C.W. Lo, and G.J. Pazour. 2012. IFT25 links the signal-dependent movement of Hedgehog components to intraflagellar transport. *Dev Cell*. 22:940-951.
Kee, H.L., J.F. Dishinger, T.L. Blasius, C.J. Liu, B. Margolis, and K.J. Verhey. 2012. A size-exclusion permeability barrier and nucleoporins characterize a ciliary pore complex that regulates transport into cilia. *Nat Cell Biol*. 14:431-437.
Kim, P.C., R. Mo, and C. Hui Cc. 2001. Murine models of VACTERL syndrome: Role of sonic hedgehog signaling pathway. *J Pediatr Surg*. 36:381-384.
Ko, H.W., A. Liu, and J.T. Eggenschwiler. 2009. Analysis of hedgehog signaling in mouse intraflagellar transport mutants. *Methods Cell Biol*. 93:347-369.
Kusano, K.F., R. Pola, T. Murayama, C. Curry, A. Kawamoto, A. Iwakura, S. Shintani, M. Ii, J. Asai, T. Tkebuchava, T. Thorne, H. Takenaka, R. Aikawa, D. Goukassian, P. von Samson, H. Hamada, Y.S. Yoon, M. Silver, E. Eaton, H. Ma, L. Heyd, M. Kearney, W. Munger, J.A. Porter, R. Kishore, and D.W. Losordo. 2005. Sonic hedgehog myocardial gene therapy: tissue repair through transient reconstitution of embryonic signaling. *Nat Med*. 11:1197-1204.
Lee, Y., H.L. Miller, H.R. Russell, K. Boyd, T. Curran, and P.J. McKinnon. 2006. Patched2 modulates tumorigenesis in patched1 heterozygous mice. *Cancer Res*. 66:6964-6971.
Liem, K.F., Jr., M. He, P.J. Ocbina, and K.V. Anderson. 2009. Mouse Kif7/Costal2 is a cilia-associated protein that regulates Sonic hedgehog signaling. *Proc Natl Acad Sci U S A*. 106:13377-13382.
Lin, Y.Y., M. Welch, and S. Lieberman. 2003. The detection of 20S-hydroxycholesterol in extracts of rat brains and human placenta by a gas chromatograph/mass spectrometry technique. *J Steroid Biochem Mol Biol*. 85:57-61.

Low, M.G. 1989. The glycosyl-phosphatidylinositol anchor of membrane proteins. *Biochim Biophys Acta*. 988:427-454.
Lu, X., S. Liu, and T.B. Kornberg. 2006. The C-terminal tail of the Hedgehog receptor Patched regulates both localization and turnover. *Genes Dev*. 20:2539-2551.
Lund, E.G., T.A. Kerr, J. Sakai, W.P. Li, and D.W. Russell. 1998. cDNA cloning of mouse and human cholesterol 25-hydroxylases, polytopic membrane proteins that synthesize a potent oxysterol regulator of lipid metabolism. *J Biol Chem*. 273:34316-34327.
Macara, I.G. 2001. Transport into and out of the nucleus. *Microbiol Mol Biol Rev*. 65:570-594, table of contents.
Marigo, V., and C.J. Tabin. 1996. Regulation of patched by sonic hedgehog in the developing neural tube. *Proc Natl Acad Sci U S A*. 93:9346-9351.
Martin, V., G. Carrillo, C. Torroja, and I. Guerrero. 2001. The sterol-sensing domain of Patched protein seems to control Smoothened activity through Patched vesicular trafficking. *Current biology : CB*. 11:601-607.
Mas, C., and A. Ruiz i Altaba. 2010. Small molecule modulation of HH-GLI signaling: current leads, trials and tribulations. *Biochem Pharmacol*. 80:712-723.
Melkonian, K.A., A.G. Ostermeyer, J.Z. Chen, M.G. Roth, and D.A. Brown. 1999. Role of lipid modifications in targeting proteins to detergent-resistant membrane rafts. Many raft proteins are acylated, while few are prenylated. *J Biol Chem*. 274:3910-3917.
Miao, E., S. Joardar, C. Zuo, N.J. Cloutier, A. Nagahisa, C. Byon, S.R. Wilson, and W.H. Orme-Johnson. 1995. Cytochrome P-450scc-mediated oxidation of (20S)-22-thiacholesterol: characterization of mechanism-based inhibition. *Biochemistry*. 34:8415-8421.
Milenkovic, L., M.P. Scott, and R. Rohatgi. 2009. Lateral transport of Smoothened from the plasma membrane to the membrane of the cilium. *J Cell Biol*. 187:365-374.
Montesano, R. 1979. Inhomogeneous distribution of filipin-sterol complexes in the ciliary membrane of rat tracheal epithelium. *Am J Anat*. 156:139-145.
Motamed, M., Y. Zhang, M.L. Wang, J. Seemann, H.J. Kwon, J.L. Goldstein, and M.S. Brown. 2011. Identification of luminal Loop 1 of Scap protein as the sterol sensor that maintains cholesterol homeostasis. *J Biol Chem*. 286:18002-18012.
Munday, A.D., and J.A. Lopez. 2007. Posttranslational protein palmitoylation: promoting platelet purpose. *Arterioscler Thromb Vasc Biol*. 27:1496-1499.
Nachtergaele, S., L.K. Mydock, K. Krishnan, J. Rammohan, P.H. Schlesinger, D.F. Covey, and R. Rohatgi. 2012. Oxysterols are allosteric activators of the oncoprotein Smoothened. *Nat Chem Biol*. 8:211-220.
Nachury, M.V., E.S. Seeley, and H. Jin. 2010. Trafficking to the ciliary membrane: how to get across the periciliary diffusion barrier? *Annu Rev Cell Dev Biol*. 26:59-87.
Nichols, A.S., D.H. Floyd, S.P. Bruinsma, K. Narzinski, and T.J. Baranski. 2013. Frizzled receptors signal through G proteins. *Cell Signal*. 25:1468-1475.
Ou, G., O.E. Blacque, J.J. Snow, M.R. Leroux, and J.M. Scholey. 2005. Functional coordination of intraflagellar transport motors. *Nature*. 436:583-587.

Pan, Y., C.B. Bai, A.L. Joyner, and B. Wang. 2006. Sonic hedgehog signaling regulates Gli2 transcriptional activity by suppressing its processing and degradation. *Mol Cell Biol*. 26:3365-3377.

Park, H.L., C. Bai, K.A. Platt, M.P. Matise, A. Beeghly, C.C. Hui, M. Nakashima, and A.L. Joyner. 2000. Mouse Gli1 mutants are viable but have defects in SHH signaling in combination with a Gli2 mutation. *Development*. 127:1593-1605.

Pazour, G.J., N. Agrin, J. Leszyk, and G.B. Witman. 2005. Proteomic analysis of a eukaryotic cilium. *J Cell Biol*. 170:103-113.

Persson, M., D. Stamataki, P. te Welscher, E. Andersson, J. Bose, U. Ruther, J. Ericson, and J. Briscoe. 2002. Dorsal-ventral patterning of the spinal cord requires Gli3 transcriptional repressor activity. *Genes Dev*. 16:2865-2878.

Pola, R., L.E. Ling, M. Silver, M.J. Corbley, M. Kearney, R. Blake Pepinsky, R. Shapiro, F.R. Taylor, D.P. Baker, T. Asahara, and J.M. Isner. 2001. The morphogen Sonic hedgehog is an indirect angiogenic agent upregulating two families of angiogenic growth factors. *Nat Med*. 7:706-711.

Polizio, A.H., P. Chinchilla, X. Chen, S. Kim, D.R. Manning, and N.A. Riobo. 2011. Heterotrimeric Gi proteins link Hedgehog signaling to activation of Rho small GTPases to promote fibroblast migration. *J Biol Chem*. 286:19589-19596.

Radhakrishnan, A., Y. Ikeda, H.J. Kwon, M.S. Brown, and J.L. Goldstein. 2007. Sterol-regulated transport of SREBPs from endoplasmic reticulum to Golgi: oxysterols block transport by binding to Insig. *Proc Natl Acad Sci U S A*. 104:6511-6518.

Rawson, R.B. 2003. Control of lipid metabolism by regulated intramembrane proteolysis of sterol regulatory element binding proteins (SREBPs). *Biochem Soc Symp*:221-231.

Ray, K., S.E. Perez, Z. Yang, J. Xu, B.W. Ritchings, H. Steller, and L.S. Goldstein. 1999. Kinesin-II is required for axonal transport of choline acetyltransferase in Drosophila. *J Cell Biol*. 147:507-518.

Reiter, J.F., and W.C. Skarnes. 2006. Tectonic, a novel regulator of the Hedgehog pathway required for both activation and inhibition. *Genes Dev*. 20:22-27.

Riobo, N.A., B. Saucy, C. Dilizio, and D.R. Manning. 2006. Activation of heterotrimeric G proteins by Smoothened. *Proc Natl Acad Sci USA*. 103:12607-12612.

Robarge, K.D., S.A. Brunton, G.M. Castanedo, Y. Cui, M.S. Dina, R. Goldsmith, S.E. Gould, O. Guichert, J.L. Gunzner, J. Halladay, W. Jia, C. Khojasteh, M.F. Koehler, K. Kotkow, H. La, R.L. Lalonde, K. Lau, L. Lee, D. Marshall, J.C. Marsters, Jr., L.J. Murray, C. Qian, L.L. Rubin, L. Salphati, M.S. Stanley, J.H. Stibbard, D.P. Sutherlin, S. Ubhayaker, S. Wang, S. Wong, and M. Xie. 2009. GDC-0449-a potent inhibitor of the hedgehog pathway. *Bioorg Med Chem Lett*. 19:5576-5581.

Rohatgi, R., L. Milenkovic, and M.P. Scott. 2007. Patched1 regulates hedgehog signaling at the primary cilium. *Science*. 317:372-376.

Rohatgi, R., and M.P. Scott. 2007. Patching the gaps in Hedgehog signalling. *Nat Cell Biol*. 9:1005-1009.

Rohatgi, R., and W.J. Snell. 2010. The ciliary membrane. *Curr Opin Cell Biol*. 22:541-546.

Rominger, C.M., W.L. Bee, R.A. Copeland, E.A. Davenport, A. Gilmartin, R. Gontarek, K.R. Hornberger, L.A. Kallal, Z. Lai, K. Lawrie, Q. Lu, L. McMillan, M. Truong, P.J. Tummino, B. Turunen, M. Will, W.J. Zuercher, and D.H. Rominger. 2009. Evidence for allosteric interactions of antagonist binding to the smoothened receptor. *J Pharmacol Exp Ther*. 329:995-1005.

Rubin, L.L., and F.J. de Sauvage. 2006. Targeting the Hedgehog pathway in cancer. *Nat Rev Drug Discov*. 5:1026-1033.

Sandhiya, S., G. Melvin, S.S. Kumar, and S.A. Dkhar. 2013. The dawn of hedgehog inhibitors: Vismodegib. *J Pharmacol Pharmacother*. 4:4-7.

Scholtz, J.R. 1961. A new corticoid for topical therapy. Fluocinolone acetonide. *California medicine*. 95:224-226.

Sever, N., T. Yang, M.S. Brown, J.L. Goldstein, and R.A. DeBose-Boyd. 2003. Accelerated degradation of HMG CoA reductase mediated by binding of insig-1 to its sterol-sensing domain. *Mol Cell*. 11:25-33.

Simons, K., and D. Toomre. 2000. Lipid rafts and signal transduction. *Nat Rev Mol Cell Biol*. 1:31-39.

Singla, V., and J.F. Reiter. 2006. The primary cilium as the cell's antenna: signaling at a sensory organelle. *Science*. 313:629-633.

Smrcka, A.V. 2008. G protein betagamma subunits: central mediators of G protein-coupled receptor signaling. *Cell Mol Life Sci*. 65:2191-2214.

Stewart, M. 2007. Molecular mechanism of the nuclear protein import cycle. *Nat Rev Mol Cell Biol*. 8:195-208.

Stone, D.M., M. Hynes, M. Armanini, T.A. Swanson, Q. Gu, R.L. Johnson, M.P. Scott, D. Pennica, A. Goddard, H. Phillips, M. Noll, J.E. Hooper, F. de Sauvage, and A. Rosenthal. 1996. The tumour-suppressor gene patched encodes a candidate receptor for Sonic hedgehog. *Nature*. 384:129-134.

Strutt, H., C. Thomas, Y. Nakano, D. Stark, B. Neave, A.M. Taylor, and P.W. Ingham. 2001. Mutations in the sterol-sensing domain of Patched suggest a role for vesicular trafficking in Smoothened regulation. *Current biology : CB*. 11:608-613.

Svard, J., K. Heby-Henricson, M. Persson-Lek, B. Rozell, M. Lauth, A. Bergstrom, J. Ericson, R. Toftgard, and S. Teglund. 2006. Genetic elimination of Suppressor of fused reveals an essential repressor function in the mammalian Hedgehog signaling pathway. *Dev Cell*. 10:187-197.

Taipale, J., J.K. Chen, M.K. Cooper, B. Wang, R.K. Mann, L. Milenkovic, M.P. Scott, and P.A. Beachy. 2000. Effects of oncogenic mutations in Smoothened and Patched can be reversed by cyclopamine. *Nature*. 406:1005-1009.

Taipale, J., M.K. Cooper, T. Maiti, and P.A. Beachy. 2002. Patched acts catalytically to suppress the activity of Smoothened. *Nature*. 418:892-897.

Tao, B., S. Bu, Z. Yang, B. Siroky, J.C. Kappes, A. Kispert, and L.M. Guay-Woodford. 2009. Cystin localizes to primary cilia via membrane microdomains and a targeting motif. *J Am Soc Nephrol*. 20:2570-2580.

Trowbridge, J.J., M.P. Scott, and M. Bhatia. 2006. Hedgehog modulates cell cycle regulators in stem cells to control hematopoietic regeneration. *Proc Natl Acad Sci USA*. 103:14134-14139.

Tseng, T.T., K.S. Gratwick, J. Kollman, D. Park, D.H. Nies, A. Goffeau, and M.H. Saier, Jr. 1999. The RND permease superfamily: an ancient, ubiquitous and diverse family that includes human disease and development proteins. *J Mol Microbiol Biotechnol*. 1:107-125.

Tsukui, T., J. Capdevila, K. Tamura, P. Ruiz-Lozano, C. Rodriguez-Esteban, S. Yonei-Tamura, J. Magallon, R.A. Chandraratna, K. Chien, B. Blumberg, R.M. Evans, and J.C. Belmonte. 1999. Multiple left-right asymmetry defects in Shh(-/-) mutant mice unveil a convergence of the shh and retinoic acid pathways in the control of Lefty-1. *Proc Natl Acad Sci U S A*. 96:11376-11381.

Tukachinsky, H., R.P. Kuzmickas, C.Y. Jao, J. Liu, and A. Salic. 2012. Dispatched and scube mediate the efficient secretion of the cholesterol-modified hedgehog ligand. *Cell reports*. 2:308-320.

Tukachinsky, H., L.V. Lopez, and A. Salic. 2010. A mechanism for vertebrate Hedgehog signaling: recruitment to cilia and dissociation of SuFu-Gli protein complexes. *J Cell Biol*. 191:415-428.

Tyler, K.M., A. Fridberg, K.M. Toriello, C.L. Olson, J.A. Cieslak, T.L. Hazlett, and D.M. Engman. 2009. Flagellar membrane localization via association with lipid rafts. *J Cell Sci*. 122:859-866.

Vandevyver, S., L. Dejager, J. Tuckermann, and C. Libert. 2013. New insights into the anti-inflammatory mechanisms of glucocorticoids: an emerging role for glucocorticoid-receptor-mediated transactivation. *Endocrinology*. 154:993-1007.

Varjosalo, M., S.P. Li, and J. Taipale. 2006. Divergence of hedgehog signal transduction mechanism between Drosophila and mammals. *Dev Cell*. 10:177-186.

Venkatakrishnan, A.J., X. Deupi, G. Lebon, C.G. Tate, G.F. Schertler, and M.M. Babu. 2013. Molecular signatures of G-protein-coupled receptors. *Nature*. 494:185-194.

Wang, B., J.F. Fallon, and P.A. Beachy. 2000. Hedgehog-regulated processing of Gli3 produces an anterior/posterior repressor gradient in the developing vertebrate limb. *Cell*. 100:423-434.

Wang, C., H. Wu, V. Katritch, G.W. Han, X.P. Huang, W. Liu, F.Y. Siu, B.L. Roth, V. Cherezov, and R.C. Stevens. 2013. Structure of the human smoothened receptor bound to an antitumour agent. *Nature*.

Wang, Y., L. Davidow, A.C. Arvanites, J. Blanchard, K. Lam, K. Xu, V. Oza, J.W. Yoo, J.M. Ng, T. Curran, L.L. Rubin, and A.P. McMahon. 2012. Glucocorticoid compounds modify smoothened localization and hedgehog pathway activity. *Chemistry & biology*. 19:972-982.

Wei, Q., Y. Zhang, Y. Li, Q. Zhang, K. Ling, and J. Hu. 2012. The BBSome controls IFT assembly and turnaround in cilia. *Nat Cell Biol*. 14:950-957.

Wilson, C.W., C.T. Nguyen, M.H. Chen, J.H. Yang, R. Gacayan, J. Huang, J.N. Chen, and P.T. Chuang. 2009. Fused has evolved divergent roles in vertebrate Hedgehog signalling and motile ciliogenesis. *Nature*. 459:98-102.

Wright, K.J., L.M. Baye, A. Olivier-Mason, S. Mukhopadhyay, L. Sang, M. Kwong, W. Wang, P.R. Pretorius, V.C. Sheffield, P. Sengupta, D.C. Slusarski, and P.K. Jackson. 2011. An ARL3-UNC119-RP2 GTPase cycle targets myristoylated NPHP3 to the primary cilium. *Genes Dev*. 25:2347-2360.

Wu, X., J. Walker, J. Zhang, S. Ding, and P.G. Schultz. 2004. Purmorphamine induces osteogenesis by activation of the hedgehog signaling pathway. *Chemistry & biology*. 11:1229-1238.

Xie, J., M. Murone, S.M. Luoh, A. Ryan, Q. Gu, C. Zhang, J.M. Bonifas, C.W. Lam, M. Hynes, A. Goddard, A. Rosenthal, E.H. Epstein, Jr., and F.J. de Sauvage. 1998. Activating Smoothened mutations in sporadic basal-cell carcinoma. *Nature*. 391:90-92.

Yamazaki, M., K. Nakamura, Y. Mizukami, M. Ii, J. Sasajima, Y. Sugiyama, T. Nishikawa, Y. Nakano, N. Yanagawa, K. Sato, A. Maemoto, S. Tanno, T. Okumura, H. Karasaki, T. Kono, M. Fujiya, T. Ashida, D.C. Chung, and Y. Kohgo. 2008. Sonic hedgehog derived from human pancreatic cancer cells augments angiogenic function of endothelial progenitor cells. *Cancer Sci*. 99:1131-1138.

Yauch, R.L., G.J. Dijkgraaf, B. Alicke, T. Januario, C.P. Ahn, T. Holcomb, K. Pujara, J. Stinson, C.A. Callahan, T. Tang, J.F. Bazan, Z. Kan, S. Seshagiri, C.L. Hann, S.E. Gould, J.A. Low, C.M. Rudin, and F.J. de Sauvage. 2009. Smoothened mutation confers resistance to a Hedgehog pathway inhibitor in medulloblastoma. *Science*. 326:572-574.

Yoo, Y.A., M.H. Kang, H.J. Lee, B.H. Kim, J.K. Park, H.K. Kim, J.S. Kim, and S.C. Oh. 2011. Sonic hedgehog pathway promotes metastasis and lymphangiogenesis via activation of Akt, EMT, and MMP-9 pathway in gastric cancer. *Cancer Res*. 71:7061-7070.

Zhang, X.M., M. Ramalho-Santos, and A.P. McMahon. 2001. Smoothened mutants reveal redundant roles for Shh and Ihh signaling including regulation of L/R asymmetry by the mouse node. *Cell*. 105:781-792.

Zhao, Y., C. Tong, and J. Jiang. 2007. Hedgehog regulates smoothened activity by inducing a conformational switch. *Nature*. 450:252-258.

Zheng, X., R.K. Mann, N. Sever, and P.A. Beachy. 2010. Genetic and biochemical definition of the Hedgehog receptor. *Genes Dev*. 24:57-71.

Chapter 2: Mechanism of Smo regulation by oxysterols

The following section contains previously published material from:

Nedelcu D., Liu J., Xu Y., Jao C. and Salic A., Oxysterol binding to the extracellular domain of Smoothened in Hedgehog signaling. Nature Chemical Biology 9: 557–564 (2013) doi:10.1038/nchembio.1290

2.1 Author contributions

I performed cellular and biochemical experiments. J.L., C.J. and A.S. designed and synthesized all reported compounds. J.L. performed the purification and characterization of the reported compounds. Y.X. and I developed the automated image analysis software, and I analyzed all the imaging data.

2.2 Abstract

Oxysterols bind the seven-spanner transmembrane protein Smoothened and potently activate vertebrate Hedgehog signaling, a pathway essential in embryonic development, adult stem cell maintenance and cancer. It is unknown, however, if oxysterols are important for normal Hedgehog signaling, and whether antagonizing oxysterols can inhibit the Hedgehog pathway. We developed azasterols that block Hedgehog signaling by binding to the oxysterol-binding site of Smoothened. We show that the binding site for oxysterols and azasterols maps to the extracellular, cysteine-rich domain of Smoothened, and is completely separable from the site bound by other small molecule modulators, located within the heptahelical bundle of Smoothened. Smoothened mutants that abolish oxysterol binding no longer respond to oxysterols, and cannot be maximally activated by the Hedgehog ligand. Our results show that oxysterol binding to vertebrate Smoothened is required for high level Hedgehog signaling, and that targeting the oxysterol binding site is an effective strategy to block Smoothened activity.

2.3 Introduction

Cell-cell signaling via the Hedgehog (Hh) pathway is critical for numerous aspects of metazoan embryonic development and regeneration, while excessive Hh signaling is involved in many cancers (Ingham and McMahon, 2001; Lum and Beachy, 2004). Among the poorly understood aspects of Hh signal transduction is the mechanism by which Hh signals are relayed across the plasma membrane, via the functional interaction between the multi-spanning membrane protein Patched (Ptc), which functions as the Hh receptor, and the seven-spanner Smoothened (Smo), a member of the Frizzled family of membrane proteins. In the absence of the Hh ligand, Ptc inhibits Smo through an unknown mechanism, ensuring that Hh signals are not relayed to the cytoplasm. Hh signaling is initiated by binding of the Hh ligand to Ptc, which leads to Smo activation and the consequent initiation of a specific transcriptional program driven by the Gli transcription factors.

A major unanswered question in Hh signaling is the mechanism by which the activity of Smo is regulated. By analogy with other seven-spanners, it is thought that Smo equilibrates between active and inactive conformations, and that this equilibrium is controlled by a ligand (Taipale et al., 2002), whose identity has remained elusive. Consistent with this hypothesis, vertebrate Smo harbors within its heptahelical bundle a binding site (Chen et al., 2002a) (hereby referred to as "Site A") reminiscent of the ligand-binding site of G protein-coupled receptors (GPCRs). Site A is targeted by a large number of small molecules, including Smo inhibitors (such as the plant alkaloid cyclopamine (Chen et al., 2002a), SANT1 (Frank-Kamenetsky et al., 2002), or the FDA-approved Smo inhibitor GDC0449 (Robarge et al., 2009)) as well as Smo activators (such as SAG (Chen et al., 2002b; Frank-Kamenetsky et al., 2002) and

purmorphamine (Sinha and Chen, 2006)). In spite of the relative ease in finding synthetic modulators of vertebrate Smo, no endogenous small molecule that regulates Smo via binding to Site A has been identified so far.

The only naturally occurring molecules that activate the Hh pathway at the level of Smo are oxysterols, a class of oxidized cholesterol derivatives known for their potent effects on many cellular processes, including signaling and metabolism. Specifically, vertebrate Hh signaling is stimulated by oxysterols carrying hydroxyl groups on the isooctyl side chain of the molecule (Corcoran and Scott, 2006; Dwyer et al., 2007), the most potent such oxysterol being 20(S)-hydroxycholesterol (20-OHC, figure 1A) (Nachtergaele et al., 2012). Oxysterols activate Smo by direct binding, and do not compete with compounds that bind to Site A, suggesting that they activate Smo by an allosteric mechanism involving a second, distinct binding site (Nachtergaele et al., 2012) (hereby referred to as "Site B"). Several important mechanistic questions about the role of oxysterols in Hh signaling are currently open. First, it is unknown where Site B is located in Smo, and whether Site B is separable from Site A. Second, while Site A is targeted by both Smo activators and inhibitors, so far we only know of oxysterol activators that bind Site B, raising the question of whether Site B can also be targeted by inhibitors. Finally, although oxysterols are potent activators of Smo, it is unknown if binding of oxysterols to Smo is required for Smo activation during normal Hh signaling in vertebrates.

We have developed azasterols that block Hh signaling triggered by the Hh ligand and by 20-OHC. These compounds compete with 20-OHC for binding to Smo, indicating that they bind to Site B; in contrast, azasterols do not compete with small molecule activators or inhibitors that

bind Site A. We used azasterol and oxysterol affinity probes to map Site B to the extracellular, cysteine-rich domain (CRD) of vertebrate Smo; furthermore, we show that Site A and B are completely separable. When Site B is mutated, 20-OHC binding to Smo is abolished and 20-OHC can no longer activate Smo, thus validating functionally the surprising identification of Site B within the CRD of Smo. These oxysterol-insensitive Smo mutants have greatly decreased responsiveness to the Hh ligand compared to wild-type Smo, indicating that binding of endogenous oxysterols to Smo is necessary for high level vertebrate Hh signaling.

2.4 Results

2.4.1 An azasterol inhibitor of vertebrate Hedgehog signaling that mimics the effects of sterol depletion

Vertebrate Hh signaling is strongly activated by 20-OHC (Nachtergaele et al., 2012); however, the consequences for Hh signaling of blocking 20-OHC are not known. To obtain a potential inhibitor of 20-OHC, we synthesized 22- azacholesterol (22-NHC, Figure 2.1a). When tested in Hh-responsive NIH-3T3 cells, 22-NHC inhibited Hh pathway activation by the Sonic Hedgehog (Shh) ligand in a dose-dependent manner, with an IC_{50} of about 3 μM (Figure 2.1b). Synthesis of 22-NHC generates a chiral center at C20, resulting in 2 possible diastereomers, 22(S)-NHC and 22(R)-NHC. The diastereomeric mix from our synthesis consisted mostly of 22(S)-NHC, and pure 22(S)-NHC recapitulated the inhibitory activity of the mix. 22-NHC did not affect the EC_{50} of the Shh ligand (Figure 2.1b) but it decreased the maximum stimulation level (Figure 2.1c), a profile indicative of non-competitive inhibition.

We first sought to determine what step in the Hh signal transduction pathway is blocked by 22-NHC. In vertebrate cells, binding of Shh to Patched (Ptc) causes the removal of Ptc from the primary cilium (Rohatgi et al., 2007), which, in turn, triggers Hh pathway activation. 22-NHC had no effect on the disappearance of Ptc from the cilium in response to Shh (Supplementary Figure S1a), suggesting that 22-NHC inhibits the Hh pathway downstream of

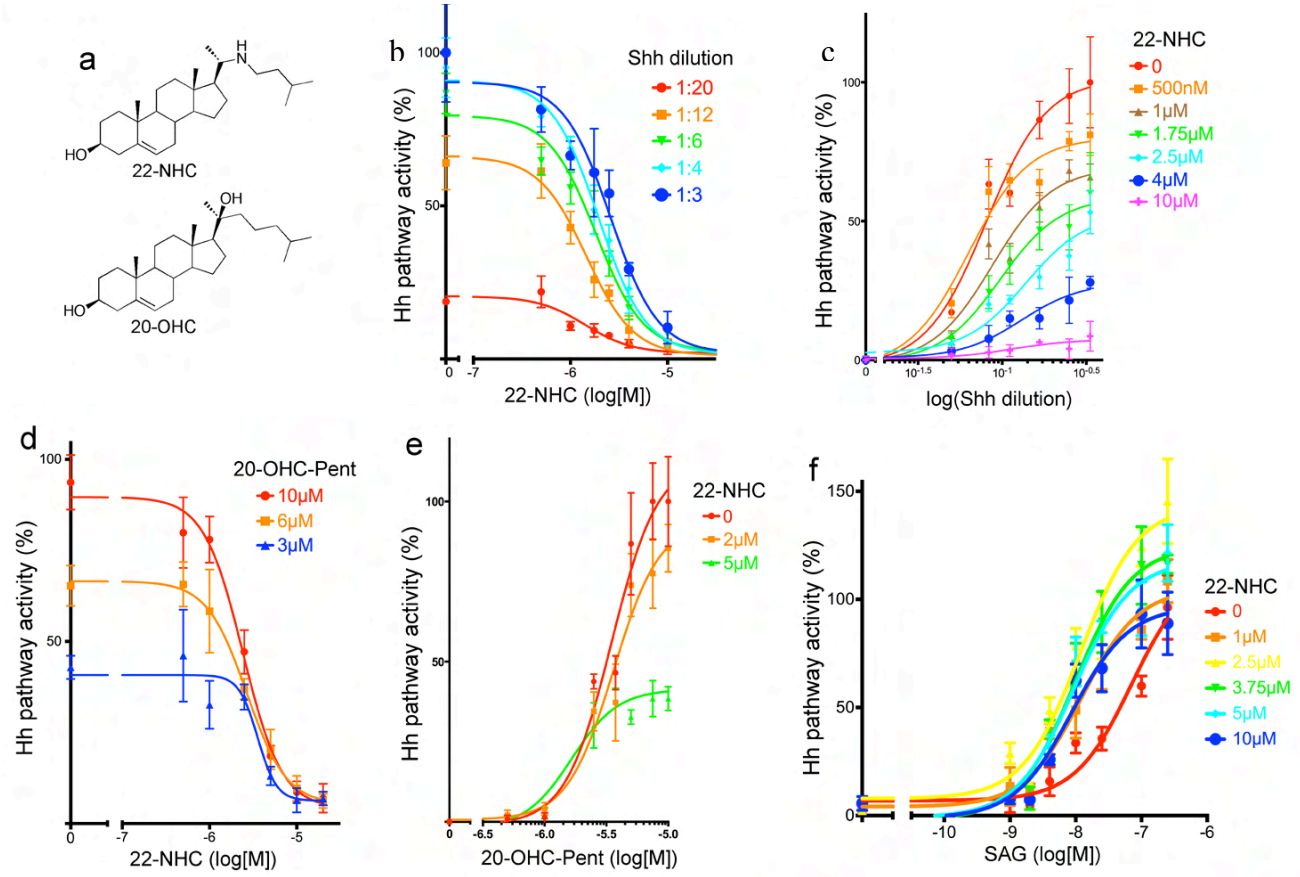

Figure 2.1 22-azacholesterol (22-NHC), an azasterol inhibitor of vertebrate Hh signaling

(a) Structures of the azasterol, 22-azacholesterol (22-NHC, shown as the S diastereomer), and of the Hh- activating oxysterol, 20(S)-hydroxycholesterol (20(S)-OHC).

(b) Shh Light II cells were treated with various concentrations of Shh, in the presence of increasing amounts of 22-NHC, and Hh pathway activation was measured by luciferase assay. All experiments were performed in quadruplicate and error bars represent the standard deviation

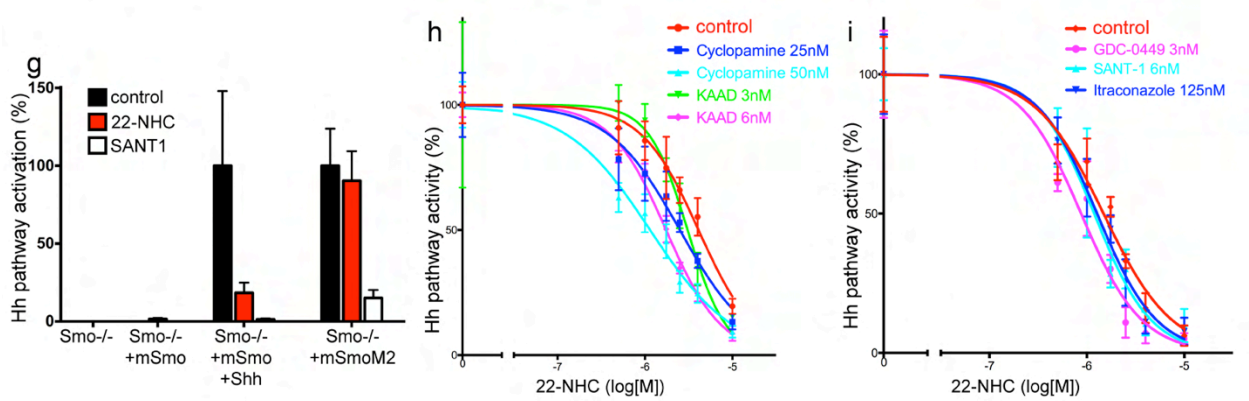

Figure 2.1 (continued) 22-azacholesterol (22-NHC), an azasterol inhibitor of vertebrate Hh signaling

of the mean. 22-NHC inhibits Hh pathway activation by Shh but does not significantly change the EC50 of Shh.

(c) The data in (b) was plotted to show that 22-NHC decreases the maximal stimulation of the Hh pathway by Shh.

(d) As in (b) but Hh signaling was activated by various concentrations of the 20-OHC analog, 20-OHC- Pent. 22-NHC inhibits Hh pathway activation by 20-OHC-Pent, without significantly changing the EC50.

(e) The data in (d) was plotted to show that 22-NHC decreases the maximal stimulation of the Hh pathway by 20-OHC-Pent.

(f) As in (b) but Hh signaling was activated by various concentrations of SAG. 22-NHC does not inhibit Hh pathway activation by SAG but decreases the EC50 for SAG.

(g) Smo-/- MEFs were rescued by stable expression of mSmo or the constitutively active mutant mSmoM2. Transcription of the Hh target gene, Gli1, was measured by Q-PCR in the absence or presence of 22-NHC (20 μM) or SANT1 (2 μM). All experiments were performed in triplicate, and error bars indicate the standard deviation of the mean. 22-NHC does not inhibit SmoM2.

(h) Shh Light II cells were stimulated with Shh, in the presence of increasing amounts of 22-NHC, with the addition of the indicated concentrations of cylopamine and cyclopamine-KAAD. Hh pathway activity was assayed as in (b)

(i) As in (h) but with addition of the indicated concentrations of SANT1, GDC0449 and itraconazole.

Ptc. We next asked if 22-NHC inhibits two activators of the Hh pathway that function at the level of Smoothened (Smo), 20-OHC and the synthetic activator, SAG. 22- NHC inhibited 20-OHC in a dose-dependent manner and non-competitively: 22-NHC did not significantly change the EC_{50} of 20-OHC (Figure 2.1d) but decreased the level of maximal stimulation (Figure 2.1e). In contrast, 22-NHC did not inhibit Hh pathway stimulation by SAG (Figure 2.1f); in fact, 22-NHC caused an increase in the responsiveness of cells to SAG (note the decrease in EC_{50} for SAG in the presence of 22-NHC, in Figure 2.1f). While we do not understand the basis for the synergy with SAG, one possibility is that it is caused by 22-NHC promoting Smo translocation to cilia (see below). Additionally, 22-NHC did not block signaling by mSmoM2 (Figure 2.1g), an oncogenic mouse Smo mutant locked in the active conformation (Taipale et al., 2000), or the constitutive Hh signaling in $SuFu^{-/-}$ MEFs (Svard et al., 2006) (Supplementary Figure S1b), in which the Hh pathway is activated downstream from Smo. Together, these results indicate that 22-NHC targets either Smo or an unknown component between Ptc and Smo. Importantly, the inhibition profile of 22-NHC mirrors the effect of sterol depletion, which blocks activation of the vertebrate Hh pathway by Shh but not by SAG, mSmoM2 or by loss of SuFu (Cooper et al., 2003).

Finally, we asked if 22-NHC synergizes with known Hh pathway inhibitors that target Smo. As shown in Figure 2.1h and Figure 2.1i, 22-NHC did not synergize with cyclopamine (Cyc), cyclopamine-KAAD, SANT1, GDC0449 and itraconazole to inhibit Hh pathway activation by Shh; conversely, these inhibitors did not significantly affect the IC_{50} of 22-NHC. Thus 22-NHC does not interact with other Smo inhibitors, suggesting a potentially different

mechanism. In summary, 22-NHC is an inhibitor that recapitulates the effect of sterol depletion on vertebrate Hh signaling, and epistatic analysis suggests Smo as a candidate target of 22-NHC.

2.4.2 22-NHC binds Smoothened at a site distinct from the cyclopamine-binding site

We next tested the effect of 22-NHC on the accumulation of Smo in primary cilia, an early response to vertebrate Hh stimulation (Corbit et al., 2005). As shown in Figure 2.2a, 22-NHC by itself caused Smo to accumulate in cilia, a behaviour reminiscent of Cyc (Rohatgi et al., 2009; Wang et al., 2009), an Hh pathway inhibitor that binds Smo at Site A. To test if 22-NHC also binds to Site A of Smo, we performed binding assays in cells with the fluorescent derivative, BODIPY-cyclopamine (Chen et al., 2002a) (BODIPY-Cyc). 22-NHC did not compete binding of BODIPY-Cyc to mouse Smo (mSmo), similar to 20-OHC (Supplementary Figure S2c); as expected, the Site A-binding small molecule SANT1 abolished BODIPY-Cyc binding. We also synthesized a fluorescent derivative of SANT1, BODIPY-SANT1 (Supplementary Figure S2d), which retains the inhibitory activity of SANT1 (Supplementary Figure S2e). 22-NHC did not compete binding of BODIPY-SANT1 to mSmo, while unmodified SANT1 did (Supplementary Figure S2c). Together, these results indicate that 22-NHC does not bind to Site A of mSmo, in contrast to Cyc.

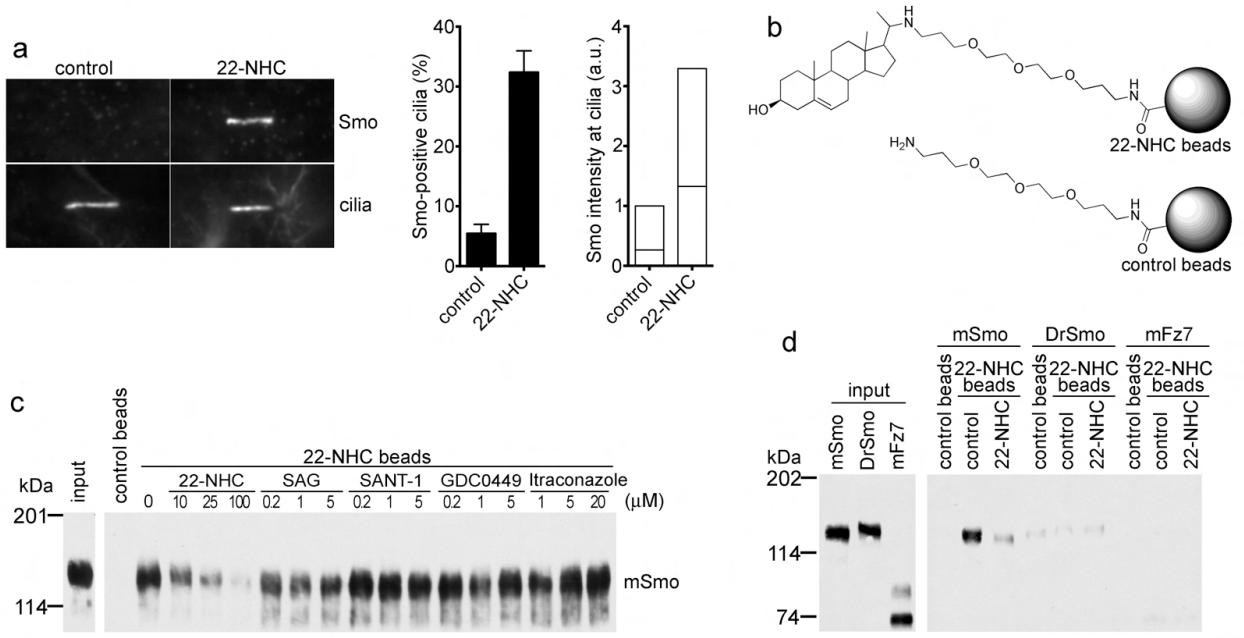

Figure 2.2 22-NHC binds Smo at a different site from cyclopamine

(a) 22-NHC causes Smo accumulation at primary cilia. NIH-3T3 cells were treated with 22(S)-NHC (10 μM) and localization of endogenous Smo was determined by immunofluorescence microscopy. The left panel shows representative micrographs of cilia. The graph in the middle shows the percentage of Smo- positive cilia. The box plot on the right shows the fluorescence intensity of Smo at cilia; the lower and

upper bounds of each box represent the 25th and 75th percentile of the intensity distribution, while the horizontal line represents the median intensity of the entire population of cilia.

(b) Schematic of the 22-NHC affinity matrix. Top: 22-NHC is covalently attached to agarose beads via a polyethylene glycol linker, to generate 22-NHC beads. Bottom: control beads.

(c) 22-NHC beads were incubated with detergent extracts of 293T cells expressing mSmo-Cherry, in the presence of the indicated concentrations of competitor compounds. The beads were washed and bound protein was eluted, separated by SDS-PAGE and immunoblotted with anti-Cherry antibodies. A portion of the extract was analyzed in parallel, to show input. MSmo binds specifically to 22-NHC beads.

(d) As in (c) but with detergent extracts of 293T cells expressing Cherry-tagged mSmo, DrSmo or mFz7. Incubation with 22-NHC beads was done in the absence or presence of free 22-NHC (100 μM). DrSmo and mFz7 do not bind 22-NHC beads.

To test if 22-NHC binds mSmo at a different site, we developed a ligand affinity assay. We focused on the alkyl side chain of 22-NHC as potential site for covalent attachment to beads, and asked if analogs with shorter side chains inhibit Hh signaling. Analogs of 22-NHC bearing N-propyl and N-ethyl groups (Supplementary Figure S2f) retain the inhibitory activity of 22-NHC, albeit they are slightly less potent (Supplementary Figure S2g). Interestingly, the stereochemistry of C20 does not matter in these 20-NHC analogs: both S and R diastereomers inhibit Hh signaling, in contrast to the strict C20 stereochemistry required for Hh pathway activation by oxysterols (Nachtergaele et al., 2012) (see also below).

Based on the structure-function analysis above, we synthesized 22-NHC-PEG-NH_2, a derivative of 22- NHC with a polyethylene glycol (PEG) linker, which was covalently attached to amine-reactive beads, to generate 22-NHC beads (Figure 2.2b). As source of mSmo protein, we used detergent extracts of 293T cells stably expressing mSmo tagged with mCherry; this fusion protein is active, as demonstrated by rescue of Hh signaling in $Smo^{-/-}$ mouse embryonic fibroblasts (MEFs) (see below). As shown in figure 2C, 22-NHC beads efficiently captured mSmo, preferentially the glycosylated species with low electrophoretic mobility, representing post-Golgi mSmo molecules; this suggests that fully mature mSmo is the predominant species that binds 22-NHC. Binding of mSmo to 22-NHC beads was competed in a dose-dependent manner by free 22-NHC added to the detergent extract (Figure 2.2c), suggesting that it was specific. SAG, SANT1 and GDC0449 had no effect on mSmo binding to 22-NHC beads (Figure 2.2c), consistent with 22-NHC not binding Site A. Itraconazole, a mSmo inhibitor that does not bind Site A (Kim et al., 2010) also had no effect on binding of mSmo to 22-NHC beads (Figure

2.2c). As negative control, we used beads derivatized with the PEG linker incorporated into 22-NHC-PEG-NH_2 (Figure 2.2b); these beads captured negligible amounts of mSmo (Figure 2.2c). As further proof of specificity, 22-NHC beads did not bind another seven-spanner related to Smo, mouse Frizzled-7 (mFz7) (Figure 2.2d). Finally, binding was specific for vertebrate Smo proteins: 22-NHC beads did not bind Drosophila Smo (DrSmo, Figure 2.2d) but bound Xenopus Smo (xSmo, see Figure 2.3b below). Together, these results demonstrate that 22-NHC binds vertebrate Smo proteins at a different site from Site A and from the hypothetical site targeted by itraconazole.

2.4.3 22-NHC binds the oxysterol-binding site of Smoothened

Oxysterols are allosteric activators of vertebrate Smo that bind to Site B, which is distinct from Site A and from the itraconazole site (Nachtergaele et al., 2012). We asked if 22-NHC binds Smo at Site B by performing competition experiments with oxysterols. Binding of mSmo to 22-NHC beads was competed in a dose-dependent manner by two active oxysterols, 20-OHC and the analog 20-OHC-Pent (see below), while the inactive 7-hydroxycholesterol (7-OHC) had no effect (Figure 2.3a). Similarly, binding of xSmo to 22-NHC beads was competed by free 20-OHC and 22-NHC, but not by 7-OHC (Figure 2.3b). Thus 22-NHC and oxysterols that activate the Hh pathway compete for binding to vertebrate Smo.

Binding of 20-OHC is strictly stereospecific: 20(S)-OHC binds Smo while 20(R)-OHC does not (Nachtergaele et al., 2012). If 22-NHC binds Site B of Smo, it would be expected that oxysterol competition be also stereospecific. To test this prediction, we prepared the pure

diastereomers of 20-OHC-Pent (Figure 2.3c). Only the active diastereomer 20(S)-OHC-Pent (see below) competed mSmo binding to 22-NHC beads, while the inactive diastereomer 20(R)-OHC-Pent had no effect (Figure 2.3d). Thus oxysterol stereochemistry at C20 is critical for competing with binding of 22-NHC to Smo.

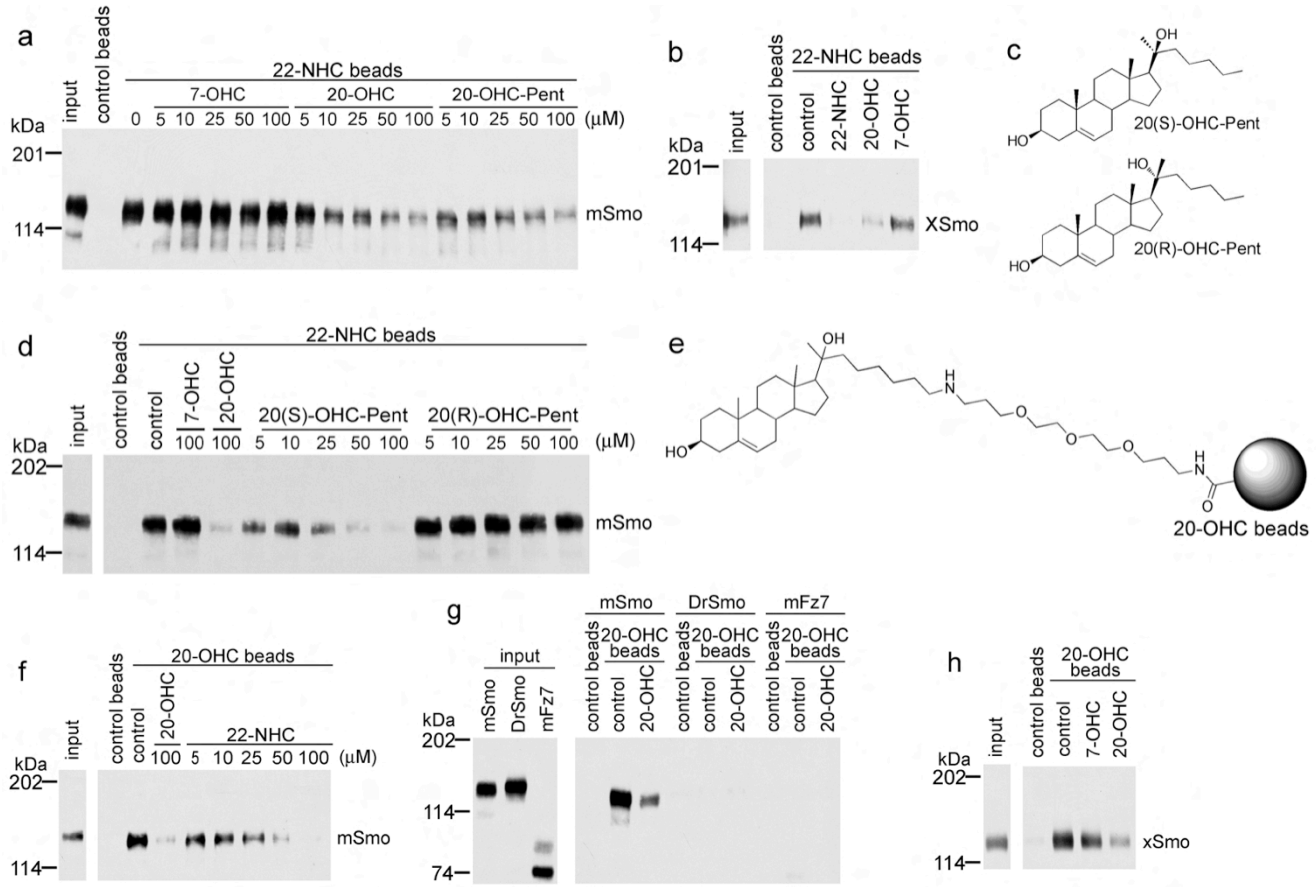

Figure 2.3 22-NHC binds Smo at the oxysterol-binding site

(a) Detergent extracts of cells expressing mSmo-Cherry were incubated with 22-NHC beads, in the presence of the indicated concentrations of the inactive oxysterol 7-OHC or the active oxysterols, 20- OHC and 20-OHC-Pent. Bound mSmo-Cherry was analyzed by SDS-PAGE and immunoblotting. Binding of mSmo to 22-NHC beads is competed in a dose-dependent manner by 20-OHC and 20-OHC- Pent, but not by 7-OHC.

(b) As in (a) but with eGFP-tagged xSmo. Binding of xSmo to 22-NHC beads is competed by free 22- NHC and 20-OHC but not by 7-OHC. All competitors were used at 100 μM.

Figure 2.3 (continued) 22-NHC binds Smo at the oxysterol-binding site

(c) Structures of the two diastereomers of the active oxysterol 20-OHC-Pent.

(d) As in (a) but with the addition of 20(S)-OHC-Pent and 20(R)-OHC-Pent. Binding of mSmo to 22- NHC beads is competed by the active S diastereomer but not by the inactive R diastereomer.

(e) Schematic of the 20-OHC beads.

(f) Detergent extracts of cells expressing mSmo-Cherry were incubated with 20-OHC beads, in the presence of the indicated concentrations of free 22-NHC or 20-OHC. Bound mSmo was analyzed as in (a). Binding of mSmo to 20-OHC beads is competed in a dose-dependent manner by free 22-NHC and 20-OHC.

(g) As in (f) but with Cherry-tagged mSmo, DrSmo or mFz7. DrSmo and mFz7 do not bind 20-OHC beads, in contrast to mSmo. Binding of mSmo was competed by free 20-OHC (100 μM).

(h) As in (f) but with eGFP-tagged xSmo. The protein bound to beads was detected by immunoblotting with anti-GFP antibodies. XSmo binds to 20-OHC beads and is competed by free 20-OHC (100 μM) but not 7-OHC (100 μM).

To perform reciprocal binding experiments, we generated 20-OHC beads (Figure 2.3e) by covalent attachment of an amine derivative of 20-OHC that incorporates the same PEG linker that we used for 22-NHC beads. These beads bound mSmo (Figure 2.3f), as previously described for a similar 20-OHC affinity matrix (Nachtergaele et al., 2012). Importantly, 22-NHC inhibited binding of mSmo to 20-OHC beads in a dose- dependent manner (Figure 2.3f). Like 22-NHC beads, 20-OHC beads did not bind DrSmo (Figure 2.3g), but bound xSmo (Figure 2.3h), consistent with the fact that oxysterols are activators of the vertebrate but not of the Drosophila Hh pathway. Furthermore, in a variety of Smo binding experiments (see below) 22-NHC and 20-OHC beads behaved virtually identically. Together, these results indicate that 22-NHC and 20-OHC bind to the same site on mSmo (Site B), and suggest that 22-NHC inhibits Hh signaling by competing with binding of 20-OHC to mSmo.

2.4.4 Oxysterols and 22-NHC bind to the extracellular domain of Smoothened

The location of Site B on mSmo has not been determined, and is unknown if Site B and Site A are physically separable, particularly in view of their allosteric interaction. We used mSmo deletion analysis (Figure 2.4a) and 22-NHC and 20-OHC ligand affinity to map the location of Site B. MSmo lacking the extracellular, cysteine-rich domain ($mSmo^{\Delta CRD}$) did not bind to 22-NHC beads (Figure 2.4b) or to 20-OHC beads (Figure 2.4c), in contrast to full-length mSmo (Figure 2.4b and Figure 2.4c) and to mSmo lacking the intracellular C-terminal domain ($mSmo^{\Delta ICD}$) (Figure 2.4d). Importantly, $mSmo^{\Delta CRD}$ bound BODIPY-Cyc (Supplementary Figure S3a) and was functional in Hh signaling in $Smo^{-/-}$ MEFs (see below), indicating that it was properly folded. These results indicate that the CRD of mSmo is required for binding to 20-OHC and 22-NHC.

We next asked if the CRD of mSmo (mSmoCRD), produced in cultured mammalian cells as a soluble, secreted protein, is sufficient to bind 22-NHC and 20-OHC. Secreted mSmoCRD bound to 22-NHC beads and was competed in a dose-dependent manner by free 22-NHC, similar to full-length mSmo (Figure 2.4e). As an additional control, we showed that secreted DrSmoCRD did not bind 22-NHC beads (Figure 2.4f), as expected from the lack of binding of full-length DrSmo.

Binding of mSmoCRD to 22-NHC beads was competed by 20-OHC and 20-OHC-Pent, but not by 7- OHC (Figure 2.4g), suggesting that, like full-length mSmo, mSmoCRD binds specifically oxysterols that activate the Hh pathway. Furthermore, the stereochemistry of oxysterol competition was identical to the one observed for full-length mSmo: the active

diastereomer 20(S)-OHC-Pent but not inactive 20(R)-OHC-Pent competed mSmoCRD binding to 22-NHC beads in a dose-dependent manner (Figure 2.4h). We obtained identical results using 20-OHC beads: mSmoCRD bound 20-OHC beads with an affinity similar to that displayed by full-length mSmo (Figure 2.4). Importantly, binding of mSmoCRD to 20-OHC beads was competed by 20(S)-OHC-Pent but not by 20(R)-OHC-Pent (Figure 2.4i). In addition, binding of mSmo and mSmoCRD to 20-OHC beads was competed by the active oxysterol 25-OHC but not by the inactive 7-ketocholesterol (Dwyer et al., 2007) (Supplementary Figure S3). Together, these results demonstrate that the oxysterol-binding site (Site B) resides in the CRD of Smo and is completely separable from Site A. Notably, it was proposed that SmoCRD might bind sterols, based on the structural similarity between the sterol-binding protein NPC2 and the CRD domain of Frizzled family proteins (Bazan and de Sauvage, 2009); our findings thus confirm this prediction.

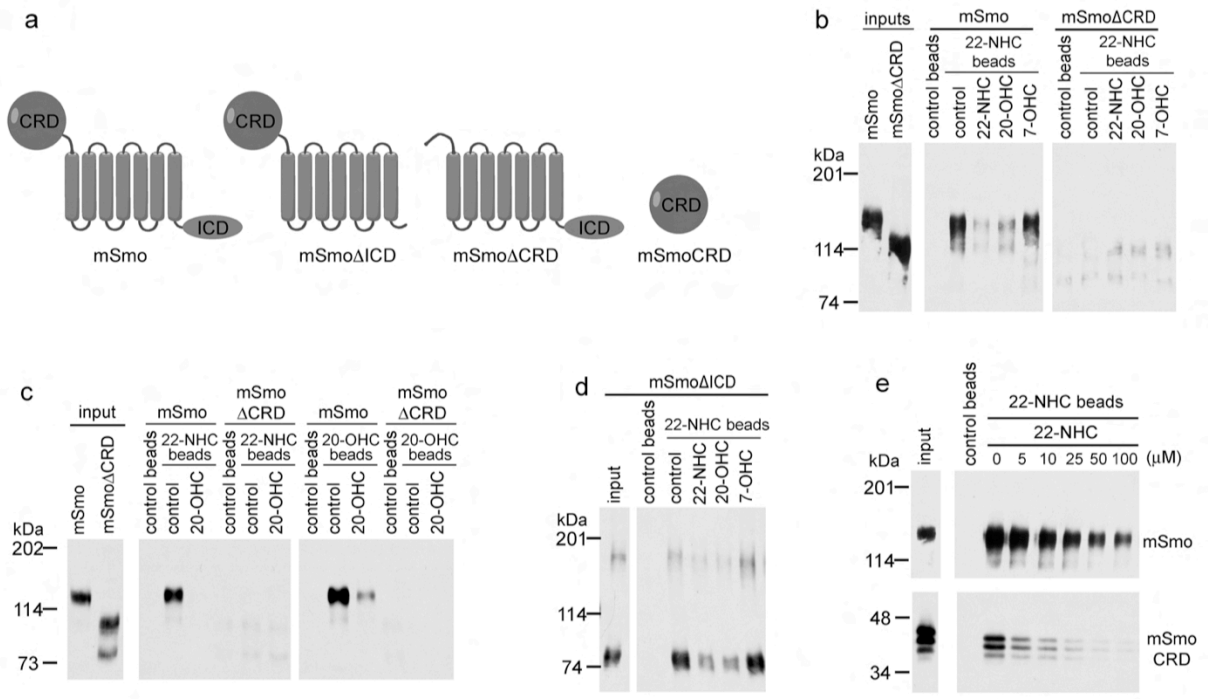

Figure 2.4 Oxysterols and 22-NHC bind the extracellular cysteine-rich domain (CRD) of vertebrate Smo

(a) Schematic of mSmo and of the mSmo deletion mutants used to map the oxysterol-binding site.

(b) Binding of Cherry-tagged mSmo or mSmoΔCRD to 22-NHC beads was tested in the presence of 100 μM of the indicated compounds. The CRD of mSmo is required for binding to 22-NHC beads.

(c) As in (b) but with 20-OHC beads. The CRD of mSmo is required for binding to 20-OHC beads.

(d) As in (b) but with mSmoΔICD-Cherry. The ICD of mSmo is not required for binding to 22-NHC beads.

(e) Secreted HA-tagged mSmoCRD and detergent extracts of mSmo-Cherry were tested for binding to 22-NHC beads, in the presence of the indicated concentrations of free 22-NHC. mSmoCRD binds 22- NHC beads, similar to mSmo.

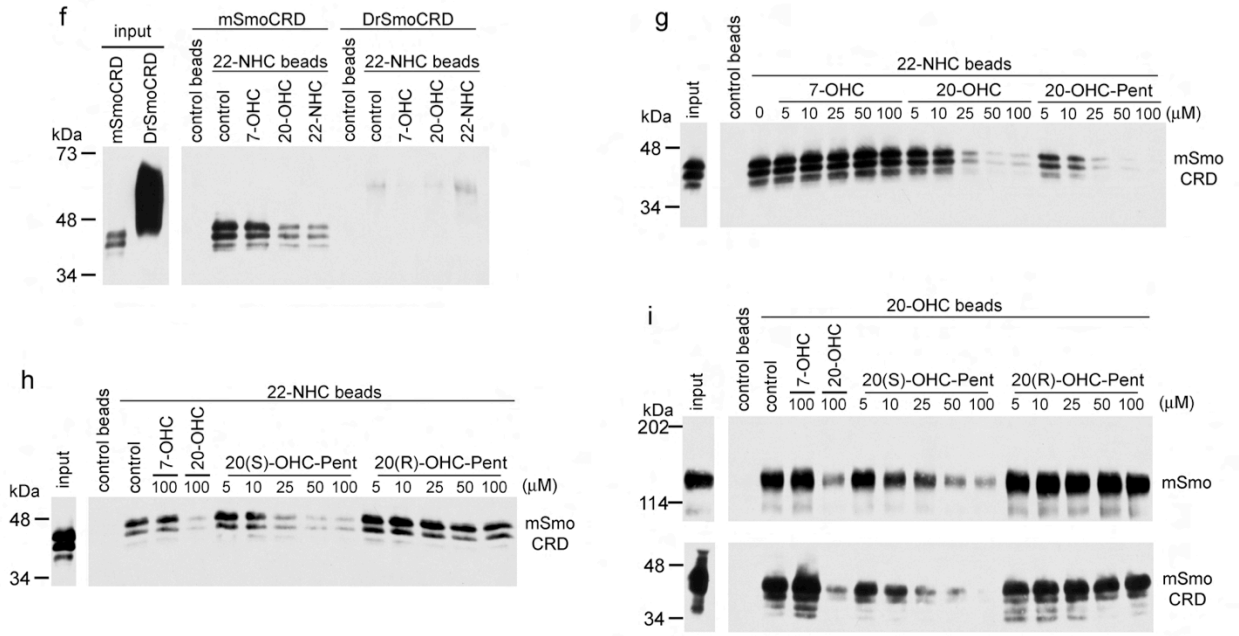

Figure 2.4 (continued) Oxysterols and 22-NHC bind the extracellular cysteine-rich domain (CRD) of vertebrate Smo

(f) As in (b) but with secreted HA-tagged mSmoCRD and DrSmoCRD. DrSmoCRD does not bind 22-NHC beads in contrast to mSmoCRD.

(g) mSmoCRD binding to 22-NHC beads was assayed as in (b), in the presence of the indicated concentrations of 7-OHC, 20-OHC and 20-OHC-Pent. Only the active sterols 20-OHC and 20-OHC- Pent compete mSmo binding to 22-NHC beads, while the inactive 7-OHC does not.

(h) As in (g) but with the indicated concentrations of the diastereomers 20(S)-OHC-Pent and 20(R)-OHC-Pent. Only the active S diastereomer competes mSmoCRD binding to 22-NHC beads.

(i) mSmoCRD and mSmo binding to 20-OHC beads was assayed as in (h). mSmoCRD binds 20-OHC beads and is competed by 20(S)-OHC-Pent. The binding affinities of mSmoCRD and mSmo to 20-OHC beads are similar.

2.4.5 Structural requirements for oxysterols in Hedgehog signaling

To gain a better understanding of the effect of oxysterols on Hh signaling, we asked what structural aspects of 20-OHC are important for mSmo activation and ciliary recruitment. We first focused on the isooctyl tail, and synthesized a series of 20-OHC analogs with progressively shorter tails (Figure 2.5a). Shortening the iso-octyl tail of 20-OHC by 1 or 2 carbons (20-OHC-Pent and 20-OHC-Bu) preserved Hh stimulatory activity. As for 20-OHC (Nachtergaele et al., 2012), the diastereomers 20(S)-OHC-Pent and 20(S)-OHC-Bu were active (Figure 2.5b) while 20(R)-OHC-Pent and 20(R)-OHC-Bu were inactive (Supplementary Figure S4a); this correlated with their ability to recruit mSmo to cilia (Figure 2.5c and Figure 2.5d). Analogs of 20-OHC with shorter side chains (20-OHC-Pr, 20-OHC-Et and 20-OHC-Me) did not stimulate Hh signaling (Supplementary Figure S4a), indicating that a tail of 6 carbon atoms is the minimum required for mSmo activation. These shorter side chain analogs also did not inhibit Hh pathway activation by Shh (Supplementary Figure S4b). Interestingly, 20(S)-OHC-Pr caused accumulation of mSmo at cilia, while 20-OHC-Me, 20-OHC-Et (R and S) and 20(R)-OHC-Pr had no effect (Figure 2.5c). Thus 20(S)-OHC-Pr is sufficient to localize mSmo to cilia but cannot activate it, suggesting that it induces a conformation of mSmo distinct from the active one induced by 20(S) analogs with longer side chains.

Finally, we asked if the Δ5 double bond and the 3β-OH group are important for the function of 20-OHC. The saturated analog, 20-OHC-PentSat (Figure 2.5a), activated Hh signaling as the S diastereomer (Figure 2.5b), while the R diastereomer was inactive (Supplementary Figure S4a); thus the Δ5 double bond is not required for activity. A 3β methyl

ether analog of 20-OHC-Pent (20-OHC-Pent-3β−OMe, Figure 2.5a) did not activate or inhibit Hh signaling (Supplementary Figure S4c), and had no effect on mSmo binding to 22-NHC beads (Supplementary Figure S4d). These results indicate that a free 3β-OH group is absolutely required for the activity of 20-OHC.

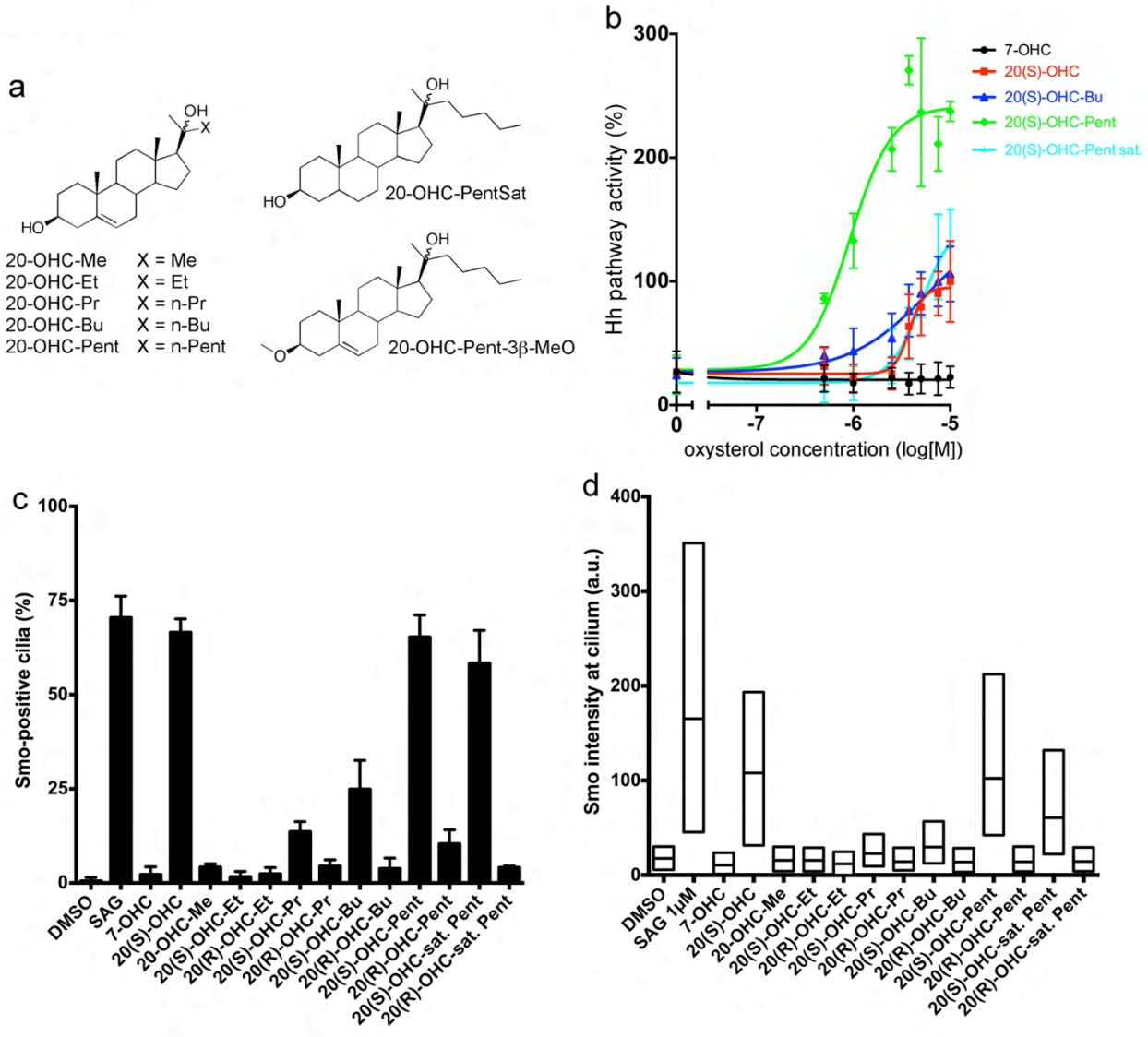

Figure 2.5 Structural requirements for oxysterol activation of Smo

Figure 2.5 (continued) Structural requirements for oxysterol activation of Smo

(a) Structures of 20-OHC analogs used in this study. All analogs except 20-OHC-Me have a chiral C20 center, and pure S and R diastereomers were isolated and assayed separately.

(b) Shh Light II cells were treated with varying concentrations of the oxysterols 20(S)-OHC, 20(S)- OHC-Pent, 20(S)-OHC-PentSat and 20(S)-OHC-Bu, followed by measuring Hh pathway activity by luciferase assay. The inactive oxysterol, 7-OHC, was used as negative control. All experiments were performed in quadruplicate, and error bars represent the standard deviation of the mean.

(c) NIH-3T3 cells were incubated overnight with the indicated oxysterols (10 μM). Cells were then fixed and processed for immunofluorescence with rabbit anti-Smo antibodies (to detect endogenous Smo) and mouse anti-acetylated tubulin antibodies (to visualize primary cilia). SAG (1 μM) and 7-OHC (10 μM) were used as positive and negative control, respectively. The graph shows the percentage of Smo-positive cilia.

(d) As in (c), but with box plots showing the fluorescence intensity of endogenous Smo at cilia. For each condition, the Smo signal was normalized to the intensity of the 20(S)-OHC treatment. The lower and upper bounds of each box represent the 25th and 75th percentile of the distribution of Smo intensity at cilia, while the horizontal line represents the median intensity across the entire population of cilia.

2.4.6 The role of oxysterols in vertebrate Hedgehog signalling

Although oxysterols are potent activators of vertebrate Smo, it is not known what role their interaction with Smo plays in normal Hh signaling. To generate mSmo mutants that do not bind oxysterols, we relied on the homology between the CRDs of Smo and Frizzled (Fz) proteins. It was proposed that SmoCRD binds sterols similar to how FzCRD binds the palmityl residue attached to Wnt proteins (Bazan and de Sauvage, 2009). Based on the crystal structure of mFz8CRD bound to palmitylated Xwnt8 (Janda et al., 2012), we focused on a stretch of 8 amino acids in mSmo, whereby the corresponding sequence in mFz8 includes 5 amino acids that form close contacts with the palmityl residue (a and (Janda et al., 2012)). This stretch is highly

conserved among vertebrate Smo orthologs but not in DrSmo, which does not bind oxysterols. To test if this stretch is important for oxysterol binding, we swapped amino acids 112-119 of mSmo for the corresponding amino acids of DrSmo. The resulting mSmo mutant ($mSmo^{DrSmoCRDmut}$) did not bind 22-NHC beads, (Supplementary Figure S5a), while the secreted $mSmoCRD^{DrSmoCRDmut}$ did not bind 20-OHC beads (Supplementary Figure S5b). Importantly, $mSmo^{DrSmoCRDmut}$ bound BODIPY-Cyc (Supplementary Figure S5c), indicating the protein is properly folded and harbors an intact Site A.

Figure 2.6 Oxysterol binding to Smo is required for high level Hh signaling

(a) Sequence alignment of a portion of the CRDs of mouse Smo (mSmo), chicken Smo (gSmo), Xenopus Smo (xSmo), zebrafish Smo (zfSmo), Drosophila Smo (DrSmo) and mouse Fz8 (mFz8). The 8-amino acid stretch indicated with red lines contains 5 residues that, in mFz8, form contacts with the palmityl moiety of Xwnt8 (Q71, F72, P74, L75 and I78).

(b) Cherry-tagged mSmo, mSmoL112D, mSmoW113Y or mSmoS114Y were tested for binding to 22- NHC and 20-OHC beads, in the presence or absence of 20-OHC (100 μM). MSmoL112D and mSmoW113Y do not bind 22-NHC and 20-OHC beads, in contrast to mSmo and mSmoS114Y.

(c) Smo-/- MEFs rescued with mSmo, mSmoL112D, mSmoW113Y or mSmoS114Y were incubated overnight with DMSO control, SAG (1 μM), 20-OHC (10 μM) or Shh. The cells were processed for immunofluorescence, to measure ciliary localization of Smo. The graph shows the percentage of Smo- positive cilia. MSmoL112D and mSmoW113Y have a defective response to 20-OHC and Shh.

(d) As in (c), but with box plots showing Smo fluorescence intensity at cilia. For each condition, the Smo signal was normalized to the intensity of the SAG treatment for the respective cell line.

(e) As in (c), but cells were processed for Q-PCR, to measure mRNA levels of the Hh target gene, Gli1. For each treatment, Gli1 levels were normalized to the level induced by SAG in the respective cell line. Each experiment was performed in triplicate, and the error bars show the standard deviation of the mean. MSmoL112D and mSmoW113Y do not respond to 20-OHC and have a reduced responsiveness to Shh.

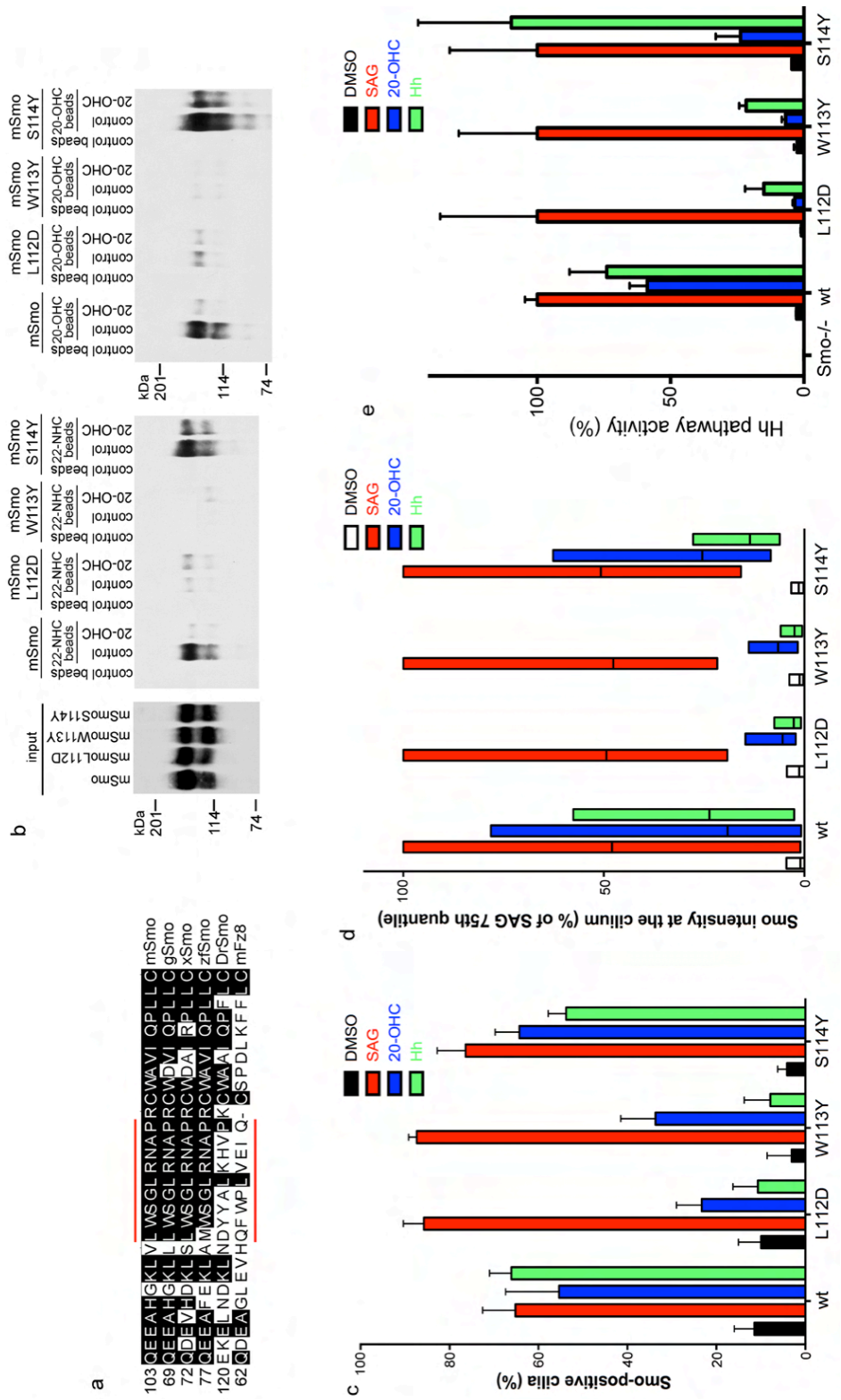

Figure 2.6 (continued) Oxysterol binding to Smo is required for high level Hh signaling

To determine if mSmo^{DrSmoCRDmut} and mSmoΔCRD respond to oxysterols, we generated Smo$^{-/-}$ MEFs that stably express the proteins at low levels, and assayed their activation by SAG and 20-OHC, both by immunofluorescence (to measure ciliary recruitment of mSmo, Supplementary Figure S5d and S5e) and by Q-PCR (to measure the transcriptional output of the Hh pathway, Supplementary Figure S5f). Both mSmo^{DrSmoCRDmut} and mSmoΔCRD rescued the response of Smo$^{-/-}$ MEFs to SAG, indicating that they are fully functional in activating the downstream steps of the Hh pathway; however, mSmo^{DrSmoCRDmut} and mSmoΔCRD did not respond to 20-OHC, in contrast to wild-type mSmo. These results validate functionally our mapping of the oxysterol-binding site within mSmoCRD.

We identified two mSmo point mutants defective in oxysterol binding by individually mutating residues in the LWS sequence (amino acids 112-114) to the corresponding DYY sequence of DrSmo. As shown in b, mSmoL112D and mSmoW113Y no longer bound 22-NHC and 20-OHC beads, in contrast to mSmoS114Y and wild-type mSmo. Importantly, mSmoL112D and mSmoW113Y showed a prominent post-Golgi band on SDS-PAGE (b) and bound BODIPY-Cyc (Supplementary Figure S5g), indicating proper folding.

To test the function of oxysterol binding to mSmo, we compared Hh signaling in Smo$^{-/-}$ MEFs stably expressing mSmo, mSmoL112D, mSmoW113Y or mSmoS114Y (see c and d for ciliary recruitment, and e for transcriptional activation). As expected, all 4 proteins rescued the response to SAG. Consistent with loss of oxysterol binding, mSmoL112D and mSmoW113Y did not respond to 20-OHC, in contrast to wild-type mSmo and mSmoS114Y. Interestingly, mSmoL112D and mSmoW113Y still responded to Shh, but the response was much reduced

compared to wild-type mSmo and mSmoS114Y. Similarly, a significantly lower response to Shh was observed in the case of mSmoΔCRD (Supplementary Figure S5h) or the double mutant mSmoL112D/W113Y (Supplementary Figure S5i). In conclusion, binding of oxysterols to the CRD is required for high-level mSmo activation by Shh; in contrast, low-level mSmo activation by Shh still occurs in the absence of oxysterol binding. This suggests that Hh signaling controls mSmo activity via Site A, or possibly via both Site A and Site B (see Discussion).

2.5 Discussion

Our findings suggest a mechanism for how the vertebrate Hh pathway is modulated by oxysterols. During Hh signaling, Shh relieves the inhibition exerted by Ptc on Smo, and a major open question is how Smo activity is regulated. Smo adopts active and inactive conformations, and it has long been hypothesized that endogenous small molecules control the equilibrium between the two conformations (Taipale et al., 2002), in turn determining the output of the Hh pathway at the membrane. Oxysterols (Corcoran and Scott, 2006; Dwyer et al., 2007), particularly 20-OHC (Nachtergaele et al., 2012), are so far the only metabolites that activate the vertebrate Hh pathway. We describe the azasterol 22-NHC, an inhibitor of Hh signaling that acts by a novel mechanism, namely by competing with 20-OHC binding to Smo. 22-NHC inhibits Shh noncompetitively, consistent with 22-NHC binding the allosteric Smo Site B. To our surprise, Site B maps to the extracellular CRD of Smo, and we show that it is completely separable from Site A (Figure 2.7a). We demonstrate that 20-OHC binding to SmoCRD is required for high Smo activation. Notably, Shh can still activate Smo mutants lacking a functional Site B, although it does so to a greatly reduced extent; thus, Site A is sufficient for

Smo to respond to Shh. These results suggest that during Hh signaling, Smo is activated by two synergistic inputs: Shh-Ptc–dependent activation of Site A and allosteric activation by oxysterol binding to Site B (Figure 2.7b). Many aspects of this mechanism remain to be deciphered, such as measuring endogenous 20-OHC, elucidating its biosynthesis and determining whether 20-OHC binding to Site B is controlled by Shh-Ptc or whether it represents an independent input.

Mapping the 20-OHC binding site to the SmoCRD confirms the prediction that the CRD of Frizzled family members is related to sterol binding proteins such as the soluble lysosomal cholesterol carrier, NPC2 (Bazan and de Sauvage, 2009). We used the crystal structure of the

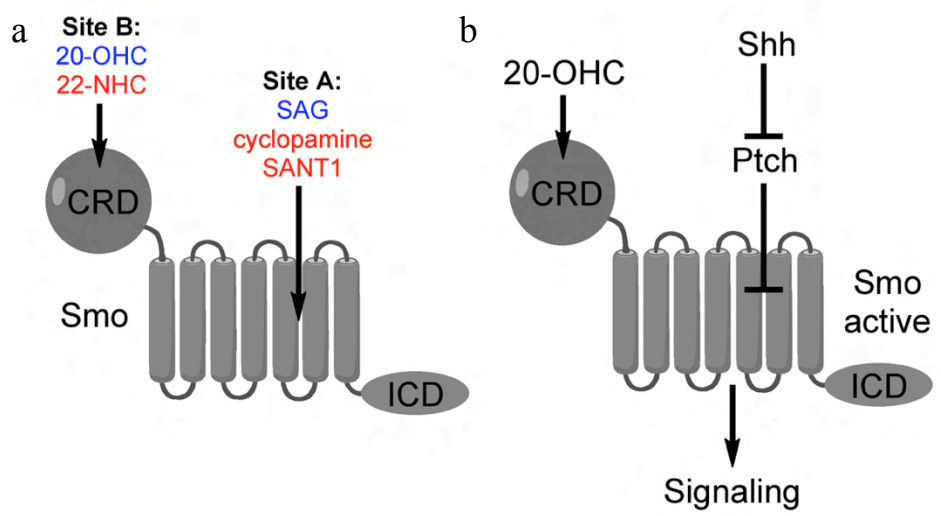

Figure 2.7 Mechanism for modulation of the vertebrate Hh pathway by oxysterols

(a) Schematic of the mSmo protein and of the location of Sites A and B. For each site, activators are in blue, while inhibitors are in red.

(b) Model for regulation of vertebrate Smo. Inhibition of Ptc by Shh results in activation of Site A of Smo. This is potentiated by the allosteric activator, 20-OHC, which binds to Site B in the extracellular domain of Smo. Active Smo then signals to the cytoplasm.

mFz8-Xwnt8 complex (Janda et al., 2012) to mutate mSmoCRD residues that align with mFz8CRD residues involved in binding the palmityl moiety of Xwnt8. These Smo mutants were defective in 20-OHC binding, suggesting that oxysterol binding to SmoCRD likely resembles binding of palmitate to mFz8CRD; structural studies will be needed to determine the exact mode of 20-OHC binding to SmoCRD. Interestingly, in the case of two other sterol-binding membrane proteins, the sterol binding sites also map to soluble portions of the protein: the Niemann-Pick protein 1 (NPC1) binds oxysterols via its N-terminal domain located in the lumen of the lysosome (Infante et al., 2008), and the SREBP cleavage-activating protein (SCAP) binds cholesterol via a large ER luminal loop (Motamed et al., 2011). It will be important to determine if this is a general feature among sterol-binding membrane proteins.

An important question is how Sites A and B of Smo are regulated during Hh signaling. No endogenous small molecule that binds Site A has been identified so far, and it is unclear whether such a molecule would be an agonist (which Ptc would prevent from reaching Smo) or antagonist (which Ptc would deliver to Smo). Our results indicate that Ptc controls Smo at least in part through regulation of Site A, but they cannot distinguish between these two alternative mechanisms. The situation is clearer for Site B, which, during Hh signaling, needs to be occupied by an endogenous activator, perhaps 20-OHC. This conclusion is based on the inhibitory effect of sterol depletion and of blocking 20-OHC binding to Smo. The endogenous concentration of oxysterols like 20-OHC is currently unknown, but is likely much lower than the micromolar EC_{50} for Hh pathway activation by oxysterols. Although higher local concentrations might exist in cells, endogenous oxysterol levels are perhaps too low to activate Smo just by

themselves, but high enough to synergize with Site A activation. One advantage of such a mechanism is that it allows a Shh-independent way to modulate Hh signaling, while ensuring that pathway activation remains strictly dependent on Shh and Ptc. Oxysterol levels might vary in different tissues, thus allowing for different levels of Hh signaling. Whole animal studies will be important in determining if the Hh pathway is differentially modulated by oxysterols in various tissues undergoing Hh signaling.

Another important question is how the allosteric interaction between Sites B and A result in Smo activation during Hh signaling triggered by Shh? It seems likely that SmoCRD binds 20-OHC and the resulting complex interacts with the heptahelical bundle of Smo, contributing to stabilizing the active conformation of Site A. An active Site A is required for oxysterols to stimulate Hh signaling, as Site A inhibitors such as Cyc and SANT1 inhibit oxysterols (Corcoran and Scott, 2006; Dwyer et al., 2007; Nachtergaele et al., 2012). SmoCRD, however, is not required for Smo activation by synthetic agonists such as SAG that bind Site A, suggesting that Site B has only a modulating role during Shh stimulation. Perhaps endogenous activation of Site A is weaker than that elicited by SAG, and as a result oxysterols are required for high-level Smo activation. Detailed biochemical and structural studies will be needed to determine how the interaction between Sites A and B controls vertebrate Smo activity.

The azasterol 22-NHC represents the first Site B-specific inhibitor of Smo. 22-NHC inhibits Hh pathway activation by Shh and by oxysterols, but cannot inhibit Smo activated by SAG, or the constitutively active SmoM2 mutant. Thus 22-NHC recapitulates the inhibitory effect of sterol depletion or of cholesterol biosynthesis defects on vertebrate Hh signalling

(Cooper et al., 2003). The simplest interpretation is that sterol depletion removes the endogenous activator of Site B, which is perhaps 20-OHC. It should be pointed out that blocking HMG-CoA reductase with statins without also depleting sterols does not block Hh signaling (Cooper et al., 2003), and thus the effect of 22-NHC is not explained by general inhibition of cholesterol biosynthesis. We cannot exclude the possibility that, in addition to binding Smo, 22-NHC might also block conversion of cholesterol into an unknown metabolite, such as an oxysterol.

2.6 Acknowledgements

We thank Yoshito Kishi and members of his laboratory for help with chiral chromatography of diastereomeric 20-OHC analogs. A.S. is supported in part by NIH grant RO1 GM092924. The authors declare no competing financial interests.

2.7 Methods

2.7.1 Antibodies

Polyclonal antibodies against Cherry were generated in rabbits (Cocalico Biologicals) and were affinity purified against recombinant Cherry immobilized on Affigel-10 beads (BioRad). Rabbit anti-Smo polyclonal antibodies were described before (Tukachinsky et al., 2010). The monoclonal anti-acetylated tubulin antibody was obtained from Sigma.

2.7.2 DNA constructs

Expression constructs were assembled by PCR in the mammalian expression vector pCS2+, from which they were subcloned into a vector for lentiviral production. Constructs encoding membrane proteins were tagged with Cherry at their C-terminus. These constructs were: full-length mouse Smo (mSmo), full-length Drosophila Smo (DrSmo), full-length mouse Frizzled (mFz7), $mSmo^{\Delta ICD}$ (aminoacids 1-554 of mSmo), mSmoM2 (constitutively active point mutant W539L), $mSmo^{\Delta CRD}$ (amino acids 183-793 of mSmo, preceded by the signal sequence of human calreticulin), $mSmo^{DrSmoCRDmut}$ (amino acids 112-119 of mSmo, LWSGLRNA, replaced by amino acids 129-136 of DrSmo, DYYALKHV), mSmoL112D, mSmoW113Y, mSmoS114Y, mSmoL112D/W113Y. Full-length Xenopus Smo (xSmo) was tagged with eGFP at the C-terminus and was expressed in Sf9 cells by baculoviral infection. The baculovirus was generated using the Bac-to-bac system (Life Sciences), according to the manufacturer's instructions. Constructs for expressing secreted extracellular cysteine-rich domains (CRDs) of Smo proteins contained the signal sequence of human calreticulin, followed by the CRD sequence lacking the

Smo signal sequence, followed by a hemagglutinin (HA) tag and 8 histidine residues. The CRD sequences were: mSmoCRD (amino acids 32-236 of mSmo), DrSmoCRD (amino acids 32-257 of DrSmo) and mSmoCRD^{DrSmoCRDmut} (amino acids 32-236 of mSmo^{DrSmoCRDmut}).

2.7.3 Cell culture and generation of stable cell lines

NIH-3T3 and Shh Light II cells were grown in Dulbecco's Modified Eagle's Medium (DMEM) supplemented with 10% bovine calf serum, penicillin and streptomycin. Mouse embryonic fibroblasts (MEFs) and 293T cells were grown in DMEM with 10% fetal bovine serum, penicillin and streptomycin. Stable cell lines were generated by lentiviral transduction, followed by selection with blasticidin 50μg/mL for 3 days. Smo$^{-/-}$ MEFs expressing low amounts of various Cherry-tagged Smo proteins were isolated by fluorescence-activated cell sorting. Expression of the tagged construct was confirmed by immunofluorescence and by QPCR assays of Hh pathway stimulation. The following compounds were obtained from commercial sources: cyclopamine (LC Laboratories), BODIPY-cyclopamine (TRC), SAG (Axxora), forskolin (Sigma), itraconazole (Sigma), SANT1 (Calbiochem), GDC0449 (LC Laboratories), 20-hydroxycholesterol (Steraloids), 7-hydroxycholesterol (Steraloids).

2.7.4 Hh ligand production

Hh ligand was produced by transiently transfecting 293T cells with an expression plasmid encoding amino acids 1-198 of human Shh. Shh was collected for 48 hours into starvation medium (DMEM supplemented with penicillin and streptomycin). For maximal

stimulation of the Hh pathway, Shh- conditioned medium was used diluted 1:3 -1:4 into fresh starvation medium.

2.7.5 Reporter assays

Hh activity assays were performed in Shh Light II cells (obtained from ATCC), a line of NIH-3T3 cells expressing firefly luciferase from a Gli-responsive promoter and Renilla luciferase from a constitutive promoter (Taipale et al., 2000). Confluent Shh Light II cultures were starved overnight in DMEM. The medium was then replaced with DMEM supplemented with the appropriate Hh pathway agonist, antagonist, and/or test compound. All small molecules were added to cellular media from concentrated stocks in DMSO, except 20-OHC-Pent-3β-MeO, which was added as a soluble complex with methyl-β-cyclodextrin (MCD), prepared as described (Klein et al., 1995). After 30 hours, Renilla and firefly luciferase levels were measured using the Dual-Glo kit (Promega). Hh pathway activity was expressed as the ratio of firefly to Renilla luciferase, normalized to 100% for maximally stimulated cells (cells treated with 1μM SAG, 10 μM oxysterol, or 1:3 Shh ligand, depending on the experiment). Each experiment was performed in quadruplicate, and error bars represent the standard deviation of the mean. For plotting dose-response curves, non-linear regression to a four-parameter curve was performed using Prism (GraphPad).

2.7.6 Real-time PCR assays of the Hh pathway

Confluent NIH-3T3 cells or MEFs were starved overnight in starvation medium, after which they were incubated for 24 hours in starvation medium supplemented with the desired

compounds. Total RNA was isolated from cells with RNA-Bee (TelTest), treated with RNase-free DNase (Promega), and purified using the GenCatch total RNA Extraction System (Epoch Biolabs). Reverse transcription was performed using random hexamers and Transcriptor reverse transcriptase (Roche). Transcription of the Hh target gene Gli1 was measured by real-time PCR using FastStart SYBR Green Master reagent (Roche) on a Rotor-Gene 6000 (Corbett Robotics). Relative gene expression was calculated using a Two Standard Curve method in which the gene-of-interest was normalized to the Ribosomal Protein L27 gene. The sequences for gene-specific primers are: L27: 5'-GTCGAGATGGGCAAGTTCAT-3' and 5'-GCTTGGCGATCTTCTTCTTG-3', Gli1: 5'-GGCCAATCACAAGTCAAGGT-3' and 5'-TTCAGGAGGAGGGTACAACG -3'. Each experiment was performed in triplicate, and error bars represent standard error of the mean.

2.7.7 Immunofluorescence

Cells were grown on glass coverslips and were fixed in PBS with 4% formaldehyde, followed by permeabilization with TBST. Non-specific binding sites were blocked by incubation in TBST with 50 mg/mL bovine serum albumin (TBST-BSA). Endogenous mSmo was detected with anti-Smo antibodies (Tukachinsky et al., 2010) and Cherry-tagged proteins were detected with anti-Cherry antibodies. Primary cilia were stained with anti-acetylated tubulin antibodies. Primary and secondary antibodies were used diluted in TBST-BSA. The primary antibodies were: rabbit polyclonal against Cherry (final concentration 1 μg/mL), rabbit polyclonal against mSmo (final concentration 2 μg/mL), mouse anti-acetylated tubulin monoclonal antibody (Sigma, final dilution dilution of 1:5,000). Alexa-594- and Alexa-488-conjugated secondary

antibodies (Life Sciences) were used at a final concentration of 1 μg/mL. The coverslips were mounted on glass slides in mounting media (0.5% p-phenylenediamine, 20 mM Tris pH 8.8, 90% glycerol). The cells were imaged by epifluorescence on a Nikon TE2000E microscope equipped with an OrcaER camera (Hammamatsu) and 40x PlanApo 0.95NA or 100x PlanApo 1.4NA oil objective (Nikon). Images were acquired using the Metamorph software (Applied Precision). Ciliary localization of Smo was measured either manually or using custom image analysis software implemented in MATLAB. Briefly, the software first identifies cilia by local adaptive thresholding of images of cells stained for acetylated tubulin. The segmented images are cleaned by automatic removal of objects whose size and shape fall outside the normal range for a typical cilium. Next, the pixel intensity of the protein of interest (Smo) in each cilium is corrected by subtracting the local background, defined as the median intensity of the pixels surrounding the cilium. Ciliary Smo is then quantified as the total corrected intensity in each cilium, normalized to the area of the cilium. To count Smo-positive cilia, fluorescence in the Smo channel is first calculated for the cilia in the negative control sample (untreated cells in case of scoring endogenous Smo, or $Smo^{-/-}$ cells in case of scoring Cherry-tagged fusions proteins stably expressed in $Smo^{-/-}$ MEFs). This data is used to calculate a threshold value that is above the fluorescence intensity for >95% of cilia in the negative control sample; note that this method overestimates the number of Smo-positive cilia in the negative control, by allowing a false positive rate of up to 5% in this sample. Using the calculated threshold value, cilia are then scored in all remaining samples, and the fraction of Smo-positive cilia is graphed. Ciliary intensity of Smo is also graphed using box plots; for each condition, the lower and upper bounds

of the box represent the 25th and 75th percentile of the Smo intensity distribution, while the horizontal line represents the median intensity across the entire cilia population. A more detailed description of the algorithm is provided in the Appendix. For the experiments presented in this study, between 150-550 cilia per condition were analyzed in this manner. For some experiments, ciliary localization of Smo was measured manually, by scoring the presence or absence of Smo in 150 cilia for each condition.

2.7.8 BODIPY-cyclopamine and BODIPY-SANT1 binding assays

Various Smo proteins, tagged at their C-termini with Cherry, were expressed in 293T cells either stably or by transient transfection. The cells were incubated for 1 hour in DMEM with 10 nM BODIPY- cyclopamine or 10 nM BODIPY-SANT1, in the presence or absence of the indicated concentration of competitor drug. The cells were washed with DMEM, fixed in PBS with 4% formaldehyde for 20 minutes, followed by 5 washes with TBST (10 mM Tris pH 7.5, 150 mM NaCl, 0.2% Triton X-100). The cells were then imaged by epifluorescence microscopy, capturing for each field of view an image of the Smo-Cherry fusion and one of the BODIPY compound.

2.7.9 Preparation of ligand affinity matrices

Free amine derivatives of 22-NHC or 20-OHC were dissolved in dry isopropanol (20 mM final concentration), and were added to amine-reactive Affigel-10 beads (BioRad). After addition of dry triethylamine (100 mM final), the beads were incubated at room temperature overnight, with end-over- end rotation. Unreacted sites on the beads were consumed by incubation with

ethanolamine (1M final in isopropanol), after which the beads were washed extensively with isopropanol. The beads were then washed extensively with water, followed by 3 washes with the wash buffer used in ligand affinity experiments (20 mM HEPES pH 7.5, 150 mM NaCl, 0.1% dodecyl-β-maltoside). Control beads were generated in parallel, by reacting Affigel-10 beads with the ethylene glycol diamine linker (4,7,10-trioxa- 1,13-tridecanediamine, 200 mM final) used in the synthesis of 22-NHC or 20-OHC amine derivatives.

2.7.10 Ligand affinity assays

Recombinant protein for ligand affinity assays was produced by stable or transient expression in 293T cells, except for xSmo-eGFP, which was produced in Sf9 cells by baculovirus infection. Cell expressing various transmembrane Smo constructs, C-terminally tagged with Cherry or eGFP, were harvested and lysed on ice for 30 minutes in lysis buffer (20 mM HEPES, pH 7.5, 150 mM NaCl, 0.5% dodecyl-β- maltoside), supplemented with protease inhibitors (leupeptin, pepstatin and chymostatin at 10 μg/mL final concentration). The detergent extract was clarified by centrifugation at 20,000g, for 30 min at 4C. The supernatant was first incubated with the desired competitor compound or DMSO control for 5 minutes on ice. All compounds were added to binding reactions from DMSO stock solutions. After this incubation, 22-NHC beads, 20-OHC beads or control beads were added, followed by end-over-end rotation for 1 hour at 4C. The beads were washed three times with wash buffer (20 mM HEPES pH 7.5, 150 mM NaCl, 0.1% dodecyl-β-maltoside), after which bound proteins were eluted in SDS-PAGE sample buffer with DTT (50 mM final) at 37C. The proteins were separated by SDS-

PAGE, followed by immunoblotting with anti- Cherry or anti-GFP antibodies. A portion of the clarified detergent extract was used as input.

Cells expressing HA-tagged secreted SmoCRD contructs were incubated for 48 hours in DMEM supplemented with 0.5% fetal bovine serum, penicillin and streptomycin. The conditioned media containing soluble SmoCRD protein was harvested, subjected to centrifugation to remove cellular debris, and concentrated 10-fold by ultrafiltration through a 10 kDa cutoff concentration device (Amicon). The media was then supplemented with dodecyl-β-maltoside (0.5% final concentration) and protease inhibitors, and was used in ligand affinity assays as described above for detergent extracts of cells expressing full-length Smo proteins.

2.8 Chemicals

A complete description of the syntheses of sterol derivatives and of BODIPY-SANT1 is provided in the Appendix.

2.9 References

Bazan, J.F., and F.J. de Sauvage. 2009. Structural ties between cholesterol transport and morphogen signaling. *Cell*. 138:1055-1056.

Chen, J.K., J. Taipale, M.K. Cooper, and P.A. Beachy. 2002a. Inhibition of Hedgehog signaling by direct binding of cyclopamine to Smoothened. *Genes Dev*. 16:2743-2748.

Chen, J.K., J. Taipale, K.E. Young, T. Maiti, and P.A. Beachy. 2002b. Small molecule modulation of Smoothened activity. *Proc Natl Acad Sci U S A*. 99:14071-14076.

Cooper, M.K., C.A. Wassif, P.A. Krakowiak, J. Taipale, R. Gong, R.I. Kelley, F.D. Porter, and P.A. Beachy. 2003. A defective response to Hedgehog signaling in disorders of cholesterol biosynthesis. *Nat Genet*. 33:508-513.

Corbit, K.C., P. Aanstad, V. Singla, A.R. Norman, D.Y. Stainier, and J.F. Reiter. 2005. Vertebrate Smoothened functions at the primary cilium. *Nature*. 437:1018-1021.

Corcoran, R.B., and M.P. Scott. 2006. Oxysterols stimulate Sonic hedgehog signal transduction and proliferation of medulloblastoma cells. *Proc Natl Acad Sci USA*. 103:8408-8413.

Dwyer, J.R., N. Sever, M. Carlson, S.F. Nelson, P.A. Beachy, and F. Parhami. 2007. Oxysterols are novel activators of the hedgehog signaling pathway in pluripotent mesenchymal cells. *J Biol Chem*. 282:8959-8968.

Frank-Kamenetsky, M., X.M. Zhang, S. Bottega, O. Guicherit, H. Wichterle, H. Dudek, D. Bumcrot, F.Y. Wang, S. Jones, J. Shulok, L.L. Rubin, and J.A. Porter. 2002. Small-molecule modulators of Hedgehog signaling: identification and characterization of Smoothened agonists and antagonists. *J Biol*. 1:10.

Infante, R.E., A. Radhakrishnan, L. Abi-Mosleh, L.N. Kinch, M.L. Wang, N.V. Grishin, J.L. Goldstein, and M.S. Brown. 2008. Purified NPC1 protein: II. Localization of sterol binding to a 240-amino acid soluble luminal loop. *J Biol Chem*. 283:1064-1075.

Ingham, P.W., and A.P. McMahon. 2001. Hedgehog signaling in animal development: paradigms and principles. *Genes Dev*. 15:3059-3087.

Janda, C.Y., D. Waghray, A.M. Levin, C. Thomas, and K.C. Garcia. 2012. Structural basis of Wnt recognition by Frizzled. *Science*. 337:59-64.

Kim, J., J.Y. Tang, R. Gong, J. Kim, J.J. Lee, K.V. Clemons, C.R. Chong, K.S. Chang, M. Fereshteh, D. Gardner, T. Reya, J.O. Liu, E.H. Epstein, D.A. Stevens, and P.A. Beachy. 2010. Itraconazole, a commonly used antifungal that inhibits Hedgehog pathway activity and cancer growth. *Cancer Cell*. 17:388-399.

Klein, U., G. Gimpl, and F. Fahrenholz. 1995. Alteration of the myometrial plasma membrane cholesterol content with beta-cyclodextrin modulates the binding affinity of the oxytocin receptor. *Biochemistry*. 34:13784-13793.

Lum, L., and P.A. Beachy. 2004. The Hedgehog response network: sensors, switches, and routers. *Science*. 304:1755-1759.

Motamed, M., Y. Zhang, M.L. Wang, J. Seemann, H.J. Kwon, J.L. Goldstein, and M.S. Brown. 2011. Identification of luminal Loop 1 of Scap protein as the sterol sensor that maintains cholesterol homeostasis. *J Biol Chem*. 286:18002-18012.

Nachtergaele, S., L.K. Mydock, K. Krishnan, J. Rammohan, P.H. Schlesinger, D.F. Covey, and R. Rohatgi. 2012. Oxysterols are allosteric activators of the oncoprotein Smoothened. *Nat Chem Biol*. 8:211-220.

Robarge, K.D., S.A. Brunton, G.M. Castanedo, Y. Cui, M.S. Dina, R. Goldsmith, S.E. Gould, O. Guichert, J.L. Gunzner, J. Halladay, W. Jia, C. Khojasteh, M.F. Koehler, K. Kotkow, H. La, R.L. Lalonde, K. Lau, L. Lee, D. Marshall, J.C. Marsters, Jr., L.J. Murray, C. Qian, L.L. Rubin, L. Salphati, M.S. Stanley, J.H. Stibbard, D.P. Sutherlin, S. Ubhayaker, S. Wang, S. Wong, and M. Xie. 2009. GDC-0449-a potent inhibitor of the hedgehog pathway. *Bioorg Med Chem Lett*. 19:5576-5581.

Rohatgi, R., L. Milenkovic, R.B. Corcoran, and M.P. Scott. 2009. Hedgehog signal transduction by Smoothened: pharmacologic evidence for a 2-step activation process. *Proc Natl Acad Sci U S A*. 106:3196-3201.

Rohatgi, R., L. Milenkovic, and M.P. Scott. 2007. Patched1 regulates hedgehog signaling at the primary cilium. *Science*. 317:372-376.

Sinha, S., and J.K. Chen. 2006. Purmorphamine activates the Hedgehog pathway by targeting Smoothened. *Nat Chem Biol*. 2:29-30.

Svard, J., K. Heby-Henricson, M. Persson-Lek, B. Rozell, M. Lauth, A. Bergstrom, J. Ericson, R. Toftgard, and S. Teglund. 2006. Genetic elimination of Suppressor of fused reveals an essential repressor function in the mammalian Hedgehog signaling pathway. *Dev Cell*. 10:187-197.

Taipale, J., J.K. Chen, M.K. Cooper, B. Wang, R.K. Mann, L. Milenkovic, M.P. Scott, and P.A. Beachy. 2000. Effects of oncogenic mutations in Smoothened and Patched can be reversed by cyclopamine. *Nature*. 406:1005-1009.

Taipale, J., M.K. Cooper, T. Maiti, and P.A. Beachy. 2002. Patched acts catalytically to suppress the activity of Smoothened. *Nature*. 418:892-897.

Tukachinsky, H., L.V. Lopez, and A. Salic. 2010. A mechanism for vertebrate Hedgehog signaling: recruitment to cilia and dissociation of SuFu-Gli protein complexes. *J Cell Biol*. 191:415-428.

Wang, Y., Z. Zhou, C.T. Walsh, and A.P. McMahon. 2009. Selective translocation of intracellular Smoothened to the primary cilium in response to Hedgehog pathway modulation. *Proc Natl Acad Sci U S A*. 106:2623-2628.

Chapter 3: Mechanisms of Smo ciliary localization

The following section contains previously published material from:

Nedelcu D., Liu J., Xu Y., Jao C. and Salic A., Oxysterol binding to the extracellular domain of Smoothened in Hedgehog signaling. Nature Chemical Biology 9: 557–564 (2013) doi:10.1038/nchembio.1290

3.1 Author contributions

I performed cellular and biochemical experiments. Y.X. and I developed the automated image analysis software, and I analyzed all the imaging data.

3.2 Abstract

Signal transduction in the vertebrate Hedgehog (Hh) pathway is sequestered at the primary cilium, which serves as an anchor point for the Hh pathway components such as Patched (Ptc) and Smoothened (Smo). However, it is unclear how these proteins reach the primary cilium, and what happens subsequent to activation. In this work, we identify two degenerate ciliary localization sequences in Smo. We further map a cytosolic domain of Smo strictly required for activation of downstream components, and show that while the ciliary localization aspect is unique to vertebrates, signaling to downstream components is conserved across phyla.

3.3 Introduction

The primary cilium is a highly conserved structure, which exists in most animal cells and serves as an anchoring point to a variety of receptors including some G-Protein Coupled Receptors to increase their local concentration; the cilium thus serves as a cellular antenna for sensing the presence of nutrients or growth factors. Structurally, the cilium is comprised of a hair-like membrane projection with a unique lipid composition which surrounds a bundle of microtubules – the axoneme.

Cell-cell signaling via the Hedgehog (Hh) pathway is critical for numerous aspects of metazoan embryonic development and regeneration, while excessive Hh signaling is involved in many cancers (Ingham and McMahon, 2001; Lum and Beachy, 2004). Signaling in the pathway is triggered when the secreted protein Hedgehog (Hh, or one of three vertebrate orthologs, primarily Sonic hedgehog, Shh) binds to its membrane receptor, Patched (Ptc) (Stone et al., 1996). Ptc normally inhibits the 7-pass transmembrane protein Smoothened (Smo). Binding of Hh inhibits Patched resulting in Smo activation; active Smo then triggers the activators of the cytoplasmic steps of the signaling pathway, which ultimately induce transcription of the Hh target genes(Rohatgi and Scott, 2007). The spatial localization of the Hedgehog pathway components in vertebrates provides an additional layer of regulation, as primary cilia are essential for transduction of the Hedgehog signal across the membrane (Huangfu and Anderson, 2005). In the absence of signal, Smo appears primarily in intracellular vesicles, while Ptc localizes to the base of the primary cilium. Upon activation by Shh, Ptc is internalized which allows Smo to accumulate at the primary cilium where the intracellular components of the Hh

signaling pathway reside, to physically associate with the ciliary protein Evc2, and to activate downstream signaling; Smo also localizes to the cilium when overexpressed (Corbit et al., 2005; Dorn et al., 2012; Rohatgi et al., 2007; Rohatgi and Scott, 2007). However, the mechanism of Smo translocation to the cilium remains unclear.

No protein synthesis takes place at the primary cilium, thus all the proteins in the cilium are synthesized in the cell body and then delivered to the cilium via specific targeting mechanisms; cargo is then moved along the cilium to and from the distal tip by intraflagellar transport (IFT) proteins; interestingly, this includes the tubulin building blocks required for elongation of the cilium. Genetic screens have identified two protein complexes involved in ciliary transport - IFT-A and IFT-B (Ou et al., 2005). The cilium is a unique structure in that, while contiguous with the plasma membrane, it is essentially isolated from the plasma membrane as a separate compartment. The IFT-A and IFT-B complexes function together in both anterograde and retrograde transport, as they associate with each other prior to movement along the cilium. The BBSome is a coat protein complex essential for ciliary formation which catalyzes the assembly of cargo-loaded IFT complexes at the base of the cilium. The IFT-A/IFT-B complexes transport both cargo and substoichiometric amounts of BBSome to the distal end of the cilium where the complex dissociates and the cargo is unloaded. The BBSome at the ciliary tip then facilitates the reassociation of the IFT-A and IFT-B, which in turn recycles both components as well as cargo (which includes the BBSome) back to the base of the cilium. The BBSome thus functions to associate IFT-A to IFT-B in both the basal body and at the ciliary tip (Wei et al., 2012).

Ciliary access is tightly regulated, as ciliary proteins must contain a cis-acting ciliary localization sequence (CLS) to access the primary cilium; several different CLS have been identified to date, but there is no conservation of sequence among them (Pazour and Bloodgood, 2008). Interestingly, certain functional CLS resemble nuclear localization sequences and consist of stretches of basic residues on soluble proteins (Dishinger et al., 2010) or a motif of adjacent hydrophobic and basic residues immediately C-terminal to the seventh transmembrane domain of certain seven spanners, in particular olfactory GPCRs (Dwyer et al., 2001). Opsin trafficking to the outer segments of vertebrate photoreceptors requires the presence of a conserved C-terminal VxP motif. However, it must be noted that other CLS exist, such as the N-terminal RVxP motif of Polycystin-2 (Geng et al., 2006), or the conserved AX[S/A]XQ motif found in the third intracellular loop of many ciliary-targeted GPCRs such as the serotonin receptor 6 (5HT6), the somatostatin receptor 3 (SSTR3) and the melanocortin concentrating hormone receptor 1 (MCHR1); this latter sequence is bound directly by the BBSome rather than by importins, and facilitates ciliary entry through a parallel mechanism (Berbari et al., 2008; Jin et al., 2010). Without exception, the CLS identified to date are all cytosolic domains, indicating that sorting into the ciliary membrane involves soluble regions. Smo ciliary localization, however, has been shown previously to be regulated by the extracellular cysteine-rich domain (CRD) (Aanstad et al., 2009); in Chapter 2, we demonstrate that the CRD functions as a sterol binding domain, and that it does not contain the ciliary localization sequence of Smo, as the mSmo$^{\Delta CRD}$ mutant localizes robustly to the cilium in response to SAG (Figure 2.S5). Thus, the identity of the cis-acting CLS of Smo remains unknown. Here we demonstrate that the CLS of Smo is found within

its cytosolic tail, the intracellular domain (ICD), and that it is degenerate as two separate sequences can mediate Smo ciliary localization; we further show that the CLS is essential but not sufficient for relaying the signal to downstream components.

3.4 Results

3.4.1 Only vertebrate but not arthropod Smo localizes to the cilia

Although Smo is conserved between vertebrates and Drosophila, we have previously shown (Chapter 2) that only vertebrate Smo binds oxysterols, raising the question of whether regulation of Smo is conserved across phyla. To begin addressing this issue, we asked if Drosophila Smo (DrSmo) retains any signaling activity in vertebrate cells. When stably expressed in $Smo^{-/-}$ MEFs, DrSmo did not localize to cilia (Figure 3.1a) and was thus inactive (Figure 3.1b); this result was not surprising, as cilia are not involved in Hh signaling in Drosophila but are essential for Hh signaling in vertebrates; it is conceivable that DrSmo cannot interact with the downstream vertebrate pathway components as they are sequestered in the ciliary compartment. Alternatively, it is also possible that DrSmo does not interact with any of the vertebrate Hh pathway components, as would be suggested by the divergent regulation of signaling downstream of Smo in arthropods and vertebrates. To distinguish these possibilities, we needed to direct DrSmo to cilia, and for this we characterized the ciliary localization determinants of murine Smo (mSmo).

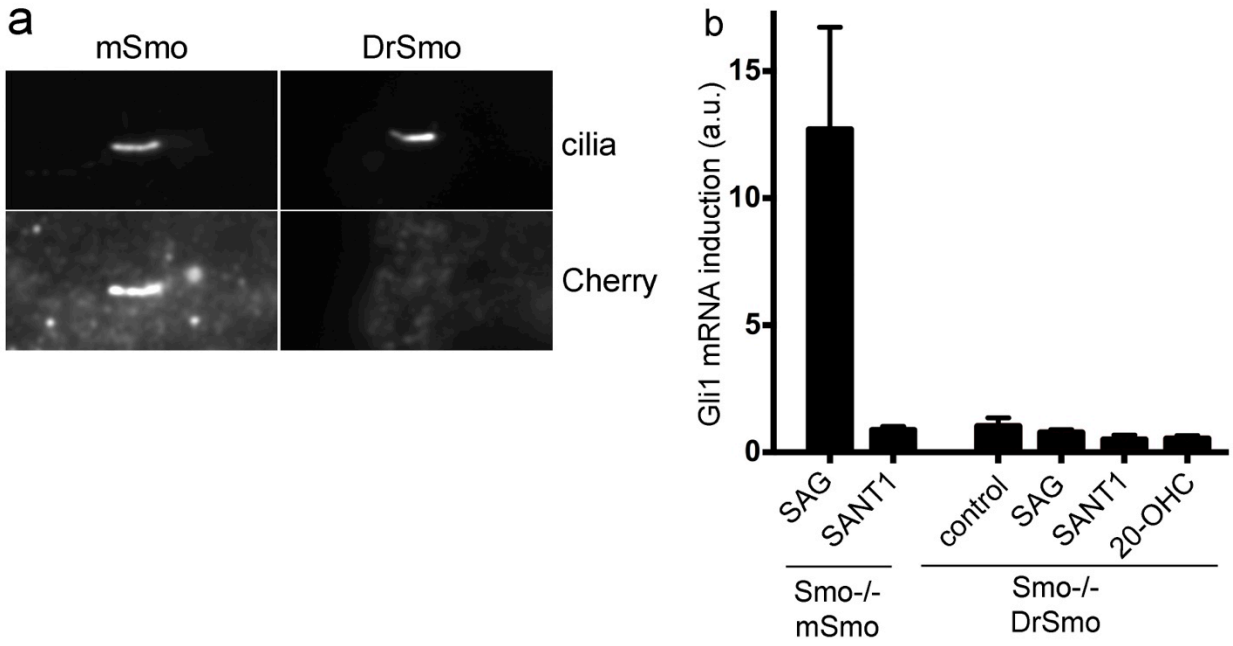

Figure 3.1 Vertebrate but not arthropod Smo localizes to the cilia

(a) DrSmo tagged with mCherry at the C-terminus, was stably expressed in $Smo^{-/-}$ MEFs. $Smo^{-/-}$ MEFs rescued with mCherry-tagged mSmo were used as positive control. Confluent cultures were starved overnight in DMEM (to promote ciliogenesis), after which the cells were fixed and processed for immunofluorescence with anti-mCherry antibodies (to visualize the fusion protein) and anti-acetylated tubulin antibodies (to visualize cilia). The micrographs show representative images of cilia. DrSmo does not localize to cilia, in contrast to mSmo.

(b) As in (a) but with overnight incubation in the presence of DMSO control, SAG (1 μM), SANT1 (1 μM), or 20-OHC (10 μM). Cells were harvested and the transcription of the target gene Gli1 was measured by Q-PCR. DrSmo does not rescue Hh signaling in $Smo^{-/-}$ MEFs, in contrast to mSmo.

3.4.2 The previously reported ciliary localization defective mutant does in fact localize to the primary cilium. The SAG binding site in the transmembrane region does not mediate ciliary localization.

Since Smo translocates to the cilium primarily through lateral diffusion from the plasma membrane in response to Shh (Milenkovic et al., 2009), and since the SAG binding site is embedded within the heptahelical transmembrane domain core of the protein, we hypothesized that Smo ciliary localization is mediated by interactions between a Smo transmembrane region and some other transmembrane protein.

We generated chimeras in which individual transmembrane domains of mSmo are replaced with the corresponding TM domains of DrSmo. The transmembrane domains show higher conservation of residues between Drosophila and vertebrates than the rest of the protein, and swapping individual domains between the two species to generate chimeras is more likely to result in a protein that folds properly (Figure 3.2a).

We have identified several mutants that are inactive when overexpressed, in stark contrast with wildtype Smo which has a high basal activity; however, all chimeras with the exception of $mSmo^{DrSmoTM7}$ respond well to stimulation by SAG. This raised the possibility that the vertebrate Smo TM7 mediates its ciliary localization; this was particularly interesting as the constitutively active mutant mSmoM2 has a point mutation which maps to a residue within TM7. However, all mutants including $mSmo^{DrSmoTM7}$ respond to stimulation with Shh or oxysterols by localizing to the cilium (data not shown) and triggering downstream activation (Figure 3.2b). Furthermore, when localized to the cilium by treatment with 20-OHC, $mSmo^{DrSmoTM7}$ binds the

Figure 3.2 mSmo mutants show variable responses to ligands, but localize to the cilium

(a) Sequence alignment of the transmembrane region of mouse and Drosophila Smo. Shaded residues are conserved across species. Individual transmembrane (TM) domains are highlighted in the alignment and were individually swapped from Drosophila Smo into mouse Smo to create the mSmo^{DrSmoTMx} chimeras

(b) mouse Smo domain swap mutants, in which individual transmembrane domains were replaced with the corresponding Drosophila Smo transmembrane domain, localize to the cilium by immunofluorescence. Smo$^{-/-}$ MEFs, stably expressing wildtype mSmo, mSmo^{DrSmoTM1}, mSmo^{DrSmoTM2}, mSmo^{DrSmoTM3}, mSmo^{DrSmoTM4}, mSmo^{DrSmoTM5}, mSmo^{DrSmoTM6}, mSmo^{DrSmoTM7}, mSmo^{CLD}, mSmo^{TM1LL} or DrSmo constructs fused at the C-terminus to mCherry, were incubated with DMEM overnight, then washed and incubated with control medium, 200nM SAG, 1μM SANT-1 or 10μM 20-OHC in DMEM for another 24hrs. The cells were fixed and processed for immunofluorescence with anti-mCherry antibodies (to visualize the fusion protein) and anti-acetylated tubulin antibodies (to visualize cilia); the positive cilia were scored visually. All mutants localize to the cilium in response to 20-OHC, even mSmoCLD which was previously reported as a ciliary localization defective mutant. All mutants except mSmo^{DrSmoTM5} and mSmo^{DrSmoTM7} also localize to the cilium when overexpressed.

(c) as in (b) but the cells were processed for Q-PCR, to measure Gli1 transcription. Each experiment was performed in triplicate, and the error bars show the standard deviation of the mean.

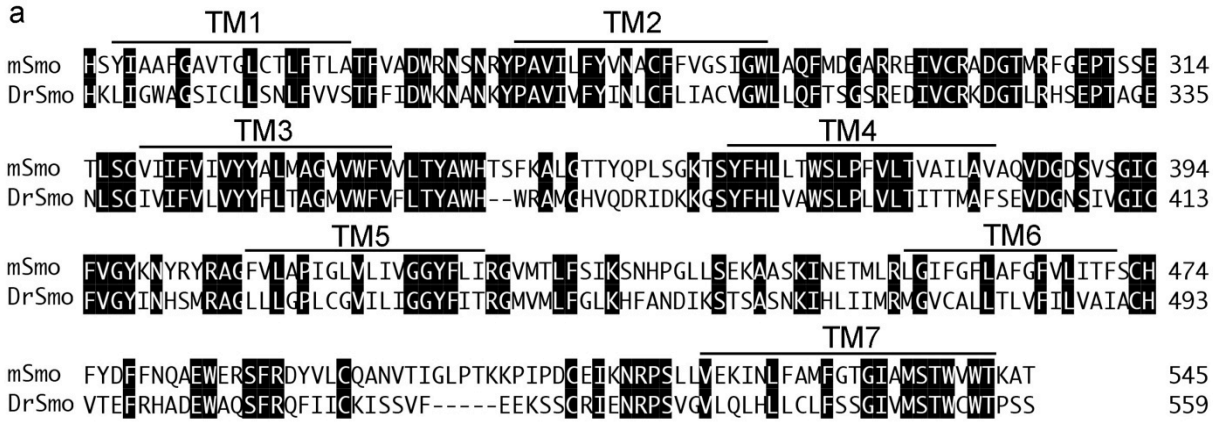

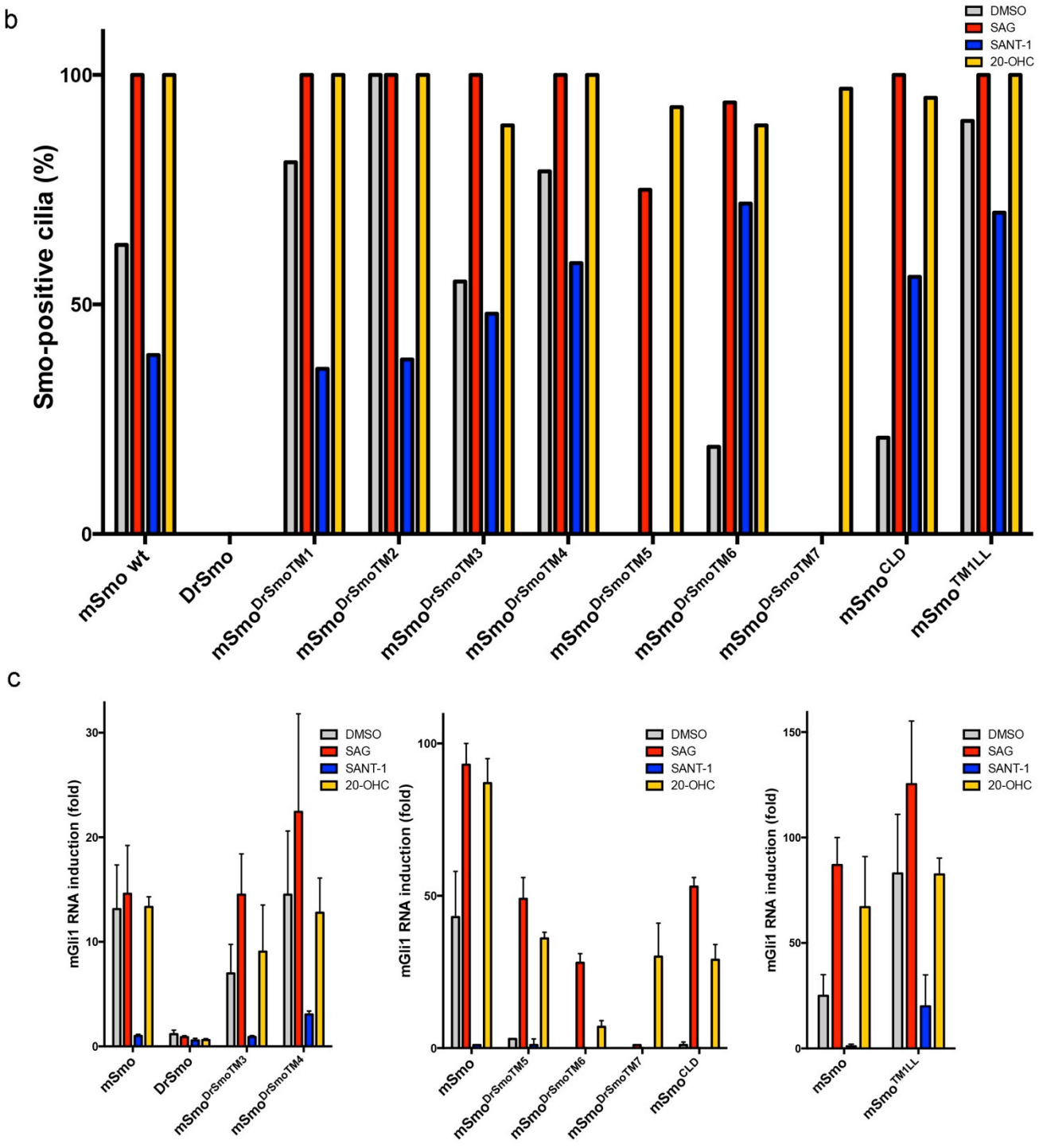

Figure 3.2 (continued) mSmo mutants show variable responses to ligands, but localize to the cilium

fluorescent cyclopamine derivative BODIPY-cyclopamine in a competitive manner. This suggests that rather than playing a role in ciliary recruitment, TM7 is intimately linked to the cyclopamine and SAG binding site, and while allowing the ligand to bind, the $mSmo^{DrSmoTM7}$ mutant fails to relay the signal to the intracellular effector part of Smo. Taken together, the $mSmo^{DrSmoTM7}$ mutant has an intact ciliary localization sequence but a defective response to binding at the SAG binding site.

Previous work has identified a putative ciliary localization motif consisting of an aromatic residue followed by a basic residue in the cytosolic tail of Smo, in close proximity to TM7 (Corbit et al., 2005). The ciliary localization defective mutant mSmoCLD mutant replaces this conserved motif, residues W549 and R550, with alanines and fails to localize at the primary cilium. The motif is also present in DrSmo which however does not localize to the cilium, casting doubt that it functions as a CLS in the first place. Thus, we asked whether the mutant was indeed unable to localize to the primary cilium, or perhaps the mutation merely stabilized the inactive conformation of Smo similarly to the effect of binding of antagonists. When stably expressed in $Smo^{-/-}$ MEFs, mSmoCLD fails to localize to the cilium and does not activate the downstream pathway components; however, in these cells mSmoCLD translocates robustly to the primary cilium in response to agonists such as SAG or 20-OHC, and is capable of rescuing the pathway defect in $Smo^{-/-}$ MEFs (Figure 3.2b, Figure 3.2c). Contrary to the previous report, we thus prove that the CLD mutation does not affect a ciliary localization sequence, but instead simply shifts the conformational equilibrium of Smo at rest towards the inactive state.

Finally, we investigated whether oligomerization of Smo is involved in ciliary translocation. In yeast, the oligomerization of the alpha-factor receptor (STE2, a GPCR) involves a GXXXG motif located in TM1 (Overton et al., 2003), while a similar motif in TM5 of the adiponectin receptor 1 triggers its dimerization (Kosel et al., 2010). Acylation and oligomerization regulate the association of proteins with lipid rafts (Shogomori et al., 2005), thus we hypothesized that they may also regulate lipid raft-mediated sortint into the ciliary compartment. A similar GXXXG motif appears in the TM1 of mouse but not Drosophila Smo suggesting that dimerization/oligomerization may have evolved as a regulatory mechanism for ciliary translocation. However, when this motif is mutated to LXXXL in $mSmo^{TM1LL}$, the mutant localizes well to the cilium and is transcriptionally active (Figure 3.2b, Figure 3.2c). Therefore, dimerization of Smo via the GXXXG motif does not regulate its ciliary entry – however, whether Smo actually forms dimers/oligomers through this motif remains unknown.

3.4.3 The intracellular domain (ICD) is necessary for targeting vertebrate Smo to the primary cilium

When overexpressed, vertebrate Smo localizes to the primary cilium. To test if the soluble cytosolic tail of vertebrate Smo is responsible for its ciliary localization, we examined the ciliary localization of $mSmo^{\Delta ICD}$ which lacks the complete cytosolic tail. We observed that the mutant $mSmo^{\Delta ICD}$ is unable to reach the primary cilium even in the presence of SAG (Figure 3.3a). This suggests that the vertebrate ICD is essential for correct sorting into the ciliary membrane compartment. $mSmo^{\Delta ICD}$ is properly folded as it binds SAG and BODIPY-

Cyclopamine in a competitive manner (Chen et al., 2002); however, it is not known whether it can localize at the cilium.

A sequence comparison of Smo from different vertebrate species highlights significant sequence homology in the cytosolic tail (ICD). In contrast, the cytosolic tail of arthropod Smo is diverged, as would be expected in the case where the cytosolic tail mediates the differential regulation of Smo in the two phyla. The ICD of vertebrate Smo contains two conserved stretches of basic amino acid residues (indicated with red lines in Figure 3.3b). These stretches each lie in close proximity to a conserved cysteine residue (denoted with * in Figure 3.3b), which could potentially function as sites of palmitoylation. Palmitoylation is used as a membrane targeting moiety, and is essential for correct ciliary localization of several transmembrane proteins such as fibrocystin (Follit et al., 2010).

In order to map the sequence requirements of the Smo CLS, we expressed a series of truncation constructs containing progressively larger C-terminal deletions and assessed their localization at the cilium. We observed that a construct lacking the first half of the cytosolic tail, (residues 543-674) is unable to localize properly to the cilium even in the presence of SAG, while absence of the second half of the ICD (residues 675-793) did not affect ciliary localization. Additional truncation constructs (Figure 3.3c) revealed that amino acid residues 614-637 are essential for ciliary localization of Smo, and thus likely contain the CLS. Furthermore, the presence or absence of the CRD did not affect the ciliary localization of the protein, as expected given our findings in Chapter 2 that. Interestingly, all C-terminal truncation mutants up to residue 637 show lower expression levels at the cilium upon overexpression and in the absence

Figure 3.3 The intracellular domain is necessary for Smo ciliary targeting

(a) Immunofluorescence of $Smo^{-/-}$ MEFs stably expressing mSmo WT or $mSmo^{\Delta ICD}$ fused at their respective C-terminus to mCherry. Cells were incubated with DMEM overnight, then washed and incubated with control medium or 200nM SAG in DMEM for another 24hrs, then fixed and processed for immunofluorescence with anti-mCherry antibodies (to visualize the fusion protein) and anti-acetylated tubulin antibodies (to visualize cilia). mSmo WT but not $mSmo^{\Delta ICD}$ localize to the primary cilium. Micrographs show representative cilia.

(b) Sequence alignment of the intracellular domain (ICD) of mouse Smo (mSmo), human Smo (hSmo), Xenopus Smo (xSmo), zebrafish Smo (Drerio Smo) and Drosophila Smo (DrSmo). Conserved residues are shaded. Two basic amino-acid stretches are indicated with red lines and contain residues conserved in vertebrate but not arthropod Smo. The basic residues in either one or both of these stretches are mutated to Alanines in the mSmo mutants $mSmo^{A11}$, $mSmo^{A10}$ and $mSmo^{A21}$ as indicated. Asterisks (*) indicate conserved cysteine residues which lie in close proximity to either of the two basic stretch, and which could potentially function as a palmitoylation site.

(c) $Smo^{-/-}$ MEFs, stably expressing constructs truncated C-terminally at the residues indicated by number and/or truncated at the N-terminus to eliminate the CRD domain (as described in Chapter 2); the constructs are fused at their respective C-terminus to mCherry. Cells were incubated with DMEM overnight, then washed and incubated with control medium or 200nM SAG another 24hrs, then fixed and processed for immunofluorescence with anti-mCherry antibodies (to visualize the fusion protein) and anti-acetylated tubulin antibodies (to visualize cilia). Micrographs show representative cilia.

(d) as in (c) but the cells were processed for Q-PCR, to measure Gli1 transcription. Each experiment was performed in triplicate, and the error bars show the standard deviation of the mean.

(e) $Smo^{-/-}$ MEFs, stably expressing wildtype mSmo, $mSmo^{A11}$, $mSmo^{A10}$, $mSmo^{A21}$ or $mSmo^{\Delta ICD}$ constructs fused at the C-terminus to mCherry, were incubated with DMEM overnight, then washed and incubated with control medium or 200nM SAG delivered as 1000X DMSO stock in DMEM for another 24hrs. The cells were processed for Q-PCR, to measure Gli1 transcription. Deletion of the ICD completely ablates the pathway response; the defect is not due to misfolding, as $mSmo^{\Delta ICD}$ binds the fluorescent Smo antagonist BODIPY-Cyclopamine(Chen et al., 2002). Each experiment was performed in triplicate, and the error bars show the standard deviation of the mean.

(f) as in (e), but the cells were fixed and processed for immunofluorescence with anti-mCherry antibodies (to visualize the fusion protein) and anti-acetylated tubulin antibodies (to visualize cilia). The percentage of cells that show ciliary localization of the fusion protein was determined by automated scoring the indicated number of cilia for each condition.

Figure 3.3 (continued) The intracellular domain is necessary for Smo ciliary targeting

Figure 3.3 (continued) The intracellular domain is necessary for Smo ciliary targeting

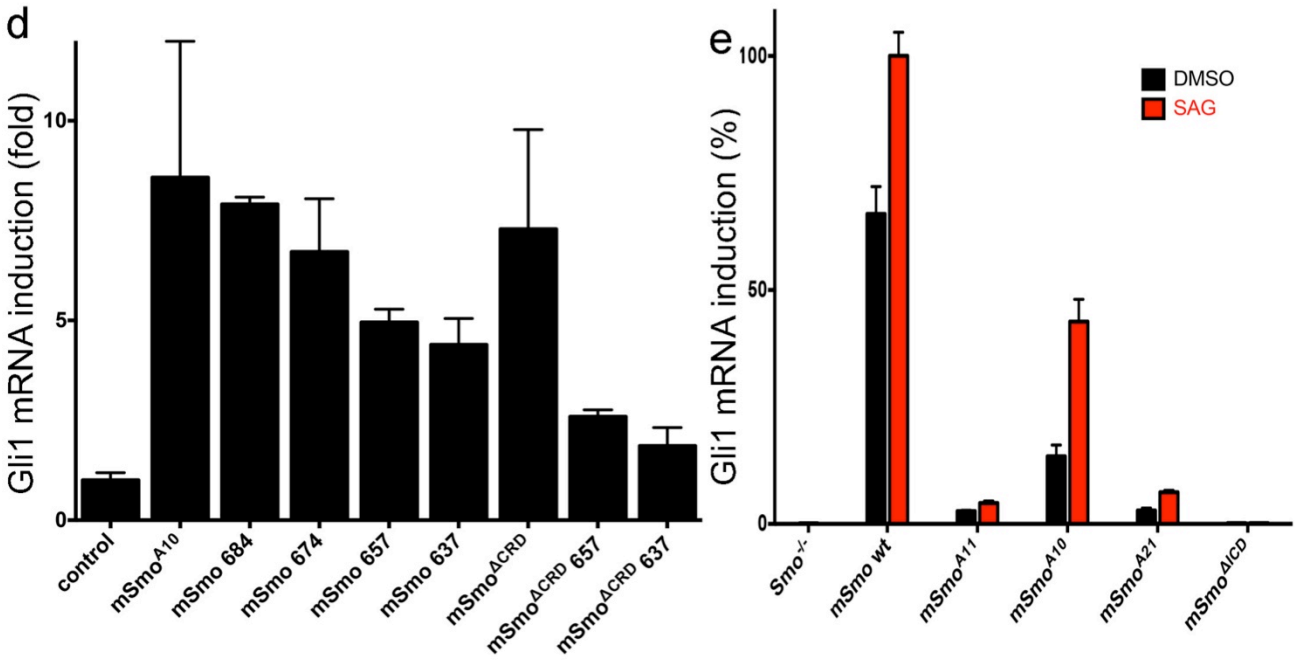

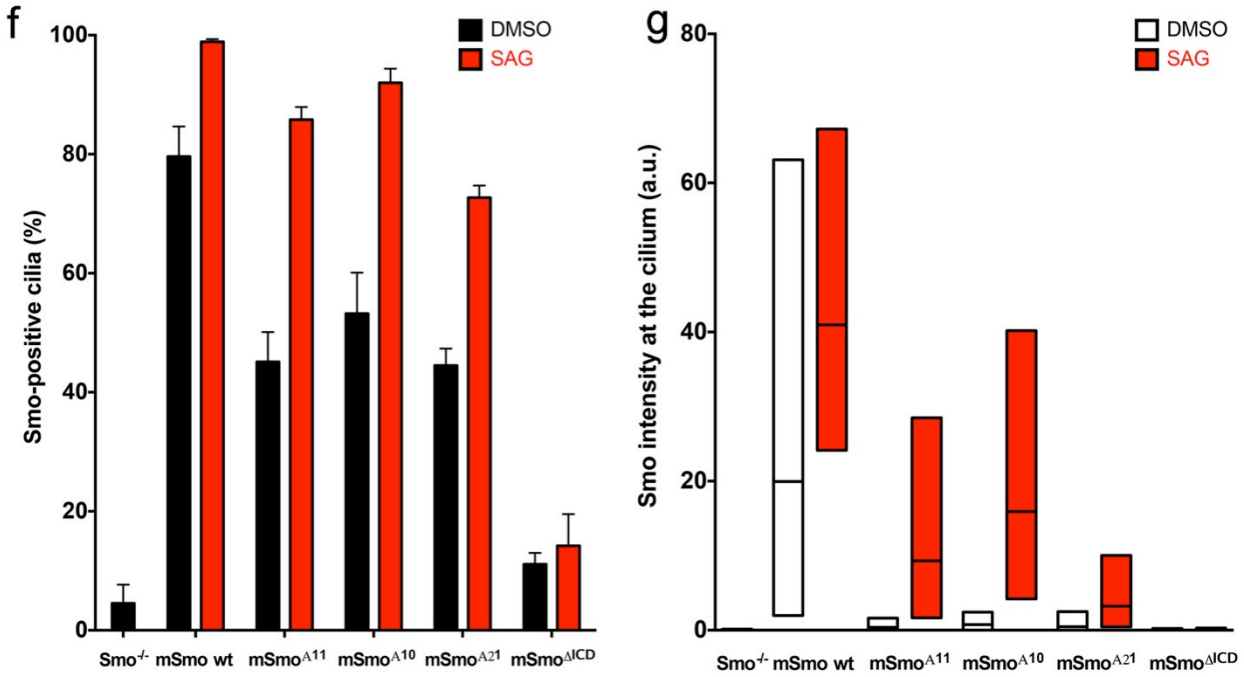

h

Cilia counted

	Smo$^{-/-}$	mSmo wt	mSmo^{A11}	mSmo^{A10}	mSmo^{A21}	mSmo$^{\Delta ICD}$
DMSO	212	429	278	363	603	469
SAG		510	484	369	813	315

Figure 3.3 (continued) The intracellular domain is necessary for Smo ciliary targeting

Figure 3.3 (continued) The intracellular domain is necessary for Smo ciliary targeting

(g) Same experiment as in (f) but with box plots showing fluorescence intensity of Smo at cilia, in arbitrary units. The lower and upper bounds of each box represent the 25th and 75th percentile of the distribution of ciliary fluorescence intensity, while the horizontal line represents the median intensity across the entire population of cilia.

(h) Same experiment as in (f) but showing the number of cilia counted

of stimulation; all of these mutants localize to the cilium robustly in response to SAG, indicating that the ciliary localization sequence is not affected by the deletions, but that the conformational equilibrium of the unstimulated protein is shifted towards the inactive conformation as if enhancer elements were lost in the deletions. $mSmo^{\Delta 638\text{-}793}$ but not $mSmo^{\Delta 615\text{-}793}$ localize to the primary cilium, indicating that the residues 615-637 of the ICD are critical for ciliary localization and likely contain the Smo CLS. However, an internal deletion construct lacking these residues ($mSmo^{\Delta 615\text{-}684}$) is still able to localize to the cilium in response to SAG, similar to the wildtype protein. This suggests the presence of a second CLS within residues 685-793 which is sufficient to localize membrane proteins to the cilium but is not necessary in the context of Smo. As expected, a truncation construct lacking both putative CLS ($mSmo^{\Delta 615\text{-}793}$) fails to localize to the cilium.

We then assessed the effect of these truncations on the hedgehog pathway activity. While the progressively larger deletion in our truncation mutants did not affect the ability of Smo to localize to the cilium, they nevertheless impacted the ability of Smo to activate the downstream pathway components as evidenced by the levels of Gli1 mRNA induction when overexpressed in $Smo^{-/-}$ MEFs (Figure 3.3d). A progressively larger truncation correlates with a lower ability to

activate the downstream pathway components. However, signaling to downstream components is never blocked completely, as overexpression of even the mSmo$^{\Delta 638\text{-}793}$ truncation stimulates the pathway above baseline. Deletion of the CRD in addition to C-terminal deletions has a synergistic effect, presumably due to folding issues. Taken together, the data suggest that the ICD contains both a CLS around the residues 615-637 as well as an additional CLS within residues 685-793; the ICD also likely contains elements in the region 637-793 that help stabilize the active conformation of the protein and enhance the response to stimulation.

Finally, since the basic stretches observed in the ICD sequence resemble palmitoylation sites, we tested whether they have any significance for the ciliary localization of Smo. We generated constructs replacing one of the basic amino acid stretches (mSmo^{A11} for the first stretch, or mSmo^{A10} for the second stretch) or both (mSmo^{A21}) with alanine residues. mSmo^{A11} and the combined mutant mSmo^{A21} but not mSmo^{A10} also show a severe signaling defect (Figure 3.3e). When stably expressed in Smo$^{-/-}$ MEFs, mSmo^{A10} rescues the pathway defect and responds well to SAG, while mSmo^{A11} or mSmo^{A21} fail to do so Figure 3.3e). This indicates that the stretch of basic residues in the region 565-581 is essential for signaling downstream. Interestingly, these mutants are not defective in ciliary localization. They also show an unaltered ciliary response to SAG, and even mSmo^{A21} shows a number of positive cilia similar to wildtype Smo (Figure 3.3f-h). Interestingly, while mSmo$^{\Delta ICD}$ fails to localize to the cilium and is thus completely inactive (as seen in Figure 3.3a), mSmo^{A11} cannot activate downstream components even in the presence of 200nM SAG - yet mSmo^{A11} localizes well to the cilium, and its ciliary localization is further enhanced by stimulation with SAG. In conclusion, the basic residues in the

region 565-581 are involved in relaying the signal to downstream components through an interaction which is ablated in the mutants, and furthermore this region does not serve as the CLS of Smo.

3.4.4 The ICD is sufficient for targeting transmembrane proteins to the primary cilium, but not for signaling

Since $mSmo^{\Delta ICD}$ does not localize to cilia, we tested if mSmoICD is sufficient for ciliary localization. We generated chimeras in which mSmoICD replaced the cytoplasmic tail of two seven-spanners that do not traffic to cilia, mouse Frizzled7 (mFz7) and the rat muscarinic acetylcholine receptor M2 (rMAChR).

Stably expressed $mFz7^{mSmoICD}$ localized to cilia in $Smo^{-/-}$ MEFs constitutively, while $rMAChR^{mSmoICD}$ did not but was strongly recruited to cilia by treatment with either agonist (acetylcholine) or antagonist (scopolamine) (Figure 3.4 a). We interpret this behavior of $rMAChR^{mSmoICD}$ as the result of improved folding caused by agonist or antagonist binding. Both $mFz7^{mSmoICD}$ and $rMAChR^{mSmoICD}$ were inactive in Hh signaling, even in the presence of the agonists acetylcholine, respectively (Figure 3.4b) and Wnt3a (Figure 3.4c). These results show that mSmoICD is sufficient for ciliary localization but is not sufficient to activate Hh signaling.

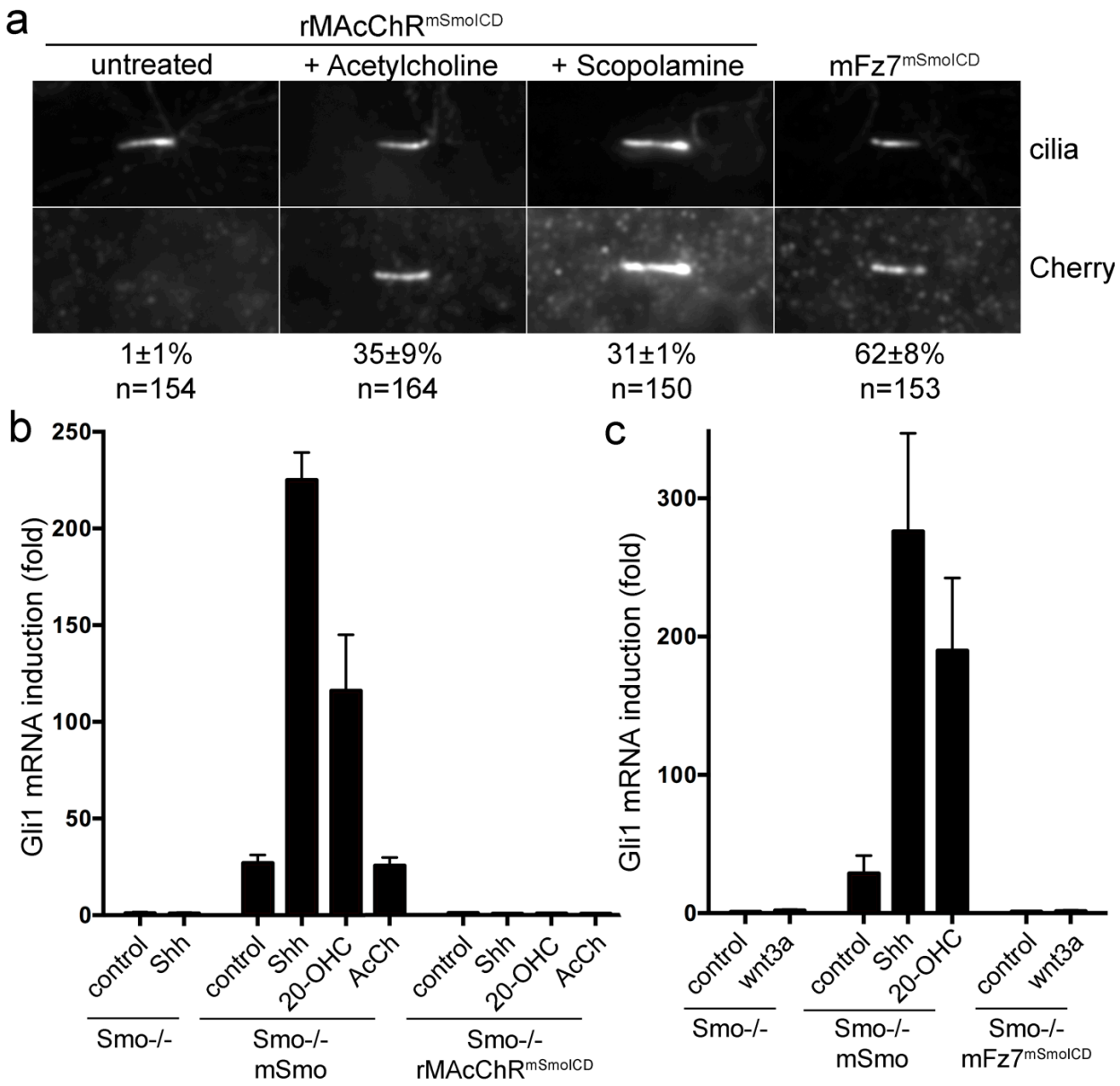

Figure 3.4 The mSmo ICD is sufficient for targeting membrane proteins to the primary cilium, but not for signaling

(a) Immunofluorescence shows that the mSmo ICD is sufficient to target a heterologous GPCR to the cilium. The cytoplasmic tail of the rat muscarinic acetylcholine receptor M2 (rMAcChR) or of the mouse Frizzled7 protein (mFz7) was replaced with the intracellular domain of mSmo (mSmoICD), to generate the chimeras rMAcChR^{mSmoICD} and mFz7^{mSmoICD}, respectively. These chimeras were C-terminally tagged with mCherry, and were stably expressed in Smo$^{-/-}$ MEFs. Confluent cultures were starved overnight in DMEM (to promote ciliogenesis) then treated as indicated for another 24hrs with ligands delivered in DMEM. In the case of rMAcChR^{mSmoICD},

Figure 3.4 (continued) The mSmo ICD is sufficient for targeting membrane proteins to the primary cilium, but not for signaling

the cells were incubated overnight with DMEM, or DMEM supplemented with the known agonist acetylcholine (100 μM) or antagonist scopolamine (100 μM). In the case of $mFz7^{mSmoICD}$, the cells were incubated overnight in DMEM. The cells were fixed and processed for immunofluorescence with anti-mCherry antibodies (to visualize the fusion protein) and anti-acetylated tubulin antibodies (to visualize cilia). The percentage of cells that show ciliary localization of the fusion protein was determined by visually scoring the indicated number of cilia for each condition. The micrographs show representative images of cilia. While $mFz7^{mSmoICD}$ localizes to cilia constitutively, $rMAcChR^{mSmoICD}$ localizes to cilia only upon treatment with either agonist (acetylcholine) or antagonist (scopolamine).

(b) Despite ciliary localization, the ICD cannot activate transcription of Hedgehog target genes when present on a heterologous protein. $Smo^{-/-}$ MEFs, stably expressing mSmo or the cilia-localized chimera $rMAcChR^{mSmoICD}$, were incubated with control medium, Shh, 20-OHC (10 μM), or Acetylcholine (AcCh, 100μM). The cells were processed for Q-PCR, to measure Gli1 transcription. $rMAcChR^{mSmoICD}$ does not rescue Hh signaling in $Smo^{-/-}$ cells, in the presence or absence of AcCh. Each experiment was performed in triplicate, and the error bars show the standard deviation of the mean.

(c) As in (b) but here $Smo^{-/-}$ cells with stable expression of mSmo or the cilia-localized chimera $mFz7^{mSmoICD}$ were incubated with control medium, Shh, 20-OHC (10 μM), or the Fz7 ligand wnt3a. $mFz7^{mSmoICD}$ did not rescue Hh signaling in $Smo^{-/-}$ cells, irrespective of the presence of the Wnt3a ligand. Each experiment was performed in triplicate, and the error bars show the standard deviation of the mean.

3.4.5 The ICD contains redundant ciliary targeting sequences

We then tried to define the minimal ciliary targeting sequence within the ICD which is sufficient to bring a heterologous membrane protein to the cilium, to supplement the previous truncation analysis. A preferred assay for candidate sequences to function as ciliary localization sequences is to fuse them to the single-spanning transmembrane receptor CD8a, replacing its cytosolic domain with the CLS of interest. This chimeric approach has successfully proven the sufficiency of several CLS to date (Jin et al., 2010; Xia et al., 2001). We observed that the C-

terminal portion of the ICD (residues 685-793) contains a CLS and was sufficient for ciliary targeting of the chimera (Figure 3.5a). Similarly, the same CLS functions in the CD8α-mSmo 675-793 chimera and targets that fusion protein to the cilium. In neither case did the presence of oxysterols affect the ciliary localization, confirming our findings from Chapter 2 where we prove that the oxysterols bind directly to the Smo CRD and not to the ICD. Surprisingly, the full-length ICD in this context was not able to target the chimera to the cilium. The most likely cause of this is a folding defect, although it cannot be ruled out that the residues 543-674 may contain a domain that functions as a repressor of ciliary targeting, and that under certain conditions this domain is derepressed to allow the ciliary trafficking to proceed.

To investigate whether the vertebrate Smo ICD is sufficient on its own to localize to the primary cilium when simply attached to lipid rafts rather than to a transmembrane protein, we fused the ICD to an N-terminal myristoylation sequence. Upon overexpression, the ICD alone is fully soluble and never enters the cilium. However, the presence of a myristoyl moiety tethers the chimera to the plasma membrane, and presumably facilitates association with lipid rafts. Similar to our previous observation in the case of the CD8α-mSmo 543-793, we were not able to observe any ciliary translocation of the myristoylated full-length ICD or of the ICD residues 543-674. However, a myristoylated construct containing only residues 675-793 of the mSmo ICD successfully translocated to the cilium (Figure 3.5b). Together with our observations from the truncation analysis, this strongly suggests that the vertebrate Smo ICD contains multiple redundant ciliary localization sequences: CLS-1 between residues 615-637, and CLS-2 located in the C-terminal residues 685-793 (and which may itself be degenerate). Each CLS is dispensable

for ciliary targeting of full-length Smo (Figure 3.5c). CLS-2 on its own is sufficient to direct transmembrane or membrane-tethered proteins to the cilium. We also interpret the inability of the myristoylated full-length ICD construct to localize to the cilium as a folding defect. What the minimal sequence sufficient for ciliary localization within these CLS is, how the two separate CLS are regulated in the endogenous protein, and whether their regulation implies additional post-translational modifications (such as palmitoylation) remains to be determined.

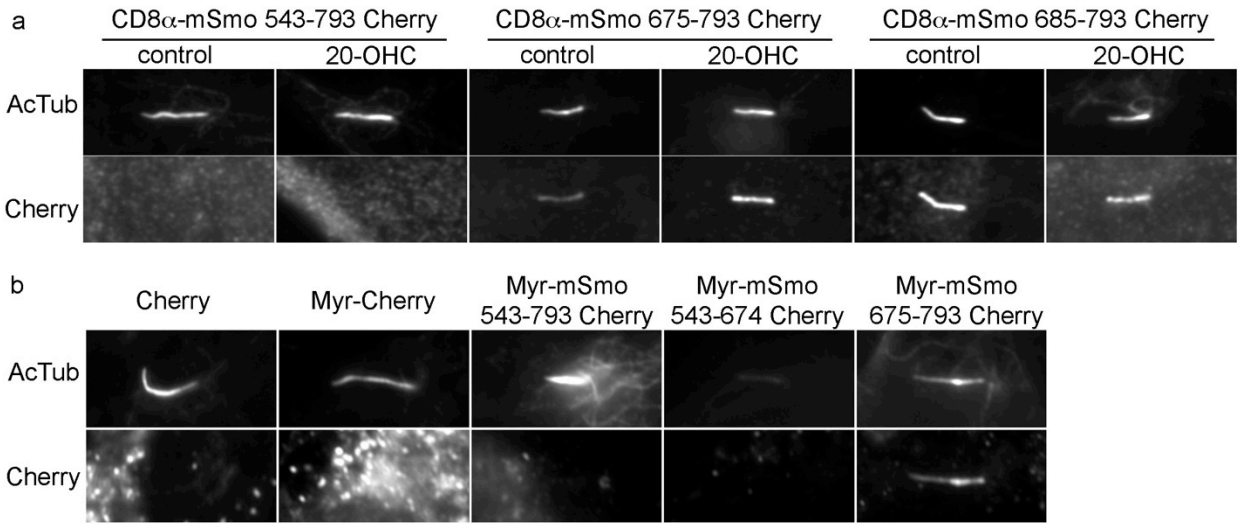

Figure 3.5 The vertebrate Smo ICD contains a C-terminal CLS sufficient for ciliary targeting of membrane proteins

(a) Immunofluorescence of indicated Smo ICD – CD8α fusion proteins reveals a C-terminal CLS. The intracellular portion of CD8α was replaced starting with residue 213 with the intracellular domain of mSmo (mSmoICD), or with portions thereof as indicated, to generate the chimeras CD8α-mSmo 543-793, CD8α-mSmo 675-793 and CD8α-mSmo 685-793. mSmo residues 675-684 represent the more c-terminal of the two basic stretches described earlier, and the chimeras allow us to test whether acylation in this region is involved at all in ciliary localization. These chimeras were C-terminally tagged with mCherry, and were stably expressed in $Smo^{-/-}$ MEFs. Confluent cultures were starved overnight in DMEM (to promote ciliogenesis) then treated with control medium or 10μM 20-OHC in DMEM for another 24hrs. The cells were fixed and processed for immunofluorescence with anti-mCherry antibodies (to visualize the fusion protein) and anti-acetylated tubulin antibodies (to visualize cilia). The micrographs show representative images of cilia.

(b) as in (a) but with 3T3 cells transiently transfected with Cs2p constructs expressing a myristoyl signal fused to the full length mSmo ICD or to portions of the mSmo ICD. Chimeras were C-terminally tagged with mCherry, and cells were transfected at 60% confluency using Mirus 3T3 transfection reagent. Cells were allowed to reach confluency in DMEM containing 10% bovine calf serum, penicillin and streptomycin. Confluent cells were starved overnight in DMEM, then fixed and processed for immunofluorescence with anti-mCherry antibodies (to visualize the fusion protein) and anti-acetylated tubulin antibodies (to visualize cilia). The micrographs show representative images of cilia. As negative controls, cells were transfected with constructs expressing mCherry or mCherry containing a myristoylation signal (Myr-mCherry). The mSmo ICD residues 675-793 contain a CLS that is sufficient for ciliary targeting when membrane anchored through a myristoyl moiety.

3.4.6 Conservation and divergence in Smo regulation

Vertebrate Smo but not Drosophila Smo signals at the primary cilium. Since the ciliary localization is mediated by two regions of the vertebrate Smo ICD, but the ICD alone is not sufficient for signaling downstream, we wondered if the downstream signaling function of Smo is conserved. To determine if DrSmo can signal at vertebrate cilia, we generated a chimera ($DrSmo^{mSmoICD}$) that consists of the CRD and heptahelical bundle of DrSmo, followed by the ICD of mSmo. As expected, $DrSmo^{mSmoICD}$ localized to cilia in $Smo^{-/-}$ MEFs (Figure 3.6a). Interestingly, $DrSmo^{mSmoICD}$ strongly activated Hh signaling (Figure 3.6b), indicating that the DrSmo portion of the chimera transduced vertebrate Hh signals. $DrSmo^{mSmoICD}$ was constitutively active, and could not be further stimulated by treatment with 20-OHC, SAG or Shh (Figure 3.6b); it was, however, inhibited by Protein Kinase A activation by forskolin, which blocks Hh signaling at a step downstream of Smo (Figure 3.6c). The lack of a response to 20-OHC and SAG is consistent with $DrSmo^{mSmoICD}$ not binding these two molecules. The inability of Shh to further stimulate $DrSmo^{mSmoICD}$ indicates that mouse Ptc cannot repress $DrSmo^{mSmoICD}$ even though the latter is targeted to cilia, thus suggesting that DrSmo is regulated differently from mSmo. Finally, in contrast to mSmo, $DrSmo^{mSmoICD}$ was not inhibited by sterol depletion (Figure 3.6d-f), indicating that oxysterols are not required for activation of $DrSmo^{mSmoICD}$. This suggests that binding of oxysterols has evolved as an additional mechanism of regulation of vertebrate Smo.

Figure 3.6 Conservation and divergence in Smo regulation

(a) The intracellular domain of DrSmo was replaced with the intracellular domain of mSmo, to generate the chimera DrSmo^{mSmoICD}, which was tagged with mCherry at the C-terminus. This fusion was stably expressed in Smo$^{-/-}$ MEFs, and Smo$^{-/-}$ MEFs expressing mCherry-tagged mSmo were used as positive control for ciliary localization. DrSmo^{mSmoICD} localizes to cilia robustly, like mSmoSmo$^{-/-}$ MEFs stably expressing mSmo or the chimera DrSmo^{mSmoICD} show robust constitutive ciliary localization. Confluent cultures were starved overnight in DMEM (to promote ciliogenesis) then the medium changed and starved for another 24hrs in DMEM, after which the cells were fixed and processed for immunofluorescence with anti-mCherry antibodies (to visualize the fusion protein) and anti-acetylated tubulin antibodies (to visualize cilia). The micrographs show representative images of cilia; cilia counts performed visually in triplicate, and the fraction of Smo-positive cilia along with the standard deviation of the mean is reported.

(b) Smo$^{-/-}$ MEFs, stably expressing DrSmo or the cilia-localized chimera DrSmo^{mSmoICD} were incubated with control medium, 20-OHC (10 μM), Shh or SAG (1μM). qPCR DrSmo^{mSmoICD} is constitutively active, and is not further activated by 20-OHC, Shh, or SAG. In contrast, DrSmo is inactive in Smo$^{-/-}$ MEFs. The cells were processed for Q-PCR, to measure Gli1 transcription. Each experiment was performed in triplicate, and the error bars show the standard deviation of the mean.

(c) As in (b), but with addition of 20 μM forskolin (FSK), to block Hh signaling downstream of Smo. Signaling by both mSmo and DrSmo^{mSmoICD} is completely blocked by FSK, indicating that the DrSmo^{mSmoICD} chimera signals through the endogenous Hh pathway components.

(d) Smo$^{-/-}$ MEFs stably expressing low levels of mCherry-tagged DrSmo^{mSmoICD} or mSmo were isolated by drug selection, followed by FACS sorting. Confluent cultures were depleted of sterols by acute treatment with 1.5% methyl-β-cyclodextrin (MCD) for 30 minutes, followed by continuous incubation with pravastatin (40 μM) to block *de novo* sterol biosynthesis. Cholesterol was added back as soluble MCD-cholesterol (Chol) complexes (100 μM in DMEM) prepared as described (Klein et al., 1995). Following sterol depletion and add-back, the cultures were incubated overnight in the presence or absence of Shh as indicated. The cells were fixed then processed for immunofluorescence with anti-mCherry antibodies (to detect Smo) and anti-acetylated tubulin antibodies (ciliary marker). The graph shows the percentage of cells with Smo- positive cilia. DrSmo^{mSmoICD} localizes to cilia, with or without sterol depletion; in contrast, mSmo accumulates in cilia upon Shh stimulation, and this accumulation is blocked by sterol depletion.

(e) As in (d), but with box plots showing fluorescence intensity of Smo at cilia, in arbitrary units. The lower and upper bounds of each box represent the 25th and 75th percentile of the distribution of ciliary fluorescence intensity, while the horizontal line represents the median intensity across the entire population of cilia.

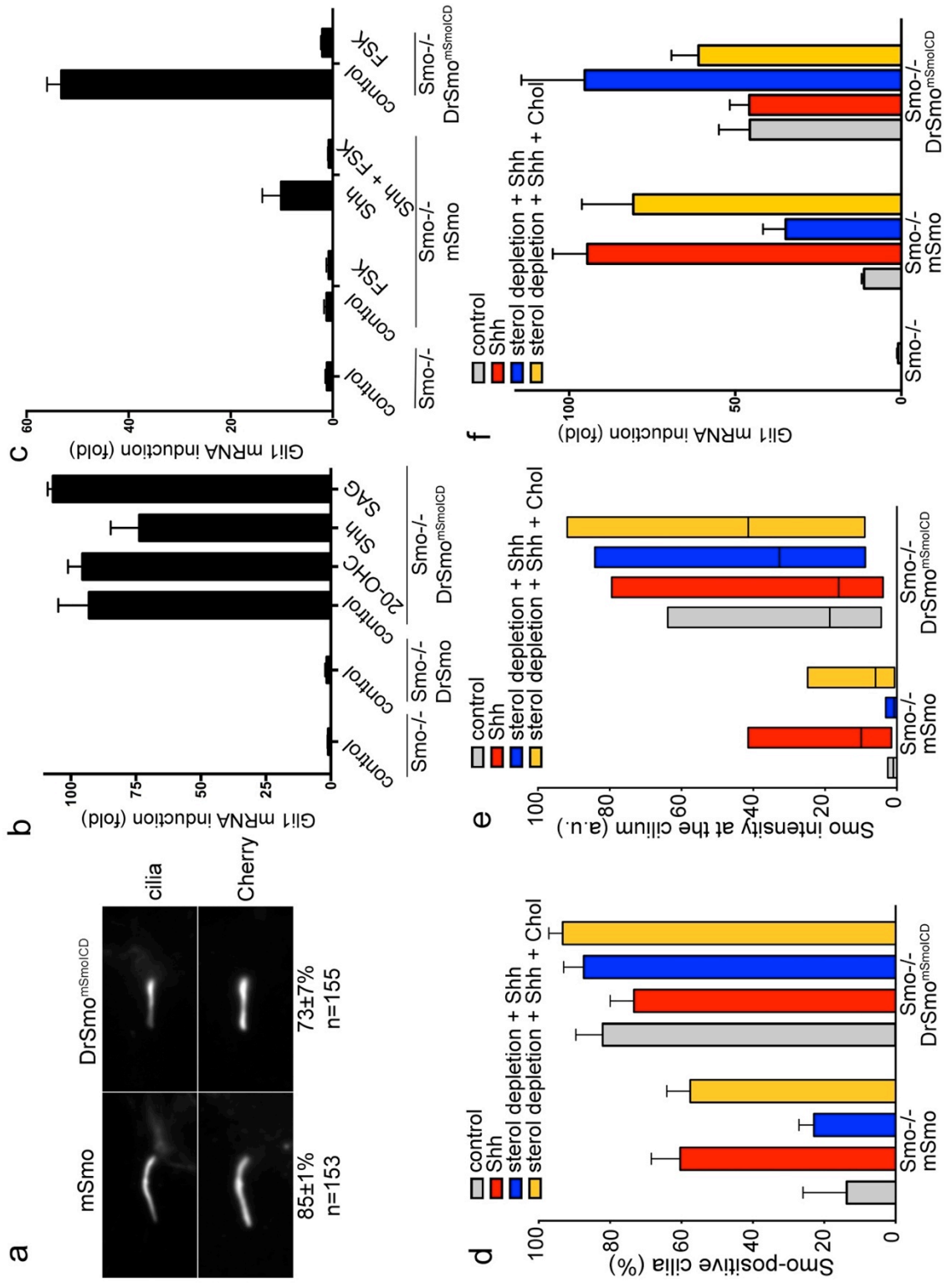

Figure 3.6 (continued) Conservation and divergence in Smo regulation

Figure 3.6 (continued) Conservation and divergence in Smo regulation

(f) The Smo ICD does not mediate sterol sensitivity. As in (d) but the cells were processed for Q-PCR, to measure Gli1 transcription relative to the L27 transcript. Each experiment was performed in triplicate, and the error bars show the standard deviation of the mean.

3.5 Discussion

We found that the vertebrate Smo ICD contains at least two redundant ciliary localization sequences: CLS-1 is embedded within residues 615-637 of mouse Smo, while CLS-2 is contained in amino acid residues 685-793. The two distinct CLS most likely function synergistically to enhance ciliary targeting; in the context of full-length Smo they appear redundant for ciliary localization, and ablation of either CLS still results in a protein that is ciliary targeted through the action of the other CLS (as summarized in Figure 3.7). Furthermore, CLS-2 is sufficient to direct other membrane proteins and even membrane-attached proteins to the primary cilium on its own. It is tempting to speculate that the different CLS are regulated differently – and perhaps have even evolved differently to satisfy distinct criteria required for Smo regulation in vertebrates. The ICD stretch 685-793 may itself contain one or more motifs sufficient for ciliary targeting. In order to pinpoint the CLS-2 at higher resolution, additional mapping is needed using constructs with shorter deletions, while the complementary fusion constructs to heterologous membrane proteins would test the sufficiency for ciliary targeting. Separately, we show that the ciliary localization of Smo and the ability of Smo to activate downstream components are mediated by different sequence motifs in the ICD. An immediate

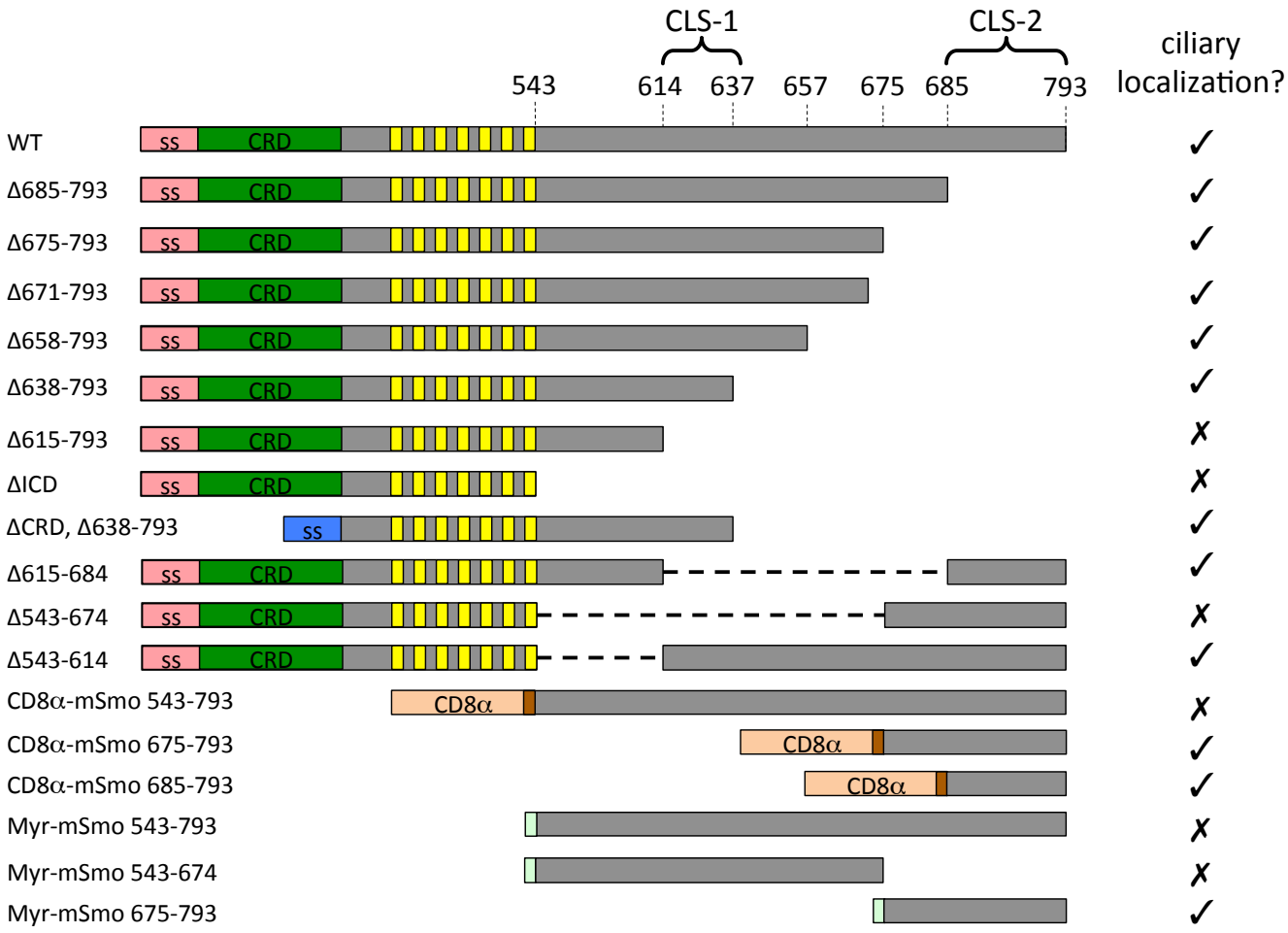

Figure 3.7 Summary of Smo deletion mapping constructs

The structure of the Smo ICD and the various deletion constructs is shown. The signal sequence (ss), the CRD and the 7 transmembrane domains, as well as the N-terminal CD8α portion used in the chimeras (which includes the CD8a transmembrane domain) and the myristoylation signal are color coded. The two regions containing the putative CLS identified are indicated.

next step will be to map the minimal domain required for activation of downstream components. The work presented herein provides a framework for such additional mapping of the downstream activating domain.

How is the translocation of Smo to the cilium regulated? One possibility is that additional dynamic post-translational modifications such as palmitoylation of cysteine residues and the ensuing incorporation into lipid rafts would be important for trafficking Smo to the primary cilium. This idea is supported by the fact that other membrane proteins such as the photoreceptor opsin or fibrocystin rely on palmitoylation for proper sorting into the ciliary compartment (Follit et al., 2010; Tam et al., 2000). Furthermore, oligomerization of Drosophila Smo and its association with lipid rafts are essential for downstream pathway activation (Shi et al., 2013). We hypothesized that Smo may be dynamically palmitoylated in response to binding ligands that trigger its ciliary translocation, and then associates with lipid rafts for cilium-directed trafficking. The vertebrate Smo ICD contains 5 cysteine residues which could be acylated, but the mutational analysis of these residues is complicated by my finding that Smo contains redundant CLS. However, genetic screens have not identified any palmitoyl transferases with a clear role in the Hh pathway downstream of Smo.

The vertebrate Smo ICD contains two stretches of basic residues in close proximity to cysteines, which are hallmarks of palmitoylation sites (Figure 3.3b) (Bijlmakers and Marsh, 2003). We found that ablation of the first basic stretch or of the full complement of basic residues in both stretches results in proteins ($mSmo^{A11}$ or $mSmo^{A21}$) that are unable to signal downstream – but localize robustly to the cilium in a regulated fashion. In the $mSmo^{A21}$ mutant, palmitoylation would not be expected. However, since Smo contains two separate CLS, it is conceivable that only one of the CLS is palmitoylation dependent, while the other one is not; in this case, the presence of a palmitoylation-independent CLS would mask the effect of loss of

palmitoylation on the palmitoylation-dependent CLS, and Smo would still localize to the cilium. The amino acid residues 615-637 in the Smo ICD, which encompass CLS-1 we identified, do not contain any cysteine residues that could be acylated, while CLS-2 we identified in the stretch 685-793 contains four cysteines but is dispensable for ciliary localization. Thus, while palmitoylation (or S-acylation in general) at those cysteine residues is not essential for the ciliary targeting of full-length Smo, it may play a crucial role in downstream signaling. In order to prove a direct role for acylation, all cysteine residues in the ICD should be mutated. A different, as yet unknown mechanism pushes Smo to the cilium. Whether this mechanism acts in addition to palmitoylation or whether ciliary localization is completely unrelated to palmitoylation remains to be established. It will be worth examining the effect of the ablation of basic stretches in the context of a Smo construct lacking either of the two CLS, such as mSmo$^{\Delta 615\text{-}684}$ or mSmo$^{\Delta 685\text{-}793}$.

If Smo signaling to downstream components is indeed regulated through palmitoylation of its ICD, then the removal of the palmitoyl moiety may likely be regulated as well, in order to maintain Smo homeostasis in the OFF state. Interestingly, cyclopamine brings inactive Smo to the primary cilium; cyclopamine may interfere with acylation of Smo, and thus block the interaction with downstream components – similar to the effect of the mSmo^{A11} mutation. Palmitoylation of Smo can be tested directly by treating cells with radioactive [^{3}H]-palmitate (Follit et al., 2010) followed by immunoprecipitation of Smo to detect the incorporation of radioactivity; in a complementary approach, an S-acylation-defective mutant could be constructed by replacing all 5 cysteine residues within the ICD with serine or alanine residues. Whether palmitoylation of Smo occurs in a signal-dependent manner, whether depalmitoylation

is involved in maintaining Smo in the OFF state outside of the cilium in the absence of signaling, and in that case what the identity of the Smo depalmitoylase is – are attractive future directions of research opened up by the present work.

Mammals have 23 proposed S-palmitoyl transferases localized to specific cellular compartments: most of them reside in the ER or the Golgi, but some localize primarily at the plasma membrane and transfer the palmitoyl moiety in a compartment-specific manner (Ohno et al., 2006); however, no palmitoyl-transferases have been reported at the primary cilium. A speculative model that reconciles the lateral movement observed for Smo with palmitoylation-mediated signaling to downstream components involves the coordinated palmitoylation of Smo under strict spatial control at the plasma membrane in a ligand-dependent manner – but how the activation state is relayed to such palmitoyl transferase remains unknown. Accordingly, a plasma membrane-resident palmitoyl transferase acts as a gate-keeper and acylates activated Smo as it is targeted to the primary cilium; at the cilium, the acyl group on Smo mediates an interaction with downstream components either directly, or indirectly by favouring the association of Smo with lipid rafts already containing a downstream component.

A crucial question is what happens at the cilium subsequent to Smo activation, in order to signal downstream. I find that the $mSmo^{A11}$ and $mSmo^{A21}$ mutants, which both lack the basic stretch within residues 565-581 of the ICD, fail to signal downstream components at the cilium. This stretch of basic residues lies in close proximity to cysteine 554, and resembles a palmitoylation site. My observation suggests the existence of a dynamic association either in the form of a direct interaction between Smo and the downstream pathway components at the level

of these residues, or in the form of a dynamic acylation of the nearby cysteine. Acylation may in turn regulate the association of Smo with lipid rafts containing downstream pathway components; alternatively, acylation may mediate the interaction with a downstream pathway component directly. Such interaction appears essential for Smo function, and we can only speculate that one possibility here is the cilium-dependent interaction with Evc2. Evc2 forms a complex with activated Smo. The interaction is spatially restricted to the transition zone of the primary cilium and is essential for transduction of the signal to the complex of Suppresor of Fused and Gli (SuFu-Gli) (Dorn et al., 2012). The mechanistic details of the interaction between Smo and Evc2 remain unknown at present. Since Smo and Evc2 co-immunoprecipitate, it will be interesting to test whether this interaction is maintained in the signaling defective $mSmo^{A11}$ and $mSmo^{A21}$ mutants. Furthermore, it will be interesting to map the minimal domain of Smo that interacts with Evc2, and to test whether the S-acylation-defective Smo mutant described above affects this interaction.

3.6 Methods

3.6.1 Antibodies

Polyclonal antibodies against mCherry were generated in rabbits (Cocalico Biologicals) and were affinity purified against recombinant mCherry immobilized on Affigel-10 beads (BioRad). The monoclonal anti-acetylated tubulin antibody was obtained from Sigma.

3.6.2 DNA constructs

Expression constructs were assembled by PCR in the mammalian expression vector pCS2p+, from which they were subcloned into a vector for lentiviral production. Constructs encoding membrane proteins were tagged with mCherry at their C-terminus. These constructs were: DrSmo^{mSmoICD} (amino acids 1- 556 of DrSmo fused to amino acids 543-793 of mSmo), mFz7^{mSmoICD} (amino acids 1-548 of mouse Frizzled7 fused to amino acids 543-793 of mSmo), rMAChR^{mSmoICD} (amino acids 1-442 of the rat muscarinic acetylcholine receptor M2 fused to amino acids 543-793 of mSmo), mSmo 684, mSmo 674, mSmo 657, mSmo 637, mSmo$^{\Delta CRD}$, mSmo$^{\Delta CRD}$ 657, mSmo$^{\Delta CRD}$ 637, mSmo A11, mSmo A10, mSmo A21.

CD8α chimeric constructs consist of the first 212 residues of the single-spanning transmembrane protein CD8α fused at the C-terminus to either residues 543-793 of Smo (the full mSmo ICD), or residues 675-793, or residues 685-793; all chimeras were assembled by PCR and tagged at their C-terminus with mCherry in the mammalian expression vector pCS2p+, from which they were subcloned into a vector for lentiviral production.

To generate the myristoylated constructs, mSmo ICD residues 543-793 (the full mSmo ICD), or residues 543-674, or residues 675-793 were fused at the N-terminus to the Src N-terminal myristoylation signal (Jia et al., 2003) and tagged at their C-terminus with mCherry in the mammalian expression vector pCS2p+.

3.6.3 Cell culture and generation of stable cell lines

Mouse embryonic fibroblasts (MEFs) and 293T cells were grown in DMEM with 10% fetal bovine serum, penicillin and streptomycin. Stable cell lines were generated by lentiviral transduction, followed by selection with blasticidin 50μg/mL for 3 days. $Smo^{-/-}$ MEFs expressing low amounts of various mCherry-tagged Smo proteins were isolated by fluorescence-activated cell sorting. Expression of the tagged construct was confirmed by immunofluorescence and by QPCR assays of Hh pathway stimulation. The following compounds were obtained from commercial sources: cyclopamine (LC Laboratories), BODIPY-cyclopamine (TRC), SAG (Axxora), forskolin (Sigma), SANT1 (Calbiochem), 20-hydroxycholesterol (Steraloids), 7-hydroxycholesterol (Steraloids), Acetyl choline (Sigma), Scopolamine (Sigma).

3.6.4 Hh ligand production

Hh ligand was produced by transiently transfecting 293T cells with an expression plasmid encoding amino acids 1-198 of human Shh. Shh was collected for 48 hours into starvation medium (DMEM supplemented with penicillin and streptomycin). For maximal stimulation of the Hh pathway, Shh- conditioned medium was used diluted 1:3 -1:4 into fresh starvation medium.

3.6.5 Wnt3a ligand production

Wnt3a ligand was produced by from a stable line of L cells expressing the the full-length protein as described (Willert et al., 2003). Wnt3a-containing supernatant was collected for 48 hours into medium (DMEM supplemented with 5% fetal bovine serum, penicillin and streptomycin). Wnt3a-conditioned medium was used diluted 1:2 -1:3 into fresh starvation medium (DMEM supplemented with penicillin and streptomycin).

3.6.6 Immunofluorescence

Cells were grown on glass coverslips to confluency and starved in DMEM overnight, then washed and incubated with control medium, 200nM or 1μM SAG, 1μM SANT-1 or 10μM 20-OHC delivered as 1000X DMSO stock in DMEM for another 24hrs, as indicated. Cells were fixed in PBS with 3.7% formaldehyde, followed by permeabilization with TBST (TBS containing 0.2% Triton X-100). Non-specific binding sites were blocked by incubation in TBST with 50 mg/mL bovine serum albumin (TBST-BSA). Endogenous mSmo was detected with anti-Smo antibodies (Tukachinsky et al., 2010) and mCherry-tagged proteins were detected with anti-mCherry antibodies. Primary cilia were stained with anti-acetylated tubulin antibodies. Primary and secondary antibodies were used diluted in TBST-BSA. The primary antibodies were: rabbit polyclonal against mCherry (final concentration 1 μg/mL), rabbit polyclonal against mSmo (final concentration 2 μg/mL), mouse anti-acetylated tubulin monoclonal antibody (Sigma, final dilution dilution of 1:5,000). Alexa-594- and Alexa-488-conjugated secondary antibodies (Life Sciences) were used at a final concentration of 1 μg/mL. The coverslips were mounted on glass

slides in mounting media (0.5% p-phenylenediamine, 20 mM Tris pH 8.8, 90% glycerol). The cells were imaged by epifluorescence on a Nikon TE2000E microscope equipped with an OrcaER camera (Hammamatsu) and 40x PlanApo 0.95NA or 100x PlanApo 1.4NA oil objective (Nikon). Images were acquired using the Metamorph software (Applied Precision). Ciliary localization of Smo was measured either manually or using custom image analysis software implemented in MATLAB. Briefly, the software first identifies cilia by local adaptive thresholding of images of cells stained for acetylated tubulin. The segmented images are cleaned by automatic removal of objects whose size and shape fall outside the normal range for a typical cilium. Next, the pixel intensity of the protein of interest (Smo) in each cilium is corrected by subtracting the local background, defined as the median intensity of the pixels surrounding the cilium. Ciliary Smo is then quantified as the total corrected intensity in each cilium, normalized to the area of the cilium. To count Smo-positive cilia, fluorescence in the Smo channel is first calculated for the cilia in the negative control sample (untreated cells in case of scoring endogenous Smo, or $Smo^{-/-}$ cells in case of scoring mCherry-tagged fusions proteins stably expressed in $Smo^{-/-}$ MEFs). This data is used to calculate a threshold value that is above the fluorescence intensity for >95% of cilia in the negative control sample; note that this method overestimates the number of Smo-positive cilia in the negative control, by allowing a false positive rate of up to 5% in this sample. Using the calculated threshold value, cilia are then scored in all remaining samples, and the fraction of Smo-positive cilia is graphed. Ciliary intensity of Smo is also graphed using box plots; for each condition, the lower and upper bounds of the box represent the 25th and 75th percentile of the Smo intensity distribution, while the

horizontal line represents the median intensity across the entire cilia population. A more detailed description of the algorithm is provided in the Appendix. For the experiments presented in this study, between 150-550 cilia per condition were analyzed in this manner. For some experiments, ciliary localization of Smo was measured manually, by scoring the presence or absence of Smo in 150 cilia for each condition.

3.6.7 Real-time PCR assays of the Hh pathway

Confluent NIH-3T3 cells or MEFs were starved overnight in starvation medium, after which they were incubated for 24 hours in starvation medium supplemented with the desired compounds. Total RNA was isolated from cells with RNA-Bee (TelTest), treated with RNase-free DNase (Promega), and purified using the GenCatch total RNA Extraction System (Epoch Biolabs). Reverse transcription was performed using random hexamers and Transcriptor reverse transcriptase (Roche). Transcription of the Hh target gene Gli1 was measured by real-time PCR using FastStart SYBR Green Master reagent (Roche) on a Rotor-Gene 6000 (Corbett Robotics). Relative gene expression was calculated using a Two Standard Curve method in which the gene-of-interest was normalized to the Ribosomal Protein L27 gene. The sequences for gene-specific primers are: L27: 5'-GTCGAGATGGGCAAGTTCAT-3' and 5'-GCTTGGCGATCTTCTTCTTG-3', Gli1: 5'-GGCCAATCACAAGTCAAGGT-3' and 5'-TTCAGGAGGAGGGTACAACG -3'. Each experiment was performed in triplicate, and error bars represent standard error of the mean.

3.6.8 Sterol depletion

Sterol depletion was performed on starved, confluent cultures of stable lines derived from $Smo^{-/-}$ MEFs. The cultures were incubated for 30 minutes with 1.5% methyl-β-cyclodextrin (MCD) in DMEM (to remove sterols), after which all subsequent incubations were in DMEM with 40 μM pravastatin (to block new sterol synthesis), with or without the indicated additives. For rescue experiments, cholesterol prepared as described (Klein et al., 1995) was added back by incubating the cells for 1 hour with soluble cholesterol-MCD complexes prepared (100 μM in DMEM supplemented with 20 μM pravastatin). After overnight incubation with the desired compounds, the cells were processed for immunofluorescence or for Q-PCR, as described above.

3.7 References

Aanstad, P., N. Santos, K.C. Corbit, P.J. Scherz, A. Trinh le, W. Salvenmoser, J. Huisken, J.F. Reiter, and D.Y. Stainier. 2009. The extracellular domain of Smoothened regulates ciliary localization and is required for high-level Hh signaling. *Curr Biol*. 19:1034-1039.

Berbari, N.F., A.D. Johnson, J.S. Lewis, C.C. Askwith, and K. Mykytyn. 2008. Identification of ciliary localization sequences within the third intracellular loop of G protein-coupled receptors. *Mol Biol Cell*. 19:1540-1547.

Bijlmakers, M.J., and M. Marsh. 2003. The on-off story of protein palmitoylation. *Trends Cell Biol*. 13:32-42.

Chen, J.K., J. Taipale, K.E. Young, T. Maiti, and P.A. Beachy. 2002. Small molecule modulation of Smoothened activity. *Proc Natl Acad Sci U S A*. 99:14071-14076.

Corbit, K.C., P. Aanstad, V. Singla, A.R. Norman, D.Y. Stainier, and J.F. Reiter. 2005. Vertebrate Smoothened functions at the primary cilium. *Nature*. 437:1018-1021.

Dishinger, J.F., H.L. Kee, P.M. Jenkins, S. Fan, T.W. Hurd, J.W. Hammond, Y.N. Truong, B. Margolis, J.R. Martens, and K.J. Verhey. 2010. Ciliary entry of the kinesin-2 motor KIF17 is regulated by importin-beta2 and RanGTP. *Nat Cell Biol*. 12:703-710.

Dorn, K.V., C.E. Hughes, and R. Rohatgi. 2012. A Smoothened-Evc2 complex transduces the Hedgehog signal at primary cilia. *Dev Cell*. 23:823-835.

Dwyer, N.D., C.E. Adler, J.G. Crump, N.D. L'Etoile, and C.I. Bargmann. 2001. Polarized dendritic transport and the AP-1 mu1 clathrin adaptor UNC-101 localize odorant receptors to olfactory cilia. *Neuron*. 31:277-287.

Follit, J.A., L. Li, Y. Vucica, and G.J. Pazour. 2010. The cytoplasmic tail of fibrocystin contains a ciliary targeting sequence. *J Cell Biol*. 188:21-28.

Geng, L., D. Okuhara, Z. Yu, X. Tian, Y. Cai, S. Shibazaki, and S. Somlo. 2006. Polycystin-2 traffics to cilia independently of polycystin-1 by using an N-terminal RVxP motif. *J Cell Sci*. 119:1383-1395.

Huangfu, D., and K.V. Anderson. 2005. Cilia and Hedgehog responsiveness in the mouse. *Proc Natl Acad Sci USA*. 102:11325-11330.

Ingham, P.W., and A.P. McMahon. 2001. Hedgehog signaling in animal development: paradigms and principles. *Genes Dev*. 15:3059-3087.

Jia, J., C. Tong, and J. Jiang. 2003. Smoothened transduces Hedgehog signal by physically interacting with Costal2/Fused complex through its C-terminal tail. *Genes Dev*. 17:2709-2720.

Jin, H., S.R. White, T. Shida, S. Schulz, M. Aguiar, S.P. Gygi, J.F. Bazan, and M.V. Nachury. 2010. The conserved Bardet-Biedl syndrome proteins assemble a coat that traffics membrane proteins to cilia. *Cell*. 141:1208-1219.

Klein, U., G. Gimpl, and F. Fahrenholz. 1995. Alteration of the myometrial plasma membrane cholesterol content with beta-cyclodextrin modulates the binding affinity of the oxytocin receptor. *Biochemistry*. 34:13784-13793.

Kosel, D., J.T. Heiker, C. Juhl, C.M. Wottawah, M. Bluher, K. Morl, and A.G. Beck-Sickinger. 2010. Dimerization of adiponectin receptor 1 is inhibited by adiponectin. *J Cell Sci*. 123:1320-1328.

Lum, L., and P.A. Beachy. 2004. The Hedgehog response network: sensors, switches, and routers. *Science*. 304:1755-1759.

Milenkovic, L., M.P. Scott, and R. Rohatgi. 2009. Lateral transport of Smoothened from the plasma membrane to the membrane of the cilium. *J Cell Biol*. 187:365-374.

Ohno, Y., A. Kihara, T. Sano, and Y. Igarashi. 2006. Intracellular localization and tissue-specific distribution of human and yeast DHHC cysteine-rich domain-containing proteins. *Biochim Biophys Acta*. 1761:474-483.

Ou, G., O.E. Blacque, J.J. Snow, M.R. Leroux, and J.M. Scholey. 2005. Functional coordination of intraflagellar transport motors. *Nature*. 436:583-587.

Overton, M.C., S.L. Chinault, and K.J. Blumer. 2003. Oligomerization, biogenesis, and signaling is promoted by a glycophorin A-like dimerization motif in transmembrane domain 1 of a yeast G protein-coupled receptor. *J Biol Chem*. 278:49369-49377.

Pazour, G.J., and R.A. Bloodgood. 2008. Targeting proteins to the ciliary membrane. *Curr Top Dev Biol*. 85:115-149.

Rohatgi, R., L. Milenkovic, and M.P. Scott. 2007. Patched1 regulates hedgehog signaling at the primary cilium. *Science*. 317:372-376.

Rohatgi, R., and M.P. Scott. 2007. Patching the gaps in Hedgehog signalling. *Nat Cell Biol*. 9:1005-1009.

Shi, D., X. Lv, Z. Zhang, X. Yang, Z. Zhou, L. Zhang, and Y. Zhao. 2013. Smoothened oligomerization/higher order clustering in lipid rafts is essential for high Hedgehog activity transduction. *J Biol Chem*. 288:12605-12614.

Shogomori, H., A.T. Hammond, A.G. Ostermeyer-Fay, D.J. Barr, G.W. Feigenson, E. London, and D.A. Brown. 2005. Palmitoylation and intracellular domain interactions both contribute to raft targeting of linker for activation of T cells. *J Biol Chem*. 280:18931-18942.

Stone, D.M., M. Hynes, M. Armanini, T.A. Swanson, Q. Gu, R.L. Johnson, M.P. Scott, D. Pennica, A. Goddard, H. Phillips, M. Noll, J.E. Hooper, F. de Sauvage, and A. Rosenthal. 1996. The tumour-suppressor gene patched encodes a candidate receptor for Sonic hedgehog. *Nature*. 384:129-134.

Tam, B.M., O.L. Moritz, L.B. Hurd, and D.S. Papermaster. 2000. Identification of an outer segment targeting signal in the COOH terminus of rhodopsin using transgenic Xenopus laevis. *J Cell Biol*. 151:1369-1380.

Tukachinsky, H., L.V. Lopez, and A. Salic. 2010. A mechanism for vertebrate Hedgehog signaling: recruitment to cilia and dissociation of SuFu-Gli protein complexes. *J Cell Biol*. 191:415-428.

Wei, Q., Y. Zhang, Y. Li, Q. Zhang, K. Ling, and J. Hu. 2012. The BBSome controls IFT assembly and turnaround in cilia. *Nat Cell Biol*. 14:950-957.

Willert, K., J.D. Brown, E. Danenberg, A.W. Duncan, I.L. Weissman, T. Reya, J.R. Yates, 3rd, and R. Nusse. 2003. Wnt proteins are lipid-modified and can act as stem cell growth factors. *Nature*. 423:448-452.

Xia, H., Z.D. Hornby, and R.C. Malenka. 2001. An ER retention signal explains differences in surface expression of NMDA and AMPA receptor subunits. *Neuropharmacology*. 41:714-723.

Chapter 4: Discussion and Future Directions

4.1 Smo is modular

An important finding of my work is that Smo contains separate modules, each with a distinct function. The seven-spanner portion of the protein contains a ligand binding site where cyclopamine binds. A crystal structure exists of this region (Wang et al., 2013) showing an inhibitor bound deeply inside the transmembrane barrel, and this cyclopamine-binding site is targeted by all Smo inhibitors developed to date. In Chapter 2, I show that the CRD contains an oxysterol-regulated module required for maximal activation of Smo. While a second ligand binding site on Smo was previously hypothesized to exist (Nachtergaele et al., 2012), this is the first report to discover the existence of a second ligand binding site on Smo that is completely distinct from the cyclopamine-binding site, and furthermore to pinpoint its location. In Chapter 3 I show that Smo contains a ciliary localization module and I map this ciliary localization module to a region of the cytosolic intracellular domain (ICD). I demonstrate that this module is sufficient to target a heterologous protein to the cilium, but is not sufficient to activate downstream components.

How, then, do the different modules interact? How does binding of a ligand at the oxysterol-binding site within the CRD elicit a response in the heptahelical bundle and then in the cytosolic tail? How does the activation state get relayed from the ligand binding sites to the effector domains that expose the ciliary targeting sequence of Smo and result in ciliary translocation? Allosteric effects most likely play a significant role in relaying the signal. The

only crystal structure of Smo solved to date contains the seven transmembrane domain region, while the CRD and the ICD, as well as the critical aspects that define the interaction between modules are missing (Wang et al., 2013).

In order to gain an understanding of how the CRD communicates with the rest of the protein, it would be very interesting to map the residues that form the sterol-binding pocket – and whether any residues from the heptahelical bundle or the extracellular loops contributes to ligand binding at this CRD site. To this end, a crystal structure of full-length Smo would be ideal but also difficult to obtain. In the absence of crystallography data, a surrogate approach would make use of my finding that 6-azi,25-OHC binds Smo specifically at the oxysterol-binding site in a competitive manner, as shown in Figure S6 in the Appendix. This sterol is photoactivatable, and exposure to UV radiation generates a reactive species that will crosslink to any amino acid residues in its immediate vicinity. Upon incubation of a Smo extract with 6-azi,25-OHC and photocrosslinking, the covalent adducts of the sterol to individual peptides can be detected by tryptic digest followed by mass spectrometry (MALDI-TOF). Such an in-vitro experiment requires a source of large amounts of protein – in Chapter 2 I showed that Xenopus Laevis Smo expressed in *Spodoptera frugiperda* Sf9 insect cells is active in detergent extracts and binds sterols at the CRD site.

In Chapter 2, I showed that Smo CRD mutations ($mSmo^{L112D}$, $mSmo^{W113Y}$ or the combined $mSmo^{LW}$) ablate the response to oxysterols, yet still responds to SAG or the endogenous Shh ligand. In Chapter 3, I demonstrate that a Smo mutant in which the seventh transmembrane domain was replaced with the Drosophila counterpart ($mSmo^{DrSmoTM7}$) fails to

respond to the Smo agonist SAG, but responds to oxysterols or the endogenous Shh ligand. An immediate question is whether a combination of a mutation at the cyclopamine binding site with a mutation at the oxysterol binding site results in a completely inactive protein that fails to respond to the endogenous ligand – or whether it still responds to the endogenous ligand, in which case additional elements in the sequence of Smo are required for activation. To test this hypothesis, a combined $mSmo^{LW,DrSmoTM7}$ mutant would be overexpressed in Smo-null MEFs, and the transcriptional response measured by qPCR at rest or upon stimulation with Shh ligand relative to WT Smo. In addition, the ciliary localization of the mutant would be scored in a complementary experiment. While a mutant that fails to respond to agonists would be expected as both ligand-binding sites would be killed, a mutant that still responds to Shh ligand would indicate that Smo activation does not rely solely on those two ligand-binding sites, and that additional sequence elements contribute to the activated state. To limit the chance that the double mutant is inactive due to misfolding, individual point mutations corresponding to the divergent residues between the mouse and Drosophila TM7 can be introduced one at a time into the cyclopamine-binding site of the $mSmo^{LW}$ mutant instead of the whole DrSmo TM7 domain. Correct folding can be tested by the presence of the mature, post-Golgi Smo band that migrates slower by SDS-PAGE. A possibility would be that while the point mutations are sufficient to ablate the response to SAG or oxysterols, they do not affect all the residues that mediate the binding of the actual endogenous ligand, and thus the endogenous ligand can still (partially) bind.

The fact that Smo is regulated at two independent sites is intriguing; my work in Chapter 2 suggests that the oxysterol-binding site is required for maximal activation of Smo for cells in tissue culture. It is possible that Smo regulation involves two separate mechanisms, and that regulation through sterols at the oxysterol-binding site in the CRD serves as a context-dependent additional layer of regulation. What is the role of the two sites in the endogenous context, and what is the relative importance of these two sites of Smo regulation? Is Smo differentially regulated in response to the levels of sterols in tissues? To answer this question, a mouse model of the $mSmo^{LW}$ would need to be generated. I would expect the mice to show subtle phenotypes, but the defects would be indicative of the relative importance of regulation of one particular site over the other. For instance, if one type of tissue requires maximal activation of Smo through the action of a sterol, then a defect will be visible, whereas no defect will be observed if Smo activation through the cyclopamine-binding site suffices. In the developing limb bud, a spatio-temporal gradient of Shh ligand specifies different digit identities (Harfe et al., 2004); in the developing neural tube, a gradient of Shh ligand specifies distinct identities for the ventral neuron types (Briscoe and Ericson, 2001). The mouse model described above will show whether the Shh gradient correlates with different levels of Smo activation – and thus the different developmental outcomes. In Drosophila, the Smo CRD is dispensable, but Drosophila Smo also lacks regulation by sterols; this mouse model will show whether the CRD is dispensable in vertebrates, and will pinpoint the location in the developing embryo where regulation of Smo through sterols plays a significant role.

4.2 Pharmaceutical inhibition of Smo ligand-binding sites

Smo contains two distinct ligand binding sites which can both be inhibited pharmaceutically. The cyclopamine-binding site can be inhibited by SANT-1, Vismodegib and the vast majority of Smo inhibitors developed to date. In Chapter 2 I introduce 22-aza cholesterol as the first Smo inhibitor specific to the oxysterol-binding site. The compound inactivates Smo with an IC_{50} of ~3μM. I suspect the main limiting effect is the high lipophilicity which forces 22-aza cholesterol to distribute into cell membranes and thus lowers its availability in solution. Together with my work defining the structure-activity relationship of the sterols that bind at the CRD site, 22-aza cholesterol can serve as lead compound for a medicinal chemistry optimization protocol to identify analogs with improved binding affinities and lower lipophilicity.

From a therapeutic perspective, inhibition of both ligand binding sites on Smo is highly desirable. I have shown in Chapter 2 that a Smo mutant completely lacking the CRD, and thus the oxysterol binding site, still shows a low-level response to agonists. This suggests that the endogenous ligand activates Smo primarily at the oxysterol-binding site, but also that ligand binding at both sites is required for a full response. Inhibition at the cyclopamine site with Vismodegib is efficient and has received FDA approval for use in patients with metastatic basal cell carcinoma. However, treatment with Vismodegib eventually results in drug resistant Smo mutants such as $mSmo^{D473H}$, which maps to the cyclopamine binding site and renders it unable to bind Vismodegib (Yauch et al., 2009). While the cyclopamine-binding site is affected in this mutant, the oxysterol-binding site is fully active and thus explains why the protein can still function while accumulating the mutations in the cyclopamine site. It is therefore conceivable

that targeting both sites simultaneously will minimize the occurrence of drug resistance by limiting the likelihood of a mutant protein with both ligand binding sites affected to still signal to downstream components. It will be very interesting to identify synergistic combinations of a cyclopamine-binding site inhibitor and of an oxysterol-binding site inhibitor.

An even better approach for a therapeutically relevant Smo inhibitor would be to develop a bidentate ligand that simultaneously targets both the cyclopamine binding and the oxysterol binding sites. Such a molecule would likely contain ligands for either site tethered to each other through a linker. Since the affinity of inhibitors at the cyclopamine binding site is low nanomolar, while 22-aza cholesterol has an IC_{50} of about 3μM, one advantage of this approach would be that the bidentate ligand will first bind to the cyclopamine site through the high-affinity moiety, thus tremendously increasing the local concentration of ligand at the oxysterol binding site and in effect increasing the affinity for the oxysterol binding site by several orders of magnitude compared to the untethered inhibitor. However, the specifics of such a bidentate ligand are not trivial in the absence of a crystal structure of full-length Smo, as the length of the linker must be chosen such that it places both the moiety targeting the cyclopamine-binding site as well as the moiety targeting the oxysterol-binding site at an optimal distance relative to each other so that both sites can be bound simultaneously.

4.3 Open questions and future directions

An important unanswered question in the Hedgehog field is how Ptc inhibits Smo. Several lines of evidence suggest a catalytic mechanism of inhibition through regulation of a

small molecule. Ptc bears resemblance to molecular pumps of the RND superfamily; furthermore, Ptc shows significant homology to another RND member, NPC1, which has been shown to transport cholesterol esters. Mutations that inactivate the pump activity of RND permeases also inactivate Ptc and are found in Gorlin syndrome patients (Taipale et al., 2002). Thus, it appears that Ptc may itself regulate a small molecule such as a sterol, but direct evidence of a pump activity for Ptc has not been reported, and no direct binding of sterols to Ptc has been reported. The identity of the small molecule intermediate between Ptc and Smo remains unknown, and I can only speculate as to what the endogenous small molecule actually is. For instance, In Chapter 2 I show that the endogenous Smo regulator is not a sterol ester, as in biological settings sterols are esterified only at the 3-OH position; in the case of sterols that activate Smo at the oxysterol-binding site, that free 3-OH position is critical and must remain unmodified. Furthermore, the iso-octyl sidechain requires at least 6 carbon atoms in order to both push Smo to the cilium as well as to stimulate the downstream pathway effectors. This evidence rules out a whole class of compounds, steroids, which are based off the structure of pregnenolone, and which generally lack the iso-octyl sidechain altogether. If there is only one endogenous small molecule regulator of Smo, and it is indeed a cholesterol derivative, it remains to be established how it can regulate both the cyclopamine-binding site and the oxysterol-binding site in the CRD – ideally through a crystal structure of the full-length Smo bound to the endogenous small molecule.

The identity of the sterol modulator of Smo at the CRD oxysterol-binding site remains elusive. A possible approach to identify the endogenous ligand would be the biochemical

purification of Smo-modulating lipids from cilia – the Smo-modulating capability of a fraction can be tested by assessing the Smo ciliary localization as well as by measuring the transcriptional response of the pathway. A major caveat to this approach is the isolation of ciliary membranes in large enough quantities to serve as a source for the lipid fractionation; my results indicate a divergence between the regulation of Smo in Drosophila and in vertebrates, therefore the biochemical fractionation should be applied to vertebrate cell membranes, while more abundant ciliary membranes from organisms like *Chlamydomonas reinhardtii* would not be expected to provide an informative answer. Chloral hydrate has been reported to deciliate kidney epithelial cells, and cilia can be recovered from the solution (Praetorius and Spring, 2003); this method may provide a sufficient supply of ciliary membranes to support a biochemical investigation.

In the absence of biochemical evidence, an indirect reverse-genetic approach to identify this elusive sterol involves targeting of its biosynthetic pathway; in brief, RNAi would be directed at all genes in the genome that resemble oxigenase enzymes, including here all CYP450 enzymes. This latter approach may highlight individual biosynthetic genes that may form the sterol modulator of Smo. However, if Smo is regulated by a ubiquitous small-molecule and not by a dedicated oxysterol with a single cellular function, pleiotropic effects due to absence of this small molecule (for instance on vesicular transport or on sorting into the proper post-ER compartment) will likely mask the Hh pathway phenotype.

The possibility that Hedgehog signal transduction is regulated through a small molecule such as a direct cholesterol metabolite is a very promising venue from a therapeutic perspective. A variety of chemical compounds that inhibit the biosynthesis of cholesterol such as statins are

currently approved for human use; the findings presented herein may lead to novel therapeutic uses of such compounds.

In Chapter 2 I find that DrSmo does not bind oxysterols. How then is DrSmo activated, and is this mechanism conserved? Unlike vertebrate Smo, which has two distinct small molecule binding sites, no small molecules (synthetic or endogenous) are known that bind DrSmo. Ptc and Smo are conserved across phyla; in fact, the transmembrane domains show the highest conservation of residues between Drosophila and vertebrate Smo. Furthermore, in vertebrate Smo, the cyclopamine-binding site maps to this transmembrane region. Taken together, the evidence points to a common Smo activation mechanism through a small molecule, and suggests that an endogenous small-molecule might bind Drosophila Smo in the transmembrane region as well in order to trigger its activation. In Chapter 3, I assayed the activity of a portion of DrSmo consisting of the CRD and heptahelical bundle in mammalian cells by targeting it to primary cilia by fusion with the intracellular domain (ICD) of mSmo. This DrSmo^{mSmoICD} construct is constitutively active and refractory to inhibition by Ptc or by sterol depletion, suggesting that DrSmo might be regulated differently from vertebrate Smo, in spite of the conservation of Ptc. I further show that the vertebrate Smo ICD is not sufficient for signaling downstream, thus the activation state of the DrSmo^{mSmoICD} mutant must be relayed downstream by the seven spanning region. In Chapter 2 I find that the vertebrate Smo CRD binds oxysterols but that Smo can be activated partially in response to pathway stimulation with the endogenous Hh ligand even in the absence of the CRD. Interestingly, DrSmo$^{\Delta CRD}$ is completely inactive in Drosophila (Nakano et al., 2004), in contrast to vertebrate Smo$^{\Delta CRD}$ (Aanstad et al., 2009; Taipale et al., 2002). Thus

DrSmo CRD does not bind sterols but is absolutely required for function, perhaps by playing a critical role in stabilizing the active conformation of DrSmo. An important implication of my findings is that Drosophila and vertebrate Smo share a similar mechanism for activation, and most likely involve a similar though not identical small-molecule ligand that binds Smo within the transmembrane region. The ciliary localization of Hh pathway components in vertebrates, and the divergence of the Smo tails as well as the insensitivity of Drosophila Smo to oxysterols, all suggest that an additional layer of regulation of Smo has evolved since the divergence of Drosophila and vertebrates. This translates to the possibility that vertebrate Smo is regulated by two separate small molecules: one that binds the cyclopamine-binding site within the transmembrane barrel and is similar to the small molecule that activates the Drosophila homolog, and a second one that binds the oxysterol-binding site in the vertebrate CRD. It is plausible that this additional mechanism of regulation is separate from the small-molecule-mediated regulation by Ptc – and this process most likely involves a second small molecule such as an oxysterol, the identity of which remains unknown. Whether vertebrate Ptc regulates a single small molecule that only targets one of the Smo sites, or perhaps regulates two separate small molecules that each target a separate site on Smo has yet to be determined. Understanding the mechanistic basis for the evolutionary divergence in Smo regulation is an important future goal.

The ciliary events subsequent to Smo activation and translocation that lead to activation of the downstream components remain unclear from a mechanistic perspective. This aspect is of particular importance given the divergence of Hedgehog pathway components downstream of Smo in vertebrates as opposed to arthropods, and may involve ciliary proteins in more direct

transduction roles than simply in the maintenance of cilia. In vertebrates, Suppresor of Fused (SuFu) forms a complex with Gli that promotes processing of Gli by the proteasome to the Gli-R repressor form. In the basal state of the pathway, the complex traffics into and out of the cilium; upon activation of Smo, however, the SuFu-Gli complex dissociates at the cilium. This liberates and stabilizes full-length activator form of Gli, which translocates to the nucleus and transcribes the Hedgehog target genes (Tukachinsky et al., 2010). From a mechanistic perspective, how the signal is transduced from Smo to SuFu and Gli is not known. Furthermore, what happens to the SuFu-Gli complex upon pathway activation, how the complex falls apart at the cilium, and how the full-length Gli activator form is stabilized and protected to avoid processing by the proteasome are all poorly understood. One possibility is that activated Smo interacts directly with the SuFu-Gli complex at the cilium and induces its dissociation; alternatively, Smo may activate a different ciliary protein, which in turn catalyzes the dissociation of the SuFu-Gli complex

Recent work has implicated Evc2, a ciliary protein which resides in a compartment immediately adjacent to the transition zone, in mediating Hh signaling at the cilium downstream of Smo (Dorn et al., 2012). Defects in Evc2 cause two human ciliopathies, Ellis-van Creveld and Weyers Acrofacial Dysostosis – which both lead to cilia with normal structure, but affected individuals show cardiac, orofacial and skeletal phenotypes resembling Hh pathway defects. Evc2 forms a complex with activated Smo; the interaction is spatially restricted to the transition zone and is essential for transduction of the signal to the SuFu-Gli complex (Dorn et al., 2012). Recessive Evc2 mutations cause Evc2 to fail to localize to the cilium, while dominant mutations

in Evc2 are mislocalized across the entire length of the cilium. Intriguingly, Evc2 or its paralog Evc are not expressed in certain tissues where Hh signaling is important, such as the nervous system, and therefore tissue-specific interactions of Smo with other ciliary proteins are likely (Dorn et al., 2012). While the Smo-Evc2 complex has been characterized, it is not known at present which domains(s) or residues of Smo mediate this interaction and how the activation state of Smo regulates the presentation of these domains to Evc2. In order to answer these questions, a deletion analysis similar to the work I present in Chapter 3 would be necessary to pinpoint the domains of Smo that interact with Evc2. The Smo-Evc2 complex can be readily identified by reciprocal immunoprecipitation followed by Western blotting of the complex partner. The deletion constructs can be tested for proper folding through their ability to bind BODIPY-cyclopamine; then, any Smo deletion constructs that fail to immunoprecipitate with Evc2 likely contain deletions in the region that interacts with Evc2. Both Evc2 and the Smo deletion constructs would be overexpressed in 293T cells, which cannot respond to Hedgehog signaling; if the forced interaction of Evc2 and the Smo deletion construct is lost even in this unregulated overexpression system, the deletion likely spans a domain of Smo required for binding Evc2. In order to prove that a candidate region interacts indeed with Evc2, a test for sufficiency is required. To this end, any candidate region of Smo that is suspected to interact with Evc2 can be fused to a heterologous protein such as the soluble eGFP; if Evc2 and the eGFP-Smo chimera co-immunoprecipitate in reciprocal experiments, this would confirm the identification of the region of Smo interacting with Evc2.

The vertebrate Smo ICD contains two stretches of basic residues in close proximity to cysteines, which are hallmarks of palmitoylation sites (Bijlmakers and Marsh, 2003). I found that ablation of the first basic stretch or of the full complement of basic residues in both stretches results in proteins (mSmo^{A11} or mSmo^{A21}) that are unable to signal downstream – but localize robustly to the cilium in a regulated fashion. One possibility is that the region 565-581 of the ICD mediates the interaction with Evc2 directly; alternatively, the region 565-581 may serve as a recognition site for a palmitoyl-transferase to acylate a nearby cysteine residue, and the presence of the palmitoyl moiety on Smo in turn facilitates the interaction with Evc2. In the mSmo^{A21} mutant, palmitoylation would not be expected; the fact that this mutant fails to signal downstream but otherwise behaves like the wildtype protein indicates that palmitoylation may play a crucial role in signaling downstream.

In order to prove a direct role for acylation, all cysteine residues in the ICD should be mutated. Palmitoylation of Smo can be tested directly by treating cells with radioactive [^{3}H]-palmitate (Follit et al., 2010) followed by immunoprecipitation of Smo to detect the incorporation of radioactivity. Alternatively, a bio-orthogonal probe such as 15-azidopentadecanoic acid can be used instead of the radioactive palmitate; the Click chemistry detection involves the copper(I)-catalyzed cycloaddition after immune-precipitation against Smo to an alkyne-fluorophore conjugate for in-gel detection (Charron et al., 2009), and the method can easily be coupled to immunofluorescence microscopy to specifically quantitate palmitoylated Smo at the cilium.

However, the interaction of activated Smo with Evc2 is not the only ciliary event required for correct signal transduction. Two proteins of the IFT-B complex, IFT25 and IFT27, form a binary complex that is conserved throughout vertebrates but is missing in Drosophila. The IFT25-IFT27 complex is not required for ciliogenesis, but appears essential for transduction of the Hh signal in vertebrates. The loss of IFT25 leads to mislocalization of Ptc, Smo and Gli2 at the cilium and disrupts the Hh pathway response upon stimulation. More specifically, Gli2 does not accumulate at the cilium in response to signaling, while Patched and Smo are constitutively localized at the cilium regardless of the presence or absence of the Hh ligand. Interestingly, despite the loss of IFT25, the cilia appear morphologically normal, and also show normal localization as well as normal amounts of other IFT proteins such as IFT88. Knock-out animals survive to birth but show severe abnormalities indicative of Hh signaling defects (Keady et al., 2012). Thus, rather than facilitating transport into the primary cilium, the IFT25-IFT27 complex enables the export of proteins from the cilium and allows the dynamic redistribution of Hh pathway components in response to signaling. In the absence of signaling Smo is efficiently removed from the cilium by the IFT25-IFT27 complex, while in the presence of stimulation Ptc is instead removed from the cilium. Which part of Smo interacts with the IFT25-IFT27 complex, whether this is a direct interaction or perhaps involves a different protein intermediary, and whether the interaction is regulated by the activation state of Smo remains to be determined.

I show that the ciliary localization of Smo and the ability of Smo to activate downstream components are mediated by different sequence motifs in the ICD. It would be very interesting to map the minimal domain required for activation of downstream components, and the work

presented herein provides a framework for such additional mapping of the downstream activating domain. To this end, one possible approach would be to fuse a heterologous well-defined CLS (for instance, the 18 amino acid CLS of Fibrocystin (Follit et al., 2010)) C-terminally to a Smo construct lacking both endogenous CLS, such as mSmo$^{\Delta 615\text{-}793}$; after additional mapping of the CLS-2, a better construct would contain two short internal deletions corresponding to the two CLS, while having the majority of the ICD intact. I expect that such a chimeric construct will be targeted to the cilium by the exogenous CLS, that it rescues the Smo$^{-/-}$ defect and that it activates the downstream pathway components. Then, internal deletions of short ICD stretches can be introduced in this construct and tested in the context of downstream pathway activation, to map out the minimal downstream activating domain. Furthermore, all constructs generated this way can be tested for successful folding by their ability to bind BODIPY-cyclopamine.

A broader biological question is what the role of the transition zone, and in particular of the Tctn1-containing transition zone complex, is in both normal ciliary function and in the context of Hedgehog signaling at the cilium. While many transition zone proteins are essential for ciliogenesis as they establish a diffusion barrier between the plasma membrane and the ciliary membrane at the base of the cilium, the Tctn1-containing complex is not essential for ciliogenesis but instead is required for proper Hh signal transduction at the cilium. Tctn1 does not associate with Smo, but loss of Tctn1 causes Smo to localize poorly to cilia even in the presence of SAG (Garcia-Gonzalo et al., 2011). Separately, Evc2 localizes to the distal end of the transition zone but does not associate with Tctn1 in the same complex. Evc2 however associates with Smo and is essential for Hh signaling (Dorn et al., 2012). Interestingly, targeting

Smo to the Evc2 expression zone artificially and thus limiting its spread throughout the axoneme results in moderate but below-maximal pathway activation, while Evc2 mutations that lead to its expression across the entire length of the cilium have dominant negative effects on the Hh pathway (Dorn et al., 2012). This raises the possibility that a hierarchical sequence of multiple events at the transition zone relays the signal from Smo to the Gli-SuFu complex before the Gli-SuFu complex reaches the tip of the cilium where it dissociates in response to signaling.

4.4 References

Aanstad, P., N. Santos, K.C. Corbit, P.J. Scherz, A. Trinh le, W. Salvenmoser, J. Huisken, J.F. Reiter, and D.Y. Stainier. 2009. The extracellular domain of Smoothened regulates ciliary localization and is required for high-level Hh signaling. *Current biology : CB*. 19:1034-1039.

Bijlmakers, M.J., and M. Marsh. 2003. The on-off story of protein palmitoylation. *Trends Cell Biol*. 13:32-42.

Briscoe, J., and J. Ericson. 2001. Specification of neuronal fates in the ventral neural tube. *Curr Opin Neurobiol*. 11:43-49.

Charron, G., M.M. Zhang, J.S. Yount, J. Wilson, A.S. Raghavan, E. Shamir, and H.C. Hang. 2009. Robust fluorescent detection of protein fatty-acylation with chemical reporters. *J Am Chem Soc*. 131:4967-4975.

Dorn, K.V., C.E. Hughes, and R. Rohatgi. 2012. A Smoothened-Evc2 complex transduces the Hedgehog signal at primary cilia. *Dev Cell*. 23:823-835.

Follit, J.A., L. Li, Y. Vucica, and G.J. Pazour. 2010. The cytoplasmic tail of fibrocystin contains a ciliary targeting sequence. *J Cell Biol*. 188:21-28.

Garcia-Gonzalo, F.R., K.C. Corbit, M.S. Sirerol-Piquer, G. Ramaswami, E.A. Otto, T.R. Noriega, A.D. Seol, J.F. Robinson, C.L. Bennett, D.J. Josifova, J.M. Garcia-Verdugo, N. Katsanis, F. Hildebrandt, and J.F. Reiter. 2011. A transition zone complex regulates mammalian ciliogenesis and ciliary membrane composition. *Nature genetics*. 43:776-784.

Harfe, B.D., P.J. Scherz, S. Nissim, H. Tian, A.P. McMahon, and C.J. Tabin. 2004. Evidence for an expansion-based temporal Shh gradient in specifying vertebrate digit identities. *Cell*. 118:517-528.

Keady, B.T., R. Samtani, K. Tobita, M. Tsuchya, J.T. San Agustin, J.A. Follit, J.A. Jonassen, R. Subramanian, C.W. Lo, and G.J. Pazour. 2012. IFT25 links the signal-dependent movement of Hedgehog components to intraflagellar transport. *Dev Cell*. 22:940-951.

Nachtergaele, S., L.K. Mydock, K. Krishnan, J. Rammohan, P.H. Schlesinger, D.F. Covey, and R. Rohatgi. 2012. Oxysterols are allosteric activators of the oncoprotein Smoothened. *Nat Chem Biol*. 8:211-220.

Nakano, Y., S. Nystedt, A.A. Shivdasani, H. Strutt, C. Thomas, and P.W. Ingham. 2004. Functional domains and sub-cellular distribution of the Hedgehog transducing protein Smoothened in Drosophila. *Mech Dev*. 121:507-518.

Praetorius, H.A., and K.R. Spring. 2003. Removal of the MDCK cell primary cilium abolishes flow sensing. *The Journal of membrane biology*. 191:69-76.

Taipale, J., M.K. Cooper, T. Maiti, and P.A. Beachy. 2002. Patched acts catalytically to suppress the activity of Smoothened. *Nature*. 418:892-897.

Tukachinsky, H., L.V. Lopez, and A. Salic. 2010. A mechanism for vertebrate Hedgehog signaling: recruitment to cilia and dissociation of SuFu-Gli protein complexes. *J Cell Biol*. 191:415-428.

Wang, C., H. Wu, V. Katritch, G.W. Han, X.P. Huang, W. Liu, F.Y. Siu, B.L. Roth, V. Cherezov, and R.C. Stevens. 2013. Structure of the human smoothened receptor bound to an antitumour agent. *Nature*.

Yauch, R.L., G.J. Dijkgraaf, B. Alicke, T. Januario, C.P. Ahn, T. Holcomb, K. Pujara, J. Stinson, C.A. Callahan, T. Tang, J.F. Bazan, Z. Kan, S. Seshagiri, C.L. Hann, S.E. Gould, J.A. Low, C.M. Rudin, and F.J. de Sauvage. 2009. Smoothened mutation confers resistance to a Hedgehog pathway inhibitor in medulloblastoma. *Science*. 326:572-574.

Appendix: Supplementary materials

A.1 Supplementary Results

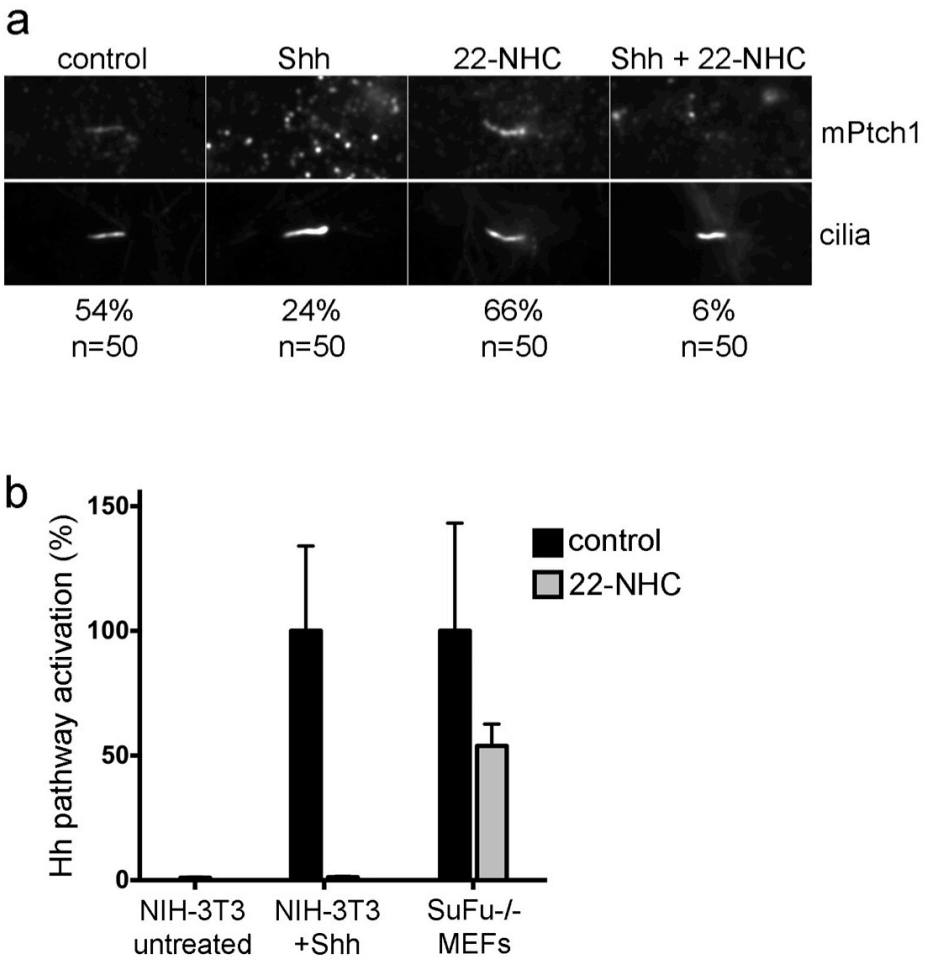

Supplementary Figure S1 related to Figure 2.1:

(a) 22-NHC does not block the disappearance of mPtch1 from primary cilia in response to Shh. Ptch1$^{-/-}$ MEFs stably expressing Cherry-tagged mPtch1 were incubated with Shh overnight, in the presence or absence of 22-NHC (10 μM). Cells were then fixed and processed for immunofluorescence with rabbit anti-Cherry antibodies (to visualize mPtch1) and mouse anti-acetylated tubulin antibodies (to visualize primary cilia). The micrographs show representative images of cilia, with Ptch1-positive cilia counts shown below the panels.

(b) 22-NHC does not block constitutive Hh signaling in SuFu$^{-/-}$ MEFs. SuFu$^{-/-}$ MEFs were incubated in the absence or presence of 22-NHC (10 μM), and the transcriptional response of the Hh pathway was measured by Q-PCR of the target gene Gli1. The same concentration of 22-NHC blocks Gli1 transcription in NIH-3T3 cells stimulated with Shh. All experiments were performed in triplicate, and error bars indicate the standard deviation of the mean.

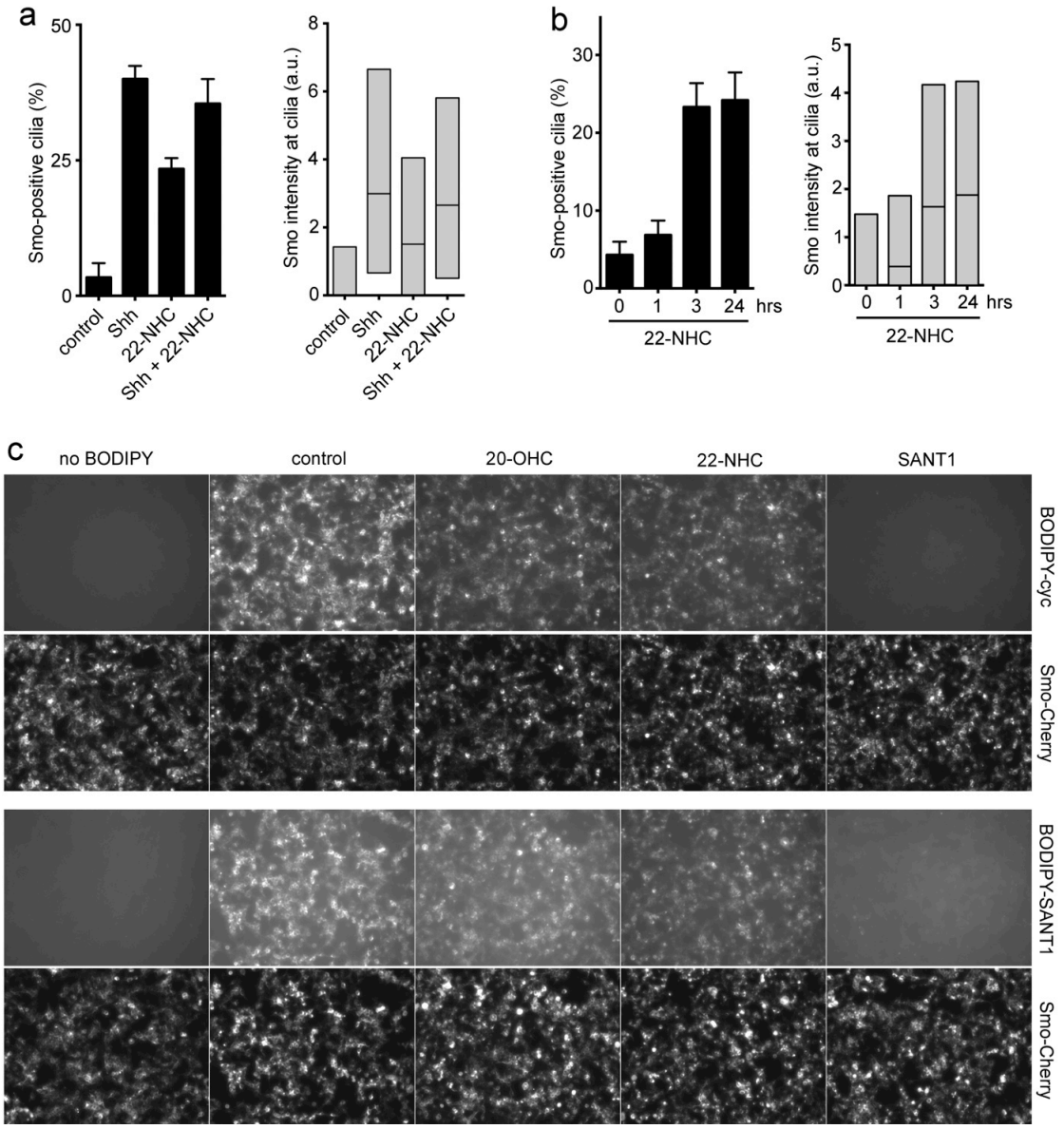

Supplementary Figure S2 related to Figure 2.2:

(a) 22-NHC does not impair ciliary localization of activated Smo in the presence of Shh. 3T3 cells were starved overnight in DMEM, then treated with control medium, 10μM 22-NHC (in DMEM) and/or Shh for another 24 hours. The cells were processed for immunofluorescence with anti-Cherry antibodies (to detect Smo) and anti-acetylated tubulin antibodies (ciliary marker). The bar graph on the left shows the percentage of cells with Smo-positive cilia. The box plot on the right shows fluorescence intensity of Smo at cilia, in arbitrary units; the lower and upper bounds of each box represent the 25th and 75th percentile of the distribution of ciliary fluorescence intensity, while the horizontal line represents the median intensity across the entire population of cilia.

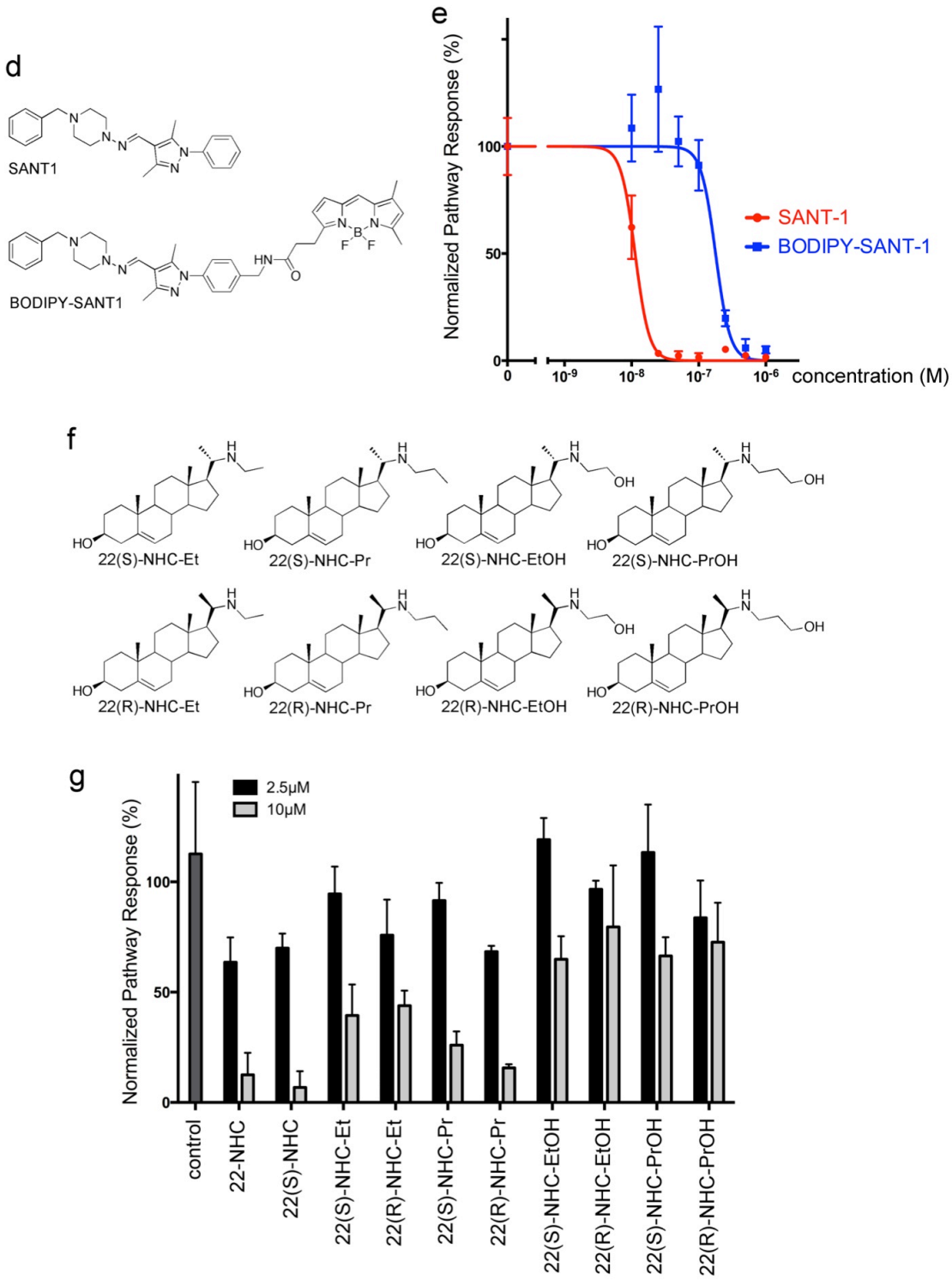

Supplementary Figure S2 (continued)

Supplementary Figure S2 (continued)

(b) Timecourse of ciliary accumulation of Smo in response to 22-NHC. 3T3 cells were starved overnight in DMEM, then treated with 10μM 22-NHC for 0, 1, 3 and 24hrs. The cells were fixed at the indicated times and processed for immunofluorescence with anti-Cherry antibodies (to detect Smo) and anti-acetylated tubulin antibodies (ciliary marker). The bar graph on the left shows the percentage of cells with Smo-positive cilia. The box plot on the right shows fluorescence intensity of Smo at cilia, in arbitrary units; the lower and upper bounds of each box represent the 25th and 75th percentile of the distribution of ciliary fluorescence intensity, while the horizontal line represents the median intensity across the entire population of cilia.

(c) 22-NHC does not compete with binding of BODIPY-cyclopamine (BODIPY-Cyc, top two rows of micrographs) or BODIPY-SANT1 (bottom two rows of micrographs) to mSmo. Human 293T cells expressing mSmo-Cherry were incubated with 10 nM BODIPY derivative, in the presence or absence of 10 μM 20-OHC, 10 μM 22-NHC or 4 μM SANT1. Cells were fixed, washed, and imaged by fluorescence microscopy, to detect mSmo-Cherry and the BODIPY conjugate.

(d) Structures of SANT1 and of the BODIPY-SANT1 derivative synthesized in this study.

(e) Shh Light II cells were stimulated with Shh in the presence of increasing concentrations of SANT1 and BODIPY-SANT1, and Hh pathway activity was measured by luciferase assay. Both SANT1 and BODIPY-SANT1 inhibit Hh signaling in a dose-dependent manner. All experiments in this panel were performed in quadruplicate, and error bars represent the standard deviation of the mean. Hh pathway activity was normalized to activity of Shh alone (100%).

(f) Structures of the 22-NHC analogs, 22-NHC-Et and 22-NHC-Pr. For each analog, the two diastereomers resulting from the two possible C20 configurations are shown (R and S).

(g) As in (c), but with Shh stimulation in the presence of the indicated concentrations of 22(S)-NHC, 22(R)-NHC-Et, 22(S)-NHC-Et, 22(R)-NHC-Pr and 22(S)-NHC-Pr. Both R and S diastereomers of 22- NHC-Et and 22-NHC-Pr inhibit Hh signaling.

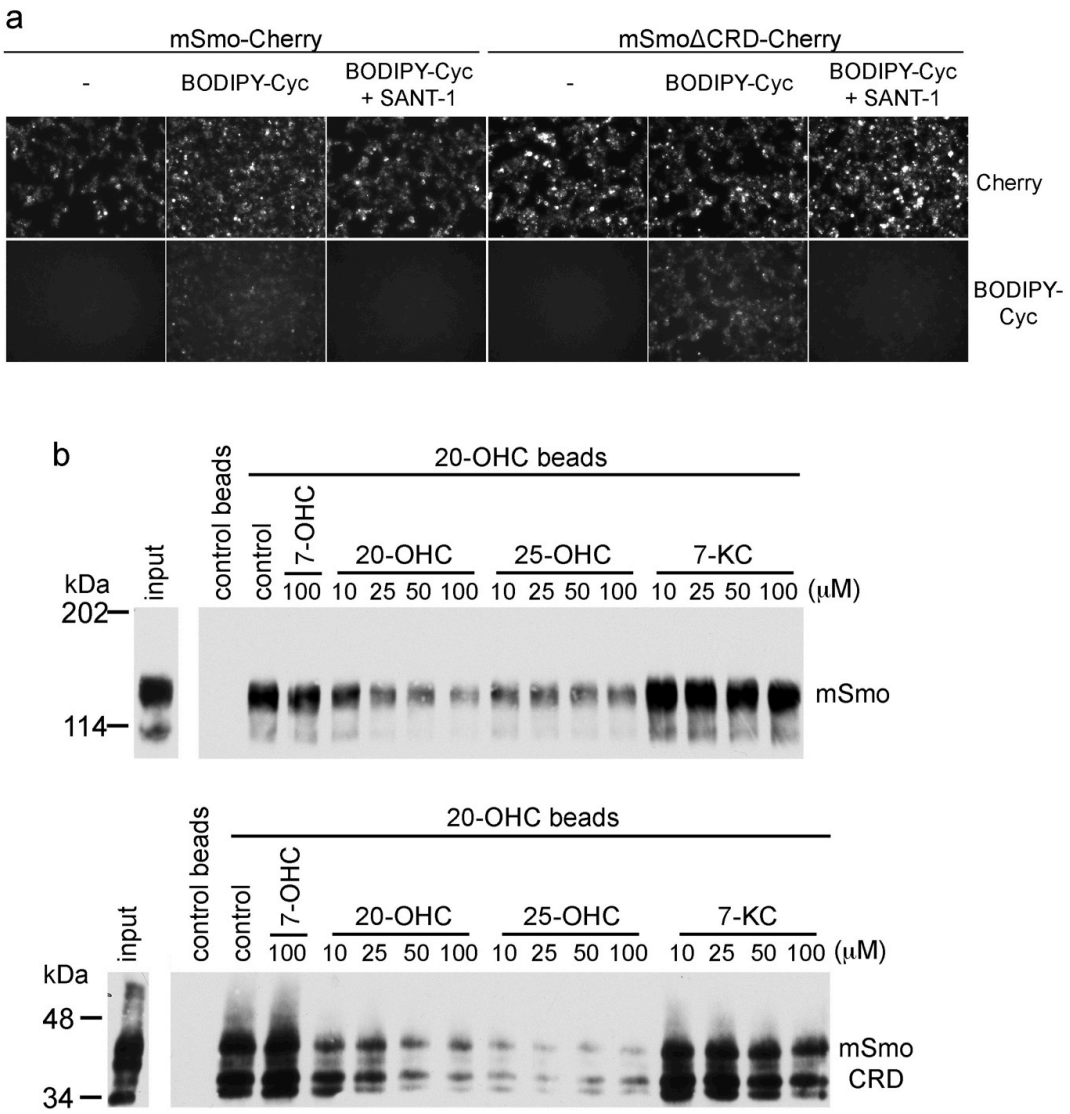

Supplementary Figure S3 related to Figure 2.4:

(a) Human 293T cells expressing mSmo-Cherry or mSmo$^{\Delta CRD}$-Cherry were incubated with 10 nM BODIPY-Cyc, in the presence or absence of 2 μM SANT1. Cells were fixed, washed, and imaged by fluorescence microscopy, to detect the Cherry fusions and the BODIPY conjugate. Both mSmo and mSmoΔCRD bind BODIPY-Cyc.

(b) Detergent extracts of 293T cells expressing mSmo-Cherry, or supernatants containing HA-tagged mSmoCRD were incubated with 20-OHC beads, in the presence of 7-OHC (negative control), or the active oxysterols 20-OHC and 25-OHC, or the inactive 7-keto-cholesterol (7-KC). Bound mSmo-Cherry and mSmoΔCRD-HA were analyzed by SDS-PAGE and immunoblotting. Binding of mSmo and mSmoCRD to 20-OHC beads is competed by 20-OHC and 25-OHC, but not by 7-KC.

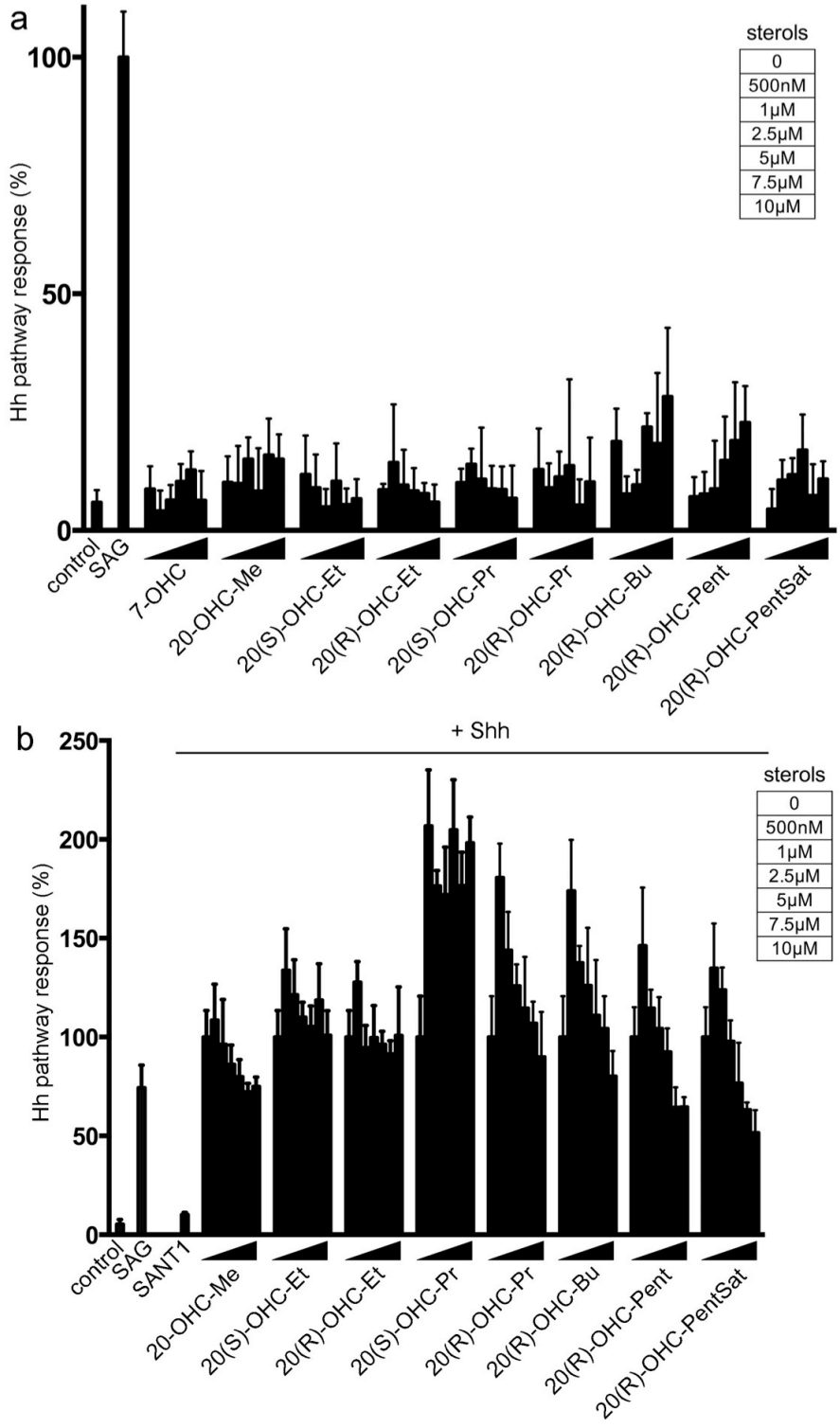

Supplementary Figure S4 related to Figure 2.5

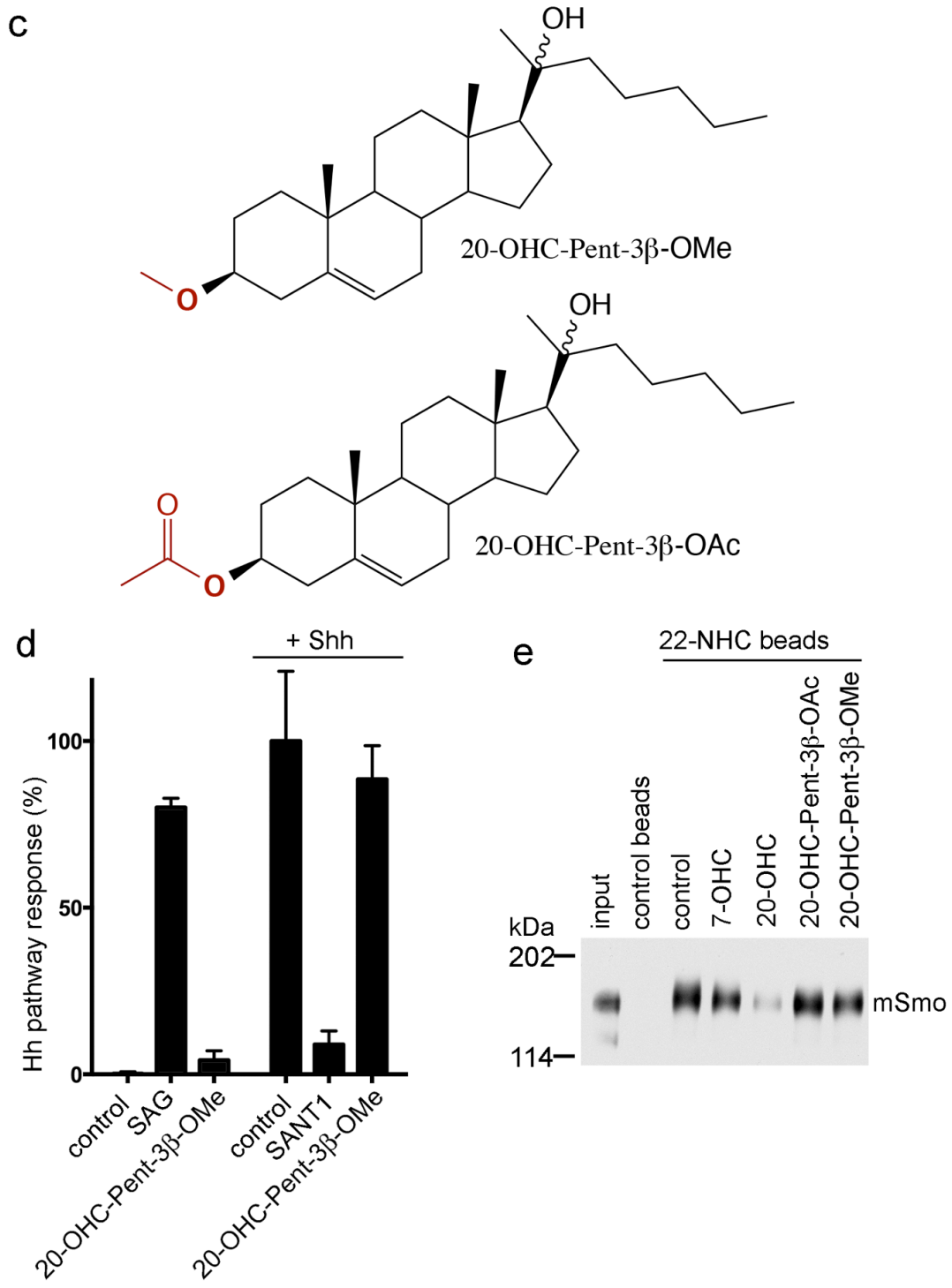

Supplementary Figure S4 (continued)

Supplementary Figure S4 (continued):

(a) Shh Light II cells were treated for 30 hours with the indicated concentrations of the oxysterol analogs 20-OHC-Me, 20(S)-OHC-Et, 20(R)-OHC-Et, 20(S)-OHC-Pr, 20(R)-OHC-Pr, 20(R)-OHC-Bu, 20(R)-OHC-Pent and 20(R)-OHC-PentSat, followed by measuring Hh pathway activity by luciferase assay. The inactive oxysterol, 7-OHC, was used as negative control, while SAG (1 μM) was used as positive control. All experiments were performed in quadruplicate, and error bars represent the standard deviation of the mean.

(b) As in (a) but with addition of Shh, to test if the oxysterol analogs have inhibitory activity on Hh signaling. The Smo inhibitor, SANT1 (1 μM) was used as positive control for Shh inhibition. All experiments were performed in quadruplicate, and error bars represent the standard deviation of the mean.

(c) Structures of 20-OHC-Pent-3β−OAc or 20-OHC-Pent-3β−OMe derivatives. The ester bond of 20-OHC-Pent-3β−OAc is labile under prolonged exposure in aqueous solutions, while the ether bond in 20-OHC-Pent-3β−OMe is chemically inert under normal assay conditions

(d) As in (a) but with addition of 20-OHC-Pent-3β−OMe, in the absence or presence of Shh. SAG1 (1 μM) was used as positive control for pathway activation, while SANT1 (1 μM) was used as positive control for Shh inhibition. The ether derivative 20-OHC-Pent-3β−OMe does not inhibit or activate Hh signaling. The ester bond in 20-OHC-Pent-3β−OAc hydrolizes under these assay conditions and was not included.

(e) Detergent extracts of 293T cells expressing mSmo-Cherry were incubated for one hour with 22-NHC beads, in the absence or presence of 100 μM 7-OHC, 20-OHC, 20-OHC-Pent-3β−OAc or 20-OHC-Pent-3β−OMe. After washing, protein bound to beads was eluted, separated by SDS-PAGE and immunoblotted with anti-Cherry antibodies. Neither 20-OHC-Pent-3β−OAc nor 20-OHC-Pent-3β−OMe compete binding of mSmo to 22-NHC beads, in contrast to 20-OHC.

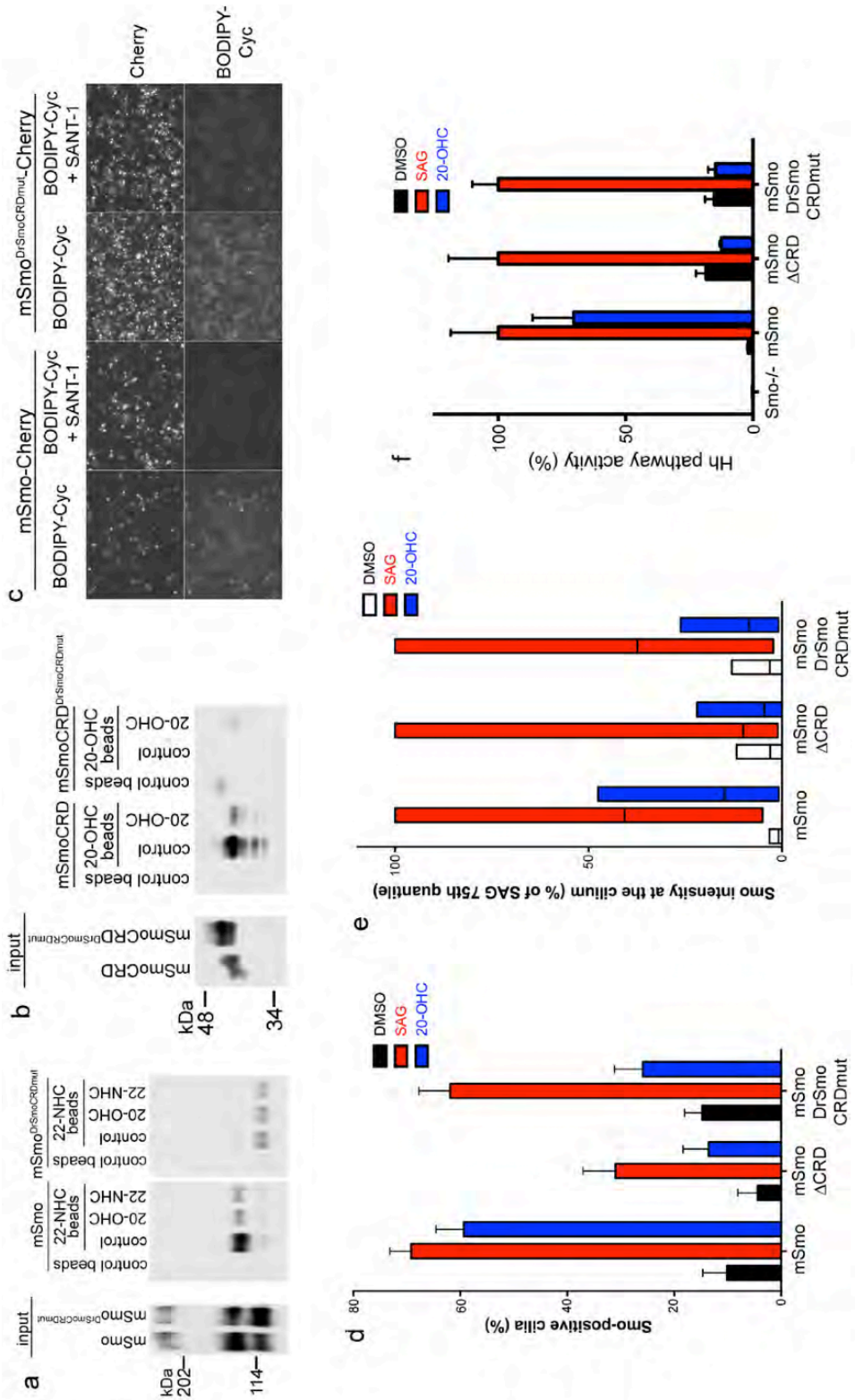

Supplementary Figure S5 related to Figure 2.6

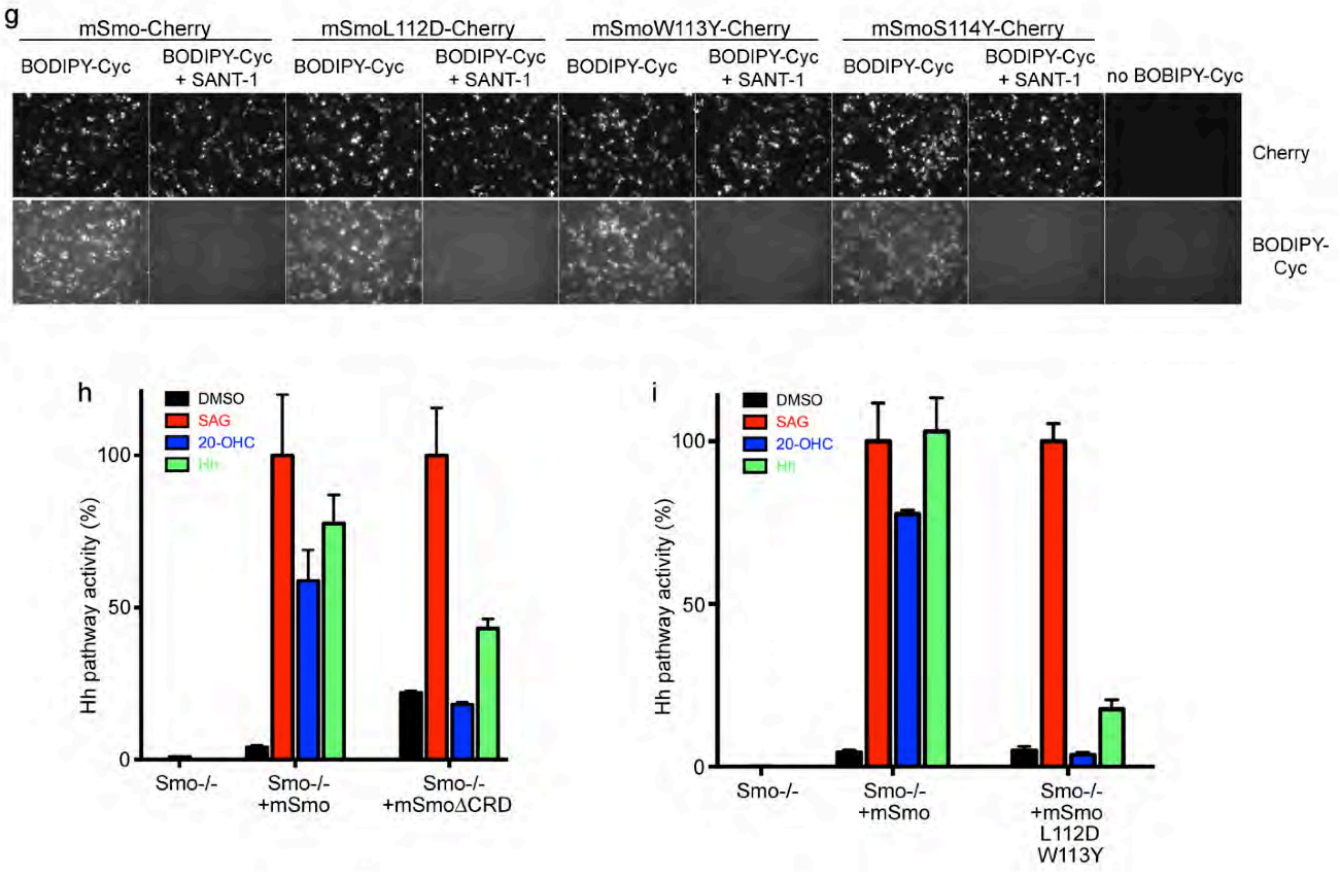

Supplementary Figure S5 (continued):

(a) Detergent extracts from 293T cells expressing Cherry-tagged mSmo or mSmo^{DrSmoCRDmut} were incubated with control beads or 22-NHC beads, in the absence or presence of 100 µM 22-NHC or 20-OHC. After washing, protein bound to beads was eluted, separated by SDS-PAGE and immunoblotted with anti-Cherry antibodies. The CRD mutant of mSmo does not bind 22-NHC beads, in contrast to wild-type mSmo.

(b) Secreted HA-tagged mSmoCRD and mSmoCRD^{DrSmoCRDmut} were incubated with control beads or 20- OHC beads, in the presence or absence of 100 µM free 20-OHC. Binding to beads was assayed as in (a), using anti-HA to detect mSmoCRD and mSmoCRD^{DrSmoCRDmut}. mSmoCRD^{DrSmoCRDmut} does not bind 20- OHC beads, in contrast to mSmoCRD.

(c) Human 293T cells expressing Cherry-tagged mSmo or mSmo^{DrSmoCRDmut} were incubated with 10 nM BODIPY-Cyc, in the presence or absence of 2 µM SANT1. Cells were fixed, washed, and imaged by fluorescence microscopy, to detect the Cherry fusion proteins and the BODIPY conjugate. Both proteins bind BODIPY-Cyc specifically.

Supplementary Figure S5 (continued):

(d) $Smo^{-/-}$ MEFs, stably expressing Cherry-tagged mSmo, mSmoΔCRD or $mSmo^{DrSmoCRDmut}$ were incubated overnight inß the presence of DMSO control, SAG (1 μM) or 20-OHC (10 μM). The cells were processed for immunofluorescence with anti-Cherry antibodies (to detect mSmo) and anti-acetylated tubulin antibodies (to visualize cilia). The graph shows the percentage of cells with Smo-positive cilia. MSmoΔCRD and $mSmo^{DrSmoCRDmut}$ respond to SAG but have a defective response to 20-OHC; in contrast, wild-type mSmo responds to both SAG and 20-OHC.

(e) As in (d), but with box plots showing the fluorescence intensity of Cherry-tagged proteins at cilia. For each condition, the Cherry signal was normalized to the intensity of the SAG treatment for the respective cell line. The lower and upper bounds of each box represent the 25th and 75th percentile of the distribution of ciliary fluorescence intensity, while the horizontal line represents the median intensity across the entire population of cilia.

(f) As in (d), but cells were processed for Q-PCR, to measure mRNA levels of the Hh target gene, Gli1. For each treatment, Gli1 levels were normalized to the level induced by SAG treatment in the respective cell line. Smo-/- MEFs were included as negative control. Each experiment was performed in triplicate, and the error bars show the standard deviation of the mean. $mSmo^{\Delta CRD}$ and $mSmo^{DrSmoCRDmut}$ respond to SAG but do not respond to 20-OHC; in contrast, wild-type mSmo responds to both SAG and 20-OHC.

(g) As in (c) but with expression of mSmo-Cherry, mSmoL112D-Cherry, mSmoW113Y-Cherry or mSmoS114Y-Cherry. All 4 proteins bind BODIPY-Cyc specifically.

(h) $Smo^{-/-}$ MEFs, stably expressing Cherry-tagged mSmo or $mSmo^{\Delta CRD}$ were incubated overnight with DMSO control, SAG (1 μM), 20-OHC (10 μM) or Shh. $Smo^{-/-}$ MEFs were included as negative control. Levels of Gli1 mRNA were measured by Q-PCR, as in (d). $mSmo^{\Delta CRD}$ does not respond to 20-OHC and has a reduced responsiveness to Shh.

(i) As in (h), but with Smo-/- MEFs stably expressing Cherry-tagged mSmo or the double point mutant mSmoL112D/W113Y. mSmoL112D/W113Y does not respond to 20-OHC and has a reduced responsiveness to Shh.

A.2 A photoactivatable probe for the oxysterol-binding site of Smo

6-azi,25-hydroxycholesterol (photo 25-hydroxycholesterol, Figure S6a) is a photoactivatable cholesterol derivative that was previously used to show direct binding of 25-hydroxycholesterol to SCAP (Adams et al., 2004). The compound contains a diazirine ring which is activated by exposure to UV radiation to eliminate nitrogen; this generates a reactive carbene radical which inserts into C-H bonds and thus crosslinks to nearby amino-acid residues. 6-azi,25-OHC also contains an iso-octyl sidechain similar to that of the Smo-activating oxysterol 25-OHC, making it likely to interact directly with Smo.

We tested whether 6-azi,25-OHC could be used to probe the oxysterol-binding site of Smo. The compound competitively inhibits binding of both full-length Smo as well as of the Smo CRD to 22-NHC beads (Figure S6b). This confirms that 6-azi,25-OHC binds directly to the oxysterol-binding site. Furthermore, we observed a similar inhibition profile as for 22-NHC: 6-azi,25-OHC inhibits the Hedgehog pathway stimulation by Shh and by oxysterols, but not by SAG (and in fact at lower doses shows a similar synergistic effect on SAG stimulation as seen for 22-NHC). In conclusion, 6-azi,25-OHC binds the same site as oxysterols and azasterols. 6-azi,25-OHC is a useful probe to map the residues which line the oxysterol-binding pocket within the Smo CRD, and any other residues which touch the bound sterols. The covalent adducts can be identified by mass spectrometric detection, or by incorporation of radioactivity if a radiolabelled 6-azi,25-OHC is used instead. To this end, the 3 position of the sterol is accessible and can be modified to generate radioactive [^{3}H]-6-azi,25-OHC using a procedure similar to that used for [^{3}H]-photocholesterol (Gehrig-Burger et al., 2005).

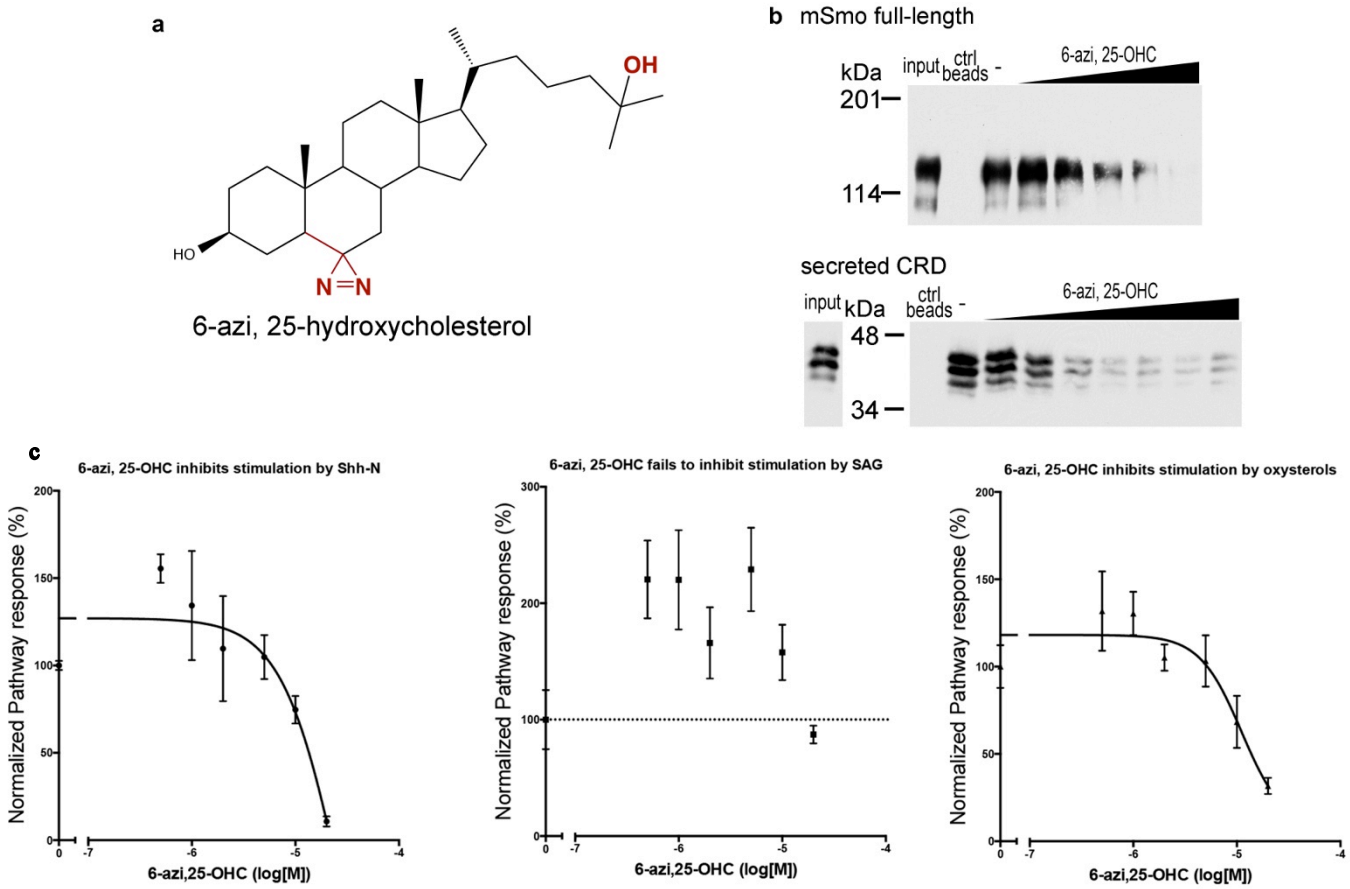

Supplementary Figure S6 6-azi, 25-hydroxycholesterol (photocholesterol) is a photoactivatable Smo inhibitor of the oxysterol-binding site

(a) structure of 6-azi, 25-hydroxycholesterol (6-azi,25-OHC). Highlighted in red are the structural modifications relative to the cholesterol structure.

(b) Detergent extracts of 293T cells expressing mSmo-Cherry, or supernatants containing HA-tagged mSmoCRD were incubated with 22-NHC beads, in the presence of 7-OHC (100µM, negative control) or 6-azi,25-OHC (5µM, 10µM, 25µM, 50µM, 100µM in the case of full-length mSmo, or 1µM, 2µM, 5µM, 10µM, 25µM, 50µM, 100µM) in the case of the CRD). Bound mSmo-Cherry and mSmo$^{\Delta CRD}$-HA were analyzed by SDS-PAGE and immunoblotting. Binding of mSmo and mSmoCRD to 22-NHC beads is competed by 6-azi,25-OHC.

(c) 6-azi, 25-OHC inhibits the stimulation by Shh (left panel) and by oxysterols such as 20-OHC-Pent (right panel) but not the stimulation by SAG (middle panel), thus recapitulating the inhibition profile of 22-NHC. Shh Light II cells were treated for 30 hours with the indicated concentrations of 6-azi, 25-OHC in the presence of Shh, 50µM SAG or 10µM 20-OHC-Pent followed by measuring Hh pathway activity by luciferase assay. Control medium was used as

Supplementary Figure S6 (continued):
negative control, while SAG (1 μM) was used as positive control. All experiments were performed in quadruplicate, the pathway response normalized to the level of stimulation in the absence of 6-azi,25-OHC and error bars represent the standard deviation of the mean.

A.3 Automated Image Analysis

A.3.1 Initial segmentation

In order to distinguish individual cilia from the local background, a locally-adaptive thresholding algorithm is used. In brief, the algorithm takes as input a 12-bit grayscale image obtained with staining for the ciliary marker acetylated Tubulin. The pixel intensities are first rescaled on a scale from 0 to 1, corresponding to the minimum and maximum pixel intensities in the picture respectively. Then, local thresholds are calculated for each pixel using a window of 100x100 neighbouring pixels. Each threshold value represents the weighted mean of the local neighbourhood minus an offset value. Pixels with thresholding values within a chosen region above the minimum are considered positive; the minimum and maximum thresholding values are chosen such that very bright or very dim pixels should not bias the filter, and the parameters may vary depending on the staining conditions or exposure settings across experiments, but stay the same within one complete experiment.

Positive pixels in close proximity to each other are then recognized as multi-connected objects, and given a unique identification number. The algorithm parses the entire list of multi-connected objects and filters them according to several criteria. Cilia have a unique elongated shape, and are easily recognizable by eye; to select cilia correctly, minimum and maximum size constraints are imposed initially on the multi-connected objects, to rule out noise or any non-ciliary staining. Then, an aspect ratio criterion is imposed such that only elongated objects are

filtered, and curved objects are generally eliminated; in conjunction with the size constraint, this criterion indirectly also filters out cilia that do not appear in focus. If the population of multi-connected objects is larger than 10, additional filtering takes place to eliminate outliers based on length or size, to ensure a more homogeneous population of cilia is recognized on the slide. Finally, each multi-connected region is extended by a 5 pixel radius, to ensure that the cilium is fully covered; the acetylated tubulin marker is internal to the primary cilium, while most of our analysis focuses on membrane staining, therefore it is imperative to integrate all the membrane staining signal.

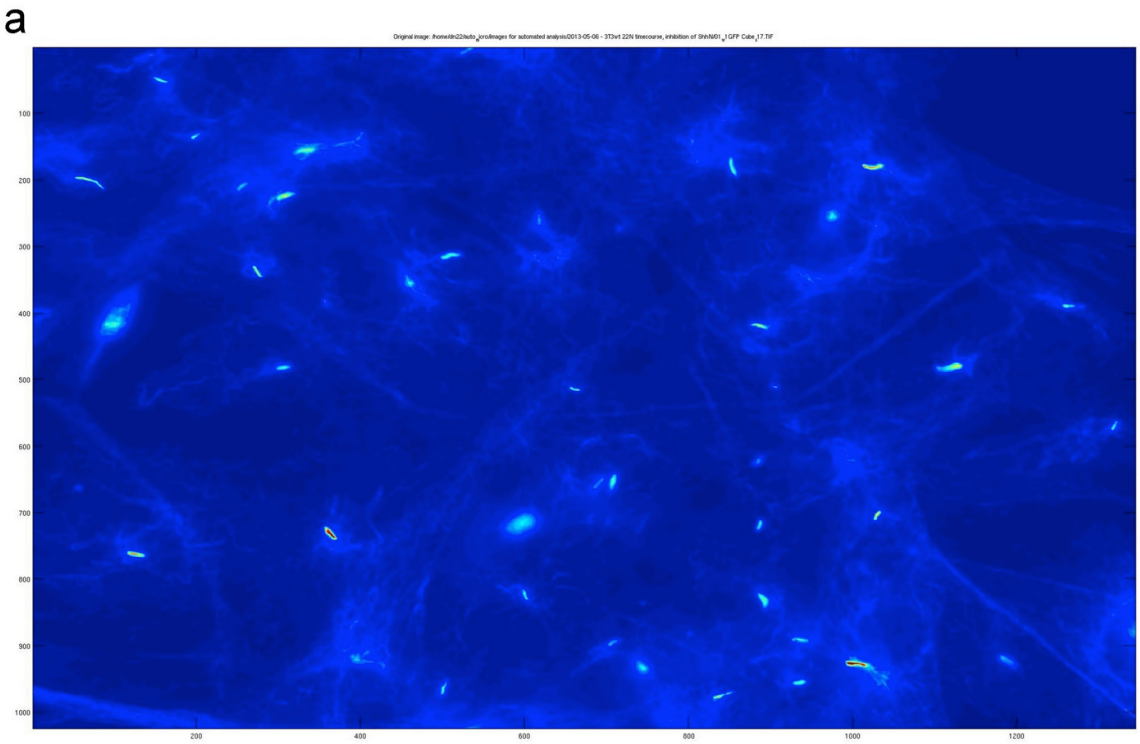

Supplementary Figure S7 Segmentation of cilia

(a) original image stained for the ciliary marker, acetylated tubulin

(b) large particles recognized that may alter the thresholding algorithm

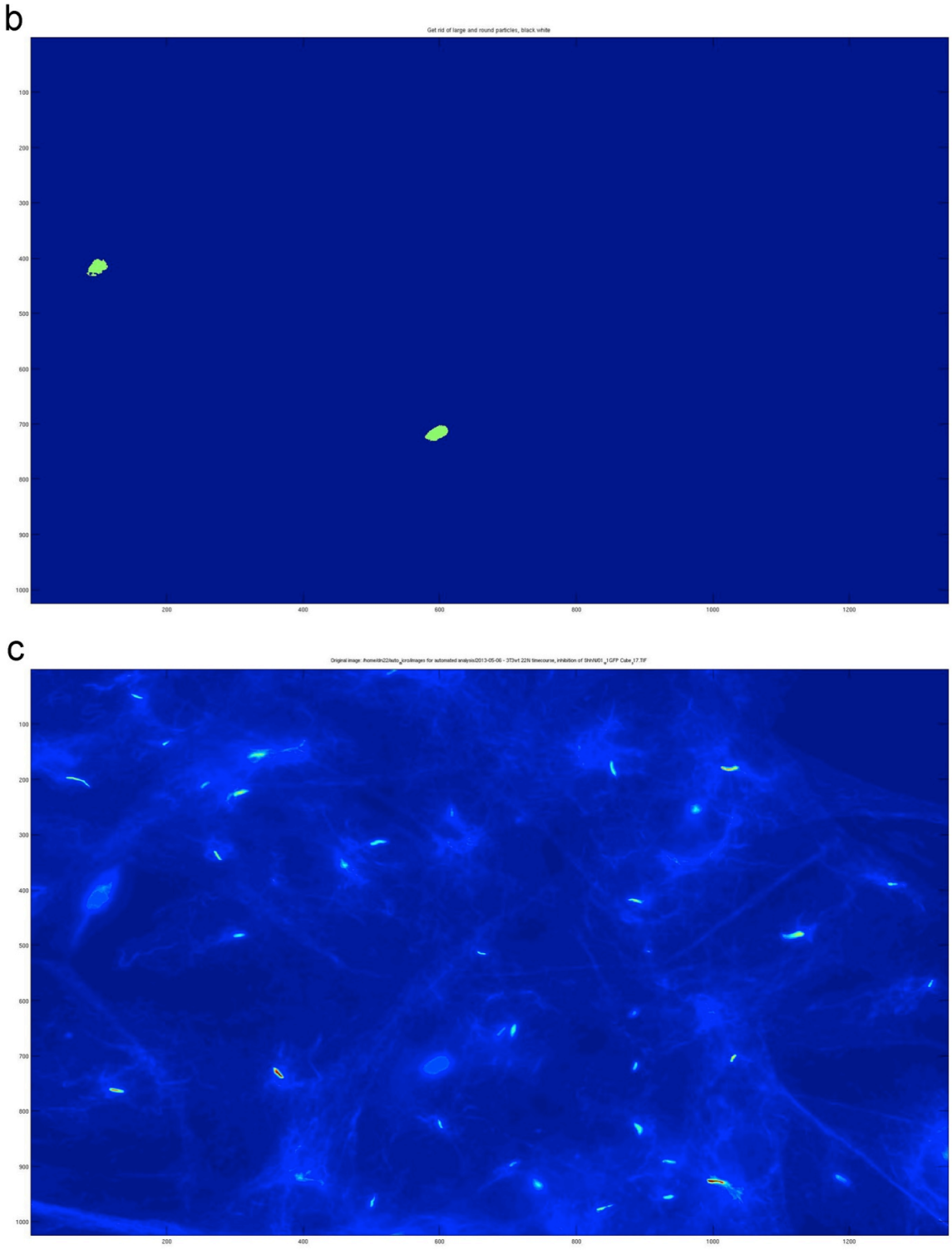

Supplementary Figure S7 (continued)

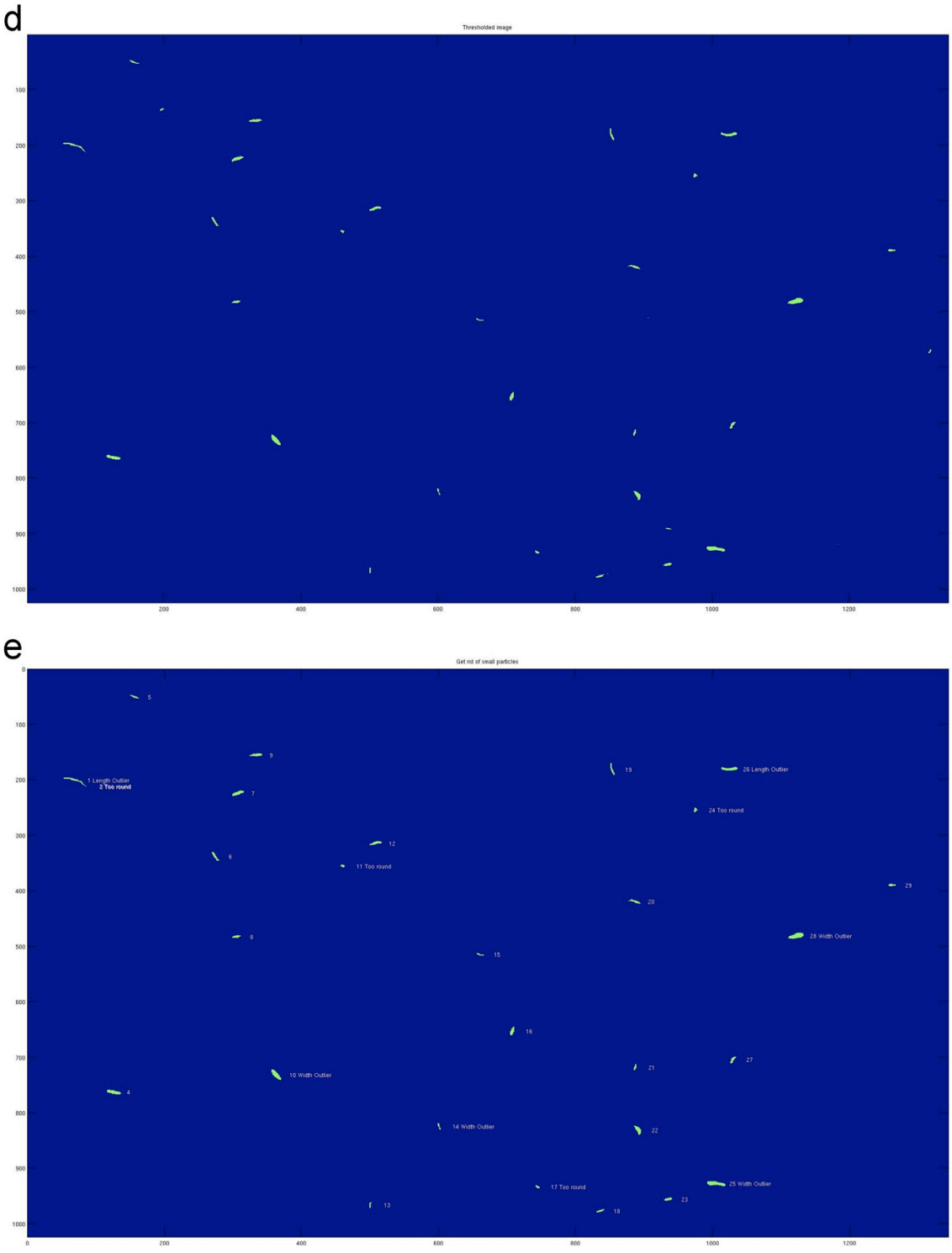

Supplementary Figure S7 (continued)

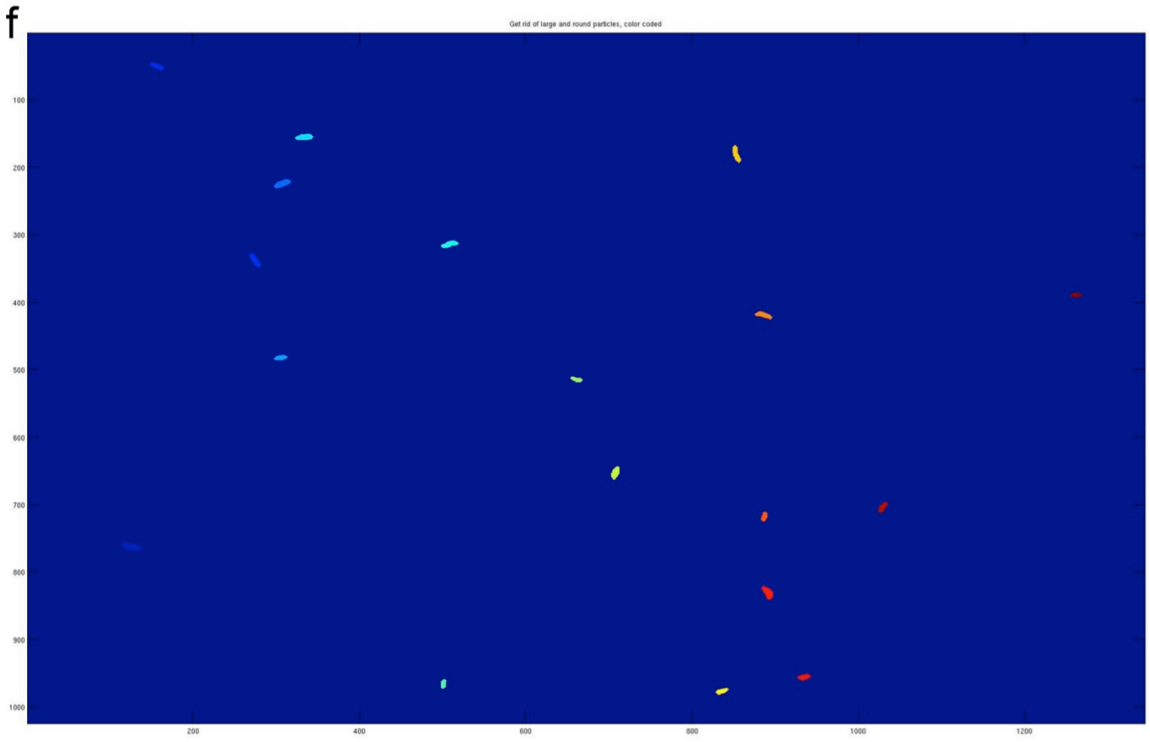

Supplementary Figure S7 (continued):

(c) original image, with large bright objects averaged out, to ensure no impact on thresholding

(d) positive pixels as a result of initial thresholding

(e) pixels recognized as multi-connected objects

(f) ciliary masks are filtered based on size and shape criteria, then the area around each remaining mask is expanded by a radius of 5 pixels, to ensure the entire cilium is covered by the mask. The mask around each cilium is shown in a different color

A.3.2 Calculation of results

We apply the masks created above based on the ciliary marker to the image of the protein to be scored (Smo or Ptc), integrates the pixel intensity in each region, and reports the mean per-pixel intensity as the ratio of the total integrated signal divided by the mask area for each cilium.

Then, we extend the original mask for each cilium by a 10 pixel radius; the local background is calculated as the per-pixel intensity in this 10-pixel donut-shaped extension around each cilium analized, and is subtracted from the per-pixel intensity in the original ciliary mask.

Since detection of low levels of signal is imperfect and can be confused with background noise, the per-pixel intensities across cilia follow a skewed distribution and not a normal one; to accurately capture this behaviour of cilia and to properly graph the high-signal tail of the distribution, we calculate the average as well as the 25^{th} and 75^{th} quantiles of the per-pixel intensities at the cilium across the population of cilia within each sample. Average intensities are reported as box plots, with the lower and upper bonds of the box representing the 25^{th} and 75^{th} quantiles respectively, and the average is indicated by a horizontal line.

In order to score positive cilia, a baseline per-pixel intensity is calculated from an untreated sample, or from a sample containing the untreated parental line in the case of overexpressed protein (thus, for the $Smo^{-/-}$ mSmo-mCherry fusion lines in Chapter 2, the baseline is calculated from the untreated $Smo^{-/-}$ sample stained at the same time as all outher samples); the baseline intensity is chosen such that either 10%, 5% or 1% false-positive results are deemed acceptable, based on the experiment. For each experimental sample, the algorithm pools the per-pixel intensities for each cilium across all the images analyzed for that particular condition and counts as positive those cilia which have a per-pixel intensity above the baseline. The result is reported as the fraction of the total cilia detected for each condition. Finally, in order to estimate the error due to sampling of only a small set of the cilia present on the coverslip, each pool of cilia (corresponding to each experimental condition) is divided in five equal sub-pools at

random, and the fraction of positive cilia in each sub-pool is calculated as for the initial large pool; the standard deviation of the fraction of positive cilia across the sub-pools represents an accurate description of the statistical sampling error, and is reported as error bars in the graphs of cilia counts.

A.4 Chemical Synthesis of Reagents used in Chapter Two

A.4.1 General methods for synthesis

All solvents and reagents were obtained from commercial sources and were used without further purification. NMR spectra were recorded on a Varian 400 MHz NMR spectrometer or a Varian Oxford 600 MHz NMR spectrometer. NMR chemical shifts were expressed in ppm relative to internal solvent peaks, and coupling constants were measured in Hz. High-resolution mass spectra were obtained at the Harvard University Mass Spectrometry Facility, or were obtained in-house on a Bruker microTOF-QII instrument, using an ESI source. LC/MS was performed on a Waters Micromass ZQ instrument using an ESI source coupled to a Waters 2525 HPLC system operating in reverse mode with a Waters Sunfire^{TM} C18 5µm 4.6×50 mm column. Flash chromatography was performed on silica gel columns using a Biotage Isolera One flash purification system. Diastereomers of 20-hydroxycholesterol analogs were purified on a chiral RegisCell (25 cm×21.1 mm) column using a preparative HPLC system composed of a Waters 1525 binary pump and Waters 2467 UV absorbance detector.

A.4.2 Preparation of 22-azacholesterol derivatives (1-6)

A.4.2.1 General procedure for reductive amination of pregnenolone

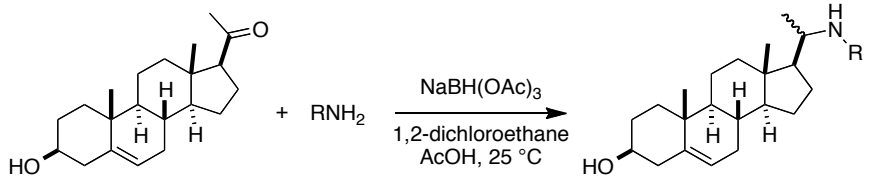

Pregnenolone 22-azacholesterol (**1-6**)

Following a reductive amination protocol (Abdel-Magid et al., 1996), pregnenolone (5-pregnen-3β-ol-20-one, 1.0 eq) and amine (1.0 eq) were mixed in 1,2-dichloroethane (c = 0.2 mol/L) and were then treated with sodium triacetoxyborohydride (1.5 eq) and AcOH (1.0 eq). The mixture was stirred at room temperature under nitrogen for 16 h. The reaction was quenched with 1M NaOH, and the product was extracted 3 times with diethyl ether. The ether layer was washed with brine and dried over Na_2SO_4. The solvent was evaporated to give the crude free base, which was purified by flash chromatography (silica gel, CH_2Cl_2/MeOH, gradient elution) to provide the 22-azacholesterol analog as a mixture of diastereomers. The ratio between the diastereomers in the mixture was estimated by LC/MS. This mixture was further purified by flash chromatography (silica gel, CH_2Cl_2/$CHCl_3$: MeOH:NH_4OH 89:10:1, gradient elution) to yield the pure diastereomers.

A.4.2.2 Preparation of (3S,8S,9S,10R,13S,14S,17S)-17-(1-(isopentylamino)ethyl)-10,13-dimethyl-2,3,4,7,8,9,10,11,12,13,14,15,16,17-tetradecahydro-1H-cyclopenta[a]phenanthren-3-ol (1)

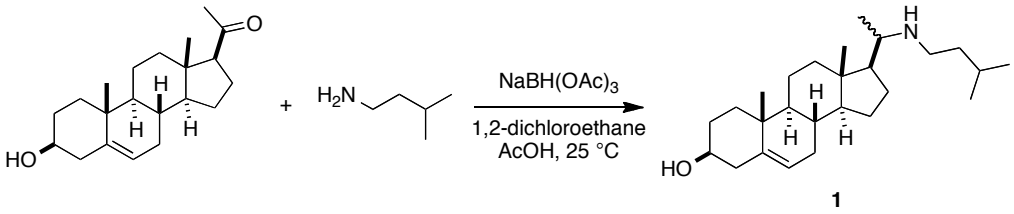

1

Following the general procedure, compound **1** was obtained from pregnenolone (1.01 g, 3.2 mmol) and 3-methylbutan-1-amine (279 mg, 3.2 mmol) as a mixture of diastereomers (20*R*:20*S*; 1:11.8) (152 mg, 12%), from which the major diastereomer **1**(20*S*) was purified as a white solid. This diastereomer was assigned the 20*S*/a configuration based on the reported

properties of 22-azacholesterol diasteromers (mp of 20a: 128–129°C, mp of 20b: 151-152°C in reference(Lu et al., 1972), and mp of 20a: 120–121°C in reference(Counsell et al., 1965)). In the case of the other analogs of 22-azacholesterol (**2-6)**, configuration of diastereomers was assigned based on similarity to the diastereomers of **1** in retention time (LC/MS, reverse-phase) and in chemical shift of H_3-20 (doublet). For all 22-azacholesterol analogs described here, the 20*R* diastereomer has a smaller retention time than 20*S*, and the H_3-20 chemical shift of the 20*R* diastereomer is smaller than that of 20*S* by 0.05-0.12 ppm.

1(20*S*/a): mp 128–129°C; $[a]_D^{24}$ = -25.2 (*c* = 0.38, MeOH); ^{1}H NMR (400 MHz, $CDCl_3$): δ 5.32-5.36 (m, 1H), 3.46-3.56 (m, 1H), 2.66-2.74 (m, 1H), 2.38-2.54 (m, 2H), 2.18-2.32 (m, 2H), 1.79-2.02 (m, 6H), 1.40-1.68 (m, 8H), 1.28-1.40 (m, 4H), 1.12-1.24 (m, 2H), 1.02-1.12 (m, 5H), 1.00 (s, 3H), 0.91-0.99 (m, 1H), 0.90 (d, *J* = 2.0 Hz, 3H), 0.89 (d, *J* = 2.0 Hz, 3H), 0.70 (s, 3H); ^{13}C NMR (100 MHz, $CDCl_3$): δ 140.8, 121.5, 71.6, 56.6, 56.3, 50.0, 44.9, 42.3, 41.9, 39.4, 39.3, 37.2, 36.5, 31.8, 31.7, 31.6, 27.1, 26.2, 24.2, 22.8, 22.5, 20.9, 19.4, 19.3, 12.2; HRMS: (ESI, m/z) calcd **[**M+H**]**$^+$ for $C_{26}H_{45}NO$: 388.3574, found 388.3582.

A.4.2.3 Preparation of (3S,8S,9S,10R,13S,14S,17S)-17-(1-(ethylamino)ethyl)-10,13-dimethyl-2,3,4,7,8,9,10,11,12,13,14,15,16,17-tetradecahydro-1H-cyclopenta[a]phenanthren-3-ol (2)

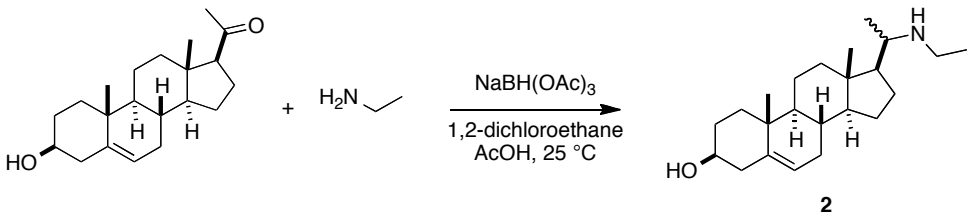

2

Following the general procedure, compound **2** was obtained from pregnenolone (1.01 g, 3.2 mmol) and ethylamine (144 mg, 3.2 mmol) as a mixture of diastereomers (20*R*:20*S*; 1.5:1) (500 mg, 45%), which was further separated to yield each pure diastereomer (**2a** and **2b)** as a white solid.

2a(20*R*): $[a]_D^{24}$ = -68.5 (*c* = 0.55, MeOH); ^{1}H NMR (400 MHz, $CDCl_3$): δ 5.32-5.35 (m, 1H), 3.47-3.57 (m, 1H), 2.69-2.80 (m, 1H), 2.57-2.66 (m, 1H), 2.44-2.54 (m, 1H), 2.18-2.32 (m, 2H), 1.92-2.02 (m, 2H), 1.71-1.87 (m, 3H), 1.41-1.65 (m, 7H), 1.20-1.40 (m, 3H), 1.02-1.15 (m, 6H), 0.91-1.02 (m, 8H), 0.72 (s, 3H); ^{13}C NMR (100 MHz, $CDCl_3$): δ 140.9, 121.3, 71.3, 56.3, 55.9, 55.7, 49.9, 42.3, 41.9, 40.9, 40.2, 37.2, 36.4, 31.7, 31.7, 31.6, 26.6, 24.1, 21.0, 19.3, 19.1, 15.5, 12.3; HRMS: (ESI, m/z) calcd **[**M+H**]**$^+$ for $C_{23}H_{39}NO$: 346.3104, found 346.3105.

2b(20*S*): $[a]_D^{24}$ = -29.0 (*c* = 0.34, MeOH); ^{1}H NMR (400 MHz, $CDCl_3$): δ 5.32-5.36 (m, 1H), 3.46-3.56 (m, 1H), 2.70-2.80 (m, 1H), 2.44-2.58 (m, 2H), 2.18-2.32 (m, 2H), 1.70-2.02 (m, 5H), 1.42-1.68 (m, 7H), 1.14-1.41 (m, 4H), 1.06-1.14 (m, 8H), 0.90-1.06 (m, 5H), 0.70 (s, 3H); ^{13}C NMR (100 MHz, $CDCl_3$): δ 140.8, 121.5, 71.6, 56.6, 56.4, 56.2, 49.9, 42.3, 41.9, 40.8, 39.3, 37.2, 36.5, 31.8, 31.7, 31.6, 27.1, 24.1, 20.9, 19.4, 19.2, 15.4, 12.2; HRMS: (ESI, m/z) calcd **[**M+H**]**$^+$ for $C_{23}H_{39}NO$: 346.3104, found 346.3108.

A.4.2.4 Preparation of (3S,8S,9S,10R,13S,14S,17S)-10,13-dimethyl-17-(1-(propylamino)ethyl)-2,3,4,7,8,9,10,11,12,13,14,15,16,17-tetradecahydro-1H-cyclopenta[a]phenanthren-3-ol (3)

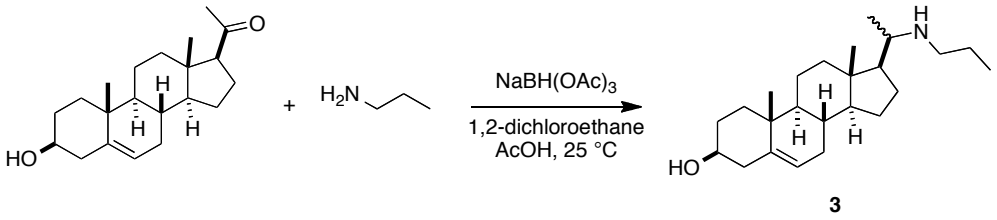

3

Following the general procedure, compound **3** was obtained from pregnenolone (1.01 g, 3.2 mmol) and propylamine (189 mg, 3.2 mmol) as a mixture of diastereomers (20R:20S; 1:1.3) (504 mg, 44%), which was further separated to yield each pure diastereomer (**3a** and **3b)** as a white solid.

3a(20*R*): $[a]_D^{24}$ = -58.0 (*c* = 0.43, MeOH); ^{1}H NMR (400 MHz, $CDCl_3$): δ 5.32-5.35 (m, 1H), 3.46-3.56 (m, 1H), 2.65-2.75 (m, 1H), 2.53-2.62 (m, 1H), 2.34-2.42 (m, 1H), 2.18-2.22 (m, 2H), 1.93-2.02 (m, 2H), 1.71-1.87 (m, 3H), 1.41-1.65 (m, 9H), 1.20-1.38 (m, 3H), 1.02-1.17 (m, 3H), 0.95-1.02 (m, 8H), 0.93 (t, *J* = 7.2 Hz, 3H), 0.72 (s, 3H); ^{13}C NMR (100 MHz, $CDCl_3$): δ 140.8, 121.5, 71.5, 56.4, 56.2, 56.0, 50.0, 49.0, 42.3, 42.0, 40.2, 37.2, 36.5, 31.8, 31.8, 31.6, 26.7, 24.2, 23.5, 21.1, 19.4, 19.2, 12.3, 12.0; HRMS: (ESI, m/z) calcd **[**M+H**]**$^+$ for $C_{24}H_{41}NO$: 360.3261, found 360.3257.

3b(20*S*): $[a]_D^{24}$ = -27.3 (*c* = 0.39, MeOH); ^{1}H NMR (400 MHz, $CDCl_3$): δ 5.32-5.36 (m, 1H), 3.46-3.56 (m, 1H), 2.61-2.69 (m, 1H), 2.46-2.54 (m, 1H), 2.36-2.44 (m, 1H), 2.18-2.32 (m, 2H), 1.78-2.02 (m, 5H), 1.40-1.68 (m, 9H), 1.28-1.40 (m, 2H), 1.05-1.24 (m, 6H), 0.94-1.05 (m,

5H), 0.88-0.96 (m, 4H), 0.69 (s, 3H); ^{13}C NMR (100 MHz, $CDCl_3$): δ 140.8, 121.4, 71.5, 56.6, 56.3, 56.3, 49.9, 48.7, 42.3, 41.8, 39.3, 37.2, 36.5, 31.8, 31.7, 31.6, 27.0, 24.1, 23.4, 20.9, 19.3, 19.2, 12.2, 11.9; HRMS: (ESI, m/z) calcd **[**M+H**]**$^+$ for $C_{24}H_{41}NO$: 360.3261, found 360.3262.

A.4.2.5 Preparation of (3S,8S,9S,10R,13S,14S,17S)-17-(16-amino-7,10,13-trioxa-3-azahexadecan-2-yl)-10,13-dimethyl-2,3,4,7,8,9,10,11,12,13,14,15,16,17-tetradecahydro-1H-cyclopenta[a]phenanthren-3-ol (6)

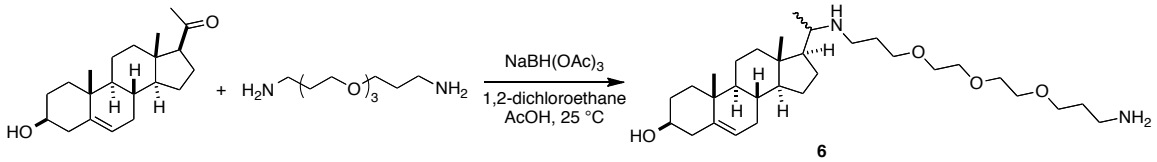

Following the general procedure, compound **6** was obtained from pregnenolone (1.01 g, 3.2 mmol) and 4,7,10-trioxa-1,13-tridecanediamine (2.2 g, 10 mmol) after silica gel column chromatography as a mixture of diastereomers (20*R*:20*S*; 2.6:1) as a yellow oil (749 mg, 45%) and was used in the next step without further purification.

6: ^{1}H NMR (600 MHz, $CDCl_3$): δ 5.33-5.36 (m, 1H), 3.47-3.67 (m, 13H), 2.77-2.89 (m, 3H), 2.45-2.70 (m, 6H), 2.20-2.32 (m, 2H), 1.91-2.05 (m, 3H), 1.69-1.89 (m, 7H), 1.39-1.69 (m, 7H), 0.90-1.39 (m, 11H), 0.72, 0.70 (2.6:1; s, 3H); HRMS: (ESI, m/z) calcd **[**M+H**]**$^+$ for $C_{31}H_{56}N_2O_4$: 521.4313, found 521.4311.

A.4.3 Preparation of 20-hydroxycholesterol analogs (7-16)

A.4.3.1 General procedure for Grignard reactions of pregnenolone

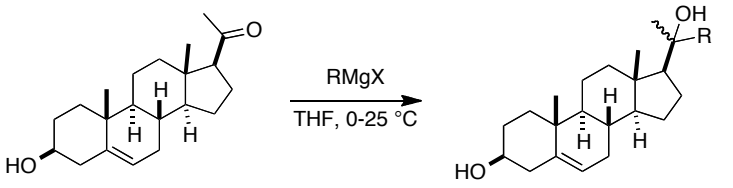

Pregnenolone

20-hydroxycholesterol (**7-11**)

Pregnenolone (1.0 eq.) was dissolved in dry THF (0.16 mol/L) and the resulting solution was cooled to 0 °C under nitrogen. A solution of alkylmagnesium bromide or chloride (3.0 eq.) was added drop-wise over 10 min. The reaction mixture was stirred at 25 °C for 16 h and was then cooled to 0 °C. A saturagted solution of NH_4Cl was added and the mixture was stirred for 30 min, after which it was extracted 3 times with EtOAc. The organic phase was washed with brine and dried over anhydrous Na_2SO_4. Evaporation of the solvent gave a residue, which was purified by flash chromatography on silica gel (step-wise gradient elution, 0-70% EtOAc/hexane) to provide the 20-hydroxycholesterol analog as a mixture of diasteromers. This mixture was subjected to normal-phase chiral HPLC purification (6% *i*-PrOH/Hexane), to yield the pure diastereomers. The configuration of the diastereomers of compounds **8-12** was assigned by comparison with the reported NMR characterization of *nat*-20(*R*)-hydroxycholesterol and related compounds (Nachtergaele et al., 2012), based on the trend in the chemical shifts of C-20 and H_3-21 (singlet). For all 20-hydroxycholesterol analogs examined here, the C-20 chemical shift of the 20*S* diastereomer is around 75.2 ppm while it is 75.8 ppm for 20*R*, and the H_3-21

chemical shift of the 20*S* diastereomer is around 1.26 ppm while it is 1.12 ppm for 20*R*. This assignment is consistent with results of biological activity assays, as the 20*R* diastereomers of **10-12** activate the Hedgehog pathway in cells and bind Smoothened, while the 20*S* diastereomers of **10-12** are inactive (see text). We also observed that the 20*S* diastereomers have a smaller retention time during the chiral HPLC separation.

A.4.3.2 Preparation of (3S,10R,13S,17S)-17-(2-Hydroxypropan-2-yl)-10,13-dimethyl-2,3,4,7,8,9,10,11,12,13,14,15,16,17-tetradecahydro-1H-cyclopenta[a]phenanthren-3-ol (7)

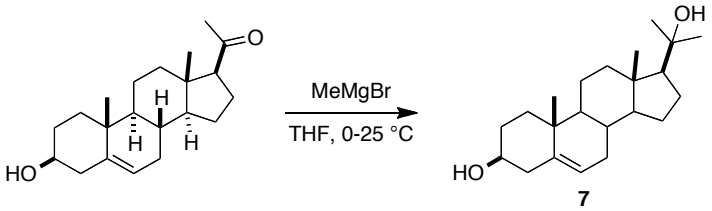

7

Following the general procedure, compound **7** was obtained from pregnenolone (1.0 g) and methylmagnesium bromide (3.2 mL of 3.0 M solution in Et_2O) in dry THF (20 mL), as a white solid (117 mg, 11% yield after HPLC purification).

7: $[a]_D^{24}$ =-43.7 (*c* = 0.21, MeOH); ^{1}H NMR (400 MHz, $CDCl_3$): δ 5.33-5.37 (m, 1H), 3.47-3.57 (m, 1H), 2.19-2.34 (m, 2H), 2.07-2.14 (m, 1H), 1.94-2.03 (m, 1H), 1.80-1.88 (m, 2H), 1.70-1.78 (m, 2H), 1.60-1.70 (m, 2H), 1.41-1.59 (m, 6H), 1.31 (s, 3H), 1.20-1.28 (m, 2H), 1.20 (s, 3H), 1.03-1.18 (m, 2H), 1.01 (s, 3H), 0.88-1.00 (m, 2H), 0.85 (s, 3H); ^{13}C NMR (100 MHz, $CDCl_3$): δ 140.8, 121.6, 73.5, 71.8, 60.2, 56.8, 50.0, 42.7, 42.3, 40.1, 37.2, 36.5, 31.8, 31.6, 31.3,

31.0, 30.1, 23.8, 23.1, 20.9, 19.4, 13.5; HRMS: (ESI, m/z) calcd **[**M+Na**]**$^+$ for $C_{22}H_{36}O_2$, 355.2613; found, 355.2630.

A.4.3.3 Preparation of (3S,10R,13S,17S)-17-(2-Hydroxybutan-2-yl)-10,13-dimethyl-2,3,4,7,8,9,10,11,12,13,14,15,16,17-tetradecahydro-1H-cyclopenta[a]phenanthren-3-ol (8)

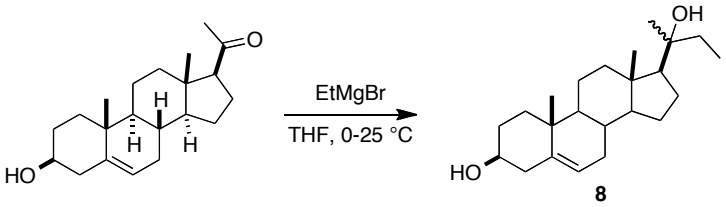

8

Following the general procedure, compound **8** was obtained from pregnenolone (1.0 g) and ethylmagnesium bromide (3.2 mL of 3.0 M solution in Et_2O) in dry THF (20 mL) as a white solid (136 mg, 12%). Further preparative chiral HPLC separation yielded the pure diastereomers (**8a** and **8b)** as white solids.

8a(20*S*): $[a]_D^{24}$ = -40.3 (*c* = 0.18, MeOH); ^{1}H NMR (600 MHz, $CDCl_3$): δ 5.34-5.37 (m, 1H), 3.49-3.55 (m, 1H), 2.28-2.32 (m, 1H), 2.20-2.27 (m, 1H), 2.07-2.12 (m, 1H), 1.95-2.01 (m, 1H), 1.82-1.87 (m, 2H), 1.70-1.78 (m, 1H), 1.57-1.70 (m, 2H), 1.44-1.57 (m, 8H), 1.36-1.44 (m, 1H), 1.25 (s, 3H), 1.02-1.24 (m, 4H), 1.01 (s, 3H), 0.90-1.00 (m, 2H), 0.87 (s, 3H), 0.86 (t, *J* = 7.2 Hz, 3H); ^{13}C NMR (150 MHz, $CDCl_3$): δ 140.8, 121.6, 75.4, 71.8, 57.2, 56.9, 50.0, 42.6, 42.3, 40.1, 37.2, 36.5, 36.1, 31.8, 31.6, 31.3, 25.7, 23.8, 22.3, 20.9, 19.4, 13.6, 8.5; HRMS: (ESI, m/z) calcd **[**M+Na**]**$^+$ for $C_{23}H_{38}O_2$, 369.2770; found, 369.2771.

8b(20*R*): $[a]_D^{24}$ = -24.4 (*c* = 0.14, MeOH); ^{1}H NMR (600 MHz, $CDCl_3$): δ 5.34-5.37 (m, 1H), 3.48-3.56 (m, 1H), 2.27-2.32 (m, 1H), 2.22-2.27 (m, 1H), 2.08-2.13 (m, 1H), 1.95-2.01 (m, 1H), 1.82-1.87 (m, 2H), 1.55-1.78 (m, 3H), 1.43-1.55 (m, 7H), 1.20-1.28 (m, 2H), 1.11-1.18 (m, 2H), 1.11 (s, 3H), 1.02-1.10 (m, 2H), 1.01 (s, 3H), 0.93-1.00 (m, 2H), 0.92 (t, *J* = 7.2 Hz, 3H), 0.86 (s, 3H); ^{13}C NMR (150 MHz, $CDCl_3$): δ 140.8, 121.6, 75.9, 71.8, 58.0, 56.9, 50.0, 42.8, 42.3, 40.2, 37.2, 36.5, 34.9, 31.8, 31.6, 31.3, 26.3, 23.8, 23.2, 20.9, 19.4, 13.7, 8.4; HRMS: (ESI, m/z) calcd **[**M+H-2H_2O**]**$^+$ for $C_{23}H_{38}O_2$, 311.2739; found, 311.2746.

A.4.3.4 Preparation of (3S,10R,13S)-17-(2-Hydroxypentan-2-yl)-10,13-dimethyl-2,3,4,7,8,9,10,11,12,13,14,15,16,17-tetradecahydro-1H-cyclopenta[a]phenanthren-3-ol (9)

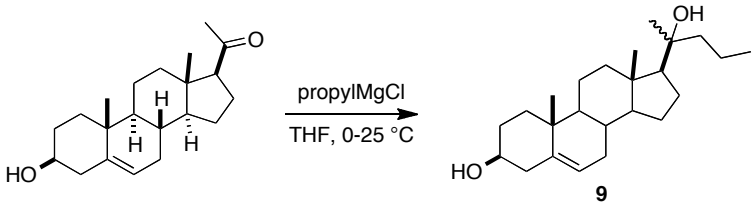

9

Following the general procedure, compound **9** was obtained from pregnenolone and (1.0 g) and propylmagnesium chloride (4.7 mL of a 2.0 M solution in Et_2O) in dry THF (20 mL) as a white solid (81 mg, 7%). Further preparative chiral HPLC separation yielded the pure diastereomers (**9a** and **9b)** as white solids.

9a(20*S*): $[a]_D^{24}$ = -39.7 (*c* = 0.20, MeOH); ^{1}H NMR (600 MHz, $CDCl_3$): δ 5.34-5.37 (m, 1H), 3.48-3.55 (m, 1H), 2.27-2.32 (m, 1H), 2.20-2.27 (m, 1H), 2.07-2.12 (m, 1H), 1.95-2.00 (m, 1H), 1.81-1.87 (m, 2H), 1.70-1.80 (m, 1H), 1.57-1.70 (m, 2H), 1.40-1.57 (m, 8H), 1.24-1.35 (m,

6H), 1.04-1.23 (m, 4H), 1.01 (s, 3H), 0.87-1.00 (m, 5H), 0.86 (s, 3H); ^{13}C NMR (150 MHz, $CDCl_3$): δ 140.8, 121.6, 75.2, 71.8, 57.7, 56.9, 50.0, 46.4, 42.6, 42.3, 40.1, 37.2, 36.5, 31.8, 31.6, 31.3, 26.4, 23.8, 22.4, 20.9, 19.4, 17.5, 14.7, 13.6; HRMS: (ESI, m/z) calcd **[**M+Na**]**$^+$ for $C_{24}H_{40}O_2$, 383.2926; found, 383.2936.

9b(20*R*): $[a]_D^{24}$ = -38.5 (*c* = 0.60, MeOH); ^{1}H NMR (400 MHz, $CDCl_3$): δ 5.33-5.37 (m, 1H), 3.47-3.57 (m, 1H), 2.18-2.33 (m, 2H), 2.06-2.12 (m, 1H), 1.93-2.02 (m, 1H), 1.79-1.87 (m, 2H), 1.44-1.79 (m, 12H), 1.33-1.44 (m, 2H), 1.21-1.30 (m, 2H), 1.05-1.20 (m, 5H), 0.97-1.05 (m, 4H), 0.88-0.97 (m, 4H), 0.87 (s, 3H); ^{13}C NMR (100 MHz, $CDCl_3$): δ 140.8, 121.6, 75.8, 71.7, 58.2, 56.9, 50.0, 45.1, 42.9, 42.3, 40.1, 37.2, 36.5, 31.8, 31.6, 31.3, 27.0, 23.8, 23.1, 20.9, 19.4, 17.3, 14.7, 13.7; HRMS: (ESI, m/z) calcd **[**M+Na**]**$^+$ for $C_{24}H_{40}O_2$, 383.2926; found, 383.2925.

A.4.3.5 Preparation of (3S,10R,13S)-17-(2-Hydroxypentan-2-yl)-10,13-dimethyl-2,3,4,7,8,9,10,11,12,13,14,15,16,17-tetradecahydro-1H-cyclopenta[a]phenanthren-3-ol (10)

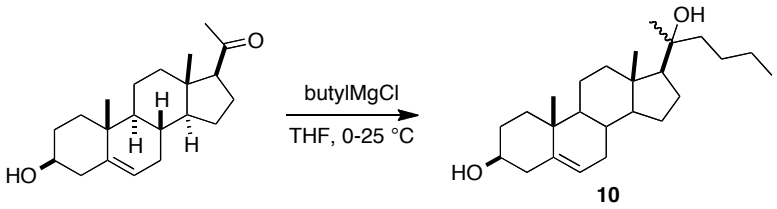

10

Following the general procedure, compound **10** was obtained from pregnenolone (1.0 g) and butylmagnesium chloride (4.7 mL of a 2.0 M solution in THF) in dry THF (20 mL) as a white solid (415 mg, 35%). Further preparative chiral HPLC separation yielded the pure diastereomers (**10a** and **10b)** as white solids.

10a(20*S*): $[a]_D^{24}$ = -54.7 (*c* = 0.42, CH_2Cl_2); ^{1}H NMR (400 MHz, $CDCl_3$): δ 5.33-5.37 (m, 1H), 3.47-3.57 (m, 1H), 2.18-2.33 (m, 2H), 2.06-2.13 (m, 1H), 1.93-2.03 (m, 1H), 1.78-1.87 (m, 2H), 1.70-1.78 (m, 1H), 1.41-1.70 (m, 11H), 1.05-1.36 (m, 11H), 0.97-1.05 (m, 4H), 0.87-0.96 (m, 4H), 0.87 (s, 3H); ^{13}C NMR (100 MHz, $CDCl_3$): δ 140.8, 121.6, 75.2, 71.8, 57.6, 56.9, 50.0, 43.7, 42.6, 42.3, 40.1, 37.2, 36.5, 31.8, 31.6, 31.3, 26.5, 26.4, 23.8, 23.3, 22.3, 20.9, 19.4, 14.1, 13.6; HRMS: (ESI, m/z) calcd **[**M+Na**]**$^+$ for $C_{25}H_{42}O_2$, 397.3083; found, 397.3083.

10b(20*R*): $[a]_D^{24}$ = -49.4 (*c* = 0.16, CH_2Cl_2); ^{1}H NMR (400 MHz, $CDCl_3$): δ 5.33-5.37 (m, 1H), 3.48-3.57 (m, 1H), 2.18-2.33 (m, 2H), 2.06-2.12 (m, 1H), 1.93-2.03 (m, 1H), 1.78-1.88 (m, 2H), 1.60-1.78 (m, 2H), 1.42-1.60 (m, 10H), 1.21-1.38 (m, 6H), 1.09-1.18 (m, 4H), 0.97-1.09 (m, 5H), 0.88-0.97 (m, 4H), 0.87 (s, 3H); ^{13}C NMR (100 MHz, $CDCl_3$): δ 140.8, 121.6, 75.8, 71.8, 58.2, 56.9, 50.0, 42.9, 42.6, 42.3, 40.1, 37.2, 36.5, 31.8, 31.6, 31.3, 27.0, 26.3, 23.8, 23.4, 23.2, 20.9, 19.4, 14.2, 13.7; HRMS: (ESI, m/z) calcd **[**M+Na**]**$^+$ for $C_{25}H_{42}O_2$, 397.3083; found, 397.3079.

A.4.3.6 Preparation of (3S,10R,13S,17S)-17-(2-Hydroxyheptan-2-yl)-10,13-dimethyl-2,3,4,7,8,9,10,11,12,13,14,15,16,17-tetradecahydro-1H-cyclopenta[a]phenanthren-3-ol (11)

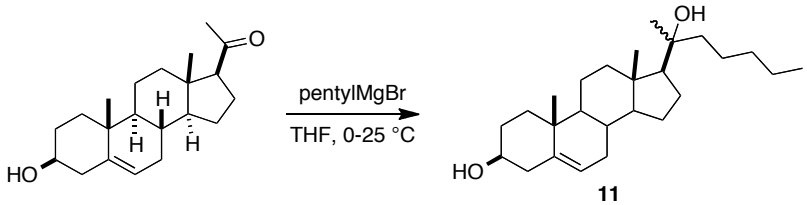

11

Following the general procedure, compound **5** was obtained from pregnenolone (1.0 g) and pentylmagnesium bromide (4.7 mL of a 2.0 M solution in Et_2O) in dry THF (20 mL) as a white solid (553 mg, 45%). Further preparative chiral HPLC separation yielded the pure diastereomers (**11a** and **11b)** as white solids.

11a(20*S*): $[a]_D^{24}$ = -54.5 (*c* = 0.31, CH_2Cl_2); ^{1}H NMR (400 MHz, $CDCl_3$): δ 5.34-5.37 (m, 1H), 3.47-3.57 (m, 1H), 2.19-2.34 (m, 2H), 2.06-2.13 (m, 1H), 1.93-2.02 (m, 1H), 1.79-1.88 (m, 2H), 1.40-1.78 (m, 12H), 1.05-1.37 (m, 13H), 0.97-1.05 (m, 4H), 0.85-0.97 (m, 7H); ^{13}C NMR (100 MHz, $CDCl_3$): δ 140.8, 121.6, 75.2, 71.7, 57.6, 56.9, 50.0, 44.0, 42.6, 42.3, 40.1, 37.2, 36.5, 32.5, 31.8, 31.6, 31.3, 26.4, 24.0, 23.8, 22.7, 22.3, 20.9, 19.4, 14.1, 13.6; HRMS: (ESI, m/z) calcd **[**M+Na**]**$^+$ for $C_{26}H_{44}O_2$, 411.3239; found, 411.3235.

11b(20*R*): $[a]_D^{24}$ = -49.7 (*c* = 0.26, CH_2Cl_2); ^{1}H NMR (400 MHz, $CDCl_3$): δ 5.33-5.37 (m, 1H), 3.48-3.57 (m, 1H), 2.18-2.34 (m, 2H), 2.06-2.12 (m, 1H), 1.94-2.02 (m, 1H), 1.79-1.88 (m, 2H), 1.42-1.78 (m, 12H), 1.20-1.40 (m, 8H), 1.09-1.18 (m, 4H), 0.97-1.09 (m, 5H), 0.85-0.97 (m, 7H); ^{13}C NMR (100 MHz, $CDCl_3$): δ 140.8, 121.6, 75.8, 71.8, 58.2, 56.9, 50.0, 42.9, 42.8, 42.3, 40.1, 37.2, 36.5, 32.5, 31.8, 31.6, 31.3, 27.0, 23.8, 23.7, 23.1, 22.7, 20.9, 19.4, 14.1, 13.7; HRMS: (ESI, m/z) calcd **[**M+Na**]**$^+$ for $C_{26}H_{44}O_2$, 411.3239; found, 411.3240.

A.4.3.7 Preparation of (3S,5S,10S,13S)-17-(2-Hydroxyheptan-2-yl)-10,13-dimethylhexadecahydro-1H-cyclopenta[a]phenanthren-3-ol (12)

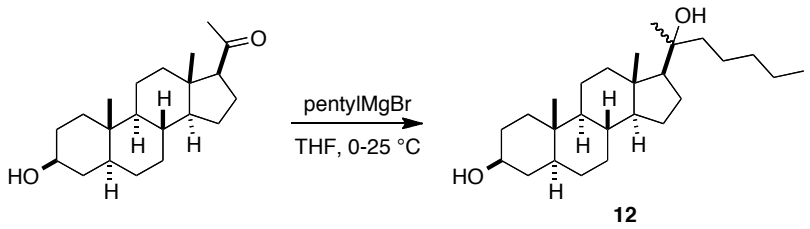

12

Following the general procedure, compound **12** was obtained from 5α-pregnan-3β-ol-20-one (1.0 g) and pentylmagnesium bromide (4.7 mL of a 2.0 M solution in Et_2O) in dry THF (20 mL) as a white solid (354 mg, 29%). Further chiral HPLC separation yielded the pure diastereomers (**12a** and **12b)** as white solids.

12a(20*S*): $[a]_D^{24}$ = 2.6 (*c* = 0.32, CH_2Cl_2); ^{1}H NMR (400 MHz, $CDCl_3$): δ 3.54-3.63 (m, 1H), 2.01-2.07 (m, 1H), 1.20-1.83 (m, 27H), 1.03-1.20 (m, 4H), 0.94-1.03 (m, 2H), 0.85-0.94 (m, 4H), 0.83 (s, 3H), 0.80 (s, 3H), 0.57-0.65 (m, 1H); ^{13}C NMR (100 MHz, $CDCl_3$): δ 75.2, 71.3, 57.7, 56.6, 54.3, 44.8, 43.9, 42.9, 40.4, 38.1, 37.0, 35.4, 34.8, 32.5, 31.9, 31.5, 28.7, 26.3, 23.9, 23.7, 22.6, 22.3, 21.1, 14.1, 13.8, 12.3; HRMS: (ESI, m/z) calcd **[**M+H-H_2O**]**$^+$ for $C_{26}H_{46}O_2$, 373.3470; found, 373.3464.

12b(20*R*): $[a]_D^{24}$ = 10.9 (*c* = 0.34, CH_2Cl_2); ^{1}H NMR (400 MHz, $CDCl_3$): δ 3.54-3.63 (m, 1H), 2.01-2.08 (m, 1H), 1.43-1.84 (m, 12H), 1.15-1.43 (m, 15H), 1.03-1.15 (m, 4H), 0.94-1.03 (m, 2H), 0.85-0.94 (m, 4H), 0.84 (s, 3H), 0.80 (s, 3H), 0.57-0.65 (m, 1H); ^{13}C NMR (100 MHz, $CDCl_3$): δ 75.8, 71.3, 58.4, 56.6, 54.3, 44.8, 43.2, 42.7, 40.4, 38.2, 37.0, 35.4, 34.9, 32.5, 31.9,

31.5, 28.7, 27.0, 23.8, 23.7, 23.1, 22.7, 21.1, 14.1, 13.9, 12.3; HRMS: (ESI, m/z) calcd [M+H-H_2O]$^+$ for $C_{26}H_{46}O_2$, 373.3470; found, 373.3482.

A.4.3.8 Preparation of (3S,10R,13S,17S)-17-(8-((tert-butyldimethylsilyl)oxy)-2-hydroxyoctan-2-yl)-10,13-dimethyl-2,3,4,7,8,9,10,11,12,13,14,15,16,17-tetradecahydro-1H-cyclopenta[a]phenanthren-3-ol (13)

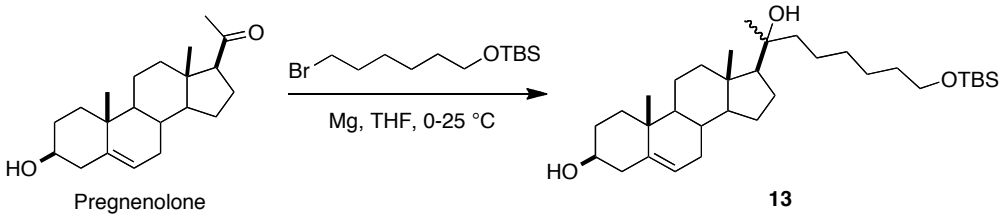

Pregnenolone **13**

In a 2-necked round bottom flask equipped with a condenser, magnesium turnings (2.2 g, 89.1 mmol) were stirred in anhydrous THF (2 mL) under nitrogen. (6-Bromohexyloxy)-*tert*-butyldimethylsilane (5.3 g, 17.8 mmol) was dissolved in anhydrous THF (18 mL) and 1/10 of this solution was added to the flask, followed by a few drops of 1,2-dibromoethane. The mixture was warmed and stirred vigorously until cloudiness and bubbling was observed. The rest of the THF solution of (6-bromohexyloxy)-*tert*-butyldimethylsilane was slowly added to the flask to keep the reaction going. The reaction mixture was heated to reflux for an additional hour, and then cooled to room temperature. The Grignard reagent thus prepared was transferred dropwise via syringe to a solution of pregnenolone (1.9 g, 5.9 mmol) in anhydrous THF (10 mL) at 0°C. The reaction was stirred at room temperature for 12 h under nitrogen and was quenched with aqueous NH_4Cl, followed by extraction with EtOAc. The organic extract was washed with brine, dried over Na_2SO_4, and concentrated *in vacuo*. The residue was purified by flash

chromatography on silica gel (step-wise gradient elution, 0-30% EtOAc/Hexanes) to yield compound **13** (1.4 g, 46%) as a colorless, amorphous solid (mixture of diasteromers).

13: ^{1}H NMR (600 MHz, $CDCl_3$): δ 5.29-5.32 (m, 1H), 3.53-3.62 (m, 3H), 3.44-3.51 (m, 1H), 2.22-2.27 (m, 1H), 2.16-2.22 (m, 1H), 2.02-2.06 (m, 1H), 1.90-1.96 (m, 1H), 1.76-1.82 (m, 2H), 1.55-1.74 (m, 4H), 1.38-1.55 (m, 8H), 1.18-1.34 (m, 8H), 0.99-1.18 (m, 4H), 0.91-0.99 (m, 4H), 0.83-0.91 (m, 12H), 0.82 (s, 3H), 0.00 (s, 6H); ^{13}C NMR (150 MHz, $CDCl_3$) (as the major diasteromer): δ 140.8, 121.6, 75.2, 71.7, 63.3, 57.6, 56.9, 50.0, 43.9, 42.6, 42.3, 40.1, 37.2, 36.5, 32.8, 31.8, 31.6, 31.3, 30.1, 26.4, 26.0, 25.8, 24.3, 23.8, 22.3, 20.9, 19.4, 18.4, 13.6, -5.3.

A.4.3.9 Preparation of 7-((3S,10R,13S,17S)-3-hydroxy-10,13-dimethyl-2,3,4,7,8,9,10,11,12,13,14,15,16,17-tetradecahydro-1H-cyclopenta[a]phenanthren-17-yl)octane-1,7-diol (14)

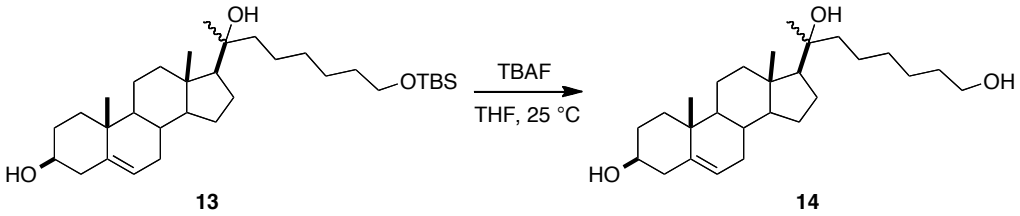

13 **14**

To compound **13** (1.1g, 2.1 mmol) in dry THF (15 mL) was added tetrabutylammonium fluoride (6.3 mL of a 1.0 M solution in THF, 6.3 mmol), and the reaction was stirred for 4 h. Upon reaction completion, water was added and most of the product was precipitated by addition of a large excess of Et_2O. The organic phase was separated and the solvent was removed by rotary evaporation. The resulting residue was washed with water and CH_2Cl_2, and was combined

with the solid obtained by ether precipitation. The combined solids were dried *in vacuo* to yield the crude **14** (0.72 g, 82 %) as a white solid (mixture of diasteromers).

14: ^{1}H NMR (600 MHz, $CDCl_3$): δ 5.34-5.37 (m, 1H), 3.62-3.67 (m, 2H), 3.48-3.56 (m, 1H), 2.27-2.32 (m, 1H), 2.20-2.26 (m, 1H), 2.06-2.11 (m, 1H), 1.95-2.01 (m, 1H), 1.81-1.87 (m, 2H), 1.62-1.78 (m, 3H), 1.43-1.62 (m, 10H), 1.24-1.41 (m, 9H), 1.04-1.24 (m, 6H), 0.96-1.04 (m, 4H), 0.90-0.96 (m, 1H), 0.86 (s, 3H); ^{13}C NMR (150 MHz, $CDCl_3$) (as a mixture of diasteromers): δ 140.8, 121.6, 75.8, 75.2, 71.8, 63.0(x2), 58.3, 57.7, 56.9(x2), 50.0, 43.8, 42.9, 42.7, 42.6, 42.3, 40.1(x2), 37.2, 36.5, 32.8, 32.7, 31.8, 31.6, 31.3(x2), 30.1, 30.0, 27.0, 26.4, 25.8, 25.7, 24.2, 24.0, 23.8(x2), 23.2, 22.4, 20.9, 19.4, 13.7, 13.6.

A.4.3.10 Preparation of 7-hydroxy-7-((3S,10R,13S,17S)-3-hydroxy-10,13-dimethyl-2,3,4,7,8,9,10,11,12,13,14,15,16,17-tetradecahydro-1H-cyclopenta[a]phenanthren-17-yl)octanal (15)

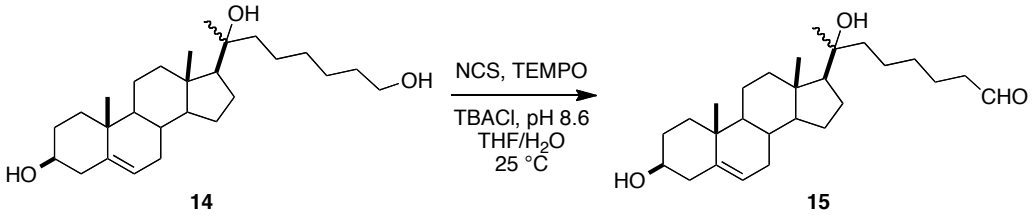

14 **15**

Compound **15** was obtained by a modification of a procedure to selectively oxidize primary alcohols to aldehydes (Gunbas and Brouwer, 2012). A solution of triol **14** (711 mg, 1.7 mmol), 2,2,6,6-tetramethyl-1-piperidinyloxy (26.6 mg, 0.17 mmol), tetrabutylammonium chloride (47.2 mg, 0.17 mmol) in THF (15 mL) and 15 mL of an aqueous solution of $NaHCO_3$ (0.5 M) and K_2CO_3 (0.05 M) were vigorously stirred at room temperature. *N*-chlorosuccinimide (340.5 mg, 2.6 mmol) was then added, and stirring was maintained for 16 h. The organic phase was

separated, and the aqueous phase was diluted with brine and extracted 3 times with CH_2Cl_2 (some precipitate might form and just filter to collect the solid and filtrate). The combined organic phases were concentrated *in vacuo*, the residue was dissolved in a small amount of CH_2Cl_2/MeOH and was subjected to purification by flash chromatography on silica gel (step-wise gradient elution, 0-40% EtOAc/hexanes) to yield aldehyde **15** (443 mg, 54%) as a white solid (mixture of diasteromers).

15: ^{1}H NMR (600 MHz, $CDCl_3$): δ 9.76-9.77 (m, 1H), 5.34-5.37 (m, 1H), 3.48-3.56 (m, 1H), 2.41-2.46 (m, 2H), 2.27-2.32 (m, 1H), 2.20-2.27 (m, 1H), 2.05-2.11 (m, 1H), 1.95-2.01 (m, 1H), 1.81-1.87 (m, 2H), 1.59-1.79 (m, 6H), 1.42-1.58 (m, 8H), 1.24-1.38 (m, 7H), 1.04-1.24 (m, 4H), 0.96-1.03 (m, 4H), 0.90-0.96 (m, 1H), 0.86 (s, 3H); ^{13}C NMR (150 MHz, $CDCl_3$) (as the major diasteromer): δ 202.8, 140.8, 121.5, 75.1, 71.7, 57.8, 56.9, 50.0, 43.8, 43.6, 42.6, 42.2, 40.1, 37.2, 36.5, 31.7, 31.6, 31.3, 29.7, 26.3, 23.9, 23.7, 22.3, 22.0, 20.9, 19.4, 13.6.

A.4.3.11 Preparation of 1-amino-21-((3S,10R,13S,17S)-3-hydroxy-10,13-dimethyl-2,3,4,7,8,9,10,11,12,13,14,15,16,17-tetradecahydro-1H-cyclopenta[a]phenanthren-17-yl)-4,7,10-trioxa-14-azadocosan-21-ol (16)

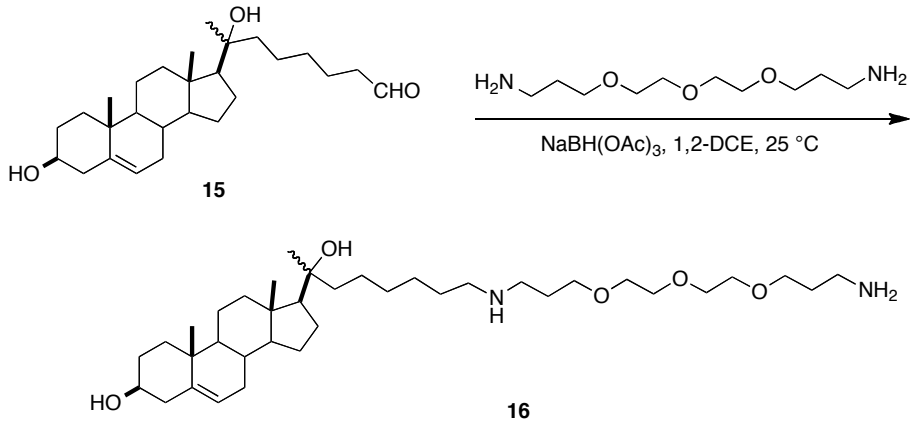

Compound **15** (208 mg, 0.5 mmol) and 4,7,10-trioxa-1,13-tridecanediamine (220 mg, 1 mmol) were mixed in 1,2-dichloroethane (5 mL) and then treated with sodium triacetoxyborohydride (159 mg, 0.75 mmol). The mixture was stirred at room temperature for 16 h until the reactants were consumed, as determined by TLC. The reaction mix was concentrated *in vacuo*, the residue was dissolved in DMSO and was purified by preparative reverse-phase HPLC on a Waters Symmetry C18 column (19 x 50 mm, 5μM). Elution was with a gradient of 15-80% MeOH in water with 0.035% trifluoroacetic acid, over 15 min and at a flow rate of 20 mL/min. The product **16** (mixture of diasteromers) was obtained as the di(trifluoroacetate) salt (yellow oil, 154 mg, 36%).

16: ^{1}H NMR (400 MHz, $CDCl_3$): δ 9.16 (br, 2H), 7.99 (br, 3H), 5.33-5.37 (m, 1H), 3.74 (t, J = 5.2 Hz, 2H), 3.56-3.66 (m, 10H), 3.47-3.56 (m, 3H), 3.04-3.22 (m, 4H), 2.72-2.98 (m, 6H), 2.18-2.33 (m, 2H), 1.93-2.11 (m, 4H), 1.79-1.88 (m, 2H), 1.58-1.79 (m, 4H), 1.38-1.54 (m, 6H), 1.22-1.38 (m, 9H), 1.06-1.22 (m, 4H), 0.87-1.06 (m, 5H), 0.85 (s, 3H); ^{13}C NMR (100 MHz, $CDCl_3$) (as the major diasteromer): δ 140.7, 121.6, 75.2, 71.8, 71.0, 70.0, 69.8, 69.5, 69.4, 68.4, 57.8, 56.8, 50.0, 48.3, 46.1, 43.6, 42.6, 42.2, 40.3, 40.0, 37.2, 36.5, 31.7, 31.6, 31.3, 29.5, 26.5, 26.1, 25.8, 25.7, 25.5, 23.8, 23.7, 22.3, 20.9, 19.4, 13.6. LC/MS: (ESI, m/z) calcd **[**M+H**]**$^{+}$ for $C_{37}H_{68}N_2O_5$: 621.5, found 621.4.

A.4.4 Preparation of BODIPY-SANT1 (17-21)

A.4.4.1 Preparation of *tert*-butyl 4-iodobenzylcarbamate (17)

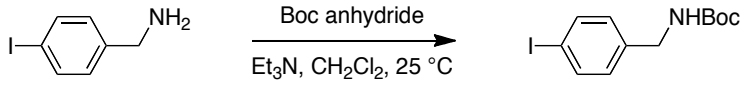

17

4-Iodobenzylamine (349.6 mg, 1.5 mmol) and triethylamine (0.44 mL, 3.15 mmol) were dissolved in dichloromethane (6 mL), and Boc anhydride (343.7 mg, 1.6 mmol) in dichloromethane (6 mL) was added dropwise. After stirring for 16 h at room temperature, the reaction mixture was washed with 1N HCl, saturated aqueous $NaHCO_3$, and brine, then dried over anhydrous Na_2SO_4 and concentrated to yield compound **17** as a white solid (499 mg, 100 %).

17: ^{1}H NMR (600 MHz, $CDCl_3$): δ 7.65 (d, J = 8.4 Hz, 2H), 7.03 (d, J = 7.8 Hz, 2H), 4.83 (br, 1H), 4.25(d, J = 4.2 Hz, 2H), 1.45 (s, 9H). Characterization matched the data reported for compound **17**(Antilla et al., 2004).

A.4.4.2 Preparation of tert-butyl 4-(4-formyl-3,5-dimethyl-1H-pyrazol-1-yl)benzyl-carbamate (18)

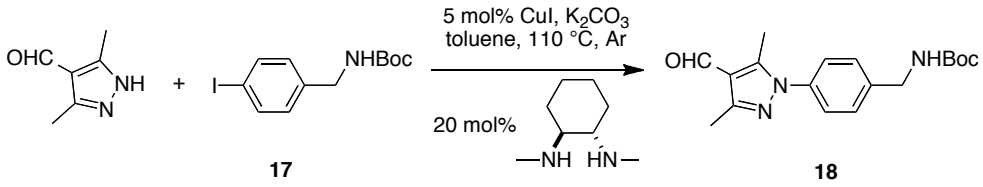

Compound **18** was obtained by *N*-arylation following a reported protocol(Fahmy et al., 2002). To a screwcap glass vial were added CuI (4.6 mg, 0.024 mmol, 5 mol%), 3,5-dimethyl-1*H*-pyrazole-4-carbaldehyde (59.5 mg, 0.48 mmol), K_2CO_3 (139.3 mg, 1.0 mmol), and a stir bar. The reaction vessel was fitted with a rubber septum, was evacuated and back-filled with argon, and this sequence was repeated twice. Aryl iodide **17** (191.8 mg, 0.58 mmol), (1*S*,2*S*)-N^1,N^2-dimethylcyclohexane-1,2-diamine (13.6 mg, 0.96 mmol, 20 mol%) and toluene (2 mL) were then added successively under a stream of argon. The reaction vial was sealed and immersed in an oil bath preheated to 110 °C, and the reaction was stirred for 24 h. The reaction mixture was cooled to room temperature, diluted with EtOAc and filtered through Celite. The filtrate was washed with aqueous NH_4OH (v/v, 1/1) and brine, then was dried over Na_2SO_4 and concentrated *in vacuo*. The resulting residue was purified by flash chromatography on silica gel (step-wise gradient from 9:1 to 2:3 hexane/EtOAc) to provide compound **18** as a yellow oil (17.0 mg, 11 %).

18: ^{1}H NMR (600 MHz, $CDCl_3$): δ 10.22 (s, 1H), 7.62 (d, J = 7.2 Hz, 2H), 7.57 (d, J = 7.8 Hz, 2H), 5.12 (br, 1H), 4.59 (br, 2H), 2.74 (s, 3H), 2.72 (s, 3H), 1.67 (s, 9H); LC/MS: (ESI, m/z) calcd $[M+H]^+$ for $C_{18}H_{23}N_3O_3$, 330.2, found 330.2.

A.4.4.3 Preparation of (E)-tert-butyl 4-(4-(((4-benzylpiperazin-1-yl)imino)methyl)-3,5-dimethyl-1H-pyrazol-1-yl)benzylcarbamate (19)

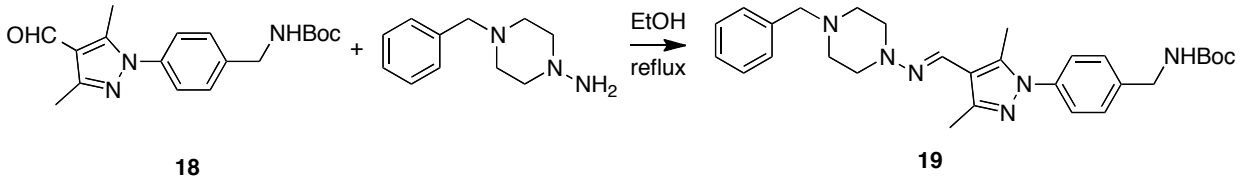

18 **19**

Following a reported protocol(Fahmy et al., 2002), an equimolar mixture of **18** (14.8 mg, 45.0 μmol) and 1-amino-4-benzylpiperazine (8.6 mg, 45.0 μmol) in absolute ethanol (0.5 mL) was heated under reflux for 12 h. After concentration, the resulting residue was purified by flash chromatography on silica gel (step-wise gradient elution from 100:1 to 9:1 CH_2Cl_2/MeOH) to provide compound **19** as a yellow oil (22.5 mg, 100 %).

19: ^{1}H NMR (600 MHz, $CDCl_3$): δ 7.53 (s, 1H), 7.17-7.31 (m, 9H), 4.88 (br, 1H), 4.28 (d, J = 5.4 Hz, 2H), 3.53 (s, 2H), 3.08-3.11 (m, 4H), 2.57-2.63 (m, 4H), 2.33 (s, 3H), 2.32 (s, 3H), 1.39 (s, 9H); LC/MS: (ESI, m/z) calcd $[M+H]^+$ for $C_{29}H_{38}N_6O_2$: 503.3, found 503.1.

A.4.4.4 Preparation of (E)-N-((1-(4-(aminomethyl)phenyl)-3,5-dimethyl-1H-pyrazol-4-yl)methylene)-4-benzylpiperazin-1-amine (20)

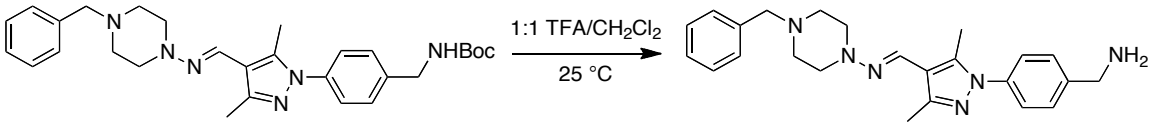

19 **20**

Compound **19** (7.5 mg, 15.0 μmol) was dissolved in a 1:1 mixture of TFA (0.8 mL) and CH_2Cl_2 (0.8 mL,) and was stirred at room temperature for 50 min. Volatiles were evaporated *in vacuo* and the resulting residue was used in the next step without further purification.

20: LC/MS: (ESI, m/z) calcd $[M+H]^+$ for $C_{24}H_{30}N_6$: 403.20, found 403.1.

A.4.4.5 Preparation of (E)-3-(3-((4-(4-(((4-benzylpiperazin-1-yl)imino)methyl)-3,5-dimethyl-1H-pyrazol-1-yl)benzyl)amino)-3-oxopropyl)-5,5-difluoro-7,9-dimethyl-5H-dipyrrolo[1,2-c:2',1'-f][1,3,2]diazaborinin-4-ium-5-uide (SANT-1-BODIPY) (21)

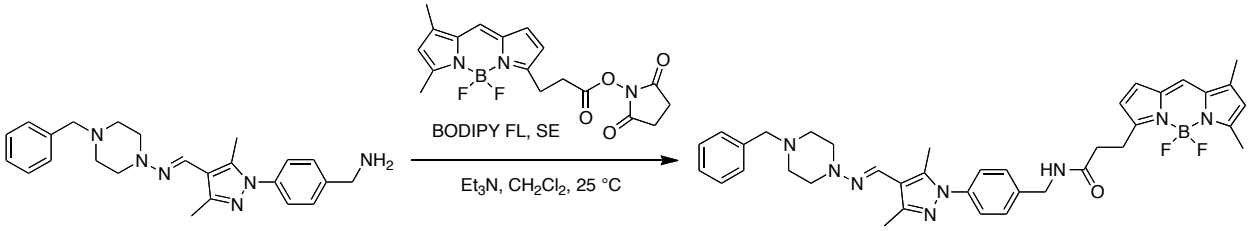

20 21

Triethylamine (9.1 μL, 65.0 μmol) and BODIPY-FL *N*-hydroxysuccinimide ester (5.0 mg, 13.0 μmol) were added to a solution of amine **20** (6.0 mg, 15.0 μmol) in dichloromethane (800 μL). The reaction mixture was stirred at room temperature for 18 h and then evaporated to dryness under a stream of nitrogen gas. Purification by flash chromatography on silica gel (step-wise gradient from 100:1 to 85:15 CH_2Cl_2/MeOH) yielded the fluorescent amide **21** as a dark red solid (7.8 mg, 89 %).

21: ^{1}H NMR (400 MHz, $CDCl_3$): δ 7.55 (s, 1H), 7.13-7.35 (m, 9H), 7.02 (s, 1H), 6.79 (d, J = 4.0 Hz, 1H), 6.22 (d, J = 4.0 Hz, 1H), 6.12 (t, J = 5.2 Hz, 1H), 6.03 (s, 1H), 4.36 (d, J = 6.0 Hz, 2H), 3.56 (d, J = 7.6 Hz, 1H), 3.52 (d, J = 7.2 Hz, 1H), 3.23 (t, J = 7.2 Hz, 2H), 3.04-3.16 (m, 4H), 2.59-2.71 (m, 6H), 2.47 (s, 3H), 2.31 (s, 6H), 2.17 (s, 3H); ^{13}C NMR (100 MHz, $CDCl_3$): δ 171.6, 160.4, 156.9, 148.1, 144.1, 138.4, 137.9, 135.2, 133.4, 129.3, 128.4, 128.2, 127.3, 125.1, 123.9, 120.5, 117.5, 63.5, 62.5, 53.0, 52.1, 51.4, 45.8, 42.9, 35.9, 24.8, 19.0, 14.9, 13.0, 11.9, 11.3, 8.1; LC/MS: (ESI, m/z) calcd $[M+H]^+$ for $C_{38}H_{43}BF_2N_8O$: 677.4, found 677.1.

A.4.5 Synthesis of 27-nor-5-cholesten-20,3β-diol methyl ether

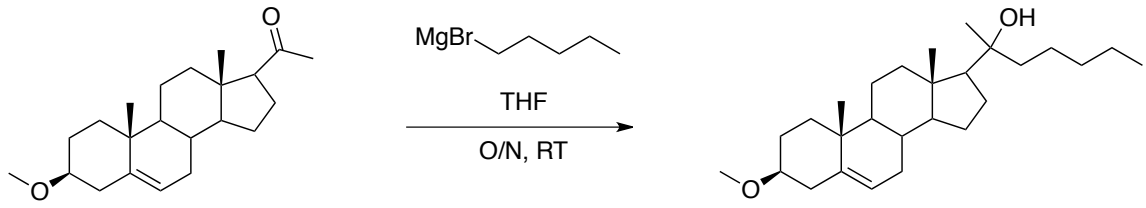

Chemical Formula: $C_{22}H_{34}O_2$
Molecular Weight: 330.50

Chemical Formula: $C_{27}H_{46}O_2$
Molecular Weight: 402.65

To a dry 250 mL flask equipped with a magnetic stir bar was added pregnenolone methyl ether (960 mg, 2.9 mmol, from Steraloids) and 5 mL anhydrous tetrahydrofuran. The solution was stirred under argon while 14.5 mL (29 mmol, 10 eq) of 2M pentyl magnesium bromide was added dropwise to the flask. The reaction was left stirring overnight under argon. The reaction was diluted with 100 mL diethyl ether and quenched by the addition of 1% aqueous acetic acid. The organic phase was washed with water and brine, dried over sodium sulfate, filtered and concentrated under reduced pressure. The crude product (TLC: 30% ethyl acetate/hexanes, starting material Rf = 0.33, product Rf = 0.38) was dissolved in a small amount of dichloromethane and purified by column chromatography using a gradient of 5-20% ethyl acetate in hexanes, yielding the product as a colorless oil (806 mg, 69%).

^{1}H NMR (400 MHz) δ 5.35 (m, 1H), 3.35 (s, 3H), 3.06 (m, 1H), 2.37 (m, 1H), 1.27 (s, 3H), 1.00 (s, 3H), 0.87 (s, 3H). ^{13}C NMR (400 MHz) 140.84, 121.46, 80.28, 75.09, 57.64, 56.90, 55.54, 50.10, 43.97, 42.61, 40.11, 38.65, 37.15, 36.85, 32.50, 31.79, 31.29, 27.96, 26.39, 23.93, 23.76, 22.65, 22.32, 20.91, 19.33, 14.07, 13.57.

A.5 Lentiviral expression

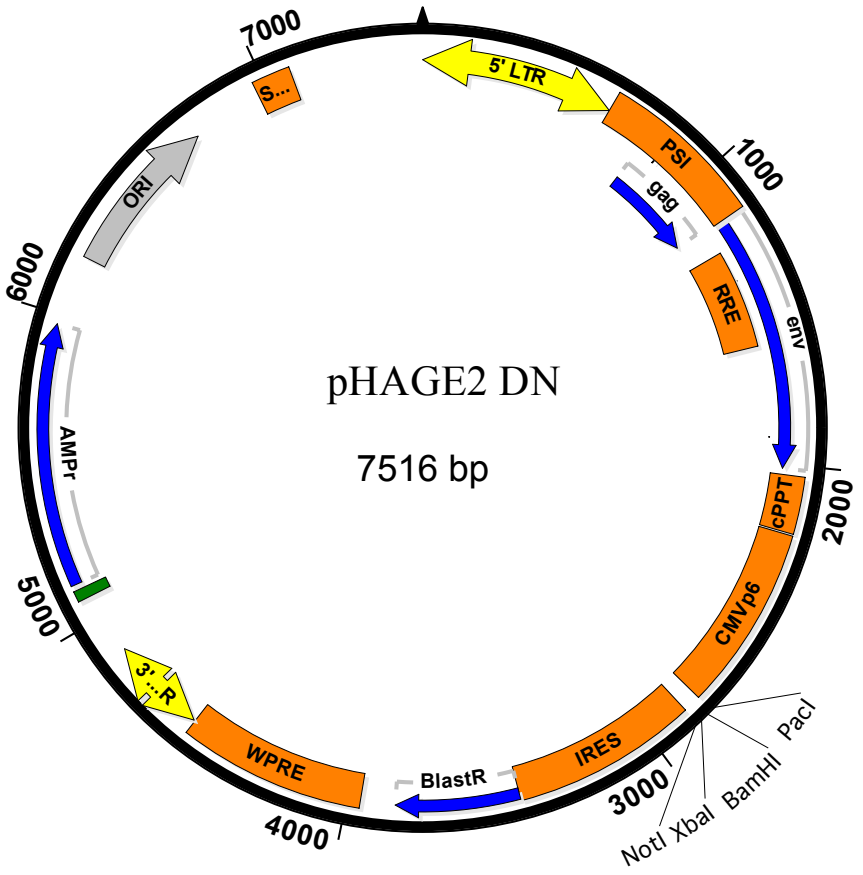

Supplementary Figure S8 Map of lentiviral packaging vector

In order to express the various constructs in Smo$^{-/-}$ MEFs, we designed a lentiviral backbone based on the pHAGE-CMV-MCS backbone (Mostoslavsky et al., 2006) to which a selectable Blasticidin resistance marker was added under the control of an internal ribosome entry site (IRES). The constructs of interest were inserted immediately downstream of the CMV promoter using the PacI and XbaI sites in a modified multiple cloning site. The resulting pHAGE2 DN constructs were cotransfected with Mirrus Trans-IT 293 into 293T cells along with packaging plasmids containing Gag-Pol, REV, TAT and VSV-G according to manufacturer's

protocol. 24 hours post-transfection, the medium was replaced and virus-containing supernatant was collected after another 48 hours. The supernatant was diluted 1:2 with regular medium, supplemented with hexadimethrine bromide (Polybrene) at a final concentration of 1μg/mL and used to infect MEFs. 24 hours post-infection, the transduction medium was replaced with medium containing 50μg/mL Blasticidin, and selection was considered complete 3 days later when no uninfected cells remained attached.

A.6 References

Abdel-Magid, A.F., K.G. Carson, B.D. Harris, C.A. Maryanoff, and R.D. Shah. 1996. Reductive Amination of Aldehydes and Ketones with Sodium Triacetoxyborohydride. Studies on Direct and Indirect Reductive Amination Procedures(1). *J Org Chem*. 61:3849-3862.

Adams, C.M., J. Reitz, J.K. De Brabander, J.D. Feramisco, L. Li, M.S. Brown, and J.L. Goldstein. 2004. Cholesterol and 25-hydroxycholesterol inhibit activation of SREBPs by different mechanisms, both involving SCAP and Insigs. *J Biol Chem*. 279:52772-52780.

Antilla, J.C., J.M. Baskin, T.E. Barder, and S.L. Buchwald. 2004. Copper-diamine-catalyzed N-arylation of pyrroles, pyrazoles, indazoles, imidazoles, and triazoles. *J Org Chem*. 69:5578-5587.

Counsell, R.E., P.D. Klimstra, L.N. Nysted, and R.E. Ranney. 1965. Hypocholesterolemic Agents. V. Isomeric Azacholesterols. *J Med Chem*. 8:45-48.

Fahmy, H.T., S.A. Rostom, and A.A. Bekhit. 2002. Synthesis and antitumor evaluation of new polysubstituted thiazole and derived thiazolo[4, 5-d]pyrimidine systems. *Arch Pharm (Weinheim)*. 335:213-222.

Gehrig-Burger, K., L. Kohout, and G. Gimpl. 2005. CHAPSTEROL. A novel cholesterol-based detergent. *FEBS J*. 272:800-812.

Gunbas, D.D., and A.M. Brouwer. 2012. Degenerate molecular shuttles with flexible and rigid spacers. *J Org Chem*. 77:5724-5735.

Lu, M.C., P. Afiatpour, C.B. Sullivan, and R.E. Counsell. 1972. Inhibition of cholesterol side-chain cleavage. 2. Synthesis of epimeric azacholesterols. *J Med Chem*. 15:1284-1287.

Mostoslavsky, G., A.J. Fabian, S. Rooney, F.W. Alt, and R.C. Mulligan. 2006. Complete correction of murine Artemis immunodeficiency by lentiviral vector-mediated gene transfer. *Proc Natl Acad Sci U S A*. 103:16406-16411.

Nachtergaele, S., L.K. Mydock, K. Krishnan, J. Rammohan, P.H. Schlesinger, D.F. Covey, and R. Rohatgi. 2012. Oxysterols are allosteric activators of the oncoprotein Smoothened. *Nat Chem Biol*. 8:211-220.